Dipartimento di Scienze Ambiente e Territorio e Scienze della Terra
Università degli studi di Milano-Bicocca

Dottorato di Ricerca in Scienze della Terra XXVI ciclo

Earthquake-induced static stress change in promoting eruptions

Tutore: Prof. Alessandro TIBALDI
Co-tutore: Dott.ssa Claudia CORAZZATO

Fabio Luca BONALI
Matr. Nr. 040546

This work is dedicated to my uncle Eugenio Marcora
who led my interest in Earth Sciences and Astronomy during my childhood

Abstract

The aim of this PhD work is to study how earthquakes could favour new eruptions, focusing the attention on earthquake-induced static effects in three different case sites. As a first case site, I studied how earthquake-induced crustal dilatation could trigger new eruptions at mud volcanoes in Azerbaijan. Particular attention was then devoted to contribute to the understanding of how earthquake-induced magma pathway unclamping could favour new volcanic activity along the Alaska-Aleutian and Chilean volcanic arcs, where 9 seismic events with $M_w \geq 8$ occurred in the last century.

Regarding mud volcanoes, I studied the effects of two earthquakes of M_w 6.18 and 6.08 occurred in the Caspian Sea on November 25, 2000 close to Baku city, Azerbaijan. A total of 33 eruptions occurred at 24 mud volcanoes within a maximum distance of 108 km from the epicentres in the five years following the earthquakes. Results show that crustal dilatation might have triggered only 7 eruptions at a maximum distance of about 60 km from the epicentres and within 3 years. Dynamic rather than static strain is thus likely to have been the dominating "promoting" factor because it affected all the studied unrested volcanoes and its magnitude was much larger.

Regarding magmatic volcanoes, the entire dataset includes a total of 51 eruptions following 9 large earthquakes ($M_w \geq 8$); 33 represent *first new* eruptions occurred at each single volcano. Comparison of the eruption rate before and after each earthquake suggests that 26 out of the 33 first new eruptions have a positive relation with the studied earthquakes; 13 out of 26 represent *awakening* events, which are first new eruptions occurred at volcanoes with not-continuous eruptive activity that had no eruptions in the five years before the earthquake. I followed a novel approach that resolves the earthquake-induced static stress change normal to the magma pathway of each volcano instead of considering the general crustal volume. I also considered other parameters that may contribute to control eruptions, such as magma composition and viscosity, magma chamber depth and local tectonic settings.

The sensitivity analysis performed for the 2010 Chile earthquake shows that the N-S- and NE-SW-striking magma pathways suffered a larger unclamping in comparison with those striking

NW-SE and E-W. Magma pathway parallel or subparallel to the strike of modelled faults suffered the highest unclamping, and this was also evident in the Alaska-Aleutian arc. Magma pathway geometry controls the magnitude of the static stress change induced by large earthquakes, with differences of up to 8 times among magma-feeding planes of different orientation at the same volcano. This range of diverse values is larger for the volcanoes closer to the epicentre. The possible error in the estimate of magma chamber depth has a minimum effect on the results since the sensitivity analysis shows that the range of stress changes with depth is about 1.5 orders of magnitude smaller than the range linked to variations in the magma pathway strike.

Result suggest that unclamping effect promoted eruptions that occurred at not-continuously erupting volcanoes (Type B) in a range of 157-543 km, while *awakening* under unclamping occurred in a range of 157-353 km. Regarding the time-gap, unclamping promoted eruptions at Type B volcanoes and *awakening* in a time window of 2 days-3 years. In the studied cases, it was also noted that unclamping enhanced eruptions preferentially at volcanoes with a deep magma chamber (> 5 km).

Regarding the role of magma pathway geometry, results suggest that 4 *awakening* events occurred along magma pathways parallel or subparallel to the σ_{Hmax}, and they are always under unclamping. Eleven *awakening* events occurred along magma pathways that have an angle from 40° to 90° respect to the σ_{Hmax}, thus unclamping favoured 8 of these events.

Finally, based on the results from this work, I suggest that earthquake-induced stress change can favour magma rise by imparting stress field modifications of the deviatoric stress acting on magma pathway in a percentage up to 5-10 %, increasing the efficiency of magma rise and consequent dyke intrusion also where the tectonic regime doesn't favour magma rise (e.g. in the older and thicker crust in Chile under contractional tectonics).

Index

1. Introduction

1.1. Aim of the project

The aim of this PhD project is to study how earthquakes could favour new eruptions, focusing the attention on earthquake-induced static effects in three different case sites (Fig. 1). First, it was tested how earthquake-induced crustal dilatation could trigger new eruptions at mud volcanoes in Azerbaijan. Second, earthquake-induced magma pathway unclamping could favour new volcanic activity along the Alaska-Aleutian and Chilean volcanic arc since 1900 AD, where 9 seismic events with $M_w \geq 8$ occurred. In particular, I applied a new numerical approach to resolve the earthquake-induced static stress change by resolving it on the magma feeding system, which was reconstructed at each single studied volcano. This approach produces a much higher resolution in the modelled static stress change than considering only a generalized crustal volume.

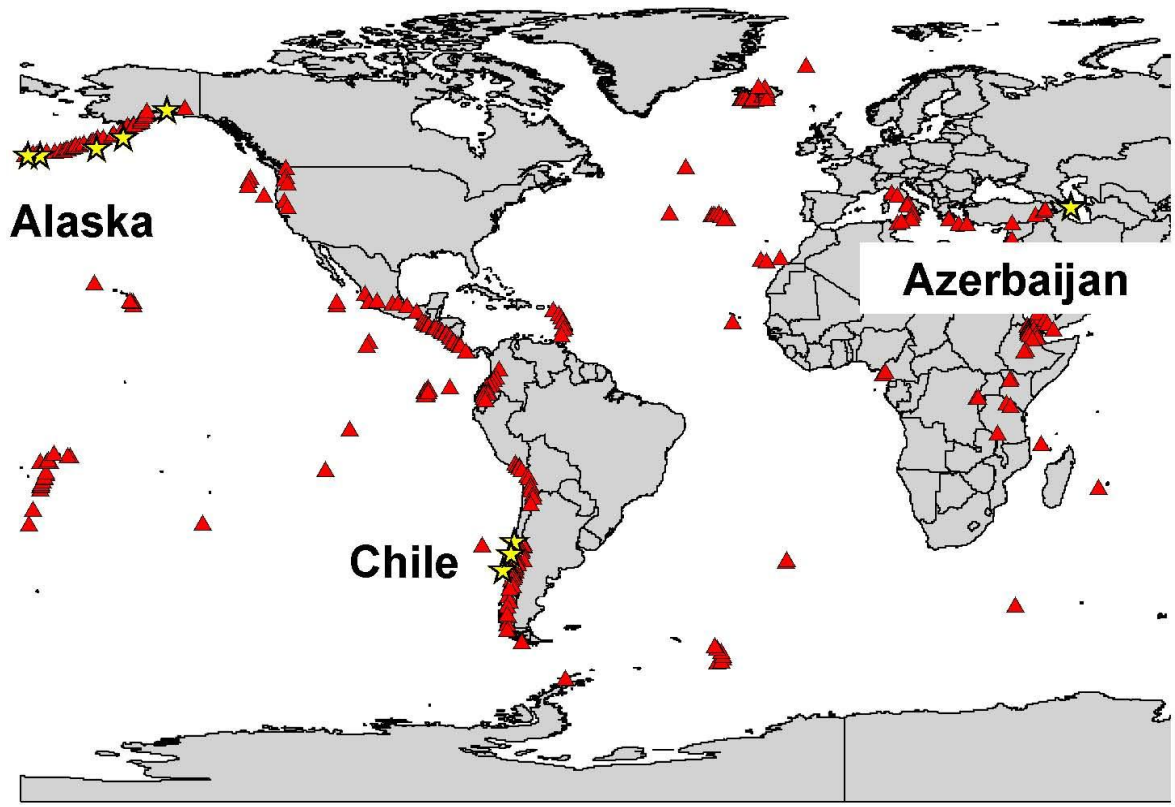

Figure 1. *Location of the studied case sites. Yellow stars locate earthquake epicentres. Red triangles represent active volcanoes (www.volcano.si.edu).*

1.2. General overview of the topic

Several authors suggest that a relation between the occurrence of large earthquakes and the following volcanic eruptions exists. They propose that a large earthquake could trigger volcanic activity at large distances from the epicentre (Linde and Sacks, 1998; Hill et al., 2002; Marzocchi, 2002; Marzocchi et al., 2002; Manga and Brodsky, 2006; Walter and Amelung, 2007; Watt et. al. 2009; Delle Donne et al., 2010; Bebbington and Marzocchi, 2011). For example, based on a global earthquake and eruption dataset, Linde and Sacks (1998) found that within two days of a large earthquake the occurrence of explosive eruptions is greater than expected as far as 750 km. This relationship has been quantified by Manga and Brodsky (2006) who showed that 0.4% of explosive volcanic eruptions occurred in a few days. For example, some volcanoes began new eruptions after the 1935 M 8.1 earthquake in Chile (Darwin, 1840), and a plinian eruption occurred at Santa Maria volcano (Guatemala) after a M 8.3 subduction earthquake in 1902 (Rockstroh, 1903); the latest eruption of Mount Fuji (Japan) in 1707 is also considered to have a relation with a major thrust earthquake occurred in that area (Koyama 2002). Some authors also argument that regional earthquakes seem to be capable of promoting effusive and explosive eruptions, and some examples regard: i) the 1960 eruption occurred Cordon Caulle volcanic complex (Chile) (Lara et al., 2004), ii) the 1975 eruption occurred at Kilauea volcano (Hawaii) (Tilling et al., 1976) and iii) the 1991 eruption occurred at Mount Pinatubo (Philippines) (Bautista et al., 1996). Eggert and Walter (2009) observed that the earthquake-eruption relations is more consistent in the near-field (0-250 km) for not continuously erupting volcanoes, and in agreement with other authors it was noted that the number of eruptions increases within a few days after the earthquake (Linde and Sacks, 1998; Manga and Brodsky, 2006; Eggert and Walter, 2009). Although such phenomena are not well constrained yet, it is suggested that the delay between the earthquake occurrence and the following volcanic events can be from seconds to years, owing to the complexity of volcanic systems (Linde and Sacks, 1998; Nostro et al., 1998; McLeod and Tait, 1999; Walter and Amelung, 2007; Eggert and Walter, 2009). For example, Watt et al. (2009) suggested that the overall eruption rate in the Southern Volcanic Zone increased after the two Chilean earthquakes of August 1906 (M_w 8.2) and May 1960 (M_w 9.5), considering a time window of one and three years after these earthquakes. Some authors suggest three principal modes for earthquake-induced stress transfer capable of promoting eruptions: i) static stress changes, ii) quasi-static stress changes, and iii) dynamic stresses induced by the seismic waves (Hill et al., 2002; Marzocchi et al., 2002; Manga and Brodsky, 2006). The static stress change is the difference in the stress field from just before an

earthquake to shortly after the seismic waves have decayed (Hill et al., 2002). It may explain processes leading to eruption in regions close to the fault rupture (e.g., Walter and Amelung, 2007) up to five years after an earthquake (Marzocchi, 2002). At greater distances, dynamic stress associated with the passage of seismic waves is often proposed as a possible eruption trigger (Linde and Sacks, 1998; Manga and Brodsky, 2006; Delle Donne et al., 2010). Quasi-static stress change is associated with slow viscous relaxation of the lower crust and upper mantle beneath the epicentre of a large earthquake, and occurs over a period of years to decades (Freed and Lin, 2002; Marzocchi, 2000; Marzocchi et al., 2002).

1.3. Overview of triggering mechanism

As discussed in Manga and Brodsky (2006) an eruption could initiate due to changes that occur both outside the magma body and changes within the subsurface magma itself. Some external factors regard: i) tectonic-induced changes in the regional stress field (e.g., Hill 1977), ii) glacial unloading (Jellinek et al. 2004), iii) sea level change (McGuire et al. 1997), or local changes caused by large landslides (Manga and Brodsky, 2006). On the contrary, changes in magmatic overpressure could initiate a new eruption (Manga and Brodsky, 2006): such increase could be induced by injection of fresh magma (e.g., Sparks et al. 1977), accumulation of bubbles (e.g., Woods & Cardoso 1997), crystallization that induces vesiculation (e.g. Blake 1984) and also earthquake-induced basaltic magma ascent and mixing with other magma reservoirs (Eichelberger, 1980). Some authors suggest that for a basaltic magmas an overpressure less than 1 MPa is necessary to generate tensile deviatoric stresses capable of promoting dike formation and propagation without cooling. For more silicic magmas this overpressure has been estimated to be 10-100 MPa (McLeod and Tait, 1999; Tait et al., 1989; Jellinek and De Paolo, 2004). Earthquake-induced static and dynamic stress changes are typically in the order of $10^{-2} \div 10^{-1}$ MPa so the overpressure must be within 99%-99.9% of the maximum overpressure for the earthquake to initiate a new eruption (Manga and Brodsky, 2006). Watt et al. (2009) suggest that eruptions within days after a large earthquake could occur only at volcanoes near a critical eruptive overpressure. On the contrary, volcanoes showing a longer response may be farther from this tipping point, but stress changes must still be significant to induced permanent pressure changes that could initiate a new eruption in a time frame of years, after an incubation period (e.g., Jupp et al., 2004).

1.3.1. Static stress change

The static stress change is the difference in the stress field from just before an earthquake to shortly after the seismic waves have decayed, it is due to the dislocation of a seismic fault and its magnitude attenuates by $1/r^3$, where r is the distance from the earthquake fault (Hill et al., 2002; Manga and Brodsky, 2006). It may explain processes leading to eruption in regions close to the fault rupture (e.g., Walter, 2007; Walter and Amelung, 2007) and delays of months to years (Hill et al., 2002). In particular, static stress changes are responsible of inducing pressure changes in a magma body and/or "unclamping" of conduits above the magma chamber (Hill et al., 2002). Two theories are discussed regarding the induced pressure changes in a magma body: i) magma is squeezed upward by increased compressional stress in the crust surrounding a magma chamber close to its critical state (e.g. Bautista et al., 1996) and ii) a decrease in compressional stress can promote additional melting, formation of bubbles and volatiles exolution (Hill et al., 2002; Walter and Amelung, 2007). The same authors suggest that the dissolved CO_2 and H_2O volatile gases are capable of influencing the density and viscosity of host magmas, playing a crucial role in promoting magma rise and the following eruption (Walter and Amelung, 2007); exolution of CO_2 decreases magma density and viscosity, which enhances the ascent of gas bubbles and magma, while exolution of H_2O may stop this process, causing the viscosity increase resulting in magma stagnation (Dixon et al., 1995). Although both hypotheses are strongly discussed in the literature, several authors agree with the second one. The first studied cases of earthquake-volcano interactions due to static stress changes regard two volcanoes located about 100 km from the epicentres, were the latest major eruption of Mount Fuji (Japan) in 1707, which occurred about one month following a M 8.2 offshore earthquake (Hill et al., 2002), and the 1991 eruption of Mount Pinatubo (Philippines) which occurred 11 months after the 1990 M 7.7 strike-slip earthquake (Bautista et al., 1996). Recently, static stress changes have been invoked to explain the rapidly triggered 1960 eruptions occurred at Cordón Caulle within 48 h of the M_W 9.5 May 22nd 1960 earthquake (Barrientos, 1994); such eruption was triggered by strain arising from extension beneath the volcano (Barrientos, 1994). Sepulveda et al. (2005) suggested that a dike raised normal to the direction of the earthquake slip - in this case the earthquake would have influenced the structural mechanism of this eruption. In fact, Hill et al. (2002) and Walter (2007) suggest that earthquake-induced static (permanent) normal stress reduction on magma pathway could have directly promoted dyke intrusion. Furthermore, Walter and Amelung (2007) suggested that volumetric strain expansion of magma could trigger eruption by magmatic decompression and gas exsolution.

They noted that the eruption rate increases in the region of permanent expansion, after a large subduction earthquake ($M_w \geq 9$). Such model provides a plausible explanation for responses on the timescale observed by Watt et al. (2009) in the Southern Volcanic zone (Chile). Such authors suggested that the overall eruption rate in the Southern Volcanic Zone (SVZ) increased after the two Chilean earthquakes of August 1906 (M_w 8.2) and May 1960 (M_w 9.5). This increase occurred in two different time windows, respectively one and three years after the earthquakes. Owing to the complexity of volcanic systems, the delay between the earthquake occurrence and the following volcanic events can be from seconds to years (Linde and Sacks, 1998; Nostro et al., 1998; McLeod and Tait, 1999; Walter and Amelung, 2007; Eggert and Walter, 2009). Several authors (e.g., Woods and Pyle, 1997; McLeod and Tait, 1999; Jellinek and De Paolo, 2004) suggest that composition and rheology of magmas, storage depth and state of volatile saturation may all play a role, as well as system overpressure. Nostro et al. (1998) proposed a coupling relationships between Apennine earthquakes and eruptions of the Vesuvius volcano. In this case static stress changes work in promoting both earthquakes and eruptions. In particular, eruptions precede and follow the earthquakes and this processes operate over a timescale several years. Marzocchi (2002) suggests a different model based on the viscous relaxation that is likely to act on longer timescales (30-35 years). Fujita et al. (2012) suggest that a pressure change of about 0.2 % of the lithostatic pressure (367.5 MPa at 15 km depth) occurred at the depth of Fuji magma reservoir. Such pressure change could be enough to trigger an eruptions in case the magma is ready to erupt and was induced by 2011 Japan earthquake and by one aftershock occurred close to the volcano. Several studies have also appealed to static stress transfer as a possible triggering mechanism for earthquakes or eruptions in such event pairs. Volcanic inflation on the Izu peninsula of Japan was followed 1-3 years later by M 6.7 and M 7.0 events at distances of 15-30 km where Thaicher and Savage (1982) calculated an increase of about 0.1 MPa in the Coulomb stress. Inflation in Long Valley was capable of inducing Coulomb failure on three of the four faults that ruptured during this geological process (Savage and Clark, 1982). Six $6.0<M<6.5$ earthquakes struck 10-40 km from Long Valley caldera during 1980-1986 (Savage and Clark, 1982; Cockerham and Cotbell, 1987). The 1978 eruption of the Asal rift, Djibouti, was followed by a series of earthquakes, Jacques et al. (1996) argued that stress transferred by the dike intrusion triggered the earthquakes.

1.3.2. Viscoelastic relaxation

In most tectonically active regions, earthquakes take place in the upper part of the crust where the deformation behaviour is elastic, while the underlying lower crust and mantle deform plastically due to higher temperatures; such depth limit is approximated to 15–20 km (Hill et al., 2002). The transition between elastic and plastic deformations corresponds to the 350-400°C isotherm (Karato and Wu, 1993; Kohlstedt et al., 1995). An earthquake is capable of inducing shear stresses in the underlying plastic zone that is coupled with the upper elastic crust. After an earthquake, the plastic zone will gradually relax and transfer stress with time to the upper crust, which continues to deform quasi-statically. Such mechanism will continue until the viscoelastic system approaches a new state of equilibrium. Phenomena triggered by viscoelastic relaxation result in a time lag of years to decades, and the magnitude of quasi-static stresses should be smaller than the static ones (Manga and Brodsky, 2006). Such mechanism has been studied for earthquake–earthquake triggering by Pollitz and Sacks (1997), Fred and Lin (2002) and Zeng (2001). These authors suggest that this process could work as far as 30-150 km from the epicentre and over periods of 7-50 years. For volcano-earthquake relations, Marzocchi (2002) noted that the largest explosive eruptions of the last Century in the World occurred within 0-5 and 30-35 years after $M_s \geq 7$ earthquakes, at distances up to 1000 km. Post-seismic stress changes were interpreted to be capable of promoting eruption in 30-35 years after earthquakes, compatibly to the relaxation time of a viscous astenosphere (Piersanti et al., 1995, 1997; Pollitz et al., 1998; Kenner and Segall, 2000). Coseismic stress changes are candidate to promote eruptions in the 0-5 years after earthquakes, where the eruptions occurred at a distance within 100-300 km (Marzocchi, 2002; Marzocchi et al, 2004). In another study, Hill et al. (2002) suggest that following the 1700 AD M = 9 megathrust earthquake, the eruption rate in the Cascade volcanic arc increased, during the early nineteenth century, due to viscoelastic relaxation. Finally, Manga and Brodsky (2006) argument that "*the stress diffusion caused by viscoelastic relaxation results in a nonlinear spatial and temporal evolution of stresses caused by the earthquake, quantifying the relationship between earthquakes and eruptions from observations will undoubtedly remain challenging*".

1.3.3. Dynamic stress changes

An earthquake generates also dynamic stress changes (transient) capable of producing greater pressure changes, although these last only seconds (Hill et al., 2002; Manga and Brodsky, 2006; Eggert and Walter, 2009). Manga and Brodsky (2006) noted that seismic waves are

transitory phenomena, and additional mechanisms are necessary to maintain the increased pressure in the magmatic system. Such processes will be discussed in this section. Dynamic stress changes may excite and promote the ascent of gas bubbles, and consequently magma ascent (Manga and Brodsky, 2006), creating new bubbles to excite volcanic eruptions (e.g., Walter et al. 2009). Earthquake-generated seismic waves travel at great distances without losing much of their energy (Hill et al., 2002) and dynamic stress change decreases more slowly than the static stress changes (Hill and Prejean, 2007), attenuation is about $1/r^{1.6}$, while for surface seismic waves attenuation is about $1/r^2$ (Manga and Brodsky, 2006; Fujite at al., 2012). Dynamic stresses can also favour bubble growth, including adjective overpressure (Linde et al., 1994), rectified diffusion (Brodsky et al., 1998) and shear strain (Sumita and Manga, 2008). In particular, Sumita and Manga (2008) suggest a common mechanism influencing both magmatic and hydrological systems. They observe a correlation among rapidly-triggered eruptions and hydrological and seismic responses, which fall within a general distance-magnitude bound. This bound appears to correspond closely to the liquefaction limit for hydrological system responses. Based on this evidence, they suggest that liquefaction may play a relevant role in eruption-triggering, as in the case of the 1960 earthquake, where all of the candidate triggered eruptions lie inside the bounds shown by Sumita and Manga (2008).

For "*bubble growth*" it is meant that the passage of seismic waves can promote nucleation of new bubbles due to small pressure changes (Manga and Brodsky, 2006). In a magma chamber, dissolved gas is added due to crystallization, and if the partial pressure of this gas is close to the critical supersaturation, earthquake-induced new bubbles could result in significant excess of nucleation and high overpressure (Manga and Brodsky, 2006). This process could result in explosive eruption in case of a crystal-poor system that can sustain a high supersaturation, because the large excess gas pressure will make the new bubbles grow rapidly (Manga and Brodsky, 2006). Also decompression of magmas stored in the crust promotes bubble nucleation (Manga and Brodsky, 2006).

As concerns "*adjective overpressure*", Steinberg et al. (1989) suggest that rising of bubbles in a closed system is capable of inducing pressure increase sufficient to trigger an eruption. Sahagian and Proussevitch (1992) suggest that this process could generate several hundred MPa of overpressure capable of fracturing the host rock. Such process is enhanced if bubbles can rise and separate fast from the magma (Woods and Cardoso 1997). A large pressure from near the bottom of a magma chamber to the surface, induced by this mechanism, and the following pressure increase, would promote eruption (Manga and Brodsky, 2006). Such

process was invoked by Linde et al. (1994) and Hill et al. (1993) to explain both deformation and seismicity in the Long Valley Caldera after the 1992 Landers earthquake. Linde et al. (1994) suggested that passage of seismic waves have dislodged bubbles.

The "*rectified diffusion*" consists in an increase in magma pressure in a closed system due to an increase in volatiles inside the bubble (Hill et al., 2002). Seismic waves could promote a small net addition of mass to (and hence volume of) the bubble (Manga and Brodsky, 2006). Brodsky et al. (1998) proposed that this process could induce an overpressure of about 10^{-2} MPa in basalts and 10^{-4} MPa in rhyolites (water was assumed as volatile phase) but only in case of sufficiently oversaturated magmatic systems. Ichihara and Brodsky (2006) suggest that such process can cause only a slight pressure increase. Finally, dynamic stresses could promote magmatic overturn where a crystal mush at the roof of a magma chamber may be dislodged as inter-crystal yield strength decreases promoting vesiculation, magma convection and rise, initiating a new eruption (Hill et al., 2002; Manga and Brodsky, 2006; Davis et al., 2007).

1.4 Contents of the following chapters

Chapter 2 – "*Methods*". The chapter presents an overview of the methods used in this work.

Chapter 3 – "*Evaluation of earthquake-induced strain in promoting mud eruptions: the case of Shamakhi-Gobustan-Absheron area, Azerbaijan*". This chapter presents a case study where both the static and dynamic strains induced by earthquakes in the substratum of mud volcanoes are evaluated. In particular, I studied the effects of two earthquakes of M_w 6.18 and 6.08 occurred in the Caspian Sea on November 25, 2000 close to Baku city, Azerbaijan.

Chapter 4 – "*Sensitivity analysis of earthquake-induced static stress changes on a volcanic arc: the 2010 Mw 8.8 Chile earthquake*". This chapter presents the sensitivity analysis of earthquake-induced static stress on the volcanic arc imparted by the 2010 Chile earthquake.

Chapter 5 – "*Earthquake-induced static stress change on magma pathway in promoting the 2012 Copahue eruption*". This chapter presents a case study where a sensitivity analysis of earthquake-induced static stress was done on the Copahue volcano magma pathway, imparted by the 2010 Chile earthquake.

Chapter 6 – "*Earthquake-induced unclamping in promoting eruptions: the Chile case*". This chapter presents a case study where earthquakes with $M_w \geq 8$ occurred in proximity of 60 Holocene volcanoes, in the Southern Volcanic Zone of the Andes (SVZ) since 1906. I analysed these events by coupled numerical modelling and field data in order to understand

the key attributes of each volcano that may lead to a seismically-triggered eruption and the general mechanisms by which earthquakes could trigger volcanic new activity.

Chapter 7 – "*Earthquake-induced unclamping in promoting eruptions: the Alaska-Aleutian case*". This chapter presents a case study where earthquakes with $M_w \geq 8$ occurred in proximity of 80 Holocene volcanoes, in the Alaska-Aleutian volcanic since 1938. I analysed these events by coupled numerical modelling and field data in order to understand the key attributes of each volcano that may lead to a seismically-triggered eruption and the general mechanisms by which earthquakes could trigger volcanic new activity.

Chapter 8 – "*Discussion*". In this chapter I discussed the dataset regarding only the eruptions following the earthquakes that have a positive statistical correlation with earthquakes. Here it is discussed the role of: i) static stress changes, ii) silica content of magmas and iii) chamber depth. Finally new relations regarding the distances from the epicentre and time-gap are proposed.

Chapter 9 – "*Final remarks*". In this chapter I summarized the results of my PhD work.

2. Methods

I analyzed earthquake-volcano interactions by seismic events with $M_w \geq 8$ occurred close to the Alaska-Aleutian and Chilean volcanic arc since 1900 AD. It was chosen to analyze the events occurred since 1900 AD in order to have reliable and confident database regarding both earthquakes and eruptions (e.g. Watt et al., 2009). Five earthquake occurred close to the Alaska-Aleutian volcanic arc in: 1938 (Shumagin Islands), 1946 (Aleutian Islands), 1957 (Andreanof Islands), 1964 (Alaska) and 1965 (Rat Islands) (Plafker, 1969; Beck and Christensen, 1991; Christensen and Beck, 1994; Johnson and Satake, 1994; Johnson and others, 1994; http://earthquake.usgs.gov/). Four earthquakes occurred close to Chilean volcanic arc in: 1906 (Valparaiso), 1960 (Valdivia), 1985 (Santiago), and 2010 (Maule) (Conte et al., 1986; Yoshida, 1991; Watt et al., 2009; http://earthquake.usgs.gov). I applied a new numerical approach to model the earthquake-induced static stress change by resolving it on the magma feeding system reconstructed at each single unrest volcano. This approach produces much higher resolution in the modelled static stress change in comparison to considering only a generalized crustal volume.

2.1. Dataset of eruption events

It was analyzed earthquake-volcano interactions induced by these seismic events within a search radius based on Delle Donne's et al. (2010) formula (Fig. 1):

$$M = -6.4 + 2.17 \log R_{max}$$

relating the earthquake magnitude (M) and an empirical maximum distance for volcanic response (R_{max}). In order to have a reliable and homogeneous dataset I consider only the eruptions occurred with certainty in the five years after each earthquake, which are classified as "*confirmed*" in the world catalogue (Global Volcanism Program, http://www.volcano.si.edu/index.cfm). I focused the analysis in the time-frame up to five years to better constrain the contribution of coseismic stress changes in promoting new eruptions (e.g. Marzocchi, 2002), considering also that static stress change is capable of inducing aftershocks (rock failure) up to 3-5 years after an earthquake (Anderson and Johnson, 1999; Stein, 1999; Hardebeck et al., 1998; Seeber and Armbruster, 2000; R. Stein, written comm., 2012). I named as "*first new*" activity the first new eruption after the earthquake within the five years, and "*awakening"* events the *first new* events that occurred at volcanoes that did not have any activity in the five years prior to the earthquake.

Similarly to Eggert and Walter (2009) and Walter and Amelung (2007), the analyzed volcanoes are classified in two classes: "Type A" are volcanoes erupting more or less continuously (i.e. more than 20 eruptions since 1900 AD), which are considered as open-conduit systems, and "Type B" are not-continuously erupting volcanoes (less than 20 eruptions). Based on these definitions, Type-A volcanoes cannot have *awakening* events since they are already in a condition of continuous eruptive activity. Type-B volcanoes that didn't have any eruption in the 5 years prior to the earthquake and then experienced *awakening* after the earthquake are defined as Type B+.

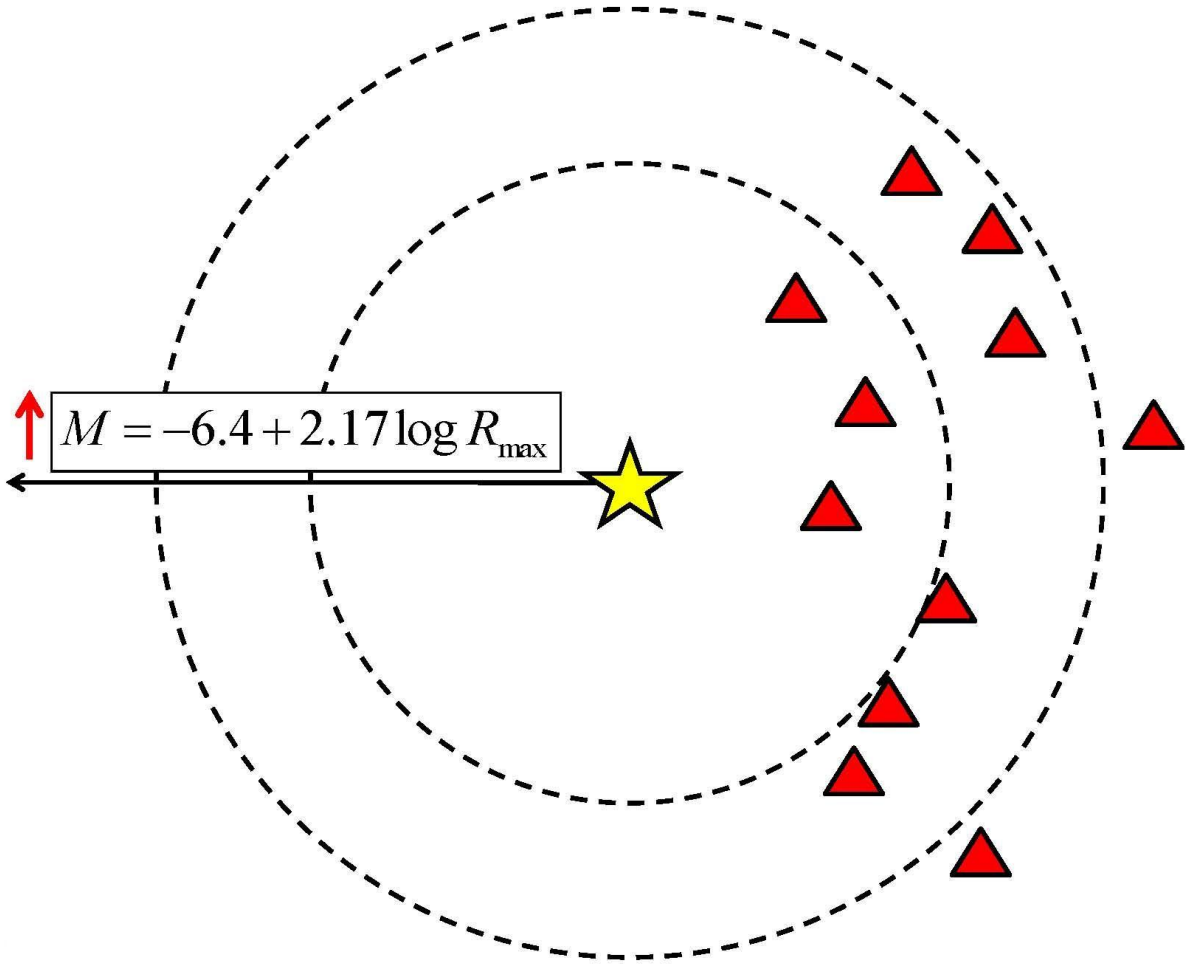

Figure 1. *It was analyzed earthquake-volcano interactions induced by seismic events within a search radius based on Delle Donne's et al. (2010) formula relating the earthquake magnitude (M) and an empirical maximum distance for volcanic response (R_{max}). Yellow stars locate earthquake epicentres. Red triangles represent active volcanoes (www.volcano.si.edu).*

In order to assess the influence of key volcanic parameters on the feedback between large earthquakes and volcanic events, I compiled all the data available for each volcano: magma chamber depth, silica content of the volcanic products, geometry of the magma pathway, volcano dimension and the tectonic setting of the volcano substratum, earthquake magnitude, distance from the earthquake epicentre and time-gap between earthquake occurrence and eruptions. Finally I compare the eruption rate before and after each earthquake, always considering eruptions within the search radius proposed by Delle Donne et al. (2010). The eruption rate before the earthquake (ER-before) has been calculated considering only eruptions occurred in the 50 years before (e.g. Walter and Amelung, 2007), while the eruption rate after the earthquake (ER-after) has been calculated for different increasing time-windows: 0-1 year, 0-2 years, 0-3 years, 0-4 and 0-5 years. This was also done analyzing only the "*first new*" eruptions, distinguishing the volcano Type (A or B) and finally considering only the eruptions occurred under magma pathway unclamping, in order to identify a consistent time-gap between the earthquake and the following volcanic eruptions.

2.2. Reconstruction of magma pathway geometry

Basic magma is supplied to the surface mostly along planar, steeply-inclined intrusive sheets that may group to form dyke swarms (Dieterich, 1988; Carracedo, 1994; Moore et al., 1994; Walter and Schmincke, 2002) and eventually volcanic rift zones formed by hundreds of such parallel dykes (Fiske and Jackson, 1972; Walker, 1999). Volcanic rift zones are usually expressed at the surface by aligned pyroclastic centres (Fig. 2) and swarms of fissures, dykes and faults (Annen et al., 2001; Walter and Schmincke, 2002). Dykes tend to propagate parallel to the horizontal greatest principal stress (σ_{Hmax}), forming aligned parasitic cones (e.g. Nakamura, 1977; Fig. 3), thus the alignment of volcanic centres and monogenetic cones can be used to infer the azimuth of local σ_{Hmax} (Johnson and Harrison, 1990; Strecker and Bosworth, 1991). Recent works suggest that a more detailed definition of the magma paths can be determined by combining dyke geometry with a series of morphometric parameters of main craters and parasitic vents (Tibaldi, 1995; Corazzato and Tibaldi, 2005; Bonali et al., 2011). Applying these criteria, the reconstruction of the azimuth of the Quaternary magma pathways was based on: i) alignment of vents, overlapping and nested calderas, nested summit craters, parasitic and flank cones, and ii) trend of vents, elongation of volcano edifice or chain, and fissure systems. In the case of those volcanoes resting along strike-slip faults, the magma pathways are assumed as vertical, extending from the surface down to the depth of magma chamber top. In the case of those volcanoes lying along reverse/thrust faults, the

geometry of the magma pathway is assumed with inclination and dip that mimic the geometry of the reverse fault. All these features were determined using satellite images, DEM-SRTM90 and geological maps, together with the available literature information and field validation.

Figure 2. *Example of volcanic rift zone from La Réunion island, Indian Ocean. In the photo the field view of a the NW-SE elongated area affected by several aligned pyroclastic cones (Bonali et al., 2011).*

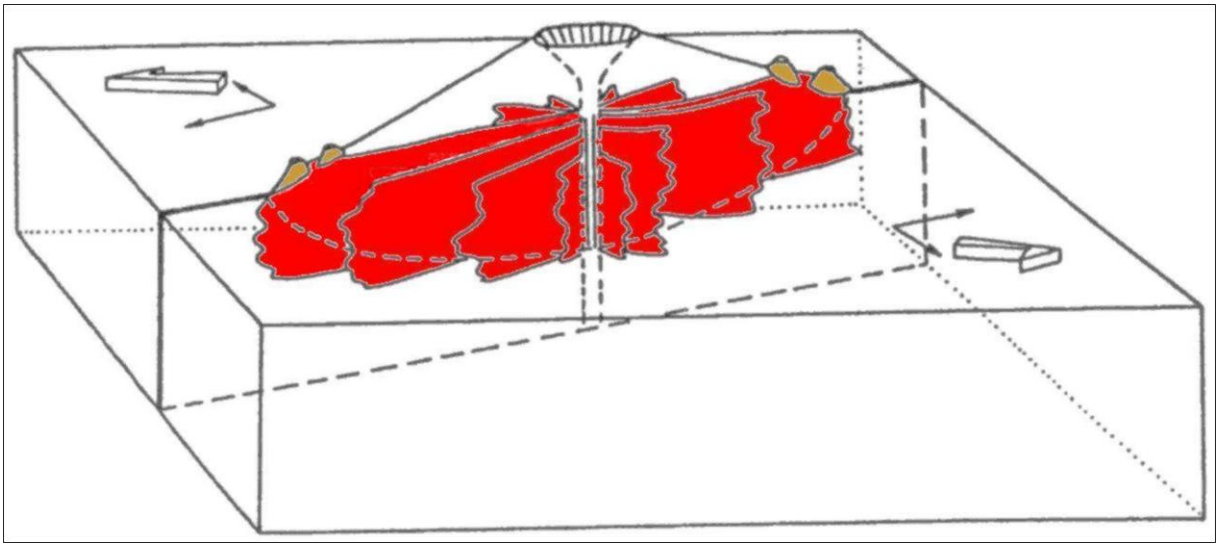

Figure 3. *Sketch view of dykes propagated parallel to the horizontal greatest principal stress (σ_{Hmax}), forming aligned parasitic cones, modified after Nakamura (1977). Dykes are highlighted in red colour, parasitic cones are highlighted in brown.*

2.3. Numerical modelling

A series of representative numerical models were developed to investigate how tectonic motions along the fault planes (of these nine earthquakes) transferred static stress on the magma pathways of the studied volcanoes. The numerical models were performed using the Coulomb 3.3 software (Lin and Stein, 2004; Toda et al., 2005), where calculations were made in an elastic halfspace with uniform isotropic elastic properties following Okada's (1992) formulae. Such formulae allow to calculate the crustal dilatation as well as the static normal stress change resolved on a receiver surface, independently from the rake angle of the receiver structure and from the friction coefficient used in the model. Such normal stress change can produce a clamping (increase in normal stress) or unclamping (decrease in normal stress) effect on any receiver surface (e.g. a magma pathway/feeder dyke). The upper crust was modelled as an elastic isotropic halfspace characterized by a Young's modulus $E = 80$ GPa and a Poisson's ratio $\nu = 0.25$, based on King et al. (1994), Mithen (1982), Lin and Stein (2004) and Toda et al. (2005); a lower value of Young's modulus would only have the effect of reducing the magnitude of static stress changes. The finite fault model used to simulate the earthquake-induced effects are based on tsunami wave form inversion, teleseismic, GPS and InSAR data and are characterized by defined fault plane geometry and variable slip rate. The input stress fields are based on data reported in the World stress map database (Heidbach et al., 2008) and tensor solutions. The subvolcanic magma feeding systems that link the volcanoes with their magma reservoirs are assumed as vertical surfaces for all volcanoes. For volcanoes that overlie thrust faults, the magma pathways are assumed 45° dipping like thrust, based on field data (Fig. 4; e.g. Cembrano and Lara, 2009). The stress changes over the area of interest has been calculated at a representative depth of 2 km below the volcano base.

2.3.1. Coulomb 3.3 code

This software was developed and implemented by the USGS and different Universities, and is available freeware www.coulombstress.org. It is designed to investigate Coulomb stress changes on mapped faults and earthquake nodal planes, and it is intended both for publication-directed research and for university teaching. It enables to calculate static displacements (on a surface or at GPS stations), strains and stresses caused by fault slip, magmatic intrusion or dike expansion. Problems such as how an earthquake promotes or inhibits failure on nearby faults, or how fault slip or dike expansion will compress a nearby magma chamber, are germane to Coulomb. Geologic deformation associated with strike-slip faults, normal faults, or fault-bend folds is also a useful application. Calculations are made in

an elastic half-space with uniform isotropic elastic properties following Okada (1992). The following processes are not included in Coulomb: dynamic stresses, pore fluid diffusion, and viscoelastic rebound. Further, basins and crustal layering modify the stresses in comparison to the elastic half-space implemented in Coulomb. Nevertheless, I believe that this tool enables to explore key aspect of fault-volcano interaction and for this reason it was used in my PhD work.

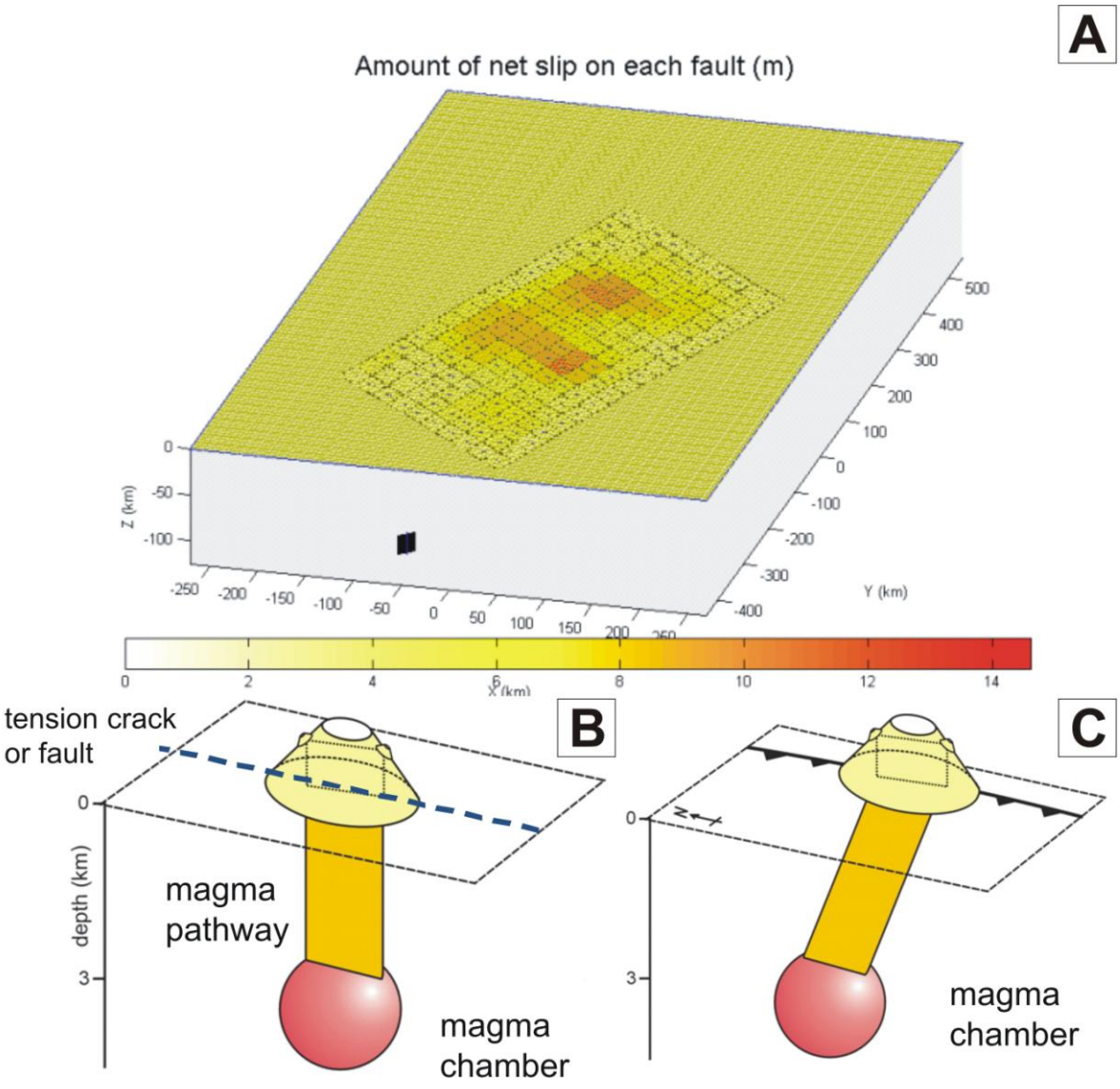

Figure 4. *(A) Coulomb 3.3 3D view of the halfspace with a finite fault model with variable fault slip and a feeder dyke (in black). (B) Subvolcanic magma feeding systems that link the volcanoes with their magma reservoirs are assumed as vertical surfaces.(C) For volcanoes that overlie thrust faults, the magma pathways are assumed 45° dipping like thrust, based on field and geophysical data (e.g. Cembrano and Lara, 2009).*

2.3.2. Elastic half-space

It is defined by isotropic and elastic properties following Okada (1992).

These proprieties are:

- the Poisson's ratio ν = 0.25 (Lin and Stein, 2004; Toda et al., 2005; Toda et al., 2008). It is the ratio, when a sample object is stretched, of the contraction or transverse (perpendicular to the applied load), to the extension or axial strain (in the direction of the applied load).
- The Young's modulus E = 80 GPa (Mithen, 1982; Lin and Stein, 2004; Toda et al., 2005; Toda et al., 2008). It is a measure of the stiffness of an isotropic elastic material. It is defined as the ratio of the uniaxial stress over the uniaxial strain in the range of stress in which Hooke's Law holds.
- The Friction coefficient μ' = 0.4, where 0.0-1.0 is typically considered the limit of the crust (Lin and Stein, 2004; Toda et al., 2005; Toda et al., 2008).
- The extent of the grid was chosen based on the specific search radius for each studied earthquake, and the grid element size is set to 5 km x 5 km.

3. Evaluation of earthquake-induced strain in promoting mud eruptions: the case of Shamakhi-Gobustan-Absheron area, Azerbaijan

This chapter reproduces the paper accepted for publication "Babayev G.[1], Tibaldi A.[2], Bonali F.L.[2], Kadirov F.[1]. Evaluation of earthquake-induced strain in promoting mud eruptions: the case of Shamakhi-Gobustan-Absheron area, Azerbaijan", Natural Hazards, December 2013.

[1]Department of Geodynamics and Seismology, Institute of Geology at Azerbaijan National Academy of Sciences, Baku, Azerbaijan.
[2]Department of Earth and Environmental Sciences, University of Milan Bicocca, Milan, Italy.

Abstract

Although a relationship between the occurrence of large earthquakes and the eruptions of close mud volcanoes is well known, several uncertainties remain on understanding the triggering mechanisms. In the present study we evaluate both the static and dynamic strains induced by earthquakes in the substratum of mud volcanoes. We studied the effects of two earthquakes of M_w 6.18 and 6.08 occurred in the Caspian Sea on November 25, 2000 close to Baku city, Azerbaijan. A total of 33 eruptions occurred at 24 mud volcanoes within a maximum distance of 108 km from the epicentres in the five years following the earthquakes. The overall eruption rate in the studied area of the 50 years before the 2000 earthquakes was 1.24 that is much smaller than the eruption rate of 6.6 of the 5 years following these earthquakes. The largest number of eruptions occurred within two years from the earthquakes with the highest frequency within six months. Our calculated earthquake-induced static effects show that crustal dilatation might have triggered only 7 eruptions at a maximum distance of about 60 km from the epicentres and within 3 years. Based on our data, dynamic rather than static strain is likely to have been the dominating "promoting" factor because it affected all the studied unrest volcanoes and its magnitude was much larger.

3.1. Introduction

Mud volcanoes have been observed to erupt shortly after close tectonic earthquakes suggesting a possible feedback effect (e.g. Chigira and Tanaka, 1997; Manga et al., 2009)

similarly to what occurs at magma volcanoes (Linde and Sacks, 1998; Nostro et al., 1998; Walter and Amelung, 2007; Eggert and Walter, 2009; Walter et al., 2009; Watt et al., 2009; Bonali, 2013; Bonali et al., 2013). Anyway, much more studies have been conducted on earthquake-triggered magma eruptions, whereas mud volcanoes received attention only in recent times; for example, Mellors et al. (2007) showed that there is a statistically significant number of mud eruptions triggered by earthquakes by analyzing their temporal-spatial relationships especially in Azerbaijan. This region hosts 190 mud volcanoes on land, a few tens of kilometers from the capital Baku, and other 150 offshore in the Caspian Sea. These onshore mud volcanoes not only represent a natural interesting phenomenon, but also impose a threat to the conterminous areas since eruptions can produce important quantities of mud capable of destroying nearby roads, pipelines and buildings. Mud volcano eruptions in fact, can produce severe social and economic impacts, such as the 29 May, 2006 eruption at Sidoarjo, Indonesia, which imposed tens of thousands of people displaced (Manga, 2007; Mazzini et al., 2007). In Azerbaijan on September 2012, Lokbatan mud volcano, located 12 km southwest of Baku, erupted with a 200-m-high fire column that posed a threat to the nearby gas and oil infrastructures. Mud volcanoes have also been studied for reconstructing the average depth of pressurized source layers because they may be indicators of mobilized fluids, with special interest to gas and oil exploration (Feyzullayev, 2012,). Mud volcanoes have been considered to be linked to the ongoing tectonics for what concerns both fault activity, which may guide the rate of mud extrusion (Kopf, 2008) and the state of stress that dictates the volcano shape and vent distribution (Bonini and Mazzarini, 2010; Bonini, 2012). Mud volcanoes are mostly located in compressional belts, have several morphological and structural similarities with lava volcanoes, and thus represent a good proxy to analyze the feeding systems under contractional tectonics. Compression in fact, with reverse or transpressional faulting, is usually considered a highly unfavourable setting for volcanism (Glazner, 1991; Hamilton, 1995; Watanabe et al., 1999) where only intrusive emplacement is expected (Cas and Wright, 1987). More recently, based on field studies of plutonic rocks (e.g. Saint Blanquat et al., 1998) and of volcanic deposits as well as analogue modelling (Tibaldi, 1992; Tibaldi and Romero, 2000; Tibaldi, 2008; Tibaldi et al., 2010), it has been showed that volcanism can also occur following reverse and transcurrent faults and folds. For all these reasons, the study of the relationships between tectonics and mud volcanism is an important recent task of research and more work is still necessary to unravel the complex picture. The complexity is particularly evident for the earthquake-eruptions relations: while time correlations between large earthquakes and mud volcano eruptions are abundant (Guliyev and

Feizullayev, 1997; Chigira and Tanaka, 1997; Delisle et al., 2002; Nakamukae et al., 2004; Baciu and Etiope, 2005; Martinelli and Dadomo, 2005; Mellors et al., 2007), uncertainties especially exist on the exact triggering mechanisms, magnitude thresholds and triggering distances (Manga et al, 2009). To contribute to this topic, we analyzed the relations between seismicity and mud volcano eruptions in Azerbaijan following two earthquakes with M_w 6.08 and 6.18, occurred in the Caspian Sea on November 25, 2000, south of Baku city (Fig. 1; Jackson et al., 2002). Previous studies on magma volcanoes suggested that large seismic events might promote eruptions due to static and dynamic stress/strain changes; these studies are based on the analysis of time coincidence between earthquakes and eruptions (Linde and Sacks, 1998; Hill et al., 2002; Marzocchi, 2002; Manga and Brodsky, 2006; Eggert and Walter, 2009; Watt et al., 2009), or on numerical models that investigated the volumetric expansion in the crust beneath volcanic chains (Walter and Amelung, 2007) or the dynamic pressure changes induced by seismic waves (transient effect) (Walter et al., 2009). Instead for mud eruptions, Manga et al. (2009) found no evidence of a correlation with earthquake-induced static stress changes at the mud volcanoes of the Niikappu group in Japan by calculating the volumetric expansion in the underlying crust. We thus analyzed the possible influence of both the static and dynamic strain changes induced by the two 2000 earthquakes in Azerbaijan on the behaviour of each single mud volcano. We are aware that a few authors for magma volcanoes also suggested the possible influence of the quasi-static stress change associated with slow viscous relaxation of the lower crust and upper mantle beneath the epicentre of a large earthquake (Freed and Lin, 2002; Marzocchi et al., 2002), but this is out of the scope of our research because we want to focus on pure dynamic and static stress change effects on mud volcanism.

3.2. Geologic and tectonic framework

The study area, corresponding to the Shemakha-Gobustan-Absheron regions, comprises the southeastern part of the Great Caucasus mega-anticlinorium and the conterminous plain located more to the south (Fig. 1) (Agabekov et. al., 1972). The area is characterized by the presence of several mud-volcanoes (Fig. 2), diapir folds and thrust faults, as well as of oil- and gas-bearing structural traps. The area was affected by intense subsidence in the Cretaceous-Tertiary period, which is reflected by the great thickness of the related deposits, especially of Palaeogene-Neogene age (Kadirov, 2000). Substantial sinking of the region comprising the Absheron peninsula, the North Absheron area and the eastern part of the Shemakha-Gobustan synclinorium occurred also in Neogene-Quaternary times

(Shikhalibeyli, 1972, 1996; Agabekov et. al., 1972). According to borehole and geophysical data, the depth of the Mesozoic top within the study area varies in the range of 1–10 km (Kadirov, 2000). The study area and the surrounding regions are characterized by mountain belts mostly trending WNW-ESE, bounded by several faults with the same orientation (Fig. 1). The ESE-trending Caucaus mountain belt is bounded along the southern side by the parallel NNE-dipping Greater Caucasus thrust, which is one of the main and recent faults of the region. Further south there is the SSW-dipping Lesser Caucasus thrust. Along the northeast side of the Caucasus belt, there is the North Caspian transpressional fault that shows important right-lateral strike-slip kinematics. On the other side of the Caspian Sea, exactly on the ideal prolongation of the North Caspian fault, there is the right-lateral strike-slip Ashkabad fault. These structures have been interpreted as originated by the ongoing Arabian-Eurasian collision that, north of the collision zone, is accommodated by shortening and lateral displacement of the lithosphere, the latter mainly along right-lateral strike-slip faults (Reilinger et al., 2006; Kadirov et al., 2012).

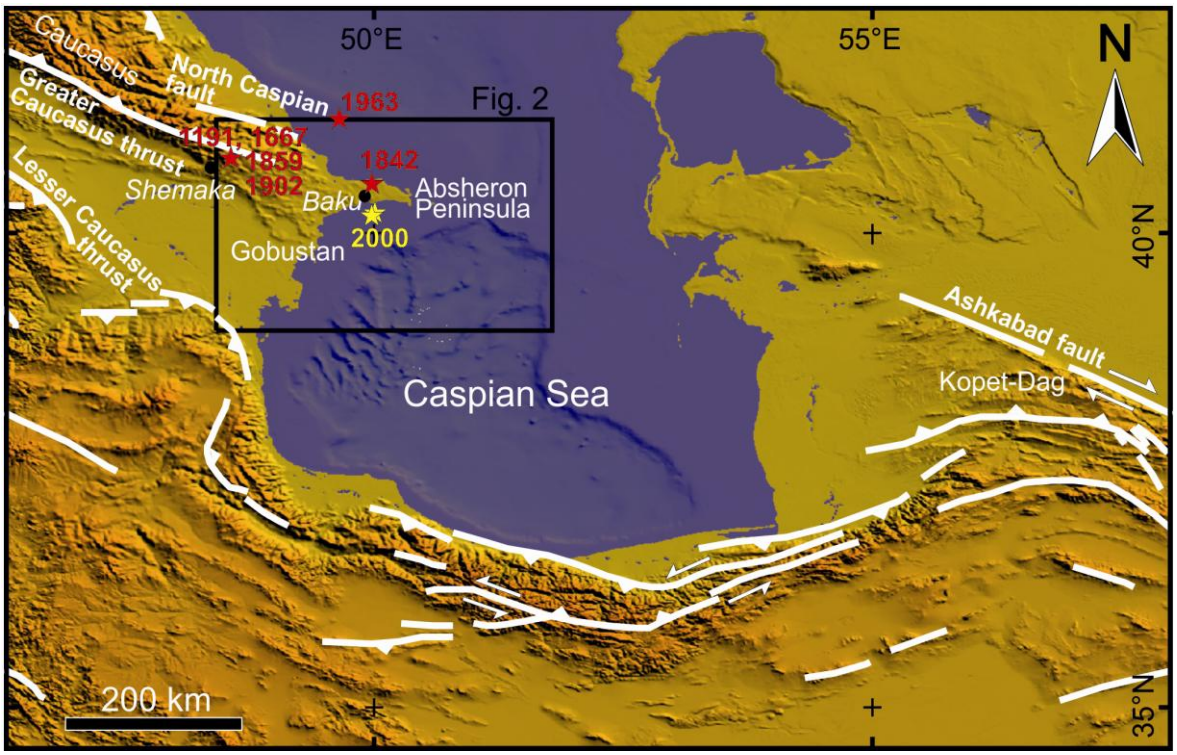

Figure 1. *Topography and simplified tectonics with the main Quaternary faults of Caucasus to Kopet-Dag region. The epicentres of the two studied 2000 earthquakes are marked by yellow stars. Red stars mark the other important earthquakes that affected Absheron Peninsula showing also their dates. Box shows the studied Shamakhi-Gobustan-Absheron area. (Tectonics modified after Jackson et al., 2002, and Babayev et al., 2010).*

3.3. Seismicity

The ongoing regional tectonic processes and lithosphere deformations produced earthquakes that have devastated the Caucasus region also during recent historic times (e.g. the 1902 Shemakha earthquake; Veber, 1904). The Absheron peninsula together with its offshore part (the Azerbaijan sector of the Caspian Sea) is located in the south-eastern extremity of the Greater Caucasus, where the orogenic active processes still occur. Earthquakes in the region migrate along the Alpine-Himalayan seismic belt (Ismail-Zadeh, 1996) and are associated with the fault zones located in the Absheron peninsula, in the Azerbaijan sector of the Caspian Sea and in the adjacent folding structures of the Greater Caucasus and Kopet-Dag (Figs. 1 and 2). Whereas the Gobustan zone can be considered even aseismic based on the available data, the Absheron peninsula is affected by low-magnitude but frequent earthquakes (Teleska et. al., 2012). However, due to their very shallow hypocentres, some of these earthquakes are capable of producing large damages with intensity of VI-VII. For example, the 1842 Mashtaga earthquake (Fig. 1) with M ~ 4,5 was characterized by intensity = VIII in the epicentral area, with ground motions limited to a relatively small area and a strong attenuation (Babayev, 2010; Babayev et. al., 2010). The larger potential threat to the Absheron peninsula comes from the earthquakes originating under the Caspian Sea. The Caspian Sea, in fact, is another seismically-active zone of Azerbaijan; the seismicity is mostly crustal (depths typically < 30 km), although events as deep as 80 km have been reported and may represent incipient subduction across the mid-Caspian (Jackson et al., 2002). The first information on the earthquakes in the study region can be found in old Arabic chronicles, hand-writings, notes of pilgrims, etc. Modern seismology here started with the 1902 Shemakha earthquake. The Shemakha town (located about 110 km west of Baku, Fig. 1) repeatedly suffered strong earthquakes in the past, like in 1191, 1667 (with a death toll of about 80,000 people) and 1859 according to Veber (1904). Besides, on February 13, 1902 a catastrophic event struck the region again, with an Intensity = X (Rossi-Forel scale) (Boghdanovitch, 1904). The earthquake resulted in complete destruction of buildings in the epicentral area, multiple rock falls and landslides, and activated several mud volcanoes. This earthquake also generated in Baku a moderate ground shaking and minor damages (e.g. cracks in some buildings). High-amplitude anomalous waves were observed in the Caspian Sea adjacent to Baku casting boats and yachts ashore (Levitski, 1902). These tsunami-like waves were likely to be generated by an underwater landslide or rocks sliding offshore, both induced by the ground shaking due to the Shemakha earthquake. The magnitude of the 1902 Shemakha earthquake was estimated = 6.9 ± 0.2 (Kondorskaya et al., 1982), although its

magnitude could be as high as 7.3 considering the duration of ground shaking of about 30–40 s and the length of the ruptured area of about 80 km (Levitski, 1902; Boghdanovitch, 1904). Finally, the November 25, 2000, earthquakes of M_w 6.18 and 6.08, which occurred in the Caspian Sea close to Baku city (Figs. 1 and 2), were characterized by focal depths of 40 and 33 km respectively (Jackson et al., 2002).

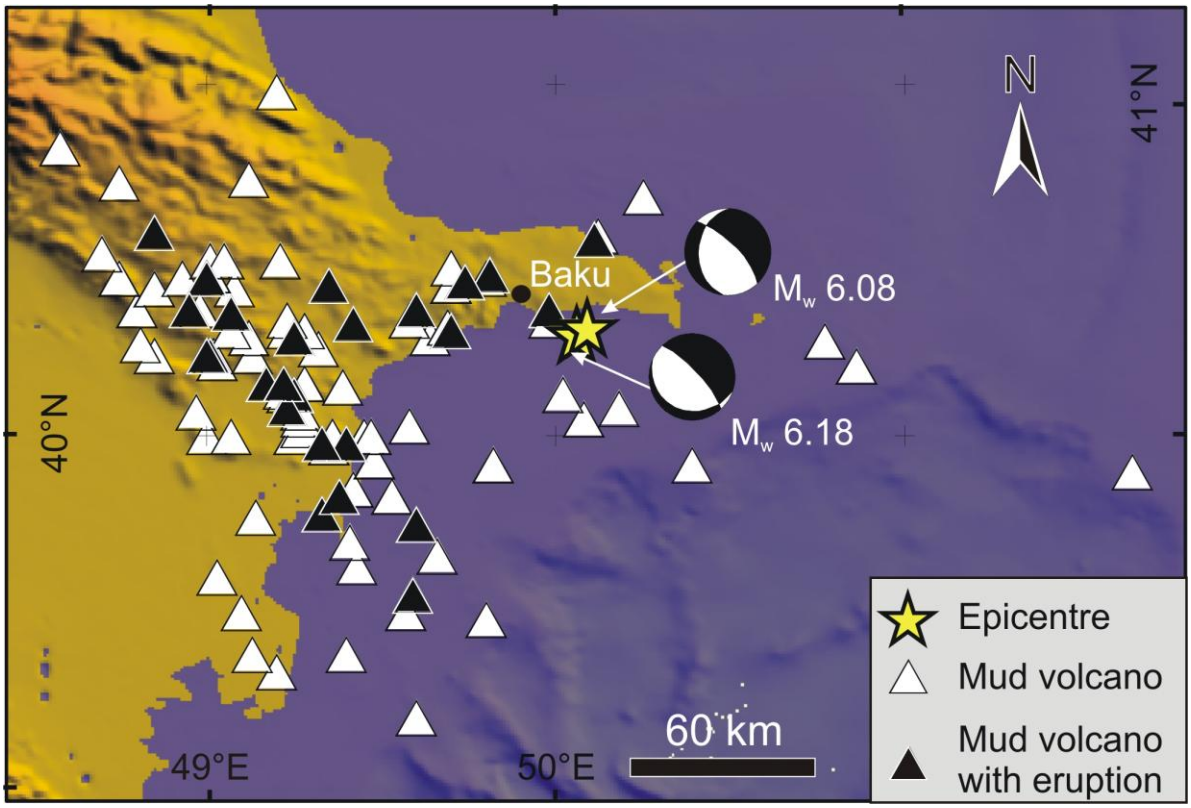

Figure 2. *Study area with distribution of mud volcanoes and location of the studied earthquakes of November 25, 2000.*

3.4. Eruptions following the November 25, 2000 earthquakes

After the two earthquakes of 2000, 33 eruptions occurred at 24 mud volcanoes within a maximum distance of 108 km from the epicentres (Fig. 3) (Aliyev et al., 2009). A first analysis of time series suggests a possible correlation between distance and time-delay, with a positive linear correlation (Fig. 3). A larger number of mud eruptions occurred at a distance greater than 50-60 km from the epicentres (Fig. 4A). The largest number of eruptions occurred within two years from the earthquakes, in particular the highest frequency is within six months (Fig. 4B). It is also possible to see that 6 eruptions occurred within 1.5 year from the earthquake at a distance < 40 km (Fig. 3). Eruptions within 2-3 years occurred at a distance between 40 and 110 km from the epicentres, on the contrary eruptions after 3 years

occurred only at a distance greater than 70 km. In particular, several eruptions occurred within 8 months from the shock, after this period the number of eruption for months is more scattered and discontinuous (Fig. 5). The average number of eruptions per year (3.2) in the overall Azerbaijan catalogue has remained fairly constant since 1950 AD; given the uncertainties, an average of 3.2 ± 1 eruptions per year seems reasonable (Mellors et al., 2007). By comparing the overall eruption rate in the studied area of the 50 years before the 2000 earthquakes (BER – before earthquakes) with the 5 years following these earthquakes (AER – after earthquakes), we can notice that 62 eruptions occurred during BER against 33 eruptions during AER, corresponding to an increase from 1.24 to 6.6 eruption per year (AER/BER = 5.32) (Fig. 6).

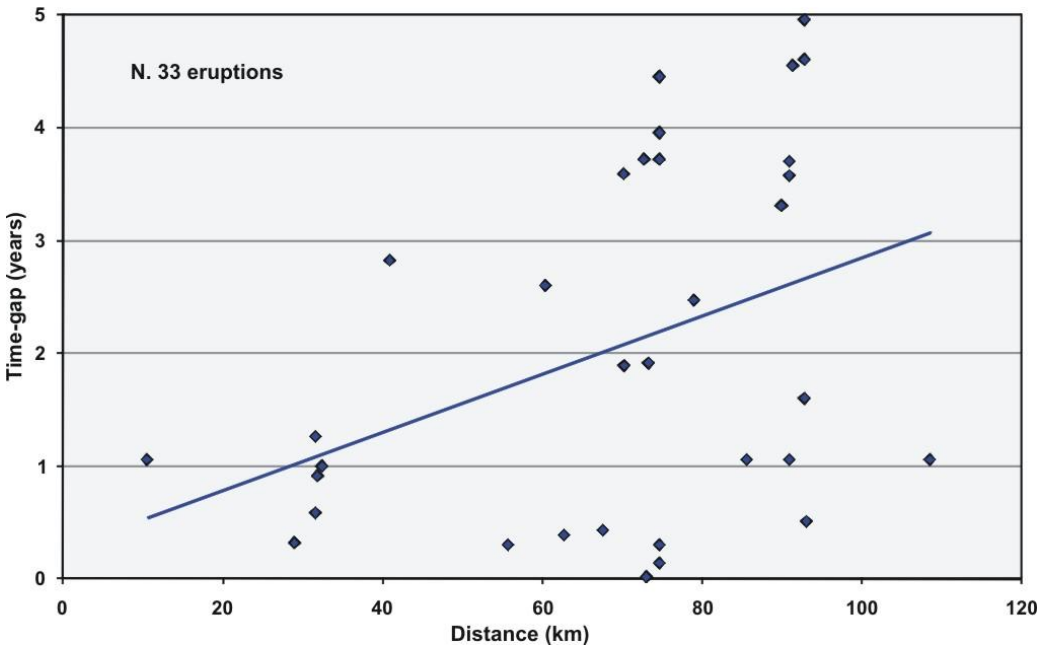

Figure 3. *Eruptions occurred in the five years following the studied earthquakes: time-gap versus averaged distance from the 2000 earthquake epicentres. The regression line is shown.*

3.5. Calculation of earthquake-induced strains

The energy delivered by an earthquake produces two different types of deformation: i) a permanent deformation and a corresponding change in the stress state of the crust, and ii) a transient deformation associated with the passage of seismic waves (Manga et al., 2009). Hereafter, we refer to these strains as static and dynamic strain, respectively. The strain amplitude depends on the distance from fault rupture zone, moment release, and mechanical properties of the involved rocks (Manga et al., 2009). In the following sections we will describe the methods and results of the calculation of both deformation types.

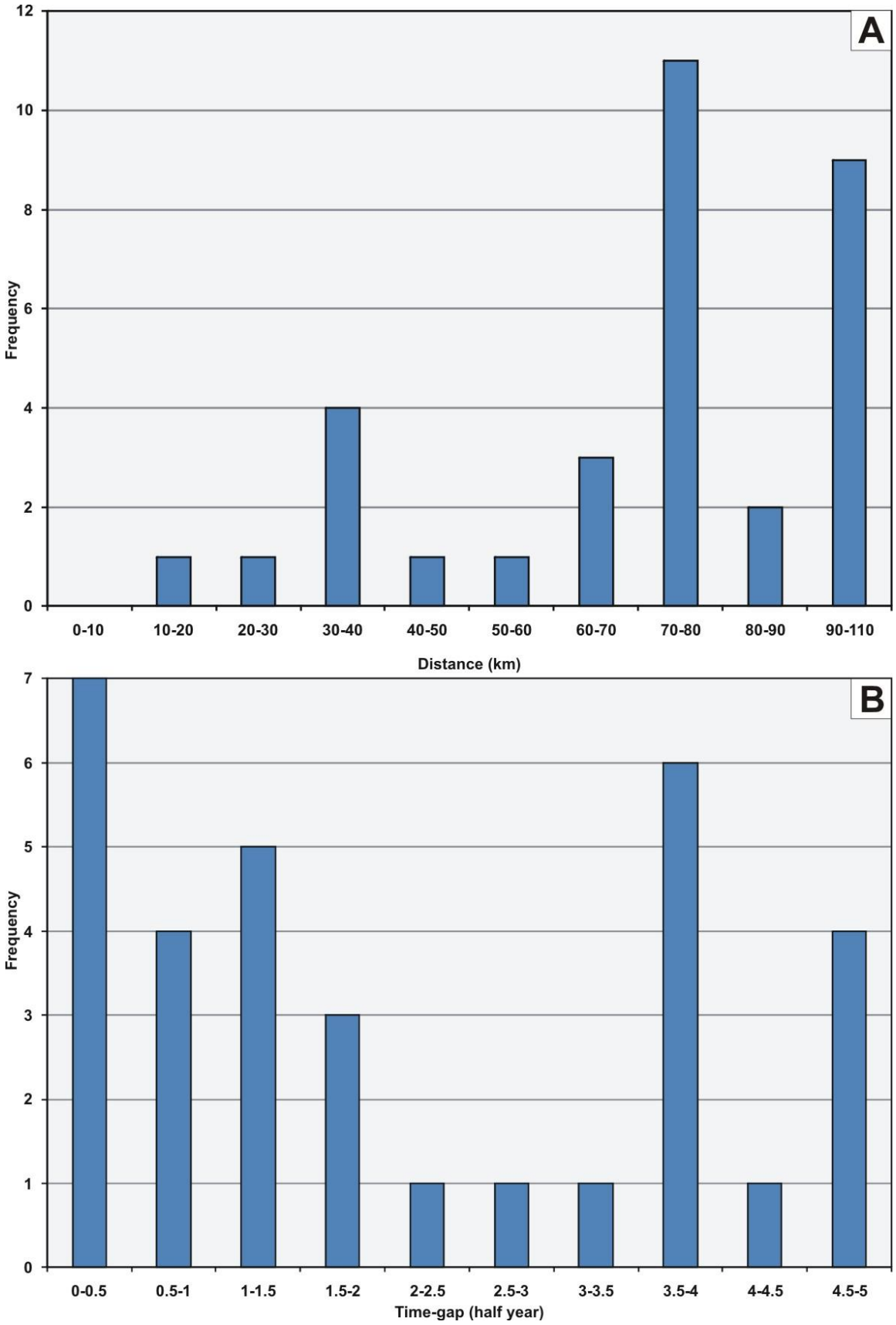

Figure 4. *Frequency of eruptions occurred in the five years following the studied earthquakes plotted versus (A) distance from the epicentres and (B) time-gap. The data have been classified in 10 classes.*

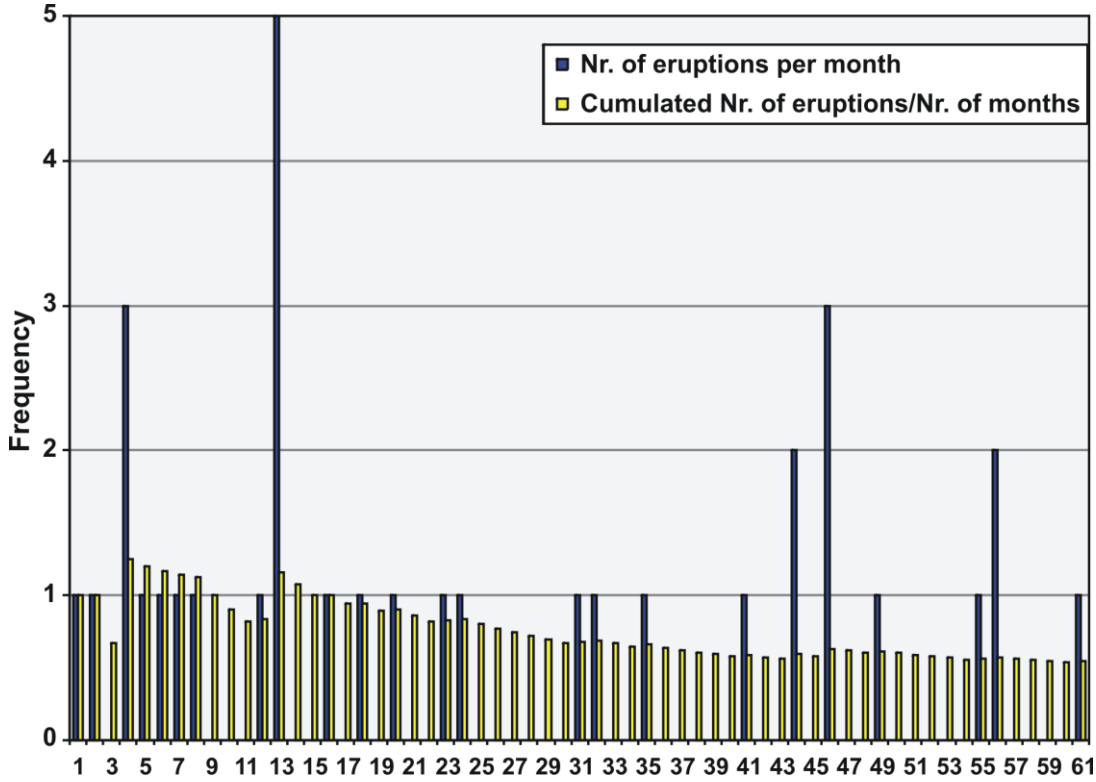

Figure 5. *Eruptions occurred in the five years following the studied earthquakes: it is reported the number of eruptions per month (blue) and the cumulative number per month/number of months (yellow).*

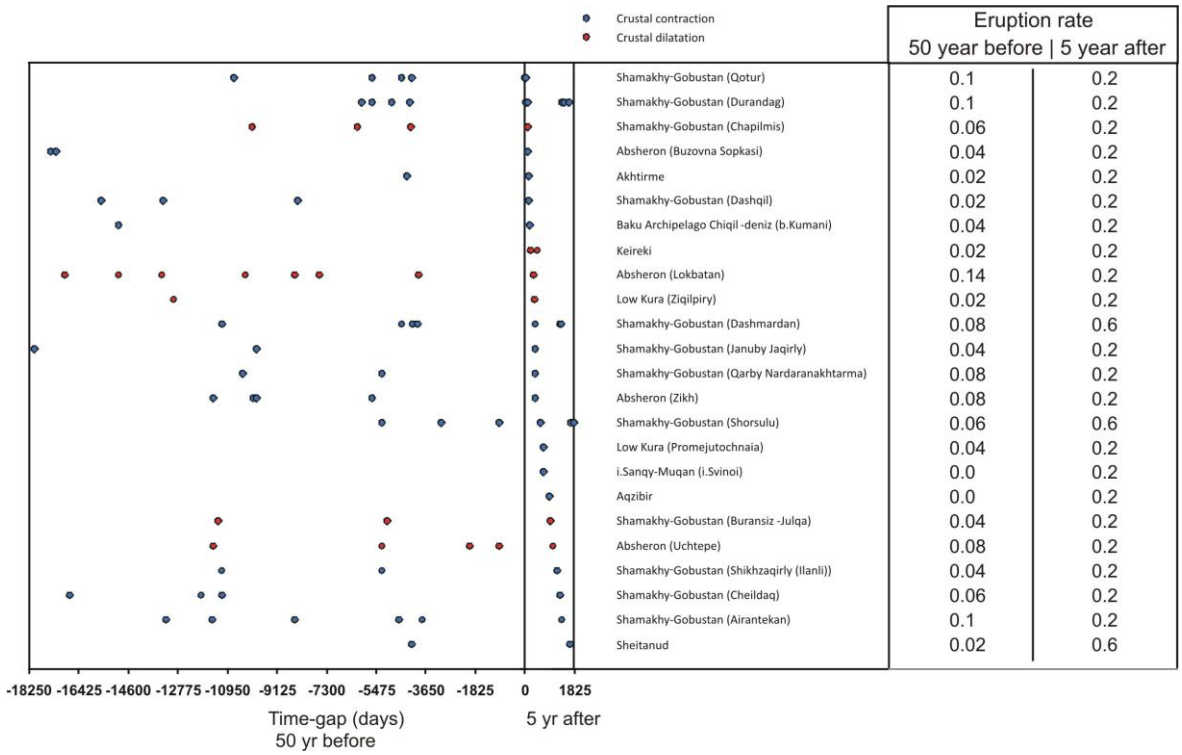

Figure 6. *List of volcanoes that suffered eruptions after the 2000 earthquakes; all the eruptions occurred in the 50 years before and in the 5 years after the earthquakes are shown, together with the values of the eruption rates of all volcanoes.*

3.5.1 Method for static strain

Crustal dilatation (volumetric expansion) is suggested as an important factor in promoting volcanic unrest (Walter and Amelung, 2007). We calculated the crustal dilatation induced by fault slip at two different depths below the sea level: 2 and 5 km (Fig. 7); these depths have been chosen based on the published data on the location of mud reservoirs (Feyzullayev, 2012). Using the Coulomb 3.3 software (Toda et al., 2011), we calculated the static strains for the volcanoes that erupted after the two 2000 earthquakes, up to a distance of about 100 km from the epicentres. We modelled the upper crust as an elastic isotropic half-space characterized by Young's modulus E = 80 GPa and Poisson's ratio $\nu = 0.25$, and the effective friction coefficient was assumed as $\mu' = 0.4$, based on King et al. (1994), Mithen (1982), Lin and Stein (2004) and Toda et al. (2005, 2011). Two different finite fault models (Tab. 1) were used to simulate the earthquake effects, providing the fault plane geometry associated to slip and rake angle values based on nodal planes and Quaternary fault geometries reported in Jackson et al. (2002). Dimension of such faults are based on empirical relations (Wells and Coppersmith, 1994; Toda et al., 2011). The focal mechanisms and depths were based on the solutions of Jackson et al. (2002) because these are the best available being based on the analysis of long-period teleseismic P and SH waveforms for events larger than M_w 5.4. The input stress fields of these tensor solutions are $\sigma_1 = 100$ bar, $\sigma_2 = 30$ bar, and $\sigma_3 = 0$ bar (King et al., 1994; Lin and Stein, 2004; Toda et al., 2005, 2011).

3.5.2 Method for dynamic strain

An earthquake generates also dynamic (transient) perturbations (Hill et al., 2002; Manga and Brodsky, 2006). Seismic waves travel at great distances without losing much of their energy (Hill et al., 2002) and dynamic stress change decreases more slowly than static stress change (Hill and Prejean, 2007). The passage of the seismic wave could encourage gas exsolution, ascent of gas bubbles and consequently magma rise (Manga and Brodsky, 2006). We estimated the peak transient strain applying the formula $\varepsilon = PGV / V_s$, where ε is strain amplitude and V_s is the shear wave velocity (Manga et al., 2009) assumed equal to 2500 m/s (Kanno et al., 2006) and PGV is the Peak Ground Velocity, although we are aware of some uncertainty of this method because it does not account for the earthquake focal mechanism or the effect of directivity and approximates rupture location by the hypocenter (Manga et al., 2009). The PGV values for the studied mud volcano region have been estimated using the relationship between moment magnitude of the events (M_w 6.18 and M_w 6.08) and the epicentral distance R (in km). The equation by Akker and Bommer (2010) was derived from

the data of Europe, Mediterranean and Middle East. Since our studied area has less recorded strong motion data, and there are many factors of uncertainty, it is better to adopt multiple equations, rather than one exact equation selection, via a logic tree method (Boore and Atkinson, 2008; Chiou and Youngs, 2008). The selected equation for PGV is well suited for our study area with soft to hard bedrocks, typical for the site conditions of the Shamakhi-Gobustan-Absheron region of Azerbaijan (Babayev et. al., 2010). Using the PGV values at bedrock as the seismic input motion parameters, all dynamic parameters of both subsurface soil and the surface PGA can be determined (Babayev et. al., 2010). Site effects, detailed surface geology, the amplification factor and the seismic response of subsurface soils have been analyzed to illustrate the influence of the site-effects terms and determine the surface motion velocity for the mud volcanoes in the study area.

3.5.3 Results of static and dynamic strain

Numerical modelling of static strain shows that the area affected by crustal dilation is SSW respect to the earthquake epicentres (Fig. 7). The value of static strain is $0.1*10^{-8}$ near the epicentres and drops to very small values at a distance of about 60 km and to 0 at about 90 km (Fig. 8A). The crustal dilatation affected the substratum of volcanoes where 7 out of 33 eruptions occurred, at a maximum distance of about 60 km. The M 6.08 event does not show variation of dilation amount with depth (Fig. 7A-B), whereas the M 6.18 earthquake produced a slight increase of dilation with depth (Fig. 7C-D). As a consequence also the cumulated effect shows an increase with depth (Fig. 7E-F). The area of crustal contraction affects the NW part of the region respect to epicentre location and the magnitude is larger than the crustal dilatation (Fig. 8A). Regarding the time-delay from earthquake occurrence, it is possible to observe that within the rock volume affected by crustal dilatation, eruptions occurred up to 3 years after the seismic events (Fig. 8B). Regarding the dynamic strain, our computation shows that all the unrest studied volcanoes are affected by this earthquake-induced transient strain (Fig. 9). In particular, the magnitude of dynamic effects decreases with distance from the epicenters (Fig. 9A). It ranges from $1.088*10^{-4}$ to $9.248*10^{-6}$ and approaches 0 at 110-120 km from the epicentres. The time-gap increases with a decrease in earthquake-induced dynamic strains (Fig. 9B).

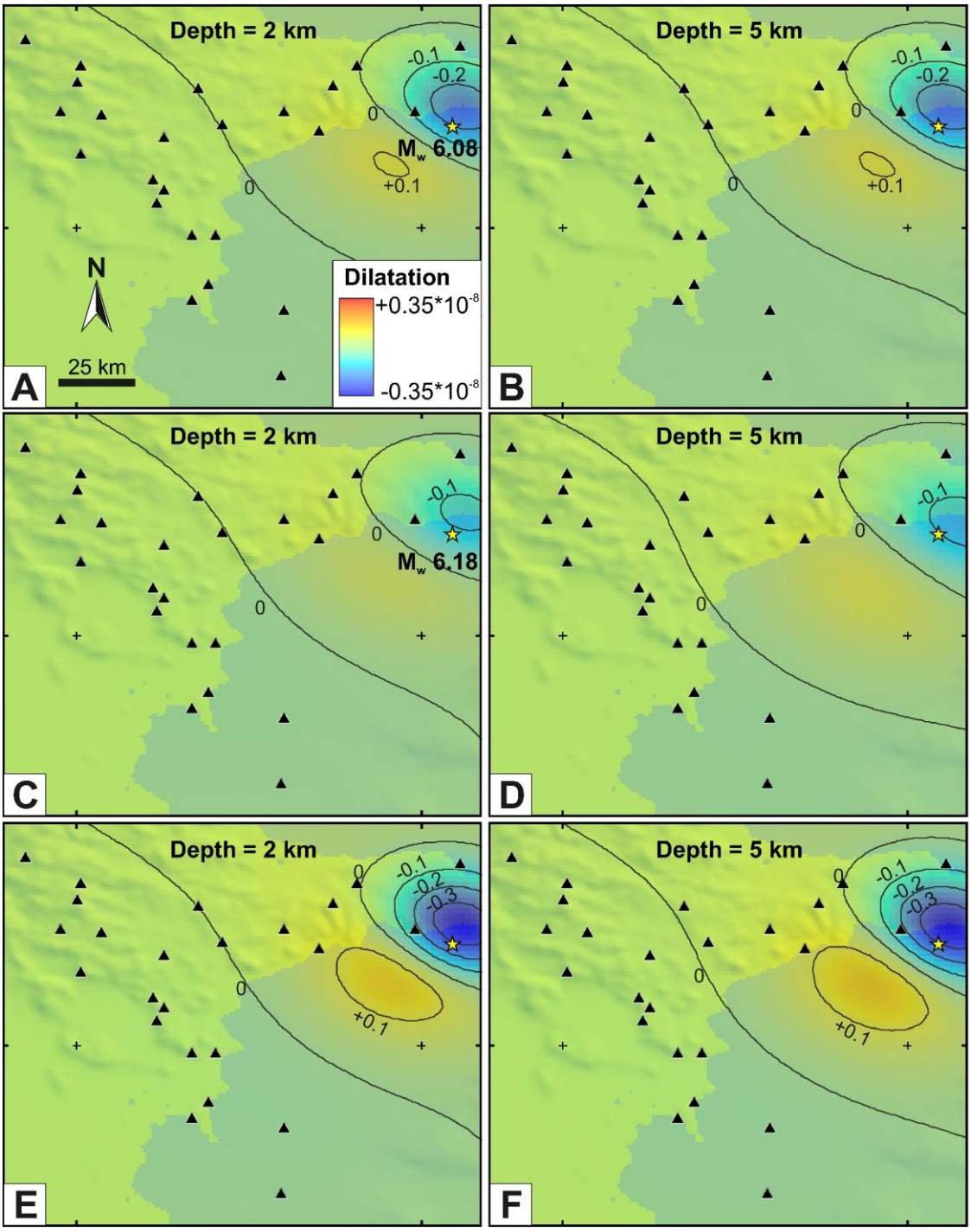

Figure 7. *Results of numerical modelling of static strains. It is reported the induced crustal dilatation at two different depths for the two earthquakes (A-B-C-D) and the cumulated effects (E-F). Red colours represent crustal dilatation, blue colours represent contraction.*

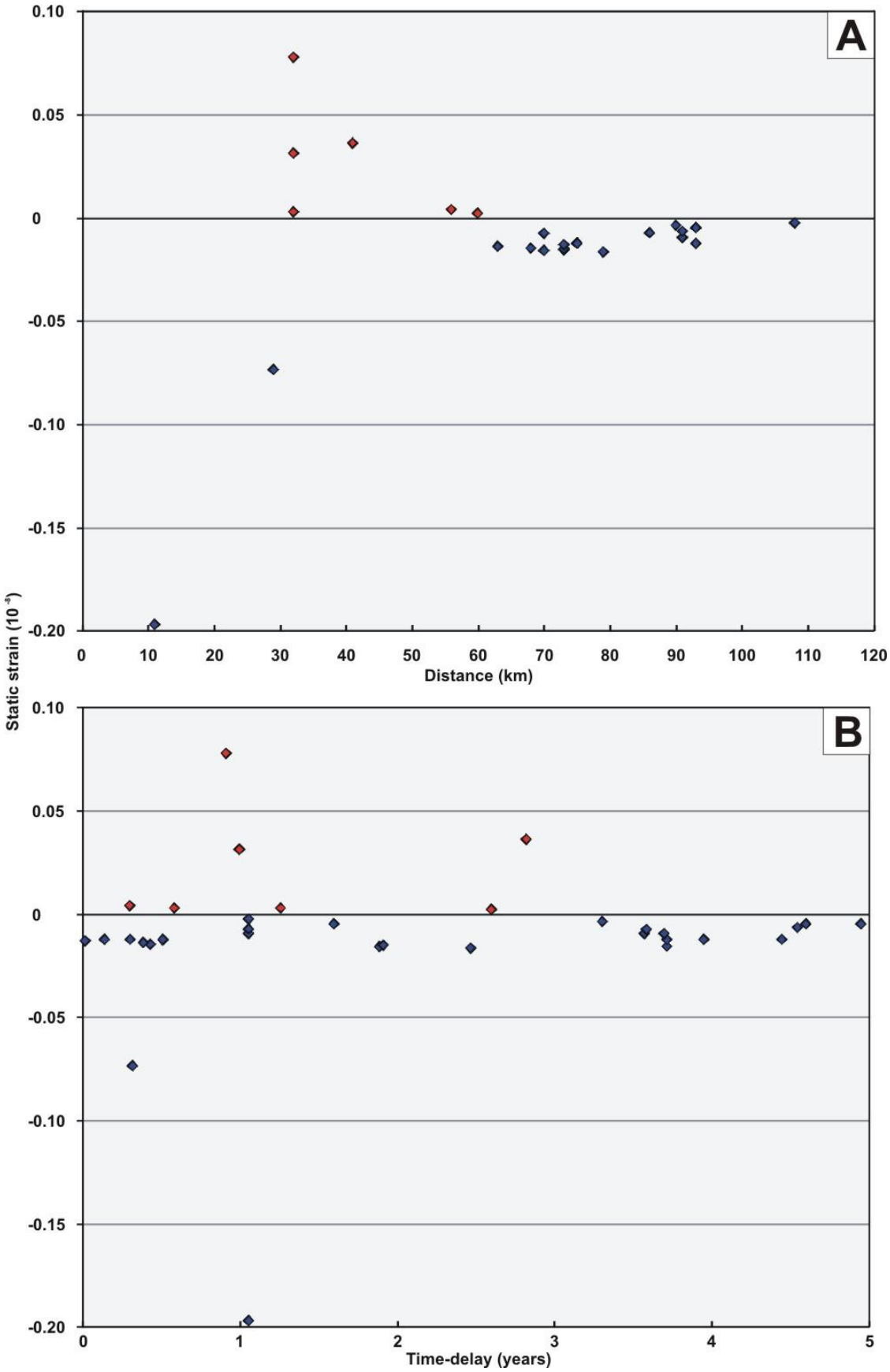

Figure 8. *Cumulated static strain versus the distance from the epicentres (A) and the time-gap (B). Red colour represent crustal dilatation, blue colour represent contraction.*

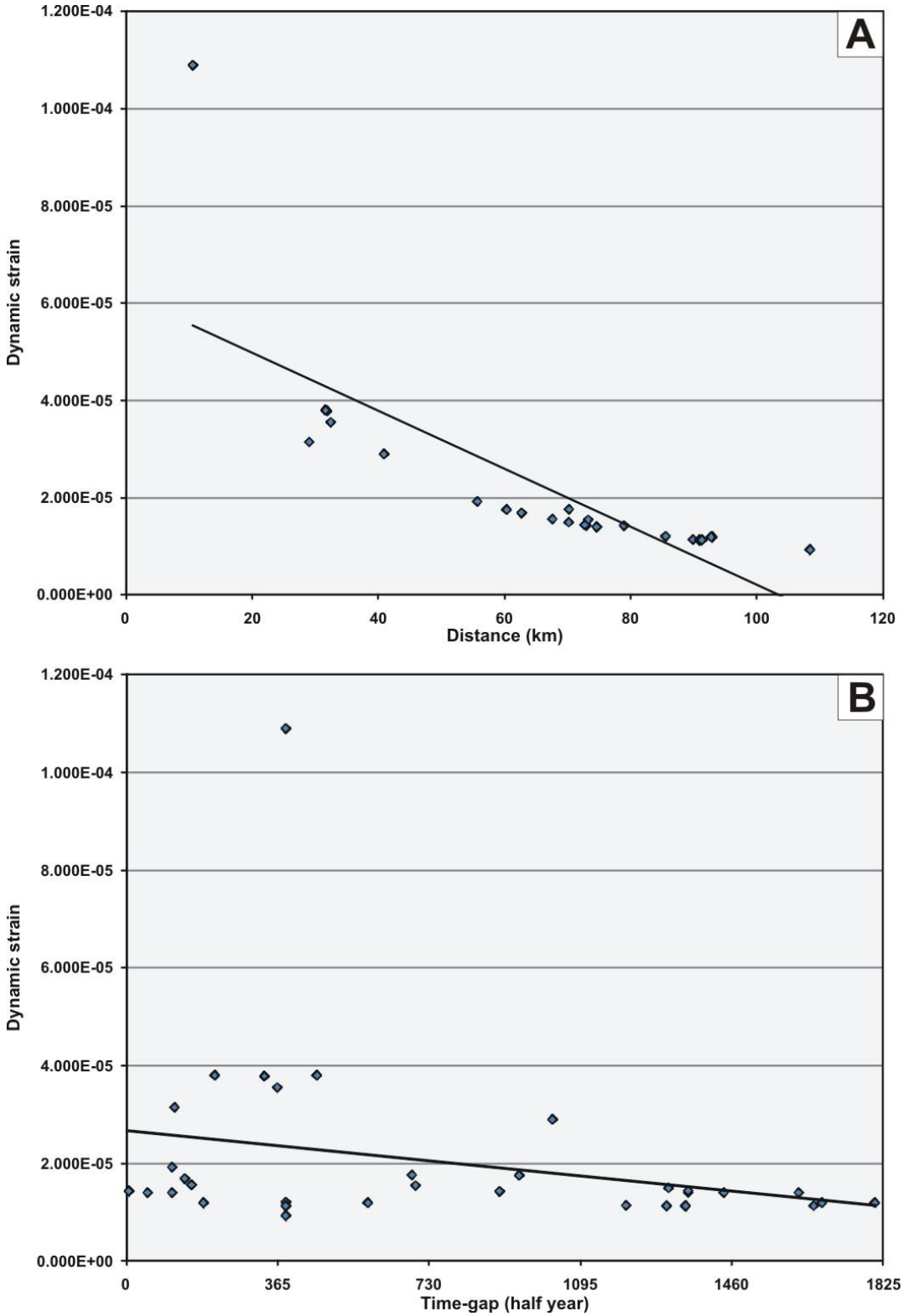

Figure 9. *Cumulated dynamic strain versus the distance from the epicentres (A) and the time-gap (B). Red colour represent crustal dilatation, blue colour represent contraction. The regression lines are shown.*

3.6. Discussion

3.6.1 Earthquake triggering

It is reported in literature that earthquake-induced stress/strain could enhance the normal activity of geysers (Gomberg and Davis, 1996; Husen et al., 2004), methane emissions (Beresnev and Johnson, 1994; Hieke, 2004; Mau et al., 2007), magma eruptions (Linde and Sacks, 1998; Manga and Brodsky, 2006; Lemarchand and Grasso, 2007; Walter and Amelung, 2007; Eggert and Walter, 2009; Bonali et al., 2013) and mud volcano eruptions (Chigira and Tanaka, 1997; Guliev and Feizullayev, 1997; Delisle et al., 2002; Nakamukae et al., 2004; Mellors et al., 2007; Manga et al., 2009; Mazzini et al., 2009), perturbing the plumbing systems also at large distances. The response of magma volcanoes to earthquakes happens on timescales of days (Linde and Sacks, 1998) to decades (Marzocchi, 2002). Many geysers exhibit strong eruption periodicity that is very sensitive to small changes in subsurface conditions (Manga et al., 2009). Geysers respond to events with static strains less than 10^{-7} and dynamic strains less than 10^{-6} (e.g. Hutchinson, 1985; Silver and Valette-Silver, 1992). While geysers in Yellowstone are not sensitive to strains less than 10^{-8}–10^{-9} (Rojstaczer et al., 2003), a lower limit has not been established for other systems (Manga et al., 2009). Mud volcanoes are commonly thought to be sourced from deep, highly overpressured shales (e.g., diapirs), liquefaction of clays, or shallow overpressured gas, hydrate, or water-rich sequences (Brown, 1990; Galli, 2000; Kopf, 2002). A trigger effect is the final step that precedes the manifestation, or the initiation of an eruption (Mazzini et al., 2009). Examples of mud volcano activity associated with seismic events have been reported for: Iran (Kopf, 2002), Pakistan (Delisle et al., 2002), Romania (Baciu and Etiope, 2005), Italy (Martinelli and Dadomo, 2005), Turkmenistan (Guliyev and Feizullayev, 1997), Japan (Chigira and Tanaka, 1997; Nakamukae et al., 2004) and Indonesia (Tingay et al., 2008; Mazzini et al., 2009). For the well studied Lusi case in Indonesia, Tingay et al. (2008) suggested that fault reactivation increased its permeability and allowed the migration of deep overpressured fluids to the surface. A research applied to the entire pre-2007 catalogue of earthquakes ($M > 5$) and eruptions (within 100 km) of Azerbaijan, has found that: i) the number of same-day earthquake/eruption pairs is significantly high, and ii) a large number of eruptions occurred in the year following the earthquakes (Mellors et al., 2007). Based on our results, in the 5 years following the two 2000 Azerbaijan earthquakes, 33 eruptions occurred at 24 volcanoes, at a maximum distance of about 108 km from these seismic events. The first eruption occurred after 6 days and 19 eruptions occurred within 2 years (Figs. 3 and 4). The average eruption rate during the 5 years following these earthquakes (6.6) is twice than the

overall averaged values for Azerbaijan (3.2 ± 1 per year; Mellors et al., 2007) and more than five times larger than the average eruption rate of the 50 years before the 2000 earthquakes (1.24) for the area studied in the present work. We believe that this demonstrates that the 2000 earthquakes may have contributed to increase the unrests at the studied mud volcanoes.

3.6.2 Static versus dynamic stress change

Earthquakes produce static and dynamic stress/strain changes and both have been cited as causes for aftershocks and magma volcanic triggering following large earthquakes (Harris,1998; Steacy et al., 2005). Static stress/strain changes, which refer to permanent changes in the absolute stress level of the crust after an earthquake, are strongest near the earthquake foci and decrease rapidly with distance. Dynamic stress changes tend to be larger in amplitude but transitory as they occur during passage of seismic waves. Dynamic stress changes also decrease more slowly with distance making them a more effective triggering agent at long distances (Mellors et al., 2007). It is reported in the literature that the near-field triggering is defined to be primarily regions within ~1 main shock fault length of the earthquake rupture zone, whereas far-field triggering extends much farther, in some observed cases more than ~5–10 fault lengths away (i.e., Hill et al., 1993; Prejean et al., 2004). Manga et al. (2009) finally suggested that an eruption can be triggered by dynamic stress changes only up to a distance of about 7 fault lengths. In our case, based on empirical relations (Wells and Coppersmith, 1994; Toda et al., 2011) for fault length, the near-field is limited to 17 km (where only one eruption occurred) and the far field extends up to 85-170 km where 32 eruptions occurred. It has been suggested that the near-field triggering results primarily from a combination of static and dynamic stress/strain changes, which at close distances are difficult to definitively separate, whereas the far-field triggering results from dynamic stress/strain changes (Steacy et al., 2005). In the studied area, our results of numerical modelling of static strain show that crustal dilatation interests a maximum distance of about 60 km within which only 7 eruptions occurred and thus can be ascribed to earthquake-induced crustal dilatation. These eruptions took place up to three years after the earthquakes. Our data also indicate that one mud eruption occurred in the far-field under crustal contraction, whereas the remaining 25 eruptions occurred under no static strain changes. Thus, 26 mud eruptions can be interpret to have been induced by earthquake-induced dynamic strain, and the other 7 eruptions might have been favoured by both static and dynamic strain.

3.6.3. Possible mechanisms of mud volcano unrest

Exactly how seismic waves from large earthquakes provoke volcanic eruptions is not clear, although a plethora of mechanisms have been suggested (e.g., Hill et al., 1993, 2002; Gomberg and Davis, 1996; Linde and Sacks, 1998; Roeloffs et al., 2003; Power et al., 2001; Feuillet et al., 2004; Moran et al., 2004; Prejean et al., 2004). These theories include large-scale seismic liquefaction, excitation of bubbles and resulting fluid overpressure, hydraulic connection between the source and the surface, hydraulic surge, changes in groundwater levels, rupturing blockages in confined aquifers, a sinking crystal plume, dyke openings and a relaxing magma body (Cayol et al., 2000; Brodsky et al., 2003; Manga and Brodsky, 2006; Mellors et al., 2007; Manga et al., 2009). Earthquake-induced long-term stress changes may also be caused by viscoelastic or pore pressure effects (Freed, 2005). At mud volcanoes, liquefaction can act to promote eruption in two ways: by increasing pore fluid pressures and by fluidizing the mud prior to eruption (Manga et al., 2009). Interestingly, liquefaction has also been observed minutes (Holzer et al., 2004) to one day (Ishihara, 1984) after earthquakes. Wang (2007) proposed that long delays arise from the creation of a hydraulic connection to pressurized aquifers. Manga et al. (2009) don't favour mechanisms that directly involve nucleating bubbles or growing bubbles because previous theoretical analyses have shown that these processes are physically implausible or require very special conditions that are not present in mud volcanoes, such as high supersaturation. If we consider the geological-structural characteristics of the studied area, we highlight the presence of several faults striking ESE and folds with hinge lines trending ESE. Several mud volcanoes are located along these structures and we think that this strong regional structural anisotropy may have acted to enhance the seismic wave propagation effects. Consistent with this idea, Miller et al. (2004) suggested that faults and fold anticlines are easily perturbed by earthquakes as they represent weak regions for the seismic wave's propagation (Mazzini et al., 2009). Earthquakes could initiate local fluid movements that cause propagation of fractures to the surface manifesting with a time delay from the main earthquake (Miller et al., 2004; Mazzini et al., 2009). The geology of the study area is also characterised by the presence of thick sedimentary successions of Palaeogene to Neogene age, following the long-lasting subsidence. This situation is consistent with the possible presence of under-consolidated deposits rich in water and gas, which may easily react under seismic solicitation with differential compaction, fracturing, and sand and mud fluidification. Under-consolidated deposits in fact, typically occur in the sedimentary sequences below mud volcanoes (Kopf, 2002). This scenario is similar to the one proposed for the Lusi case where dynamically

induced stress changes generated by the Yogyakarta earthquake (Brodsky et al., 2003) caused sediment consolidation, overpressure development and associated redistribution of fluid pressures at the eruption site (Manga, 2007). The delay up to 3 years of unrest at the mud volcanoes affected by earthquake-induced static stress change is consistent with the long-lasting effects of large seismic events suggested by various authors. For example, Anderson and Johnson (1999) showed significant correlations between aftershock occurrence and static stress increase during 1.4-2.8 years after the mainshock, Hardebeck et al. (1998) suggested a relation up to 5 years, and Stein (1999, and written comm., 2012) indicated evidence that static stress change is capable of inducing rock failure up to 5 years after a large earthquake. Similarly, we suggest there are no reasons why the static stress change on the rocks surrounding a mud volcano plumbing system should not endure for the same time amount. Regarding the delay between the 2000 earthquakes and the unrest at the volcanoes affected by the dynamic stress change, which is a transient effect, we believe that it may be explained based on the complexity of the involved parameters and the different response due to local site conditions. The dynamic stress change, in fact, might have promoted compaction in the typical underconsolidated sedimentary deposits of the area, as already suggested above. This in turn promoted, immediately after the earthquakes or within a short time delay, an increase in fluid pressures below the volcano and mud fluidification that, in the case of reaching the critical value, promoted the eruptions occurred shortly after the 2000 earthquakes. But for those eruptions occurred months or years after the 2000 earthquakes, we believe that this time delay was necessary to accumulate further gas in order to reach the critical overpressure value respect to the surrounding host rock and consequent wall-rock fracturing. We retain that the upwards-propagation of a fracture network is a necessary process in order to allow fluid migration to the surface, similarly to igneous stoping (Barber et al., 1986; Morley et al., 1998; Kopf and Behrmann, 2000; Morley, 2003). Once the deep mud reaches an overpressure that must exceed the horizontal compressive stress perpendicular to the fracture plane plus the tensile strength of the surrounding rocks, failure of the host rock begins and mud can intrude along the fractures. The stoping process slowly propagates towards the surface with the majority of the fracture network being produced by hydrofractures (Jolly and Lonergan, 2002; Planke et al., 2003). This mechanic model is also consistent with recent findings at eroded mud volcanoes that highlight a complex network of fractures used as ascending mud paths (Roberts et al., 2010). The strength of the surrounding rock (stiffness) depends upon the local characteristics of the deposits and thus can vary from one volcano substratum to another one, whereas the depth of the "mud chamber" together with the density of the overburden

rocks dictate the contribution of the lithostatic stress amount. The different time delay can thus be ascribed, for example, to diverse: i) accumulation of gas previous to the 2000 seismic events, ii) degree of original fracturing of the host rock surrounding the mud plumbing system, iii) stiffness of the host rock, iv) depth of the gas reservoir, v) density of the overburden succession, or to a combination of these factors. We think that these conclusions are also consistent with the data showing that the delay increases with the decrease in earthquake-induced dynamic strains (Fig. 9B). In fact, the lower the dynamic strain and the lower the initial earthquake-induced increase of pressure in the system, requiring longer times to recharge until reaching the critical overpressure value.

3.7. Concluding remarks

- After the two earthquakes of 2000, 33 eruptions occurred at 24 mud volcanoes within a maximum distance of 108 km from the epicentres;
- the average eruption rate during the 5 years following these earthquakes (6.6) is twice than the overall averaged values for Azerbaijan (3.2 ± 1 per year) and more than five times larger than the average eruption rate of the 50 years before the 2000 earthquakes (1.24) for this area;
- the largest number of eruptions occurred within two years from the earthquakes, in particular the highest frequency has been within six months;
- crustal dilatation affected the substrate of only 7 erupting volcanoes at a maximum distance of about 60 km; these eruptions occurred up to three years after the earthquakes;
- these 7 eruptions might have been triggered with the contribution of static strain, whereas dynamic strain have involved all the studied eruptions;
- since the eruption rate has been maintained much higher in the five years following the 2000 earthquakes, it is possible to suggest that earthquake-induced static and dynamic strains might predispose the plumbing system to unrest, but eruption occurs even years after the seismic event with a delay dependant from the various local conditions that characterise the substratum.

Date	25/11/2000	25/11/2000
M_w	6.18	6.08
Lat (dd)	40.29	40.31
Lon (dd)	50.06	50.09
Focal depth (km)	40	33
Fault length (km)	16.14	13.89
Fault strike (°)	317	313
Fault dip (°)	76	70
Rake angle (°)	-80	-115
Fault top (km)	34.88	28.55
Fault bottom (km)	45.12	37.45
σ_1 (trend°/plunge°)	240/58	189/57
σ_2 (trend°/plunge°)	135/10	322/24
σ_3 (trend°/plunge°)	39/30	62/22

Table 1. *Characteristics of the two studied earthquakes and related finite fault models (based on Jackson et al., 2002).*

4. Sensitivity analysis of earthquake-induced static stress changes on a volcanic arc: the 2010 M_w 8.8 Chile earthquake

The content of this chapter has been submitted to Terra Nova as "Bonali, F.L.[1], Tibaldi, A.[1], Corazzato, C.[1], Tormey, D.R.[2]. Sensitivity analysis of earthquake-induced static stress changes on a volcanic arc: the 2010 Mw 8.8 Chile earthquake".

[1]*Department of Earth and Environmental Sciences, University of Milan-Bicocca, Milan, Italy*
[2]*Cardno ENTRIX Inc., Los Angeles, CA, USA*

Abstract

We studied how the 2010 Chile earthquake could have induced stress changes along the Southern Volcanic Zone as possible positive feedbacks in promoting new volcanic eruptions. The test area is characterized by the presence of 24 historic/Holocene volcanoes, near the fault zone. The fault-slip-induced static normal stress changes have been resolved on the reconstructed magma pathway of each volcano, testing six different finite fault models. The calculation on each magma pathway indicates different patterns of stress change due to the heterogeneity of magma pathway geometry and orientation. In particular, N-S and NE-SW striking magma pathways suffered a greater decompression (unclamping) in comparison with those striking NW-SE and E-W. Based on similitude with seismic effects, earthquake-induced magma pathway unclamping might contribute to promote new eruptions up to 5 years after the earthquake and up to 450 km from the epicentre.

4.1. Introduction

The analysis of volcanic eruption time-series shows a good coincidence between large earthquakes and subsequent eruptions up to large distances from the earthquake epicentre (Linde and Sacks, 1998; Manga and Brodsky, 2006; Marzocchi, 2002; Marzocchi et al., 2002; Bebbington and Marzocchi, 2011; Watt et al., 2009), but this is most evident in the near-field (0-250 km) and within a few days after the earthquake (Linde and Sacks, 1998; Manga and Brodsky, 2006; Eggert and Walter, 2009). It is commonly suggested that the delay between the earthquake occurrence and the following volcanic events can be from seconds to years due to the complexity of volcanic systems (Linde and Sacks, 1998; Nostro et al., 1998; McLeod and Tait, 1999; Walter, 2007; Walter and Amelung, 2007; Eggert and

Walter, 2009) although the mechanisms of triggering are not well constrained yet. Some authors summarized the earthquake-induced triggering phenomena in three main categories: i) static stress changes, ii) quasi-static stress changes and iii) dynamic stresses induced by the seismic waves (Hill et al., 2002; Marzocchi et al., 2002; Manga and Brodsky, 2006; Walter et al., 2009). I focused this study on the earthquake-induced static perturbations on the fault's hanging wall block, capable of promoting aftershocks (Lin and Stein, 2004; Motagh et al., 2010; Asano et al., 2001; Toda et al., 2011a,b), secondary faulting (Lin and Stein, 2004; Toda et al., 2011) and volcanic eruptions (Barrientos S.E., 1994; Walter and Amelung, 2007; Bonali et al., 2013a,b). In particular, this work is the natural follow-up of a previous paper by Bonali et al. (2013a,b) that preliminary investigated the effects of the four major earthquakes occurred in Chile since 1906 AD. In the present work I propose a new and more detailed analysis focusing on the stress changes induced by the 27 February 2010 M_w 8.8 earthquake that occurred along the Chile subduction zone with a hypocentral depth of 35 km (Fig. 1). I resolved the earthquake-induced static stress change on each volcano magma pathway, instead of only calculating a general volumetric expansion in the crust beneath the volcanic chain as done by all previous authors. Moreover, for the first time it has been carried out a sensitivity analysis to study how differently oriented magma pathways react to the same seismic event. Results contribute to better define the role of earthquake-induced static effects in promoting new volcanic eruptions, and suggest that at the same distance from the epicentre, the magnitude of the static change is strongly controlled by the orientation of the magma pathway. Our new results better constrain the cause-and-effect relationships between this earthquake and the following volcanic activity in a time-window of 3 years.

4.2. Geological framework

The study area is the Southern Volcanic Zone (SVZ, 33°S-46°S) of the Chilean Andes, which has over 60 volcanoes considered to have been active during the Holocene (Siebert et al., 2010). Its tectonic setting is characterized by slightly dextral-oblique convergence between the Nazca and South American plate margins that has prevailed for the last 20 Ma (Fig. 1) (Pardo-Casas and Molnar, 1987; Somoza, 1998; Angermann et al., 1999; Cembrano and Lara, 2009). The plate boundary at these latitudes is characterized by a partitioning of deformation with dominant large thrust earthquakes in the subduction zone and intra-arc transcurrent faulting events (Barrientos and Ward, 1990; Cisternas et al., 2005; Watt et al., 2009). The SVZ shows significant variations in crustal thickness and tectonic style (Cembrano and Lara, 2009, and references therein; Fig. 1).

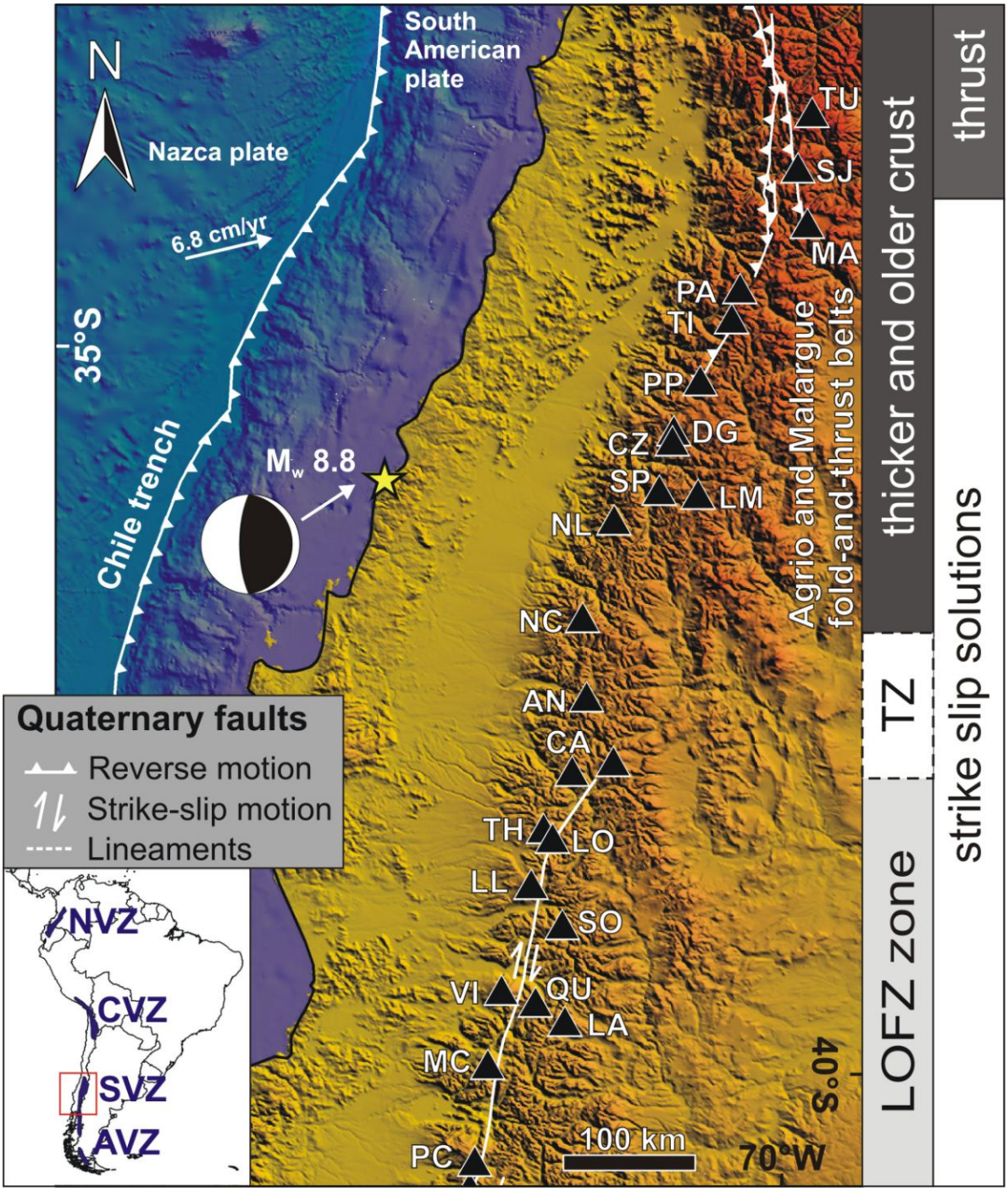

Figure 1. *Active volcanoes (Holocene) belonging to the Southern Volcanic Zone near the 2010 earthquake fault zone. The white arrow indicates the approximate convergence direction of the plates and estimated velocity. Main intra–arc faults with reverse motions in the north and right- lateral strike-slip motions in the south (redrawn after Cembrano and Lara, 2009) are reported; LOFZ = Liquiñe–Ofqui Fault Zone, TZ = Transition Zone. NVZ, CVZ, SVZ and AVZ correspond to Northern, Central, Southern and Austral Volcanic Zone. Volcanoes are reported in Table 1.*

The transpressional Liquiñe-Ofqui Fault Zone (LOFZ) is one of the controlling structures for the volcanic activity at the volcanic front between 37°S and 47°S (Lavenu and Cembrano, 1999; Rosenau, 2004); the LOFZ appears to allow more rapid magma ascent through the crust and lesser occurrence of assimilation or magma mixing compared to the more contractional setting further north in the SVZ (Cembrano and Lara, 2009; López-Escobar et al., 1995). Further north, the LOFZ merges into the Agrio and the Malargue fold-and-thrust belts at approximately 37°S (Folguera et al., 2006). The transition from the LOFZ to the thrust zone corresponds also to a thickening and ageing of the continental crust, longer crustal magma residence times, and greater differentiation, crustal assimilation and magma mixing (Tormey et al., 1991). Eruptions following the 2010 Chile earthquake occurred along the LOFZ (Puyehue-Cordón Caulle), the transition zone (Copahue) and the fold and thrust belt (Planchón-Peteroa).

4.3. Modelling strategy

I calculated the static stress changes for each of the 24 Holocene volcanoes of the SVZ proximal to the fault zone using the Coulomb 3.3 software (Toda et al., 2011c), based on Okada's (1992) formulae. Such formulae allow to calculate the static normal stress change resolved on a receiver surface, independently from the rake angle of the receiver structure and from the friction coefficient used in the model. I modelled the upper crust as an elastic halfspace with uniform isotropic elastic properties characterized by a Young's modulus $E = 80$ GPa and Poisson's ratio $\nu = 0.25$, and the effective friction coefficient was assumed as $\mu' = 0.4$, based on King et al. (1994), Mithen (1982), Lin and Stein (2004) and Toda et al. (2005, 2011c). I used six different finite fault models to simulate the earthquake-induced effects on the volcanic arc. They are based on tsunami, teleseismic, GPS and InSAR data and are characterized by defined fault plane geometry and variable slip rate (Tab. 2). The input stress field is based on the following tensor solutions: USGS WPhase, Global CMT and USGS Centroid Moment (http://earthquake.usgs.gov). First I present a sensitive analysis of stress changes along magma-feeding fractures with diverse theoretical orientations; then I develop the analysis on the most plausible reconstructed magma paths for each volcano.

ID	Name	Latitude (dd)	Longitude (dd)	Type	SiO_2 (wt. %)	Depth of M.C. (km)
TU	Tupungatito	-33.4	-69.83	B	56-65[3]	7-10[2,3,5]
SJ	San José	-33.82	-69.9	B	55-67[3]	7-10[2,3,5]
MA	Maipo	-34.17	-69.82	B	54-58[3]	4-7[13]
PA	Palomo	-34.6	-70.32	B	53-66[3]	unknown
TI	Tinguiririca	-34.82	-70.35	B	56-63[3]	unknown
PP	Planchón-Peteroa	-35.2	-70.52	B	51-69[3]	2-3[9]
DC	Descabezado Grande	-35.58	-70.62	B	53-71[3]	7-10[2,3,5]
CA	Cerro Azul	-35.65	-70.76	B	51-70[3]	7-10[2,3,16]
SP	San Pedro-Pellado	-35.99	-70.85	B	52-72[3]	unknown
LM	Laguna del Maule	-36.05	-70.5	B	52-72[1]	unknown
NL	Nevado de Longaví	-36.17	-71.17	B	56-65[3]	unknown
NC	Nevados de Chillán	-36.87	-71.38	B	55-69[3,10]	2-3[2,3,5]
AN	Antuco	-37.4	-71.37	B	50-60[3]	4-7[2,3,5]
CO	Copahue	-37.85	-71.17	B	51-74[15]	9-20[12]
CA	Callaqui	-37.93	-71.43	B	> 60[17]	unknown
TH	Tolhuaca	-38.3	-71.63	B	unknown	unknown
LO	Lonquimay	-38.37	-71.58	B	51-67[2,5]	2-3[2,5]
LL	Llaima	-38.7	-71.73	A	51-62[18]	2-3[3,5]
SO	Sollipulli	-38.97	-71.52	B	52-62[8]	unknown
VI	Villarrica	-39.42	-71.95	A	50-56[6]	2-3[2,5]
QU	Quetrupillan	-39.5	-71.77	B	unknown	unknown
LA	Lanín	-39.63	-71.5	B	unknown	unknown
MC	Mocho-Choshuenco	-39.93	-72.03	B	53-62[4]	unknown
PC	Puyehue-Cordón Caulle	-40.5	-72.25	B	50-73[14,19]	2-3[2,5]

Table 1. *Holocene volcanoes belonging to the Southern Volcanic Zone with the available volcanological features for each volcano: name, type, location (decimal degrees), SiO_2 content of erupted lavas and estimated depth of the magma chamber. Data based on satellite images, SRTM90 DEM and data reported in the literature, Global Volcanism Program Digital Information Series, http://www.volcano.si.edu/gvp/world/ (Frey et al., 1984[1]; Hickey-Vargas et al., 1984[2]; Hildreth and Moorbath, 1988[3]; Mcmillan et al., 1989[4]; Tormey et al., 1991[5]; Gonzalez-Ferran, 1995[6]; López-Escobar et al., 1995[7]; Gilbert et al., 1996[8]; Tormey et al., 1995[9]; Dixon et al., 1999[10]; Déruelle and López-Escobar, 1999[11]; Mamaní et al., 2000[12]; Sruoga et al., 2005[13]; Lara et al., 2006b[14]; Varekamp et al., 2006[15]; Maskimow et al., 2007[16]; Rea et al., 2009[17]; Reubi et al., 2011[18]; Collini et al., 2013[19]).*

Source model	Avarage strike (°)	Avarage dip (°)	Length (km)	Width (km)	N. of slip patches	Method
Pollitz et al. (2011)	17	15	650	185	200	GPS, InSAR
Delouis et al. (2010)	15	18	720	280	126	HRGPS, InSAR
Vigny et al. (2011)	13.5	15.7	~500	~200	375	cGPS
Koper et al. (2012)	18	18	460	160	184	Teleseismic
Lin et al. (2013)	18	13	500	100	292	GPS, InSAR, teleseismic
Lorito et al. (2011)	16.4	17.1	~620	200	200	GPS, InSAR, tsunami

Table 2. *Finite fault models used for the modelling. GPS, Global Positioning System; cGPS, Continuous Global Positioning System; HRGPS, High resolution Global Positioning System; InSAR, Interferometric Synthetic Aperture Radar.*

4.4. Earthquake-induced stress changes

4.4.1 Sensitivity analysis

To better constrain a cause-and-effect relationship between large earthquakes and volcanic activity, I resolved the earthquake-induced static stress changes on receiver surfaces with four different strikes, representing possible volcano magma pathways: N-S, NE-SW, E-W and NW-SE. The different pathways were modelled as vertical planes and each calculation was performed at three different depths below the volcano base: 2, 5 and 10 km. In Figure 2 I report the results for calculations made at a depth of 2 km, being the results for 5 and 10 km are very similar and reported in the Figure 3 and 4. For each of the six different finite fault models, the static stress changes were plotted versus the distance from the epicentre. It is possible to note that at a general level, the magnitude of the earthquake-induced stress changes decreases with distance. Comparing the calculated values on different magma pathways at the same distance from the epicentre, it is possible to note that there are relevant changes using different finite fault models, for all the four studied directions of vertical magma pathway. This is due to slight differences in geometries and slip models of the used input fault models (Tab. 2). Nevertheless, it is evident that the surfaces striking N-S suffered the largest values of decompression (unclamping), followed by the NE-striking planes, where the normal stress reduction acted as far as 450 km. The NW- and E- striking magma pathways suffered lower values of unclamping. In Figure 5 it is also possible to note that the stress change has a large range of variation for the four studied directions, and this range decreases with increasing distance from earthquake epicentre for all the six fault models. On the contrary, for the same magma pathway directions, the magnitude of the stress change has very minor changes with depths (Figs. 6 and 7). Results suggest that the direction of magma pathway strongly controls the stress values, while the depth of calculation is much less relevant. Taking into account that several volcanoes have a shallow chamber, I suggest that a calculation at a depth of 2 km is a good way to estimate and quantify earthquake-induced effects on volcano magma pathways.

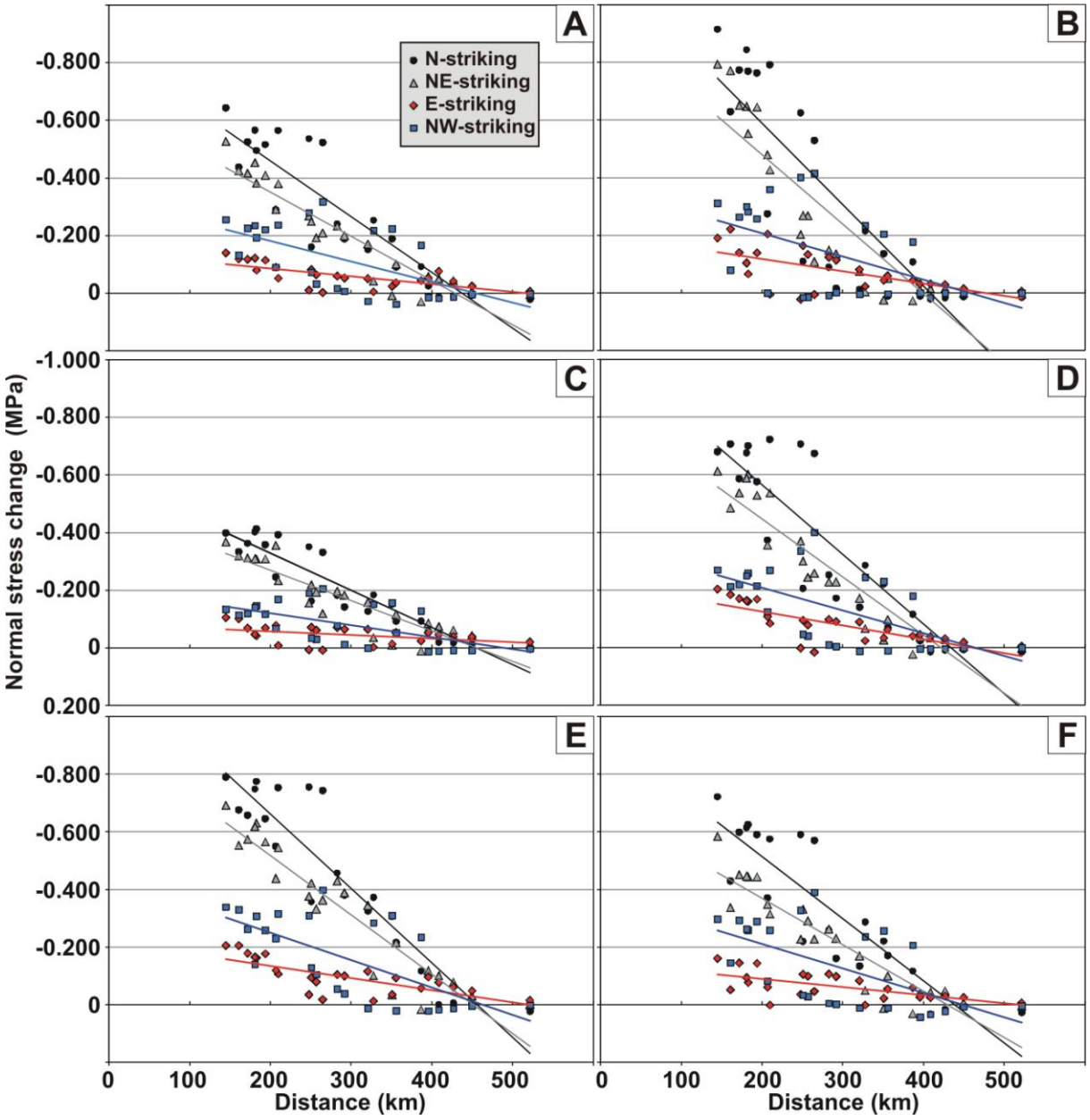

Figure 2. *Earthquake-induced static stress changes resolved on vertical magma pathways with four different directions at a depth of 2 km below the volcano base, versus the distance from the epicentre. Regression lines are reported. I used six different finite fault models: (A) Delouis et al. (2010), (B) Koper et al. (2012), (C) Lin et al. (2013), (D) Pollitz et al. (2011), (E) Lorito et al. (2011) and (F) Vigny et al. (2011) (Tab. 2).*

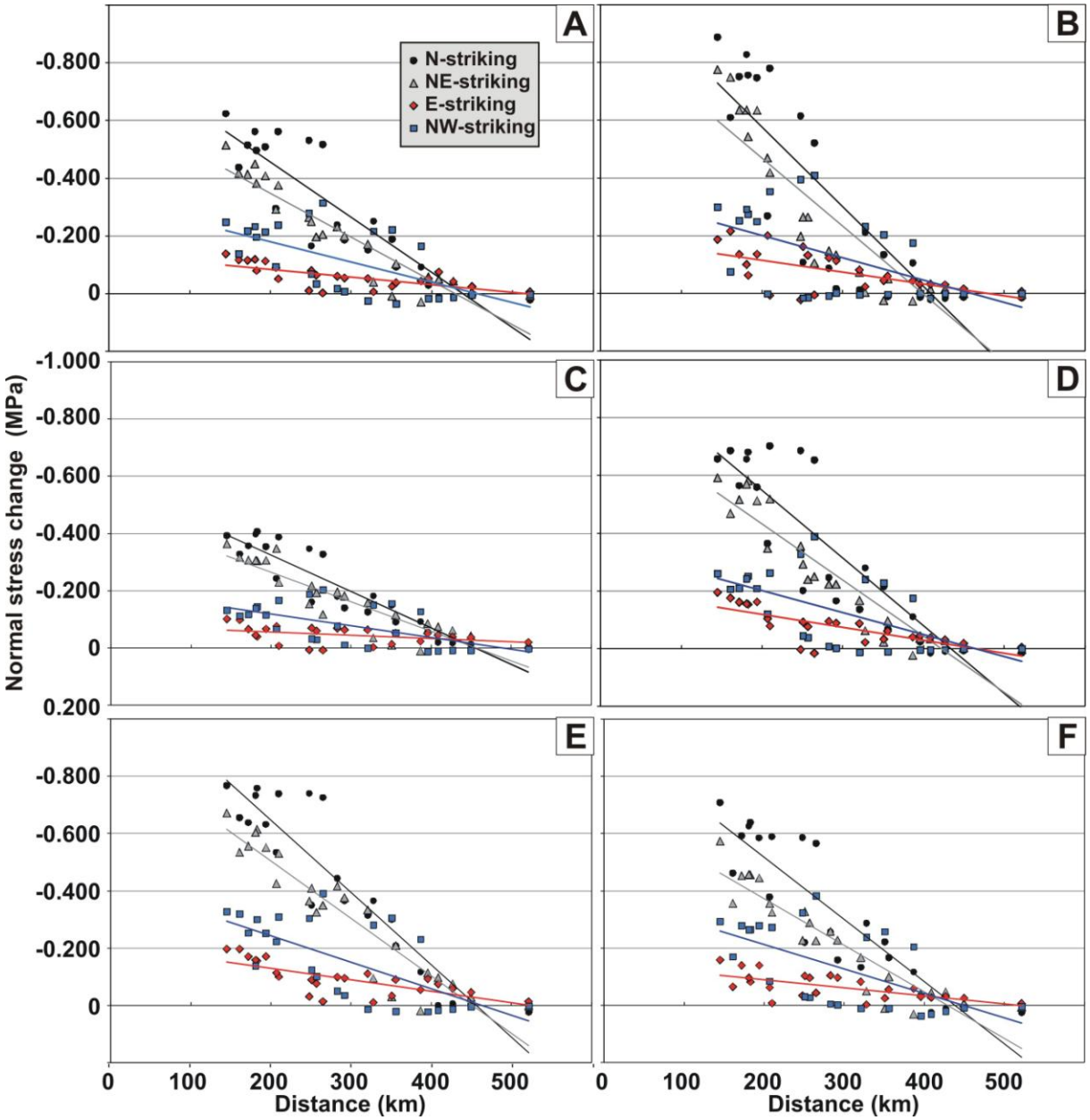

Figure 3. *Earthquake-induced static stress changes resolved on vertical magma pathways with four different directions at a depth of 5 km below the volcano base, versus the distance from the epicentre. Regression lines are reported. We used six different finite fault models: (A) Delouis et al. (2010), (B) Koper et al. (2012), (C) Lin et al. (2013), (D) Pollitz et al. (2011), (E) Lorito et al. (2011) and (F) Vigny et al. (2011) (Tab. 2).*

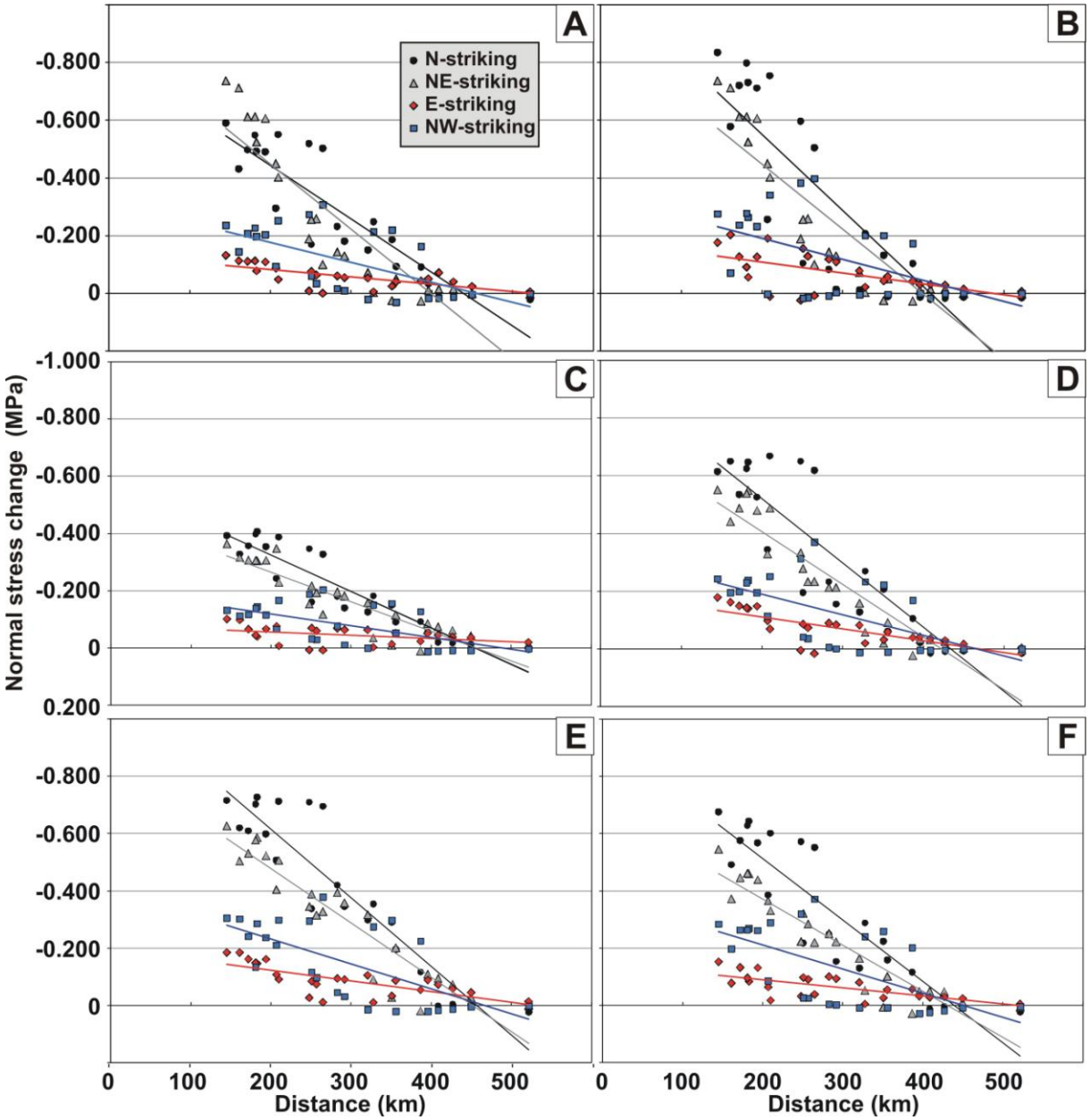

Figure 4. *Earthquake-induced static stress changes resolved on vertical magma pathways with four different directions at a depth of 10 km below the volcano base, versus the distance from the epicentre. Regression lines are reported. I used six different finite fault models: (A) Delouis et al. (2010), (B) Koper et al. (2012), (C) Lin et al. (2013), (D) Pollitz et al. (2011), (E) Lorito et al. (2011) and (F) Vigny et al. (2011) (Tab. 2).*

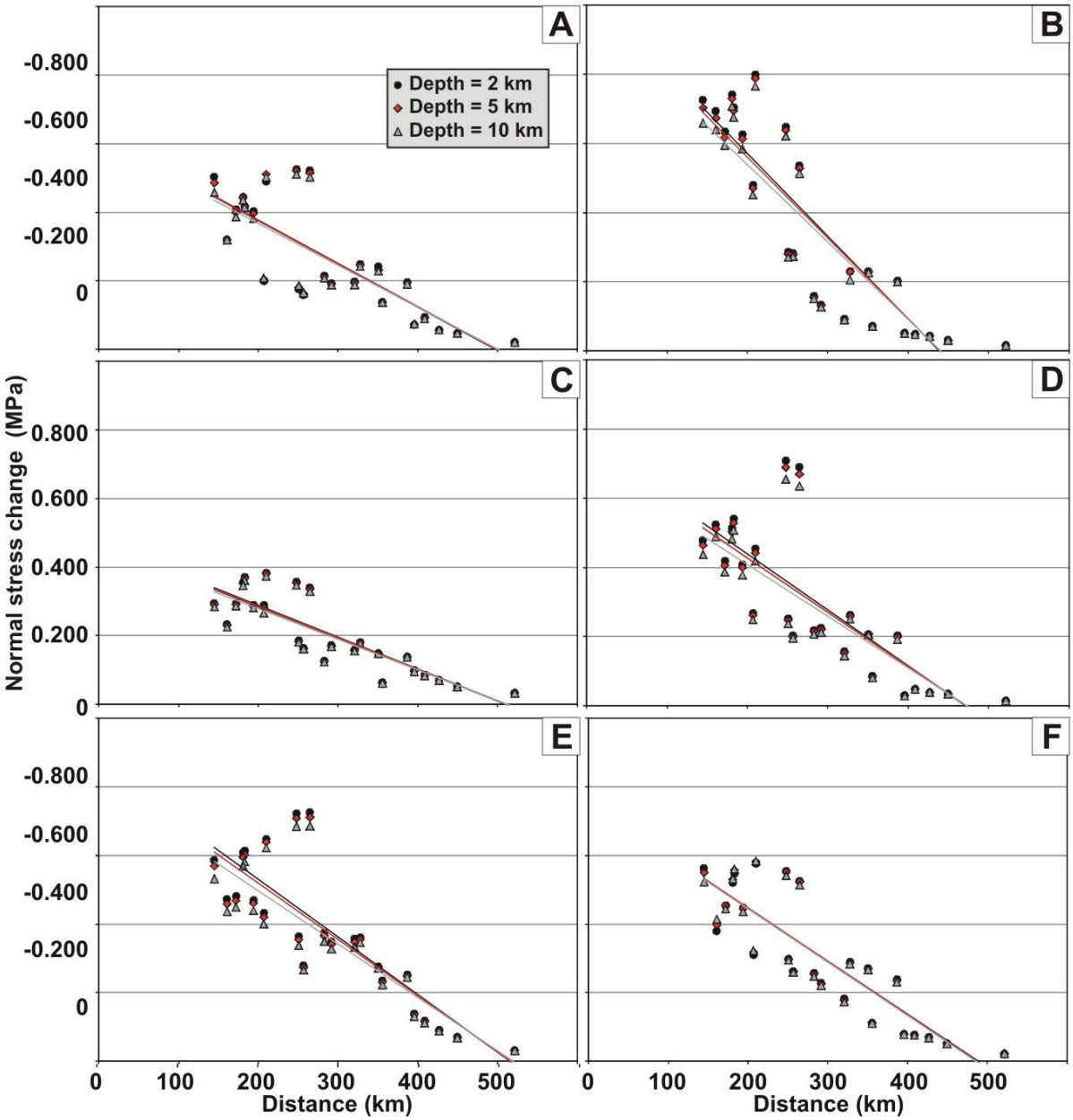

Figure 5. *The graphs shows the range between the smallest and greatest stress changes measured along the four different magma pathways for each volcano, at the three depths of 2, 5 and 10 km. Regression lines are reported. Different finite fault models as in Figure 2.*

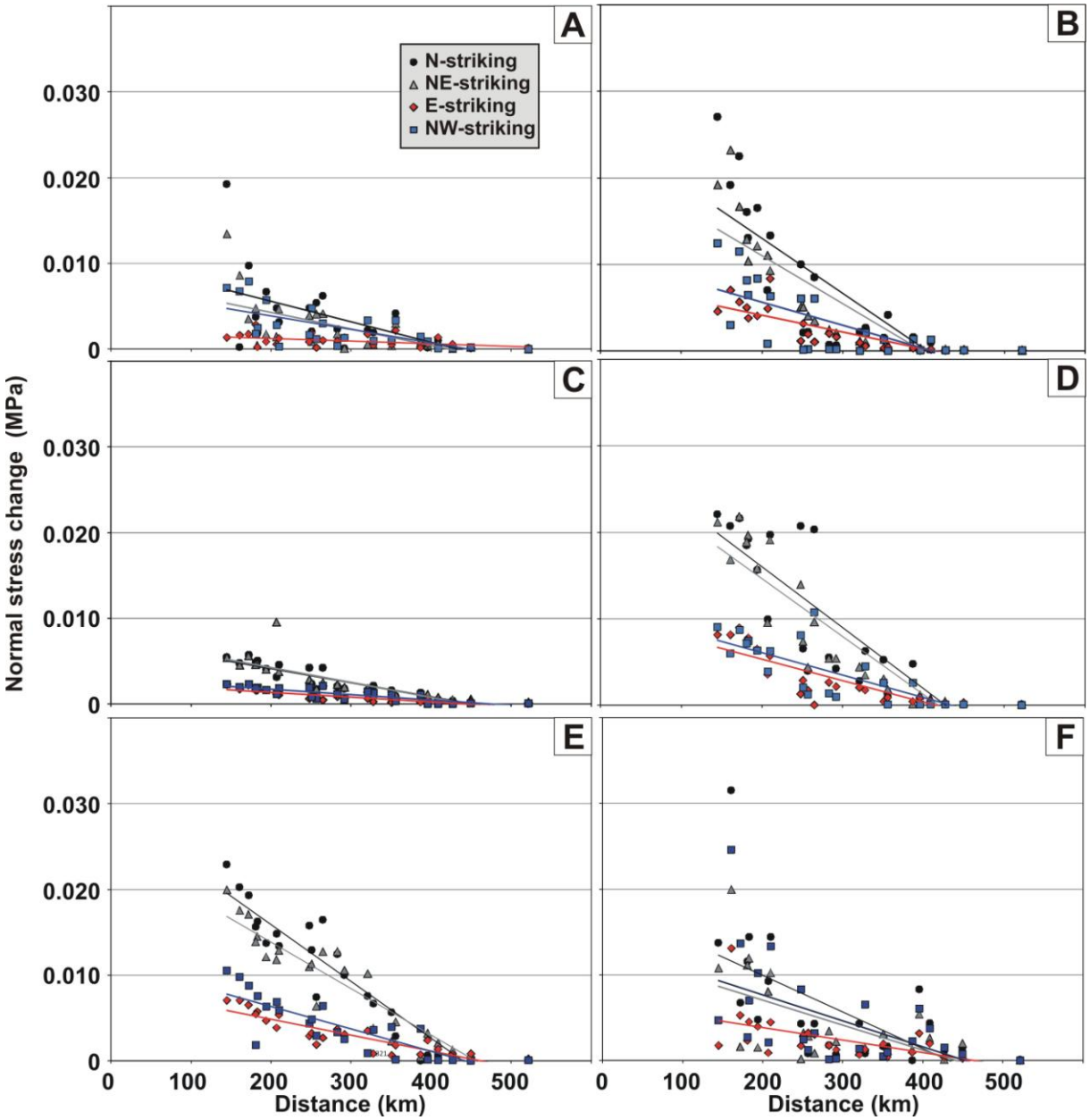

Figure 6. *Variation of the earthquake-induced static stress changes (resolved on vertical magma pathways) between 2 and 5 km of depth, versus the distance from the epicentre. Regression lines are reported. Different finite fault models as in Figure 2.*

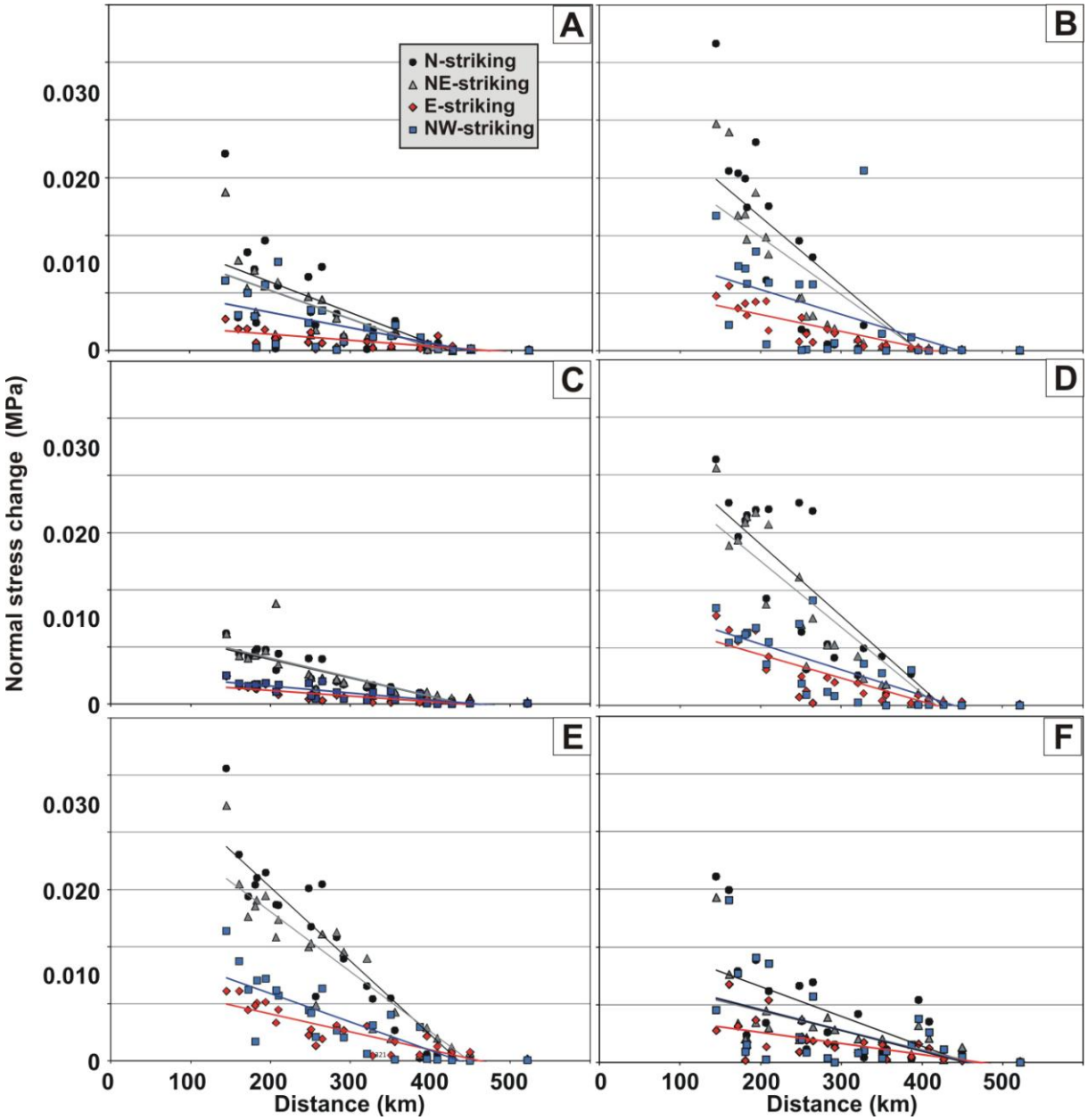

Figure 7. *Variation of the earthquake-induced static stress changes (resolved on vertical magma pathways) between 5 and 10 km of depth, versus the distance from the epicentre. Regression lines are reported. Different finite fault models as in Figure 2.*

4.4.2 Stress changes resolved on reconstructed magma pathways

For each volcano I also reconstructed the most plausible magma pathway geometry (Figs. 8A-B) by means of geological-structural studies of dykes, morphometric characteristics of the volcanoes and spatial distribution of vents (reviews in: Nakamura, 1977; Tibaldi, 1995; Cembrano and Lara, 2009; Bonali et al., 2011), along with local geophysical data and

structural data on faults. For those volcanoes that overlie thrust faults (Maipo, Palomo, Planchón-Peteroa, San José, Tinguiririca and Tupungatito), the magma pathway was assumed 45°-west-dipping based on focal mechanism solutions and field data of fault attitude (Cembrano and Lara, 2009, and references therein); south of the thrust fault zone, magma paths were assumed vertical as the strike-slip faults of the area. Our results show that the unclamping in a direction normal to the magma pathway affects magma plumbing systems to a maximum distance from the epicentre of about 450 km (i.e. Tupungatito volcano). The N-, NNE- and NE-striking magma pathways experienced larger values of unclamping, in comparison with those striking NNW (Fig. 8C and Tab. 3). At present, static stress change contributed to volcanic eruptions at Planchón-Peteroa and Copahue volcano, at a maximum distance of 256 km, while the Puyehue-Cordón Caulle volcanic complex underwent only a very low normal stress increase (clamping).

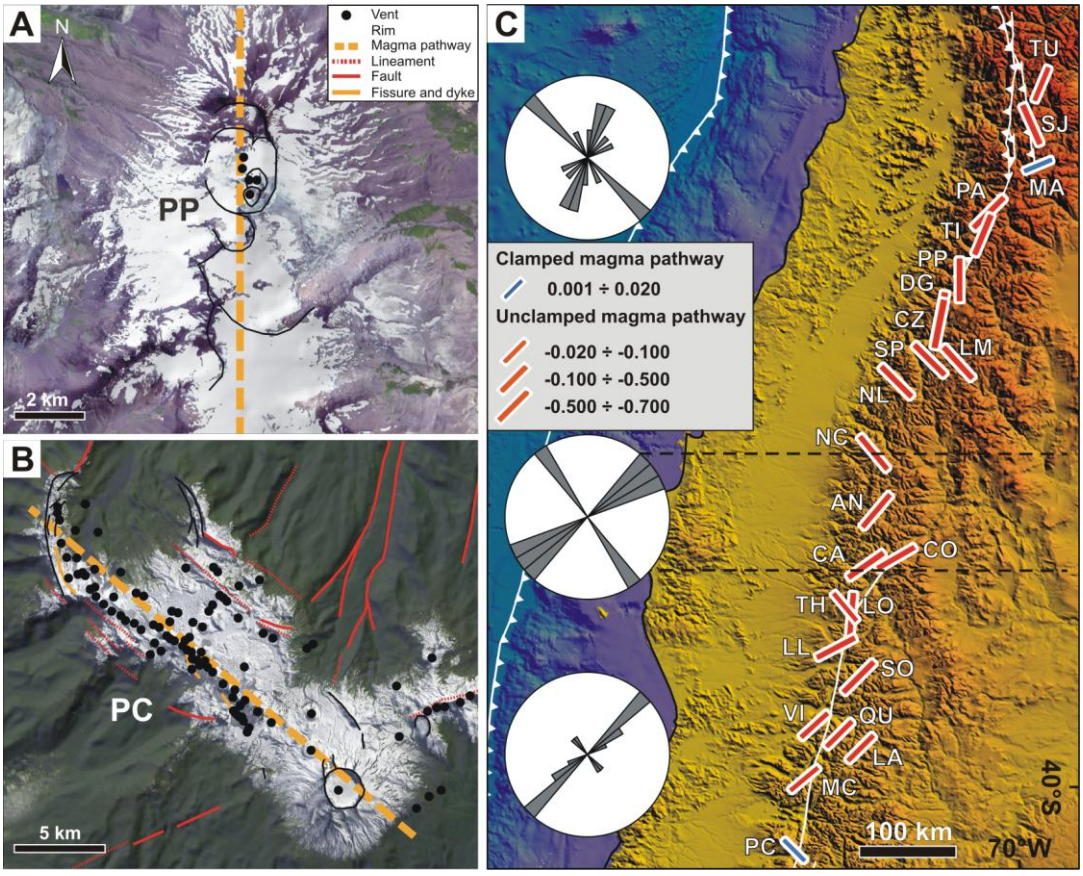

Figure 8. *Reconstructed magma pathway geometry based on dyke orientation, vent alignment and morphometric characteristics of volcanoes for (A) Planchón-Peteroa and (B) Puyehue-Cordón Caulle. (C) Orientation of magma pathways with the values of clamping/unclamping obtained by numerical modelling; rose diagrams represent the azimuth of volcano magma pathways. Volcanoes are reported in Table 1.*

4.5. Discussion

Coseismic and postseismic-induced stress/strain might remotely promote eruptions, particularly for volcanoes close to a critical state (Marzocchi, 2002; Marzocchi et al., 2002; Walter and Amelung, 2007), in addition to dynamic shaking that is another important factor for triggering eruptions (Manga and Brodsky, 2006). Regarding the coseismic induced effects, Marzocchi et al. (2002) showed a complex situation, because eruptions occurred in areas where large earthquakes induced strong compression and/or shear perturbations. Walter and Amelung (2007) suggest that earthquake-induced volumetric expansion causes an increase in the magma-gas pressure and so encourages eruptions in a time frame of years. Coseismic stress changes are candidate to promote eruptions within 5 years after a major earthquake, where the eruptions occurred at a distance of 100-300 km (Marzocchi, 2002). The time delay of 0-5 years can be attributed to the inertia of the volcanic system in reacting to the static stress changes, to a delay due to a not perfect elasticity of the crust, and/or to the stress corrosion effect (e.g., Main and Meredith, 1991). Postseismic stress changes were interpreted to be capable of promoting eruption in 30-35 years after earthquakes, compatibly to the relaxation time of a viscous asthenosphere (Piersanti et al., 1995, 1997; Pollitz et al., 1998; Kenner and Segall, 2000). Our results of numerical modelling suggest that in Chile fault-slip induced magma pathway unclamping as far as 450 km from the epicentre (Fig. 2) and that N-S and NE-SW striking magma pathways suffered the largest effect in comparison to E-W and NW-SE striking magma paths. The eruptions of Planchón-Peteroa and Copahue volcanoes occurred in correspondence of unclamped magma pathways, whereas the eruptions at Puyehue-Cordón Caulle were accompanied by very small clamping (an explanation of this phenomena was provided in Bonali et al., 2013). Furthermore other volcanoes suffered magma pathway unclamping suggesting that these volcanoes are the most prone to unrest from the point of view of the stress state of the rocks hosting their plumbing system (Fig. 8). This does not mean that such volcanoes have necessarily to erupt, due to the complication and different various factors that control magma upwelling. We also compared the volcanic activity in the 50 years preceding the 2010 Chile earthquake and in the following 3 years (Fig. 9) for those volcanoes that do not have a continuously-erupting behaviour (Type B volcanoes in Eggert and Walter, 2009, and Bonali et al., 2013). No eruptions occurred in the six years prior to the earthquake. In the 50-years period before the earthquake the average eruption rate (BER) in the studied area is 0.48, while in the 3-years period following the earthquake (AER), eruptions occurred at three different volcanoes with an average eruption

rate = 1. This could indicate an increase in the eruption rate for Type B volcanoes due to earthquake-induced effects (AER/BER = 2.08).

Name	Latitude (dd)	Longitude (dd)	ID	Distance (km)	Delouis et al. (2010)	Koper et al. (2012)	Lorito et al. (2011)	Lin et al. (2013)	Pollitz et al. (2011)	Vigny et al. (2011)
Tupungatito	-33.40	-69.83	TU	387	-0.007	-0.011	-0.016	-0.015	-0.026	-0.011
San José	-33.82	-69.90	SJ	351	-0.125	-0.104	-0.091	-0.136	-0.186	-0.144
Maipo	-34.17	-69.82	MA	328	0.011	0.015	0.006	0.002	0.002	0.011
Palomo	-34.60	-70.32	PA	265	-0.284	-0.059	-0.062	-0.134	-0.190	-0.115
Tinguiririca	-34.82	-70.35	TI	248	-0.230	-0.232	-0.144	-0.310	-0.334	-0.235
Planchón-Peteroa	-35.20	-70.52	PP	210	-0.284	-0.398	-0.197	-0.363	-0.378	-0.288
Descabezado Grande	-35.58	-70.62	DC	183	-0.515	-0.794	-0.429	-0.744	-0.812	-0.639
Cerro Azul	-35.65	-70.76	CA	181	-0.590	-0.882	-0.421	-0.720	-0.787	-0.629
San Pedro-Pellado	-35.99	-70.85	SP	172	-0.225	-0.263	-0.119	-0.218	-0.261	-0.292
Laguna del Maule	-36.05	-70.50	LM	194	-0.390	-0.535	-0.247	-0.469	-0.468	-0.469
Nevado de Longaví	-36.17	-71.17	NL	145	-0.255	-0.311	-0.134	-0.269	-0.338	-0.297
Nevados de Chillán	34.80	-71.38	NC	161	-0.161	-0.119	-0.136	-0.242	-0.371	-0.179
Antuco	-37.40	-71.37	AN	207	-0.305	-0.481	-0.270	-0.377	-0.473	-0.373
Copahue	-37.85	-71.17	CO	257	-0.157	-0.256	-0.151	-0.197	-0.246	-0.242
Callaqui	-37.93	-71.43	CA	251	-0.216	-0.273	-0.194	-0.264	-0.349	-0.295
Tolhuaca	-38.30	-71.63	TH	283	-0.029	-0.029	-0.022	-0.017	-0.081	-0.011
Lonquimay	-38.37	-71.58	LO	292	-0.188	-0.144	-0.175	-0.221	-0.364	-0.224
Llaima	-38.70	-71.73	LL	321	-0.164	-0.081	-0.154	-0.170	-0.332	-0.167
Sollipulli	-38.97	-71.52	SO	356	-0.099	-0.051	-0.115	-0.096	-0.213	-0.098
Villarrica	-39.42	-71.95	VI	396	-0.059	-0.013	-0.086	-0.038	-0.120	-0.038
Quetrupillan	-39.50	-71.77	QU	409	-0.049	-0.015	-0.074	-0.033	-0.099	-0.042
Lanín	-39.63	-71.50	LA	427	-0.043	-0.015	-0.061	-0.027	-0.077	-0.047
Mocho-Choshuenco	-39.93	-72.03	MC	450	-0.011	-0.001	-0.031	-0.005	-0.033	-0.011
Puyehue-Cordón Cau	-40.50	-72.25	PC	522	0.003	0.001	0.004	0.000	0.002	0.005

Table 3. *2010 M_w 8.8 earthquake-induced static normal stress change resolved on each reconstructed volcano magma pathway at a depth of 2 km below the volcano base. Results are given for the six different finite fault models (Delouis et al., 2010; Koper et al., 2012; Lin et al., 2013; Pollitz et al., 2011; Lorito et al., 2011; Vigny et al., 2011).*

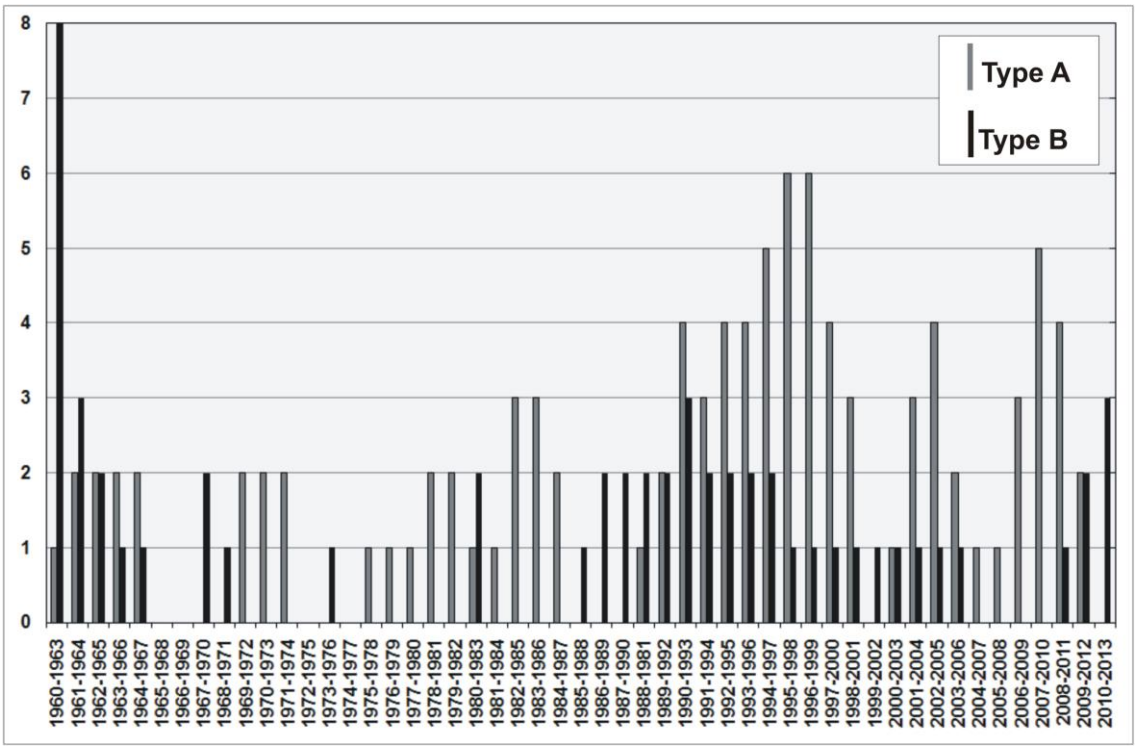

Figure 9. *Volcano activity in the 50 years preceding the 2010 Chile earthquake (average eruption rate = 0.48) and in the following 3 years (average eruption rate = 1). In accord with Eggert and Walter (2009), I considered the average eruption rate for only those volcanoes that do not have a continuously-erupting behaviour (Type B).*

4.6. Final remarks

Combining the reconstruction of the geometry of each volcano's magma pathway with a numerical study of earthquake-induced static stress changes is a powerful tool to quantitatively identify those volcanoes that have a higher probability of new eruptions induced by a large earthquake, based on the state of stress of magma plumbing system.

Our results show that:

- the magma pathway geometry controls the magnitude of the static stress change induced by large earthquakes, with differences of up to 8 times between magma-feeding planes of different orientation at the same volcano;
- this range of diverse values is larger for the volcanoes closer to the epicentre;
- the possible error in the estimation of magma chamber depth has a minimum effect on the results since our sensitive analysis shows that the range of stress changes with depth is about 1.5 orders of magnitude smaller than the range linked to variations of the magma pathway strike;
- in the 2010 Chile earthquake, the N-S- and NE-SW-striking magma pathways suffered a larger unclamping in comparison with those striking NW-SE and E-W;
- in Chile, the unclamping affects the plumbing system of several SVZ volcanoes at a maximum distance of up to 450 km from the epicentre;
- the volcanoes undergoing magma pathway unclamping could experience new earthquake-induced activity up to 5 years after the earthquake.

5. Earthquake-induced static stress change on magma pathway in promoting the 2012 Copahue eruption

This chapter reproduces the published paper "Bonali,F.L.[1], 2013. Earthquake-induced static stress change on magma pathway in promoting the 2012 Copahue eruption. Tectonophysics 608, 127-137".

[1]*Department of Earth and Environmental Sciences, University of Milan-Bicocca, Milan, Italy*

Abstract

It was studied how tectonic earthquake-induced static stress changes could have contributed to favouring the 22 December 2012 major eruption at Copahue volcano, Chile. Numerical modelling indicates that the vertical N60°E-striking magma pathway below Copahue was affected by a normal stress reduction induced by the M_w 8.8 Chile earthquake of 27 February 2010. A sensitivity analysis suggests that N-, NE- and E-striking vertical planes are affected by normal stress decrease (maximum at the NE-striking plane), and that also a possible inclined N60°E plane is affected by this reduction. Copahue did not have any magmatic event since 2000. Seismic signals of awakening started in April 2012 and the first volcanic event occurred on July 2012. Thus, it is here suggested a possible earthquake-induced feedback effect on the crust below the volcanic arc up to at least 3 years after a large subduction earthquake, favouring new eruptions.

5.1. Introduction

Subduction earthquakes are capable of inducing static stress perturbations in the crust with relevant effects on the fault's hanging wall block (Barrientos S.E., 1994; Lin and Stein, 2004; Walter and Amelung, 2007). These stress changes in turn, are capable of promoting aftershocks (Lin and Stein, 2004; Motagh et al., 2010; Asano et al., 2011; Toda et al., 2011a,b) as well as secondary faulting (Lin and Stein, 2004) at a maximum distance of 425 km (Toda et al., 2011b). Furthermore, some authors suggested that large earthquakes could trigger volcanic activity at large distances from the epicentre (Linde and Sacks, 1998; Hill et al., 2002; Marzocchi, 2002; Marzocchi et al., 2002; Manga and Brodsky, 2006; Walter and Amelung, 2007; Bebbington and Marzocchi, 2011), but this is most evident in the near-field (0-250 km) (Eggert and Walter, 2009) and within a few days after the earthquake (Linde and

Sacks, 1998; Manga and Brodsky, 2006; Eggert and Walter, 2009). Owing to the complexity of volcanic systems, the delay between the earthquake occurrence and the following volcanic events can be from seconds to years (Linde and Sacks, 1998; Nostro et al., 1998; McLeod and Tait, 1999; Walter and Amelung, 2007; Eggert and Walter, 2009), but it is not well constrained yet. In the literature, three principal modes for earthquake-induced stress transfer capable of promoting eruptions are proposed: i) static stress changes, ii) quasi-static stress changes and iii) dynamic stresses induced by the seismic waves (Hill et al., 2002; Marzocchi et al., 2002; Manga and Brodsky, 2006). The static stress change is the difference in the stress field from just before an earthquake to shortly after the seismic waves have decayed (Hill et al., 2002). It may explain processes leading to eruption in regions close to the fault rupture (e.g., Walter and Amelung, 2007; Bonali et al., 2013). At greater distances, dynamic stress associated with the passage of seismic waves is often cited as a possible eruption trigger (Linde and Sacks, 1998; Manga and Brodsky, 2006; Delle Donne et al., 2010). Quasi-static stress change is associated with slow viscous relaxation of the lower crust and upper mantle beneath the epicentre of a large earthquake, and occurs over a period of years to decades (Freed and Lin, 2002; Marzocchi, 2000; Marzocchi et al., 2002). Watt et al. (2009) suggested that the overall eruption rate in the Southern Volcanic Zone (SVZ) increased after the two Chilean earthquakes of August 1906 (M_w 8.2) and May 1960 (M_w 9.5). This increase occurred in two different time windows, respectively one and three years after the earthquakes. After the 27 February 2010 Chile earthquake, new volcanic activity took place within 23 months (Bonali et al., 2013). With the present work I am proposing a detailed analysis of the earthquake-induced static stress/strain changes on the Copahue volcano. The results integrate the study of the volcanic events that followed the 2010 Chile earthquake, demonstrating what might be the static effect of a large earthquake in promoting new volcanic eruptions, and suggesting a time-window, possibly larger than previously studied in the literature, for the earthquake-induced static effects (Walter and Amelung, 2007) on magma pathway (Walter, 2007; Bonali et al., 2013).

5.2. Geological framework

5.2.1 The Southern Volcanic Zone

The SVZ (33°S-46°S) is located along the Chilean subduction zone, which absorbs part of the slightly dextral-oblique convergence between the Nazca-American plate margins (Fig. 1), a movement that has prevailed for the last 20 Ma (Pardo-Casas and Molnar, 1987; Somoza, 1998; Angermann et al., 1999; Cembrano and Lara, 2009). The plate boundary at these

latitudes is characterized by a partitioning of deformation, with dominant large thrust earthquakes in the subduction zone and intra-arc transcurrent faulting events (Barrientos and Ward, 1990; Cisternas et al., 2005; Watt et al., 2009). The main cordillera is controlled by dextral strike–slip moment tensor solutions dominating between 34° and 46°S (e.g. Chinn and Isacks, 1983; Lange et al., 2008), although field evidence of long-term strike-slip faulting at the surface can be observed only south of 38°S (Fig. 1) (Cembrano and Lara, 2009). This major intra-arc fault system is the 1200 km-long Liquiñe–Ofqui fault zone (LOFZ; Cembrano et al., 1996; Folguera et al., 2002; Adriasola et al., 2006; Rosenau et al., 2006; Cembrano and Lara, 2009). The transpressional LOFZ is one of the controlling factors of magmatic activity along the volcanic front between 37° and 47°S (Lavenu and Cembrano, 1999; Rosenau, 2004). The LOFZ appears to allow more rapid magma ascent through the crust and lesser occurrence of assimilation or magma mixing compared to the more contractional setting further north in the SVZ (Cembrano and Lara, 2009; López-Escobar et al., 1995). The LOFZ merges into the Agrio and the Malargue fold-and-thrust belts at approximately 37°S (Fig. 1) (Folguera et al., 2006). The transition from the strike-slip LOFZ to the thrust zone corresponds also to a thickening and ageing of the continental crust, to longer crustal magma residence times, and to greater differentiation, crustal assimilation and magma mixing (Tormey et al., 1991).

5.2.2 Volcano-tectonic features of Copahue

Copahue is a 2997-m-high stratovolcano located in the eastern side of the SVZ at the Chile-Argentina (Province of Neuquén) border, (Varekamp et al., 2001). The volcano evolution was subdivided in three stages, started 1.2 Ma ago (Delpino and Bermudez, 1993). Its Holocene activity was characterized by the emission of basaltic–andesitic products, expressed by fissure-related pyroclastic flows, aligned parasitic cones and activity from the summit craters (Melnick et al., 2006). A new eruptive cycle started in July 1992 and continued until 1995; the activity was characterized by crater-lake explosions with ejection of hydrothermally altered rock fragments, siliceous white dust, copious amounts of green and yellow liquid sulphur (Delpino and Bermudez, 1995) and some basaltic-andesitic juvenile fragments (Bermudez and Delpino, 1995; Delpino and Bermudez, 1993). Major eruptions occurred in December 1994 and September 1995 (Varekamp et al., 2001) and in 2000 (Naranjo and Polanco, 2004). No further activity has been documented up to April 2012. Quaternary volcanic activity in the Copahue area concentrates along the NE-trending, 90-km-long Callaqui–Copahue–Mandolegüe lineament (CCM; Fig. 1), the longest of the SVZ.

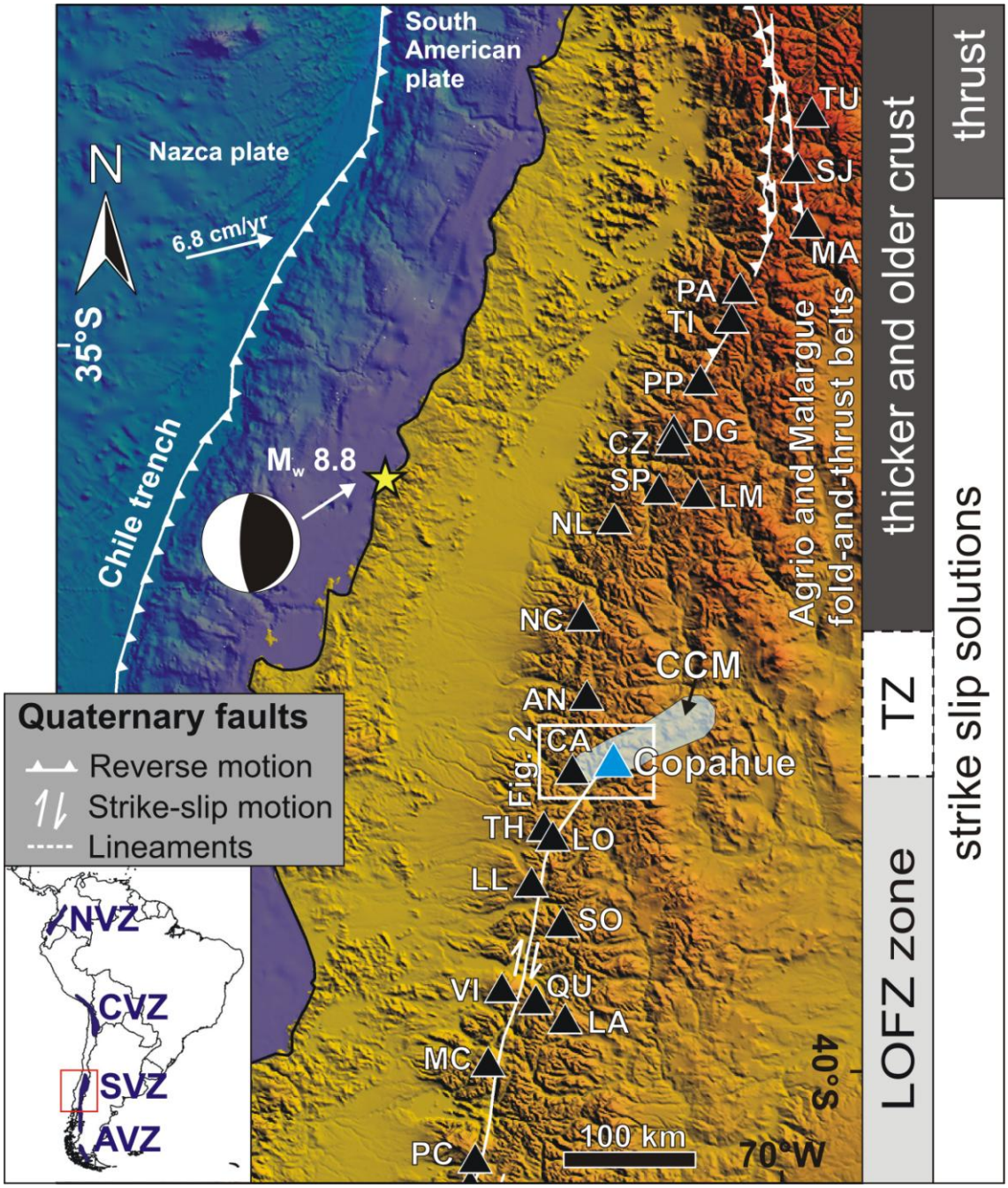

Figure 1. *Active Holocene volcanoes belonging to the Southern Volcanic Zone. The white arrow indicates the approximate convergence direction of the plates with estimated velocity. Main intra–arc faults with reverse motion in the north, and right lateral strike–slip motion in the south are reported (redrawn after Cembrano and Lara, 2009 and Melnick et al., 2006). LOFZ, Liquiñe–Ofqui Fault Zone; TZ, Transition Zone; CCM, Callaqui–Copahue–Mandolegüe lineament. NVZ, CVZ, SVZ and AVZ correspond to Northern, Central, Southern and Austral Volcanic Zone. TU, Tupungatito; SJ, San José; MA, Maipo; PA, Palomo; TI, Tinguiririca; PP, Planchón-Peteroa; DG, Descabezado Grande; CZ, Cerro Azul; NL, Nevado de Longavi, NC, Nevados de Chillán; AN, Antuco; CA, Callaqui; TH, Tolhuaca; LO, Lonquimay; LL, Llaima; VI, Villarrica; QU, Quetrupillan; LA, Lanin; MC, Mocho-Choshuenco; PC, Puyehue-Cordón Caulle.*

This lineament is interpreted as an inherited crustal-scale transfer zone from a Miocene rift basin (Melnick et al., 2006). The CCM is expressed by the alignment of the N60°E-elongated Callaqui volcano to the SW, the Copahue stratovolcano, and the Caviahue caldera to the NE (Fig. 2; Moreno and Lahsen, 1986; Melnick et al., 2006). Volcanic activity along the Copahue volcano-Caviahue caldera alignment is controlled by local structures that formed at the intersection of regional fault systems (Melnick et al., 2006). The main active fault of the area is the NE-striking Lomìn fault that affects the Holocene lavas from Copahue (Melnick, 2000). This fault is considered as the main expression of the horsetail-like array formed at the northern end of the LOFZ (Fig. 2; Melnick et al., 2006). Furthermore, the post-glacial vent alignment on Copahue volcano and the Holocene fault scarps on the eastern slope of the edifice show a general N60°E-striking structural control like the CCM transfer zone (Fig. 2; Melnick et al., 2006).

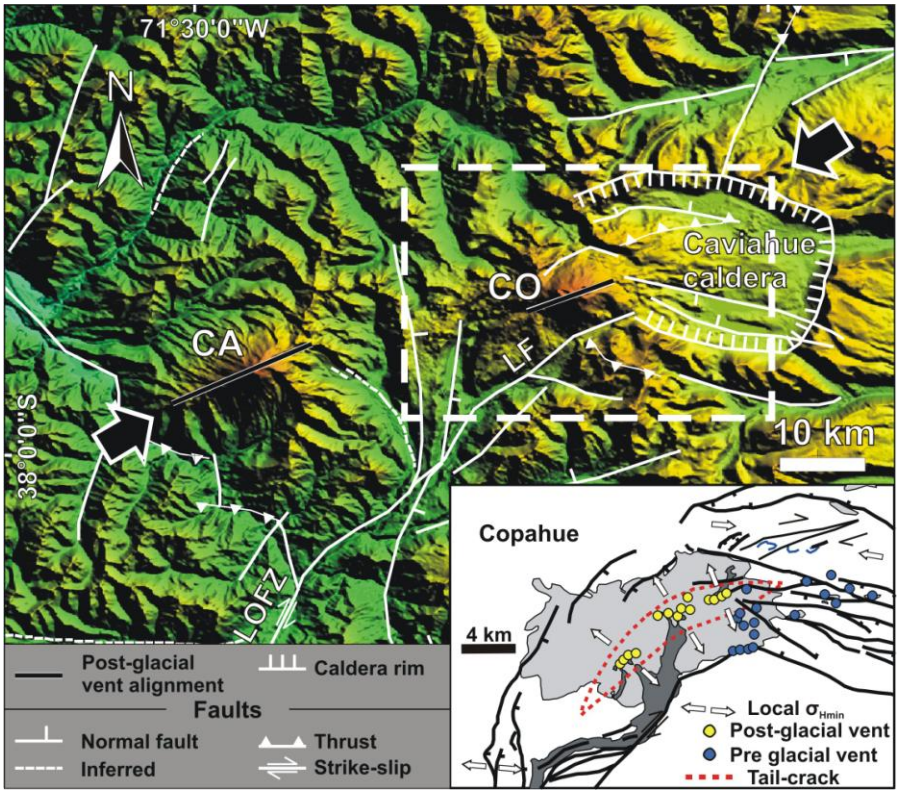

Figure 2. *Tectonic map of the Callaqui-Copahue-Mandolegüe transfer zone. LOFZ, Liquiñe-Ofqui fault zone; LF, Lomìn fault; CA, Callaqui; CO, Copahue. Black arrows represent the regional* σ_{Hmax}. *Shaded-relief digital elevation model from SRTM90 data (datum WGS84) (http://srtm.csi.cgiar.org/). Inset: structural model of the Copahue volcanic complex characterized by a N60°E trending post-glacial vent alignment. Redrawn from Melnick et al. (2006).*

Based on vent alignment and fault geometry, and in agreement with Melnick et al. (2006), I consider that magma rises along N60°E-striking vertical planes perpendicular to the least principal horizontal stress (σ_{Hmin}). This is in conformity with the fact that basic magmas rise to the surface along planar, steeply-inclined intrusive sheets that may group to form dyke swarms (Carracedo, 1994; Dieterich, 1988; Walter and Schmincke, 2002), and with Nakamura (1977) who suggested that dykes tend to propagate normal to the σ_{Hmin}, forming subaerial aligned parasitic cones. The inversion of fault–slip data throughout the SVZ between 37°S to 46°S for the Quaternary stress tensor documents a mostly sub-horizontal, NW-trending least principal stress axis (σ_3) (Lavenu and Cembrano, 1999; Arancibia et al., 1999; Cembrano et al., 2000; Potent and Reuther, 2001; Lara et al., 2006; Cembrano and Lara, 2009). Mamani et al. (2000) suggested a possible depth of the Copahue magma chamber between 9 and 20 km, based on magnetotelluric soundings.

5.3. Volcanic unrest and eruptive crisis

5.3.1 Volcanic events

The new eruptive cycle of Copahue volcano began on 19 July 2012 with phreatic explosions (Caselli et al., 2013). These Authors on 22 December 2012 observed evidence of phreatic activity that turned into hydromagmatic and magmatic activity in a few hours. Magmatic activity reached a paroxysm with an eruption of VEI = 1-2 on the same 22 December, with the emission of a plume of white gas and dark ash rising to 1-1.5 km above the crater and then drifting 400 km SE (OVDAS-SERNAGEOMIN). On 23-24 December 2012, strombolian activity was observed, with ejection of incandescent blocks; during 25-29 December white plumes rose 450-850 m and drifted NE and E (OVDAS-SERNAGEOMIN). On 5-7 January 2013 incandescence was noted in proximity of the summit craters, as well as gray ash plumes rising up to 200 m above the crater (OVDAS-SERNAGEOMIN). During 9-15 January the camera installed near Copahue recorded white gas plumes rising 0.9-1.5 km above the crater, and incandescence at night. On 15-18 January white gas plume raised 250-1300 m above the crater, and on 22 January an explosion produced a gas plume (with no ash) that rose 1.45 km above the crater. Volcanic activity was present up to May 2013 (OVDAS-SERNAGEOMIN).

5.3.2 Recorded seismic signals

Starting from April 2012, the monitoring network of Copahue detected Volcano-Tectonic (VT), Long Period (LP) and tremor (TR) seismic signals. In particular, a large number of VT

and LP events were recorder before and during the eruptive crisis started on 22 December 2012, while TR were recorded in July, August, September as well as during the crisis (OVDAS-SERNAGEOMIN).

Relevant VT events were recorded on: i) 22/06/2012 (M_L= 1.7-1.9) at a depth of 1.8 km and located 8.4-9.2 km NE of Copahue; ii) 18/07/2012 (M_L= 1.8) at a depth of 1.5 km, 10 km NE of the volcano; iii) 24/08/2012 close to the volcano, at a depth of 8.1 km; iv) October 2012 (M_L= 1.5) at a depth of 3.2 km, 3 km E of the volcano (OVDAS-SERNAGEOMIN). These volcano-tectonic signals are regarded as generated by brittle rock failure induced by magma movements in the crust beneath the volcano, and are often the first indicator of renewed volcanic activity (Chouet, 1996, and references therein) or support the idea of a change in the stress state of the volcanic system (Palma et al., 2008). LP earthquakes are produced by injection of magma in the crust and/or inside the volcano and are related to pressure changes during the unsteady transport of magma. When magma injection is sustained, a large amount of these earthquakes are produced (Chouet, 1993) suggesting that a volcano is about to erupt. The overall seismicity recorded on 31 December 2012, and on the 2 and 4-5 January 2013 suggested that magma movement was focused at 4 km below the crater and was moving to shallower depths (OVDAS-SERNAGEOMIN). A LP seismic swarm started at 14:20 on 22 January 2013. The earthquakes were initially deep but became shallower, and VT events were more frequently detected, until the next report posted at 22:00 (OVDAS-SERNAGEOMIN).

5.4. Modelling strategy

In order to constrain a possible cause-and-effect relationship between large earthquakes and volcanic activity, I calculated the earthquake-induced normal stress change on the Copahue magma pathway (e.g. Nostro et al., 1998; Walter, 2007; Bonali et al., 2012; 2013) and the dilatation in the crust at the depth of the magma chamber (e.g. Barrientos, 1994; Walter and Amelung, 2007). The numerical models were performed using the Coulomb 3.3 software (Lin and Stein, 2004; Toda et al., 2005), where calculations were made in an elastic halfspace with uniform isotropic elastic properties following Okada's (1992) formulae. Such formulae allow to calculate the crustal dilatation as well as the static normal stress change resolved on a receiver surface, independently from the rake angle of the receiver structure and from the friction coefficient used in the model. The Copahue magma pathway was assumed as a vertical surface striking N60°E as explained before. A sensitivity analysis is also proposed, where different dip angles (50°, 70° and 90°) for the reconstructed N60°E Copahue magma

pathway were tested, along with different directions (N-S, NE-SW, E-W, NW-SE) of the magma pathway.

The upper crust was modelled as an elastic isotropic halfspace characterized by a Young's modulus E = 80 GPa and a Poisson's ratio ν = 0.25 based on King et al. (1994), Mithen (1982), Lin and Stein (2004) and Toda et al. (2005); a lower value of Young's modulus would only have the effect of reducing the magnitude of static stress changes. Regarding the finite fault model, we tested six different fault solutions to simulate the earthquake-induced effects. They are based on tsunami, teleseismic, GPS and InSAR data and are characterized by defined fault plane geometry and variable slip rate (Tab. 1). The input stress field is based on three comparable tensor solutions: USGS WPhase, Global CMT and USGS Centroid Moment (Fig. 1; http://earthquake.usgs.gov).

Furthermore, it has been evaluated the possible contribution of earthquake-induced static stress changes due to crustal earthquakes occurred between the last pre-2010 volcanic eruption (2000) and the 2010 Chile earthquake. Fault geometries and kinematics are based on focal mechanism solutions (http://earthquake.usgs.gov; http://www.gmtproject.it/) when available, and geometries and kinematics of active faults reported in the literature (Melnick et al., 2006; Cembrano and Lara, 2009). Fault dimensions were based on empirical relations (Wells and Coppersmith, 1994; Toda et al., 2011c). I considered earthquakes with $M_w \geq 4$ (http://earthquake.usgs.gov) and a depth between 0 and 70 km.

Source model	Avarage strike (°)	Avarage dip (°)	Length (km)	Width (km)	N. of slip patches	Method
Pollitz et al. (2011)	17	15	650	185	200	GPS, InSAR
Delouis et al. (2010)	15	18	720	280	126	HRGPS, InSAR
Vigny et al. (2011)	13.5	15.7	~500	~200	375	cGPS
Koper et al. (2012)	18	18	460	160	184	Teleseismic
Lin et al. (2013)	18	13	500	100	292	GPS, InSAR, teleseismic
Lorito et al. (2011)	16.4	17.1	~620	200	200	GPS, InSAR, tsunami

Table 1. *Finite fault models used for the modelling. GPS, Global Positioning System; cGPS, Continuous Global Positioning System; HRGPS, High resolution Global Positioning System; InSAR, Interferometric synthetic aperture radar.*

5.5. Earthquake-induced static stress and strain changes

A first set of simulations was performed to evaluate the M_w 8.8 2010 earthquake-induced crustal dilatation. The calculations were performed at a depth of 14.5 km, coincident with the hypothetical centre of the magma chamber (Mamani et al., 2000). Results suggest that for all the six different finite fault models the crust is affected by dilatation (Fig. 3). A second set of simulations was performed to evaluate the static stress changes resolved on the N60°E

striking Copahue magma pathway, considering the pathway as both a vertical or inclined surface. For all the six different finite fault models the results suggest that the magma pathway is affected by a normal stress reduction (unclamping) within a depth range of 1 to 9 km below the volcano base (Figs. 4 and 5). The Copahue magma pathway is always involved in an area of normal stress reduction, although the overall area of unclamping exhibits different patterns of normal stress change (Fig. 4). Such difference is due to the different characteristics of the finite fault models used as input for the simulations (Tab. 1). At a general level, the highest magnitude of this perturbation on Copahue occurs when considering a vertical pathway, slightly decreasing with depth, and ranges from -0.258 to -0.147 MPa. The magnitude of unclamping decreases with decreasing dip angle of the magma pathway (Fig. 5). In particular with increasing depth and the dip angle being the same, the unclamping is greater for pathways dipping to the NW. In order to complete the sensitivity analysis on magma pathway geometry, different strikes were tested for a vertical surface, again considering the six different finite fault models to impart the normal stress change (Tab. 1). Results suggest that the N-, NE- and E-striking vertical planes are always affected by unclamping, the NE-striking plane suffering, in most cases, the largest decrease in stress on the modelled surface (Fig. 6). On the contrary, the NW-striking receiver plane is sometimes affected by normal stress increase (Fig. 6B and 6D).

Regarding the possible contribution of earthquake-induced static stress changes due to crustal earthquakes with M_w 4 ÷ 6.6 (http://earthquake.usgs.gov), only one out of 193 earthquakes (Fig. 7A) was capable of inducing static normal stress changes on the Copahue magma pathway (Fig. 7B). This earthquake occurred on 31/12/2006 with a M_w of 5.6 and hypocenter at a depth of 20.6 km (http://earthquake.usgs.gov) with dextral strike-slip kinematics (Fig. 7A), at a distance of about 11 km from the volcano. Results suggest that both the N60°E-striking vertical magma pathway and SE-dipping inclined pathways suffered a normal stress reduction, while the subvertical NW-dipping pathway is sometimes affected by normal stress increase with depth. The less inclined NW-dipping pathway instead didn't suffer relevant normal stress changes (Fig. 7B). In any case, the stress change imparted by the 2006 earthquake is two orders of magnitude less than the contribution of the 2010 seismic event.

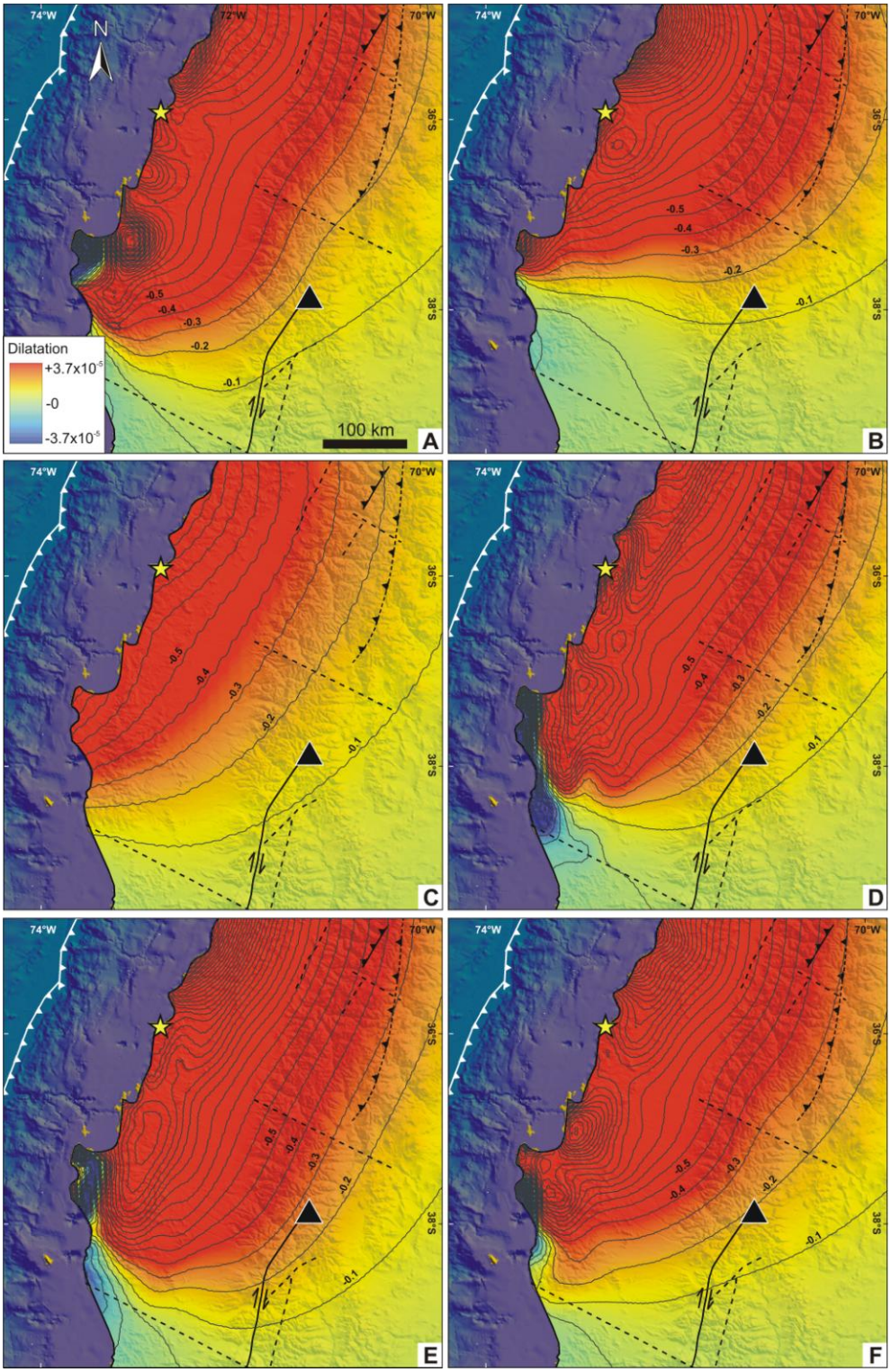

Figure 3. *Earthquake-induced dilatation. The calculations were performed at a depth of 14.5 km, coincident with the hypothetical centre of the magma chamber (Mamani et al., 2000), using different finite fault models from: (A) Delouis et al. (2010), (B) Koper et al. (2012), (C) Lyn et al. (2013), (D) Pollitz et al. (2011), (E) Lorito et al. (2011) and (F) Vigny et al. (2011) (Tab. 1). A black triangle locates the Copahue volcano. Red colours represent dilatation, blue colours represent contraction.*

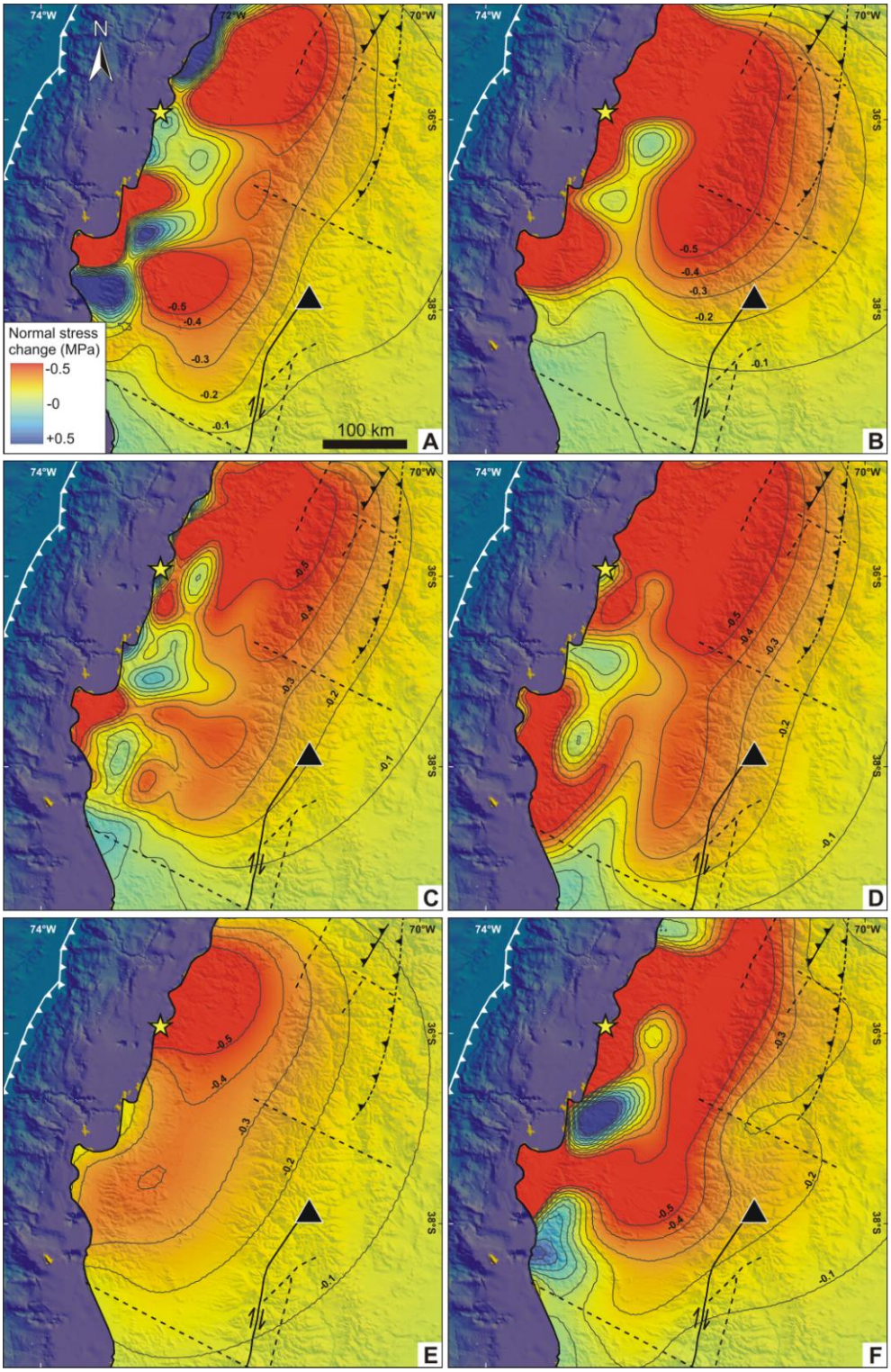

Figure 4. *Earthquake-induced normal stress change resolved on the N60°E-striking Copahue magma pathway at a depth of 4.5 km below the volcano base, using different finite fault models from: (A) Delouis et al. (2010), (B) Koper et al. (2012), (C) Lyn et al. (2013), (D) Pollitz et al. (2011), (E) Lorito et al. (2011) and (F) Vigny et al. (2011) (Tab. 1). A black triangle locates the Copahue volcano. Red colours represent a normal static stress reduction on the receiver plane, blue colours represent an increase.*

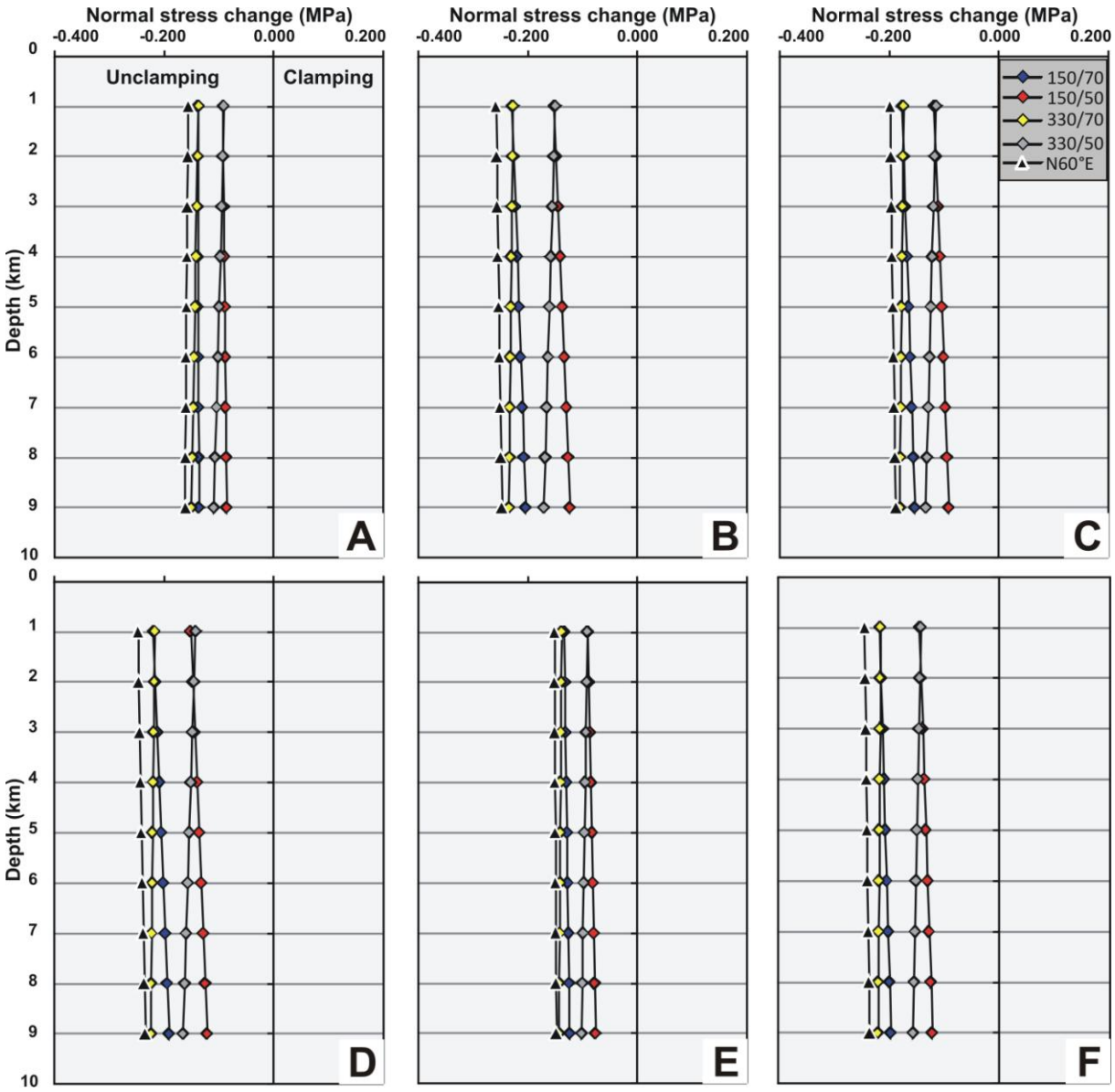

Figure 5. *2010 M_w 8.8 earthquake-induced normal stress change resolved on the N60°E-striking reconstructed Copahue magma pathway, considering both vertical and inclined receiver surfaces, and depths of 1 to 9 km below the volcano. The attitude of the inclined receiver surfaces is expressed as dip direction/dip angle. I used six different finite fault models: (A) Delouis et al. (2010), (B) Koper et al. (2012), (C) Lyn et al. (2013), (D) Pollitz et al. (2011), (E) Lorito et al. (2011) and (F) Vigny et al. (2011) (Tab. 1).*

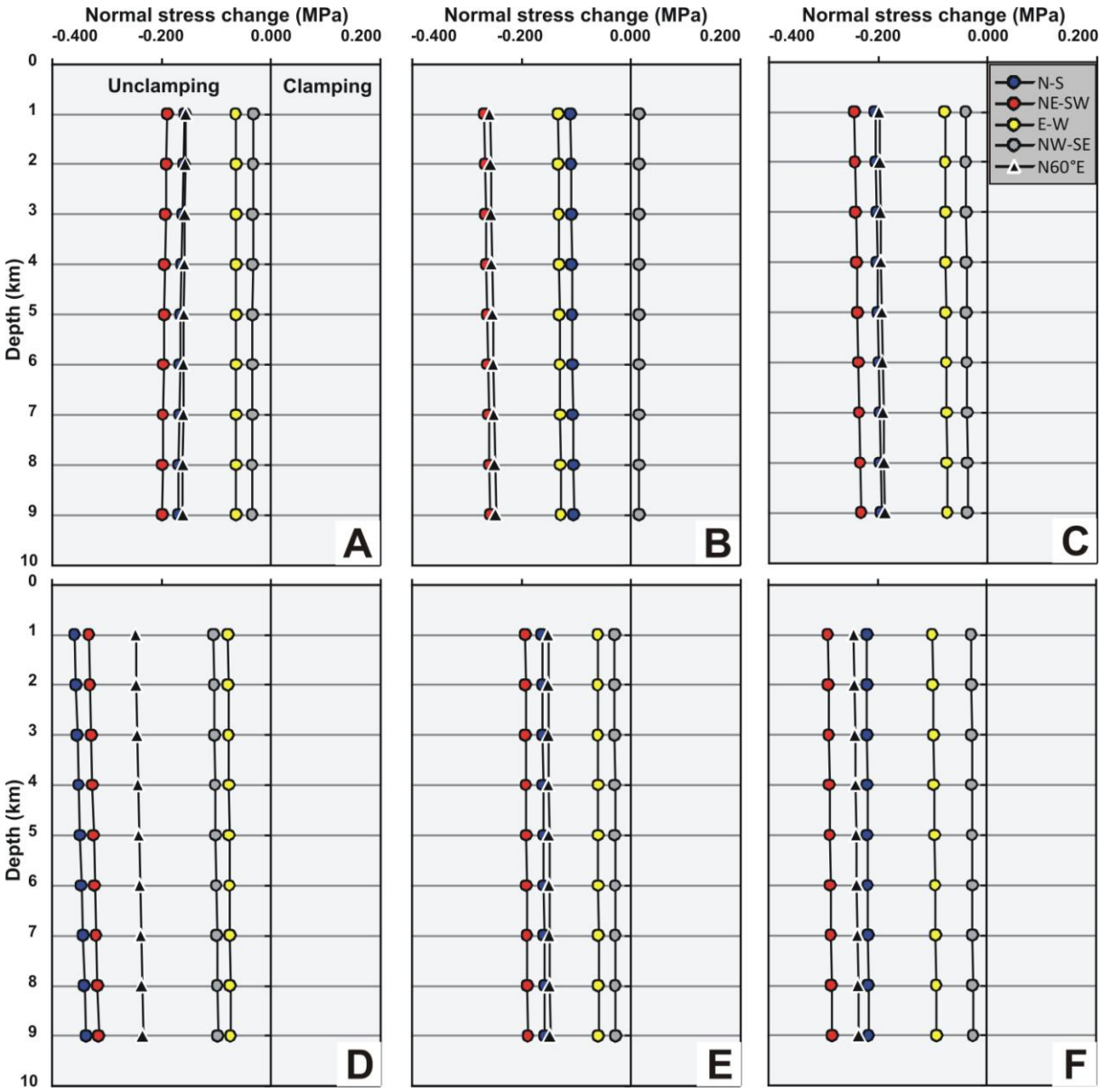

Figure 6. *2010 M_w 8.8 earthquake-induced static normal stress change resolved on: N-, NE-, E- and NW-striking magma pathway within depths of 1 to 9 km below the volcano. The output for the N60°E strike is reported for comparison. I used six different finite fault models: (A) Delouis et al. (2010), (B) Koper et al. (2012), (C) Lyn et al. (2013), (D) Pollitz et al. (2011), (E) Lorito et al. (2011) and (F) Vigny et al. (2011) (Tab. 1).*

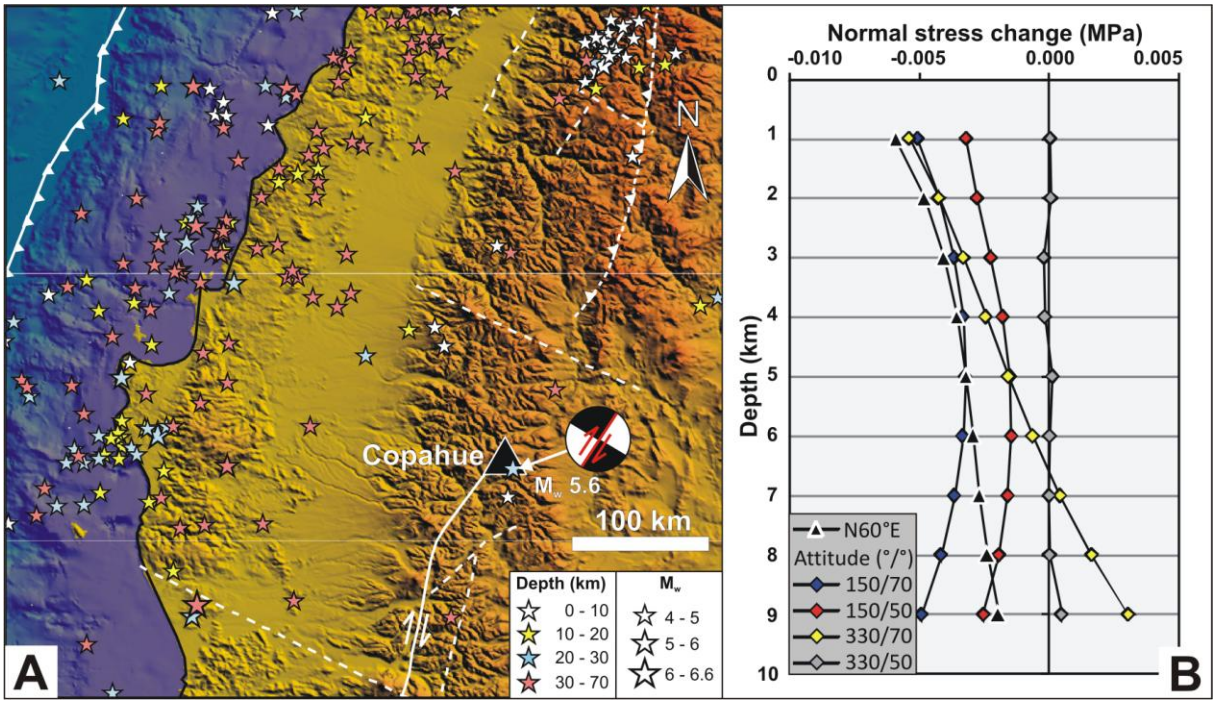

Figure 7. *(A) Crustal earthquakes with $M_w \geq 4$ (http://earthquake.usgs.gov) occurred between the last pre-2010 volcanic eruption (July 2000) and the 2010 Chile earthquake. The focal mechanism of the 31/12/2006 with a M_w of 5.6 (http://earthquake.usgs.gov; http://www.gmtproject.it/) is shown along with the red line representing the fault strike and kinematics, based on focal mechanism solution and active faults reported in the literature (Melnick et al., 2006; Cembrano and Lara, 2009). (B) 2006 M_w 5.6 earthquake-induced normal stress change resolved on the N60°E-striking reconstructed Copahue magma pathway, considering both vertical and inclined receiver surfaces, and depths of 1 to 9 km below the volcano. The attitude of the inclined receiver surfaces is expressed as dip direction/dip angle.*

5.6. Discussion

Coseismic and postseismic-induced stress/strain might remotely promote eruptions, particularly for volcanoes close to a critical state (Marzocchi, 2002; Marzocchi et al., 2002; Walter and Amelung, 2007), in addition to dynamic shaking that is another important factor for triggering eruptions (Manga and Brodsky, 2006). Regarding the coseismic induced effects, Marzocchi et al. (2002) showed a complicated situation, because eruptions occurred in areas where large earthquakes induced strong compression and/or shear perturbations. Walter and Amelung (2007) suggest that earthquake-induced volumetric expansion causes an increase of the magma-gas pressure and so encourages eruptions in a time frame of years. Bonali et al. (2013) suggest that magma pathway unclamping is a key factor in promoting eruption at volcanoes with deep magma chambers. It was also demonstrated that quasi-static

stress change, which is a postseismic-induced effect, could occur over a period of years to decades (Freed and Lin, 2002) and promote large volcanic eruptions (Marzocchi et al., 2002). Dynamic stress changes may excite and promote ascent of gas bubbles, and consequently magma ascent (Manga and Brodsky, 2006), the details of the feedback mechanisms remaining unclear. Dynamic effects can also favour bubble growth, including adjective overpressure (Linde et al., 1994), rectified diffusion (Brodsky et al., 1998; Ichihara and Brodsky, 2006) and shear strain (Sumita and Manga, 2008). Furthermore, Hill (2008) suggests that volcanoes in extensional tectonic regimes are more vulnerable to dynamic triggering in comparison with those in compressional regime. All the proposed mechanisms can result in a delayed triggering. Results of numerical modelling suggest that the upper crust was affected by M_w 8.8 2010 earthquake-induced crustal dilatation. The Copahue magma pathway was affected by a static normal stress reduction due to the 2006 M_w 5.6 earthquake that occurred close to the volcano, while the main contribute was induced by the February 2010 Chile earthquake, occurred at a distance of about 257 km from the volcano (Fig. 1). In the preceding 12 years, Copahue did not have any volcanic activity, since the latest major eruption occurred on July-October 2000 (Fig. 8). On April and July 2012, seismic and volcanic events started to occur (26 months after the earthquake), developing into the major eruption of December 2012. Recorded seismic signals suggested rock fracturing and magma rise (OVDAS-SERNAGEOMIN; cfr. § 3.2); magma movements were suggested at a depth of about 4 km, and rock fracturing was recorded at depths of 8.1 and 3.2 km near the volcano. This indicates that magma raised along the earthquake-unclamped Copahue magma pathway. I therefore consider that the static stress change can have played an important role in promoting unrest at this volcano. Copahue had 10 eruptions since 1900 (Global Volcanism Program Digital Information Series), five of which occurred in the last 21 years (Fig. 8). In particular, four eruptions occurred between 1992 and 2000, while the recentmost eruption occurred after the 2010 Chile earthquake, under unclamping conditions of the magma pathway. The same conditions occurred also after the 1960 Valdivia earthquake, when the Copahue magma pathway was affected by normal stress reduction and the volcano erupted (Bonali et al., 2013). For volcano-earthquake relations, Marzocchi (2002) noted that the largest explosive eruptions of the last Century in the World occurred within 0-5 and 30-35 years after $M_s \geq 7$ earthquakes, at distances up to 1000 km. Postseismic stress changes were interpreted to be capable of promoting eruption in 30-35 years after earthquakes, compatibly to the relaxation time of a viscous asthenosphere (Piersanti et al., 1995, 1997; Pollitz et al., 1998; Kenner and Segall, 2000). Coseismic stress changes are candidate to promote eruptions

in the 0-5 years after earthquakes, where the eruptions occurred at a distance within 100-300 km (Marzocchi, 2002). The time delay of 0-5 years can be attributed to the inertia of the volcanic system in reacting to the static stress changes, to a delay due to a non perfect elasticity of the crust, and/or to the stress corrosion effect (e.g., Main and Meredith, 1991). Instead, for earthquake-aftershocks relations, it was noted that static stress change is capable of inducing rock failure up to 3-5 years after an earthquake (Anderson and Johnson, 1999; Stein, 1999; Hardebeck et al., 1998; Seeber and Armbruster, 2000; R. Stein, written comm., 2012). In fact, from a seismological perspective, the earthquake-induced static stress changes are evaluated to better constrain the distribution of aftershocks and to understand which faults may be close to future failure due to earthquake-induced stress transfer (Stein, 1999). In the studied case, magma pathway failure at Copahue occurred 3 years after the M_w 8.8 2010 earthquake, as testified by recorded seismic signals (OVDAS-SERNAGEOMIN; cfr. § 3.2). This failure was promoted by the earthquake-induced static stress change. Although positive feedbacks due to dynamic and postseismic stress changes could not be excluded, in the Copahue case the earthquake-induced static (permanent) normal stress reduction on magma pathway could have directly promoted dyke intrusion (e.g. Hill et al., 2002; Walter, 2007) at a distance of 257 km, increasing the efficiency of magma rise. Such hypothesis confirms that unclamping of a magma pathway plays an important role in promoting volcanic unrest at volcanoes with deep magma chambers like Copahue.

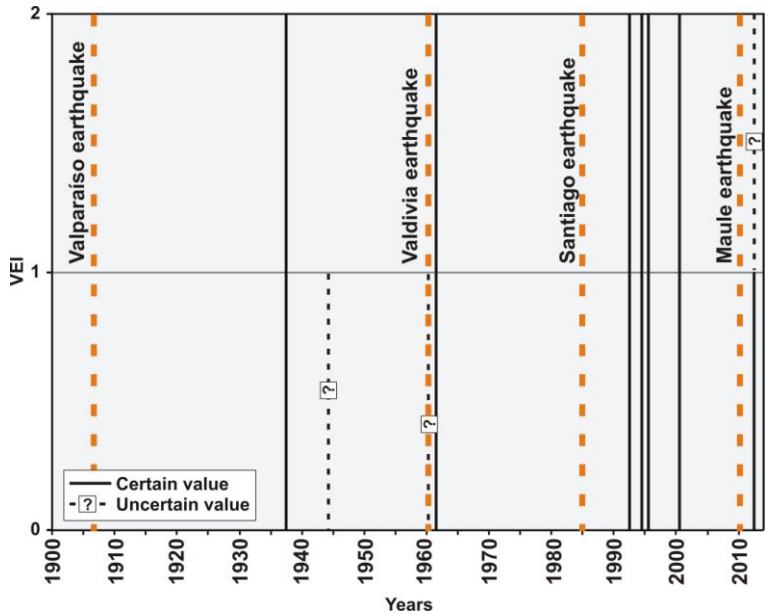

Figure 8. *Significant earthquakes (M_w>8) along the SVZ and eruptions occurred at Copahue volcano since 1900 AD (Global Volcanism Program Digital Information Series). The first day of the reported years is marked. VEI, Volcanic Explosivity Index.*

5.7. Final remarks

The results indicate that the most plausible Copahue magma pathway (vertical and striking N60°E) was affected by a normal stress reduction of -0.258 to -0.147 MPa, induced by the M_w 8.8 2010 Chile earthquake, at a distance of 257 km from the epicentre. A slight unclamping was also induced by the M_w 5.6 2006 earthquake. The sensitivity analysis shows that a similar reduction would have occurred also in the case of N- and E-striking, or inclined N60°E-striking, magma pathways. As a consequence, I suggest a possible earthquake-induced feedback effect on the volcanic arc up to at least 3 years after a large subduction earthquake, provided that the magma pathway is suitably oriented. Furthermore, based on previous studies regarding earthquake-induced static effects, it is advisable to explore the static stress changes induced on the entire volcanic arc close to the 2010 fault zone, in order to define which other volcanoes could have been affected by magma pathway unclamping.

6. Earthquake-induced magma pathway unclamping in promoting eruptions: the Chile case

This chapter is based on the published paper "Bonali F.L.[1], Tibaldi A.[1], Corazzato, C.[1], Tormey, D.R.[2], Lara L.E.[3], 2013. Quantifying the effect of large earthquakes in promoting eruptions due to stress changes on magma pathway: the Chile case. Tectonophysics 583, 54-67", integrated with new unpublished data and methodological improvements from this doctoral work.

[1]Department of Earth and Environmental Sciences, University of Milan-Bicocca, Milan, Italy
[2]Cardno ENTRIX Inc., Los Angeles, CA, USA
[3]Servicio Nacional de Geología y Minería, Volcano Hazards Program, Santiago, Chile

Abstract

Four earthquakes with $M_w \geq 8$ occurred in proximity to 60 Holocene volcanoes, in the Southern Volcanic Zone of the Andes (SVZ) since 1906. We analysed these events by numerical modelling and field data to understand the key attributes of each volcano that may lead to a seismically-triggered eruption, and the general mechanisms by which earthquakes could trigger volcanic new activity. We developed a new approach by resolving the earthquake-induced normal static stress change on the magma pathway of each volcano instead of considering the general crustal volume. We also considered other parameters that may lead to eruption, such as magma chamber depth, magma composition and viscosity, local tectonic settings and volcano dimension. The dataset includes a total of 29 eruptions following large earthquakes, 20 out of 29 represent *first new* eruption occurred at each single volcano. Out of these 20 events, 10 represent eruptions occurred at volcanoes that had no activity in the five years before the earthquake. Results indicate that the static stress change was capable of triggering the observed volcanic phenomena up to a distance of 353 km from the epicentre. *First new* eruptions occurred at volcanoes with shallow magma chambers (2-3 km) under conditions of unclamping or very weak clamping, as well as a*wakening* event. *Awakening* at volcanoes with deeper magma chambers (>7 km) occurred only by magma pathway unclamping. Considering the regional tectonics of the SVZ, 5 volcanoes lying along strike-slip faults, 4 in the thickened and older crust of the fold-and-thrust belt, one along a transition zone and one in the Austral Volcanic Zone, experienced *first new* eruptions. Based

on numerical modelling and statistical analysis, results show that magma pathway unclamping plays a fundamental role in dictating unrest at volcanoes that are already in a critical state up to 2.8 years after a large earthquake. These studies contribute to possible individuation of those volcanoes that are more prone to seismically-triggered eruptive events.

6.1. Introduction

There is a growing acceptance that large earthquakes could trigger volcanic activity (Linde and Sacks, 1998; Walter and Amelung, 2007; Eggert and Walter, 2009; Watt et al., 2009; Delle Donne et al., 2010; Bebbington and Marzocchi, 2011). Linde and Sacks (1998) and Manga and Brodsky (2006) identified a large portion of the 1400-km-long Southern Volcanic Zone of the Andes (SVZ) where eruptions can be rapidly-triggered by large subduction earthquakes; Watt et al. (2009) suggested that the eruption rate increased after the two Chilean earthquakes of August 1906 and May 1960. The above authors suggest a feedback effect between large earthquakes and volcanic eruptions mainly based upon two approaches: i) focusing on the time-relationships between seismic and volcanic events, or ii) the reconstruction of earthquake-induced crustal stress (dilation). One of the main problems in assessing the real triggering effect of earthquakes is that the inherent complexity of the magmatic systems and associated feedbacks might induce eruptions with a delay of days, months or years after the seismic event (Linde and Sacks, 1998; Nostro et al., 1998; Walter and Amelung, 2007; Watt et al., 2009). With longer time delays, it can be difficult to discern a seismically-induced eruption from the normal background rate of eruptions. Understanding the relative importance of the parameters that might control earthquake-induced volcanism is of paramount importance if we are to achieve the goal of predicting this type of volcanic eruption. In the present work we evaluate these parameters by analyzing the four post-1900, $M_w \geq 8$ earthquakes of Chile, and the documented volcanic phenomena (Tab. 1) in the five years following each earthquake (Tab. 2) within a search radius calculated following Delle Donne et al. (2010). We took into consideration the following attributes of each volcano: magma chamber depth, magma rheology, tectonic settings and dimension of volcanic edifice. We applied a new numerical approach to model the earthquake-induced static stress change by resolving it on the magma feeding system reconstructed at each single unrested volcano of the SVZ. This approach produces much higher resolution in the modelled static stress change in comparison to considering only a generalized crustal volume.

6.2. Tectonics and geological background

6.2.1. Tectonics of the Southern Volcanic Zone

The SVZ (33°S-46°S) has over 60 volcanoes considered to have been active during the Holocene (Siebert and Simkin, 2010). Its tectonic setting is characterized by slightly dextral-oblique convergence between the Nazca and South American plate margins that has prevailed for the last 20 Ma (Fig. 1) (Pardo-Casas and Molnar, 1987; Somoza, 1998; Angermann et al., 1999; Cembrano and Lara, 2009). The plate boundary at these latitudes is characterized by a partitioning of deformation with dominant large thrust earthquakes in the subduction zone and intra-arc transcurrent faulting events (Barrientos and Ward, 1990; Cisternas et al., 2005; Watt et al., 2009). The main cordillera is controlled by dextral strike–slip moment tensor solutions dominating between 34° and 46°S (e.g. Chinn and Isacks, 1983; Lange et al., 2008), although field evidence of long-term strike-slip faulting at the surface can be observed only south of 38°S (Fig. 1) (Cembrano and Lara, 2009). This major intra-arc fault system is the 1200 km-long Liquiñe–Ofqui fault zone (LOFZ; Cembrano et al., 1996; Folguera et al., 2002; Adriasola et al., 2006; Rosenau et al., 2006; Cembrano and Lara, 2009). Inversion of fault–slip data for the central and southern Chilean Andes for the Quaternary stress tensor documents a NE-trending sub-horizontal greatest principal stress axis (σ_1) throughout the SVZ between 37°S to 46°S, and a mostly sub-horizontal, NW-trending least principal stress axis (σ_3) (Lavenu and Cembrano, 1999; Arancibia et al., 1999; Cembrano et al., 2000; Potent and Reuther, 2001; Lara et al., 2006a; Cembrano and Lara, 2009). Only in the main cordillera, between 33°S and 34°S, the recorded focal mechanism solutions suggest a switch from strike–slip to reverse faulting with σ_3 becoming vertical (Farías et al., 2006; Pardo et al., 2006; Cembrano and Lara, 2009).

6.2.2. Volcano-tectonics of the Southern Volcanic Zone

Cembrano and Lara (2009) suggested that individual stratovolcanoes and clusters of stratovolcanoes/monogenetic cones of the SVZ show several types of spatial distributions and internal organization with respect to both the overall strike of the volcanic arc and the first and second order active/inactive basement faults. The kinematically-coupled volcano–tectonic associations include individual volcanoes and groups of volcanoes primarily controlled by the present-day contractional (33–34°30′) or dextral–transpressional (34°30′–46°S) tectonics of the volcanic arc, and contractional tectonics of the back arc (33°–38°S), which are in turn responsible for the geometry and kinematics of the second order structures such as tension cracks, shear fractures and volcanic fissures (Cembrano and Lara, 2009).

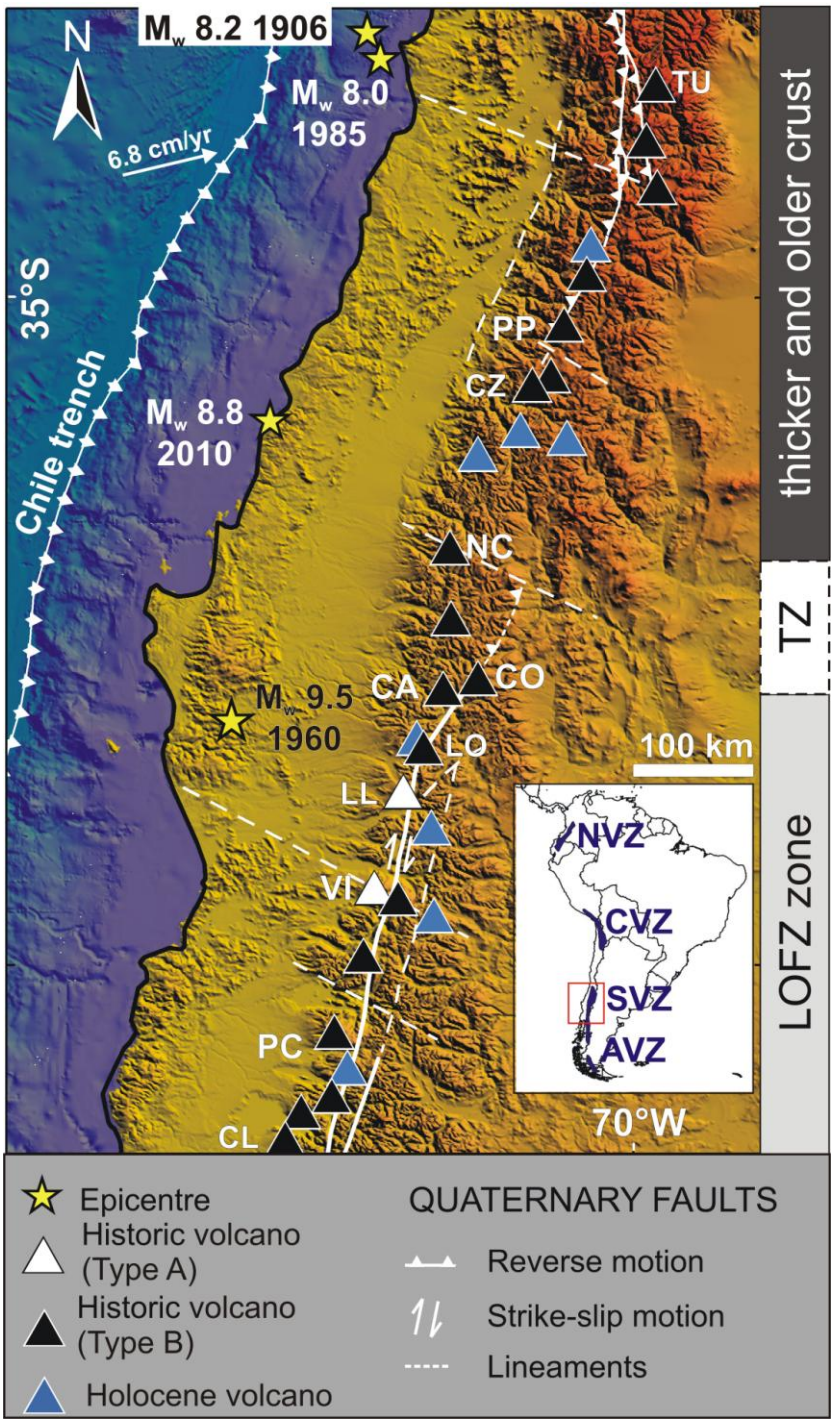

Figure 1. *Volcanoes active historically and in the Holocene belonging to the Southern Volcanic Zone. The white arrow indicates the approximate convergence direction of the plates and estimated velocity. Main intra–arc faults with reverse motion in the north and right-lateral strike-slip motion in the south (redrawn after Cembrano and Lara, 2009) are reported; LOFZ = Liquiñe–Ofqui Fault Zone. TZ = Transition Zone. NVZ = Northern Volcanic Zone, CVZ = Central Volcanic Zone, SVZ = Southern Volcanic Zone, AVZ = Austral Volcanic Zone. TU = Tupungatito, PP = Planchón-Peteroa, CZ= Cerro Azul\Quizapu, NC = Nevados de Chillán, CO = Copahue, CA = Callaqui, LO = Lonquimay, LL = Llaima, VI = Villarrica, PC = Puyehue-Cordón Caulle, CL = Calbuco.*

The kinematically-uncoupled volcano–tectonic association includes individual volcanoes and groups of volcanoes where the spatial distribution and overall morphology is controlled by the inherited basement structures: reverse and strike–slip faults that underlie the volcanic arc or the LOFZ master faults (Cembrano and Lara, 2009). At the arc-scale, crustal tectonics would control whether basaltic magmas reach the surface or evolve to more differentiated products at crustal levels: i) NE-trending volcanic alignments contain mainly basaltic to basaltic-andesitic lithologies in either stratovolcanoes or minor eruptive centres, ii) NW-trending alignments, where only stratovolcanoes occur, include a wide range of compositions with some centres that have erupted only rhyolitic products in historical times (e.g. Lara et al., 2004a,b).

6.3. Methods

Earthquakes with $M_w \geq 8$ occurred close to the SVZ in: 1906 (Valparaiso), 1960 (Valdivia), 1985 (Santiago) and 2010 (Maule). We analyzed the earthquake-volcano interactions induced by these seismic events (Tab. 2) within a search radius for volcanic events based on Delle Donne's et al. (2010) formula: $M = -6.4+2.17\log R_{max}$, relating the earthquake magnitude (M) and the distance (R) defining an empirical maximum distance for volcanic response (R_{max}). Considering the fact that the eruption record catalogue (Global Volcanism Program, http://www.volcano.si.edu/index.cfm) might be incomplete for older events, in order to have a homogeneous data set we consider only the eruptions that occurred certainly in the five years following the earthquake (Fig. 2), with confident location and a reported VEI (Tab. 1). The choice of a five-year investigation is based on the evidence that static stress change is capable of inducing aftershocks up to five years after an earthquake (R. Stein, written comm., 2012). We also evaluated the volcanic activity in the five years before the earthquake. By this way we were able to constrain which volcanoes had new activity due to earthquake-induced static stress change and better understand the seismic trigger. In particular, in this paper "*first new*" activity represents the first new eruption after the earthquake within the five years; "*awakening"* events are the *first new* events that occurred at volcanoes that did not have activity in the five years prior to the earthquake. Similarly to Eggert and Walter (2009) and Walter and Amelung (2007), the analyzed volcanoes are classified in two classes: "Type A" are more or less continuously erupting volcanoes (i.e. more than 20 eruptions since 1900 AD), which are considered as an open-conduit system, and "Type B" are not-continuously erupting volcanoes (less than 20 eruptions). Type A (open-vent) volcanoes cannot have *awakening* events since they are already awake, Type B volcanoes that didn't have eruptions

in the 5 years prior to the earthquake and that experienced *awakening* events are defined "Type B+".

6.3.1. Reconstruction of magma pathway geometry

Basic magma is supplied to the surface mostly along planar, steeply-inclined intrusive sheets that may group to form dyke swarms (Dieterich, 1988; Carracedo, 1994; Moore et al., 1994; Walter and Schmincke, 2002) and eventually volcanic rift zones formed by hundreds of such parallel dykes (Fiske and Jackson, 1972; Walker, 1999). Volcanic rift zones are usually expressed at the surface by aligned pyroclastic centres and swarms of fissures, dykes and faults (Annen et al., 2001; Walter and Schmincke, 2002). Dykes tend to propagate parallel to the horizontal greatest principal stress (σ_{Hmax}), forming aligned parasitic cones (e.g. Nakamura, 1977), thus the alignment of volcanic centres and monogenetic cones can be used to infer the azimuth of local σ_{Hmax} (Johnson and Harrison, 1990; Strecker and Bosworth, 1991). Recent works suggest that a more detailed definition of the magma paths can be determined by combining dyke geometry with a series of morphometric parameters of main craters and parasitic vents (Tibaldi, 1995; Corazzato and Tibaldi, 2005; Bonali et al., 2011). Applying these criteria, the reconstruction of the azimuth of the Quaternary magma pathways (Tab. 1) was based on: i) alignment of vents, overlapping and nested calderas, nested summit craters, parasitic and flank cones, and ii) trend of vents, elongation of volcano edifice or chain, and fissure systems. In the case of those volcanoes resting along strike-slip faults, the magma pathways are assumed as vertical, extending from the surface down to the depth of magma chamber top. In the case of volcanoes lying along reverse/thrust faults, the geometry of the magma pathway is assumed with inclination and dip that mimic the geometry of the reverse fault. All these features were determined using satellite images, DEM-SRTM90 and geological maps, together with the available literature information and field validation.

6.3.2. Numerical modelling

A series of representative numerical models were developed to investigate how tectonic motions along the fault planes (of these four earthquakes) transferred static stress on the magma pathways of the 12 studied volcanoes (Tab. 1), with the aid of Coulomb 3.2 software (www.coulombstress.org; Lin and Stein, 2004; Toda et al., 2005). Such normal stress change can produce a clamping (increase in normal stress) or unclamping (decrease in normal stress) effect on any receiver surface (e.g. a magma pathway/feeder dyke). In particular, the model function "calculate stress on receiver faults", based on Okada (1992)'s formulas, was used to

compute the normal stress change on the receiver magma pathways. The numerical models were computed in an isotropic and elastic half-space defined, for the examined crust portion, by the following properties, based on Mithen (1982), King et al. (1994), Lin and Stein (2004) and Toda et al. (2005, 2008): Young's modulus E = 80 GPa, Poisson's ratio ν = 0.25, and effective friction coefficient μ' = 0.4. In agreement with King et al. (1994), the increase of μ' slightly increases the effects, while dropping the friction to zero reduces them. Lower values of Young's modulus have the effect of reducing the magnitude of static stress changes. The characteristic of the four finite fault models (source faults) for the earthquakes are listed in Table 2. For each four cases the input stress field is based on the T, P, N-axis proposed in the focal mechanism, where σ_1 has a magnitude of 100 bar, σ_2 has magnitude of 30 bar and σ_3 has magnitude of 0 bar (King et al., 1994; Toda et al., 2005,2008). The subvolcanic magma feeding systems that link the volcanoes with their magma reservoirs are assumed as vertical surfaces for most volcanoes, being associated with strike-slip faulting. For volcanoes that overlie thrust faults (Planchon-Peteroa and Tupungatito), the magma pathways are assumed to dip 45° west, based on field data (Cembrano and Lara, 2009). The stress change over the area of interest is calculated at a representative depth of 2 km below the volcano base.

6.4. Results

6.4.1. Volcanic eruptions following the earthquakes

A total number of 29 volcanic eruptions occurred after these four earthquakes at 11 different volcanoes, listed in Table 1. From north to south, they are located in the thickened and older crust of the fold-and-thrust belt (Tupungatito, Planchon-Peteroa, Cerro Azul/Quizapu, Nevados de Chillan), in the transition zone (Copahue), and along the LOFZ (Llaima, Lonquimay, Villarrica, Puyehue-Cordon Caulle, Calbuco; Fig. 1). Few volcanoes erupted more than once following the same earthquake or following more than one earthquake (Tab. 1). A total of 20 out of 29 represent *first new* volcanic eruptions, and 10 out of these 20 represent *awakening* (volcanoes that had no activity in the five years before the earthquakes, all are "Type B+"). Eight out of these 10 *awakening* events experienced unclamping of the magma pathway (Tab. 1). At general level, the number of eruptions classified as *awakening* increases with earthquake magnitude (Fig. 2A), and the latter only one occurred after three years following the earthquakes (Fig. 2B). These events are more represented at a shorter distance from the epicentre (Fig. 2C) and at shallow magma chambers (i.e. only at one deep chamber, Fig. 2D). The historical records report five *first new* eruptions that occurred after the M_w 8.2 August 1906 earthquake (Tab. 1): Tupungatito erupted on 15/02/1907, Villarrica

erupted on 05/05/1907, Cerro Azul/Quizapu erupted on 28/07/1907 (Maksimov, 2007) and both Nevados de Chillán and Llaima erupted in 1907 (sometimes months are not reported). Nevados de Chillán (Type B), Llaima and Villarrica (both Type A) erupted also in the five years before the earthquake; on the contrary Tupungatito and Cerro Azul (both Type B+) had no eruptions. After the M_w 9.5 May 1960 earthquake, 8 *first new* eruptions are reported in the literature (Tab. 1): Puyehue-Cordon Caulle erupted just two days after the earthquake, Planchón-Peteroa erupted on 10/07/1960, Tupungatito erupted on 15/07/1960, Calbuco erupted on 01/02/1961, both Copahue and Villarrica erupted in 1961 (sometimes months are not reported). Llaima erupted in 1964 but moths and day are not reported, Lautaro (Type B) in October 1961. Such volcano is the only one located in the Austral Volcanic Zone. Planchón-Peteroa, Tupungatito and Lautaro (all Type B) and Villarrica (Type A) erupted also in the five years before the earthquake; on the contrary Puyehue-Cordon Caulle, Calbuco and Copahue (all Type B) had no eruptions. After the M_w 8.0 1985 earthquake Tupungatito erupted on 20/01/1986 and Llaima erupted on 25/11/1990 (Tab. 1). Llaima (Type A) had erupted also in the five years before, while Tupungatito (Type B) had no eruptions. Lonquimay (Type B) erupted on 25/12/1988 and had no eruptions in the five years before. Volcanic activity following the February 2010 earthquake, new eruptions occurred along the LOFZ (Puyehue-Cordon Caulle, Villarrica), in the transition zone (Copahue) and in the fold and thrust belt (Planchon-Peteroa) (Tab. 1). After 12 years of inactivity at Planchón-Peteroa volcano (35.2°S), an explosive vulcanian eruption of ash and vapor began on 6 September 2010 and continued until October 2010 (Fig. 3B). Ash plumes up to 7-km-high drifted over a distance of 30 km (OVDAS, http://www2.sernageomin.cl/ovdas/). After a brief period of quiescence, new vapor and ash plumes were reported on 17 February 2011 to at least May 2011 (OVDAS) and a new eruption took place from 17/02/2013 to 25/06/2011. At Villarrica volcano (39.4°S), increased fumaroles were reported the day after the 2010 earthquake (OVDAS). In addition, thermal anomalies (MODVOLC, http://modis.higp.hawaii.edu/; Fig. 3C) became more frequent beginning 5 April 2010 (18 days in April and 14 days in May), seismicity increased accompanied by a rise in the lava lake level, and more vigorous fumarolic and Strombolian activity occurred. Also between April and October 2010, nearly continuous gas plumes were observed from Villarrica (OVDAS). Villarrica has been active since 22 November 2009 to 20 April 2012, but from April 2009 to February 2010 only tremors and thermal anomalies were detected (OVDAS). A new eruption started on 25/07/2013 and finished on 29/07/2013. At Puyehue-Cordon Caulle volcanic complex

(40.5°S), shallow seismicity increased beginning 27 April 2011, and explosive eruptive activity began on 4 June 2011 (Fig. 3A and B).

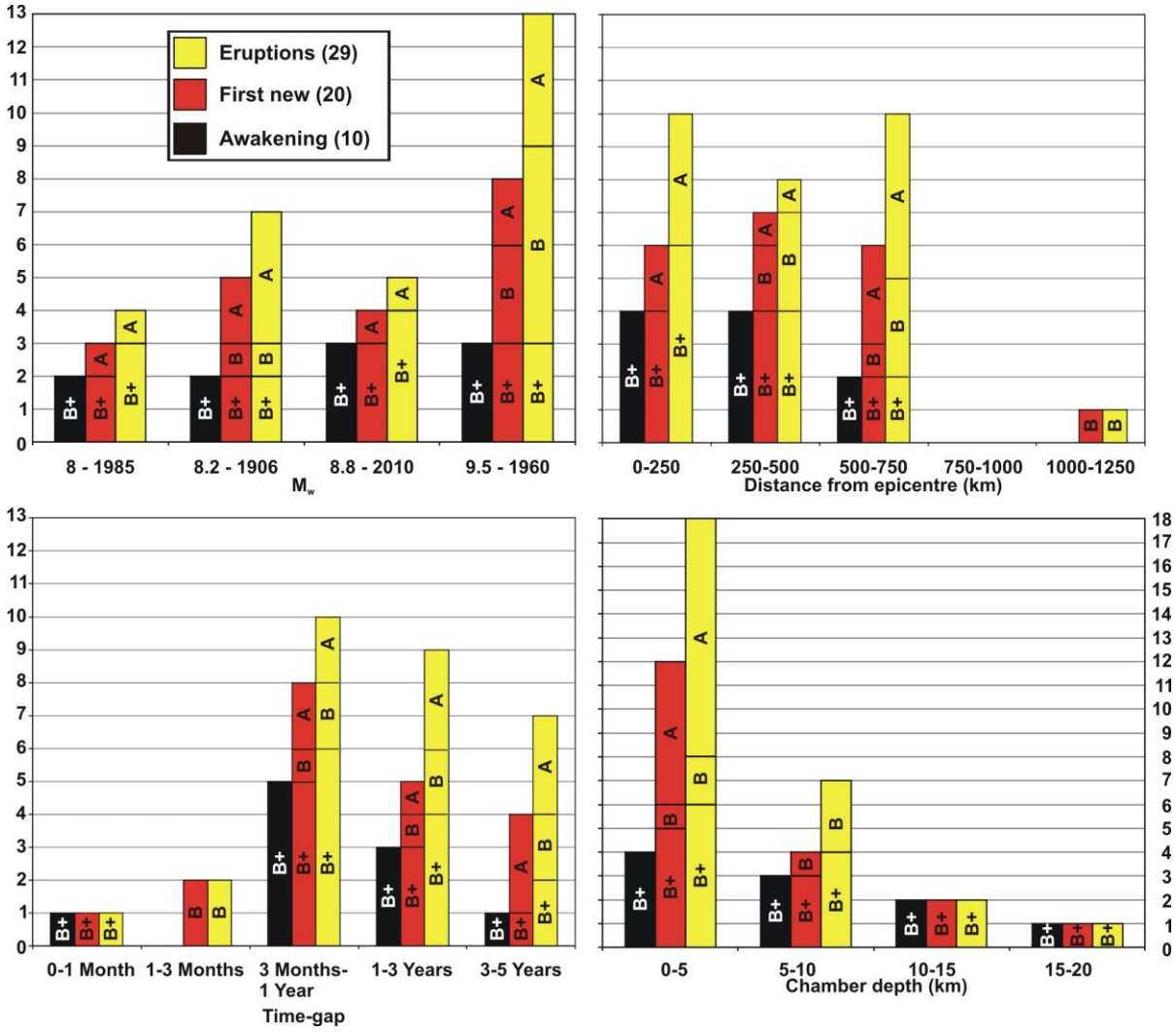

Figure 2. *Volcanic events occurred in the five years following the studied earthquakes, distinguished in Type A and Type B. (A) Number of: volcanic events, first new events and awakening events (volcanoes that had no volcanic events in the five years before the earthquake) versus earthquake magnitude. (B) Number of volcanic events versus time-gap. (C) Number of volcanic events versus the distance from earthquake epicentre (km). (D) Number of volcanic events versus magma chamber depth (km).*

The ash plume rose to an altitude of 14 km and disrupted aviation. A lava flow was observed in the summit area on 20 June (OVDAS). Based on seismicity data and visual observations, OVDAS reported that the eruption from the Puyehue-Cordón Caulle continued up to 21 April 2012 with discontinuous white plume emissions. The Puyehue-Cordón Caulle is a large NW-SE-trending late-Pleistocene to Holocene basaltic-to-rhyolitic transverse volcanic chain.

Historical eruptions are from the Cordón Caulle rift zone. Both Villarrica and Puyehue-Cordón Caulle erupted after both the 1906 and 1960 earthquakes (Siebert and Simkin, 2010). Villarrica (Type A) had activity in the five years before the earthquake, while Planchon-Peteroa and Puyehue-Cordón Caulle (all Type B) had no activity. Furthermore a new eruption started at Copahue (Type B) volcano on 22 Decembre 2012 after 12 years of inactivity. Minor events regard: i) Nevados de Chillan (36.9°S), where field observations detected a new hydrothermal vent approximately 200 m north of the longstanding hydrothermal field, three days after the earthquake; ii) Callaqui (37.92°S), where an ash plume was reported by the Buenos Aires Volcanic Ash Advisory Center (http://www.ssd.noaa.gov/VAAC) based on pilot observation on 2 January 2012; iii) OVDAS reported that during 1-28 February seismicity increased at Descabezado Grande.

6.4.2. Numerical modelling of static stress changes

The computation of static stress changes induced by the earthquakes, resolved on the reconstructed magma pathway (Fig. 4A), indicates that of the 18 *first new* volcanic eruptions (including both eruptions and minor events) occurred at volcanoes that experienced minor increases in normal stress or decreases in normal stress, while two *first new* eruptions occurred at volcanoes that experienced no changes on magma pathway. Seven out of the 20 *first new* eruptions occurred at volcanoes where modelling shows weak clamping (normal stress increase <0.02 MPa); three occurred at volcanoes that experienced minor unclamping (normal stress change between 0 and -0.1 MPa), and the remaining eight events occurred at volcanoes where modelling shows moderate unclamping (normal stress change between -0.1 and -2.277 MPa). Specifically, considering the static stress changes, the 1906 earthquake induced unclamping on Tupungatito (Fig. 4B) and on Cerro Azul/Quizapu (Fig. 4C), and very weak clamping on Nevados de Chillan, Llama and Villarrica (Fig. 4D-E-F). The 1960 earthquake induced very weak clamping on Planchon-Peteroa, Tupungatito (Fig. 5A and B) and Lautaro, while medium-high unclamping was experienced by Copahue, Llaima, Villarrica, Puyehue-Cordon Caulle and Calbuco (Fig. 5C-D-E-F-G). The 1985 earthquake induced weak unclamping on the Tupungatito (Fig. 5H) and no changes on Llaima and Lonquimay (Fig. 5I). The 2010 earthquake induced medium unclamping on Planchon-Peteroa (Fig. 6), Copahue (Fig. 4 chapter 4) and Villarrica (Fig. 7), while it induced very weak clamping on Puyehue-Cordon Caulle (Fig. 8).

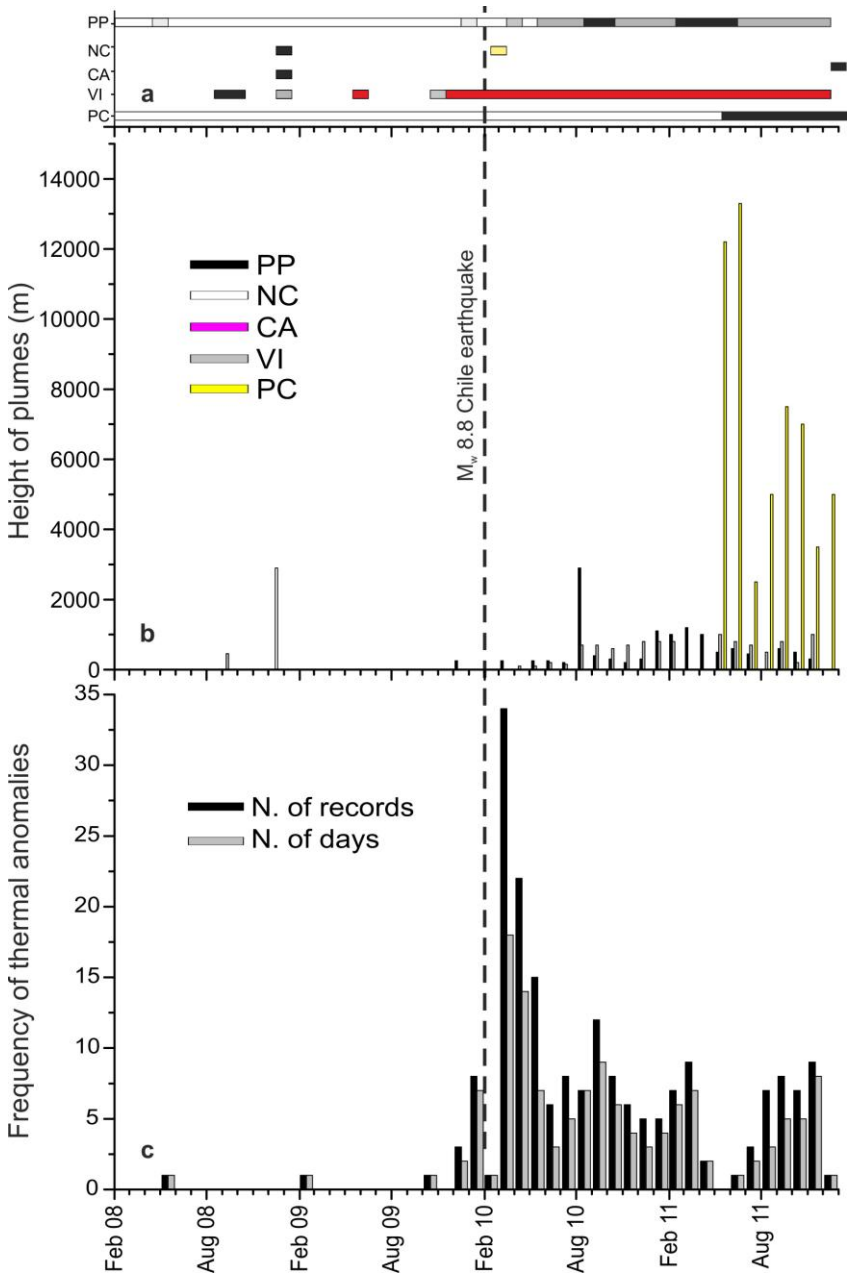

Figure 3. *Available data representing the activity for restless volcanoes from January 2009 to July 2011. Note the very strong increase in activity after the Mw 8.8 earthquake. (A) Plumes and fumarolic activity for restless volcanoes (data from OVDAS; POVI, http://www.povi.cl). White–no activity, light gray–discontinuous fumarolic activity (steam and sometimes gas), dark gray–discontinuous plume activity (gas and sometimes SO2), black–discontinuous ash emissions, red–discontinuous plume emissions with incandescence visible at night, green–new hydrothermal vent opening. (B) Maximum height of plumes (data from OVDAS, Global Volcanism Program). Values for Puyehue-Cordón Caulle (PC) only are out of scale. (C) Number of recorded thermal anomalies and days of anomaly for each month at Villarrica volcano (data from MODVOLC, http://modis.higp.hawaii.edu/). PP = Planchón-Peteroa, NC = Nevados de Chillán, CA = Callaqui, VI = Villarrica, PC = Puyehue-Cordón Caulle.*

6.4.3. Analysis of the eruption rate

It was also compared the volcanic activity in the 50 years preceding each earthquake (e.g. Walter and Amelung, 2007) and in the following years. In particular it has been calculated the eruption rate the 50 years prior to the earthquake (ER-before), while ER-after is calculated for different increasing time-windows, from 0-1 to 0-5 years. Such analysis was done considering the first new eruptions for both Type A and B (volcanoes that do not have a continuously-erupting activity) and also considering the unclamping effect induced by the earthquake. When the ratio ER-after/ER-before > 1, a relation between the earthquakes and the following eruptions is supposed. A first analysis of the eruption rates has done considering all the *first new* eruptions. Such analysis suggests that a relation between the earthquakes and following eruptions may exist for only the 1906 and 1960 earthquakes for time windows of 0-4 and 0-5 years respectively (Fig. 9A). Considering all the *first new* eruptions occurred at volcanoes that suffered earthquake-induced unclamping effect a relation between the earthquakes and following eruptions may exist for only the 1906 and 1960 earthquakes for time windows of 0-1 and 0-2 years respectively (Fig. 9B). It was also analyzed the eruption rate for different type of volcanoes that erupted after the studied earthquakes. In particular the ER-before and ER-after have been calculated Type A and B respectively. Considering all the *first new* eruptions involving volcanoes of Type A, a relation between the earthquakes and following eruptions may exist only for the 1906 earthquake for a time window of 0-3 years (Fig. 9C). Considering all the *first new* eruptions involving volcanoes of Type B, a relation between the earthquakes and following eruptions may exist for all the four studied earthquakes. In particular, for the 1906 earthquake could be considered a time window of 0-3 years, for both 1960 and 2010 earthquakes could be considered a time window of 0-5 years and for the 1985 earthquake could be considered a time window of 0-1 year (Fig. 9D). Considering the eruptions occurred at volcanoes that experienced unclamping these considerations change. In particular there is not a relation between earthquakes and eruptions occurred at volcanoes of Type A under unclamping (Fig. 9E), while a relations exist for volcanoes of Type B (Fig. 9F). In particular, for the 1906 earthquake could be considered a time window of 0-2 years, for both 1960 and 2010 earthquakes could be considered a time window of 0-3 years and for the 1985 earthquake could be considered a time window of 0-1 year (Fig. 9F).

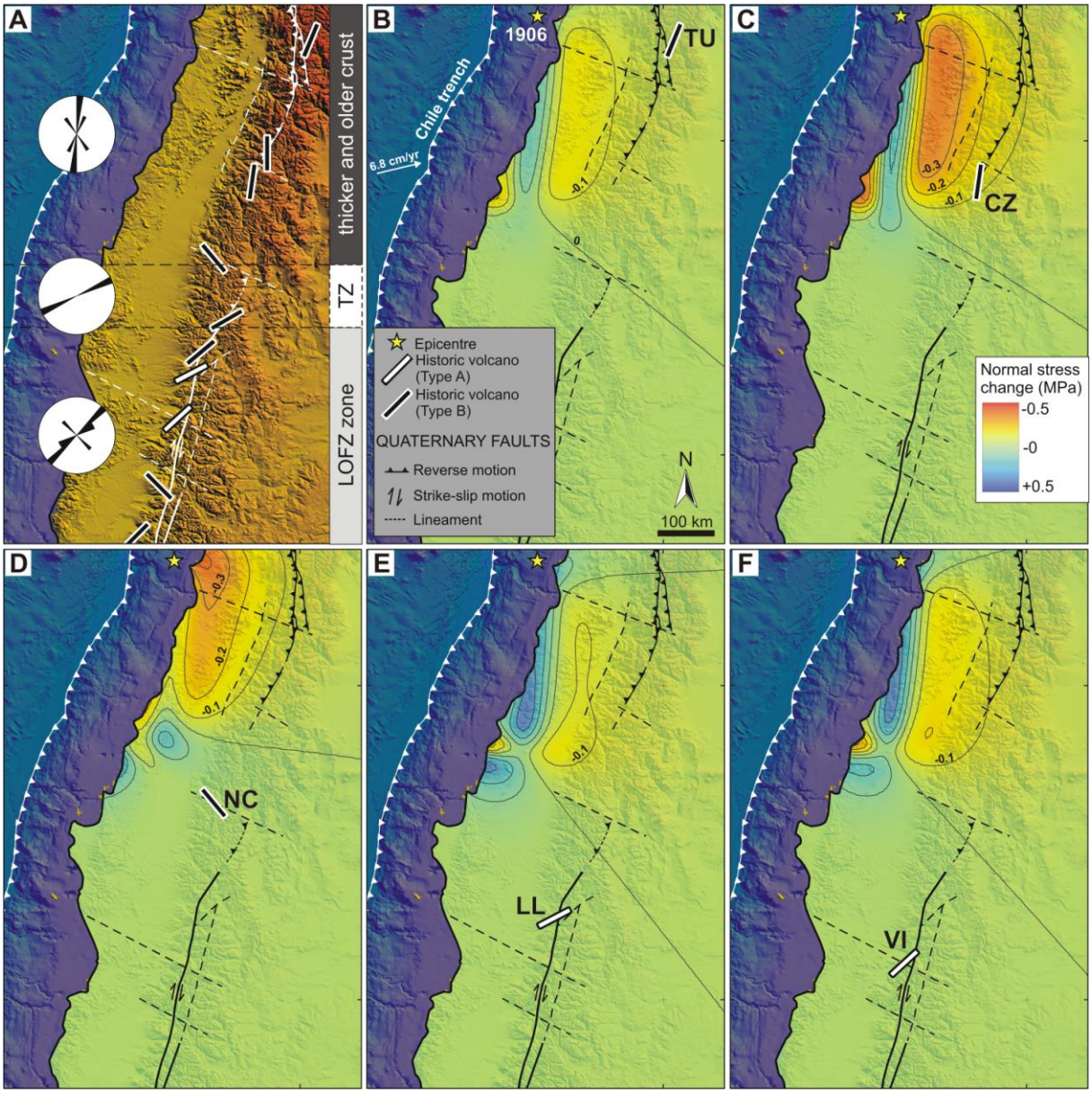

Figure 4. *(A) Reconstructed magma pathway orientation for the studied volcanoes. Each rose diagram shows the azimuth summarized for each tectonic zone. TZ = Transition Zone. (B-F) Normal stress change induced by the 1906 earthquake on the magma pathways of the five volcanoes that erupted in the three years following the earthquake: (B) Tupungatito, (C) Cerro Azul/Quizapu, (D) Nevados de Chillán, (E) Llaima and (F) Villarrica. Red colours represent a normal static stress reduction on the magma pathway, blue colours represent an increase.*

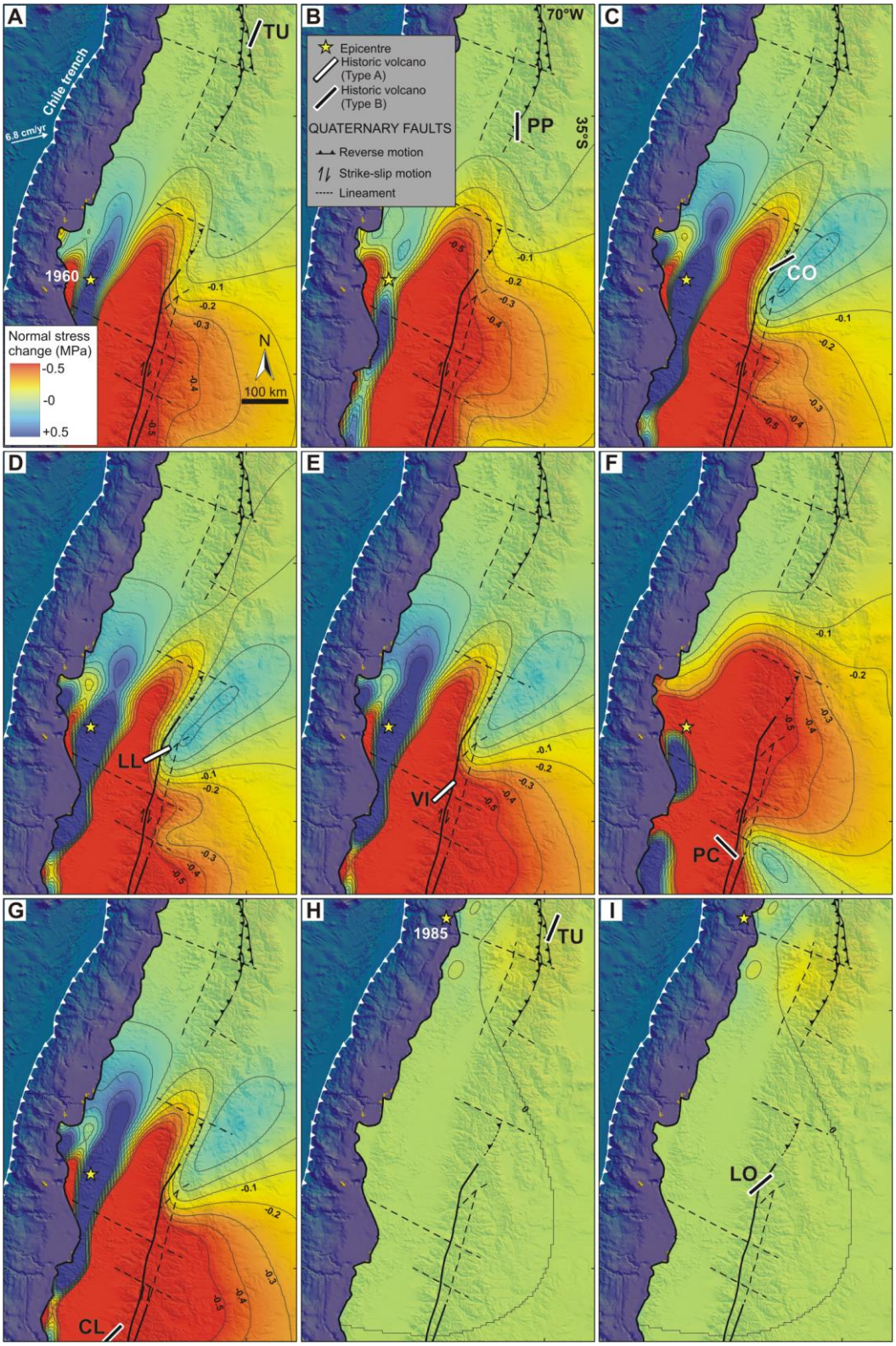

Figure 5. *Normal stress change induced by the 1960 earthquake on the magma pathways of the volcanoes that erupted in the five years following the earthquake: (A) Tupungatito, (B) Planchón-Peteroa, (C) Copahue, (D) Llaima, (E) Villarrica, (F) Puyehue-Cordón Caulle, (G) Calbuco. Normal stress change induced by the 1985 earthquake on Tupungatito (H) and (I) Lonquimay. Red represents unclamping, blue represents clamping*

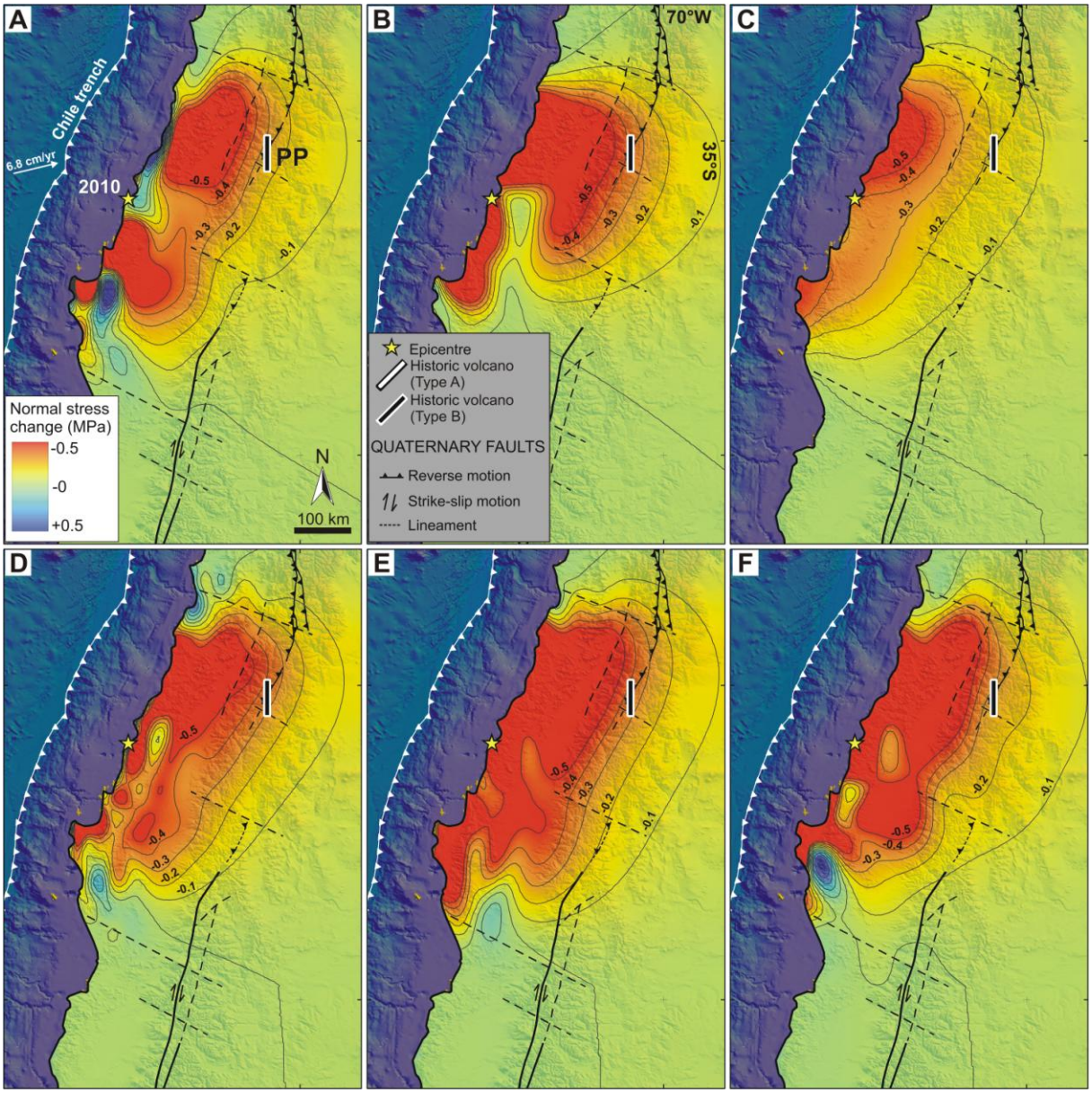

Figure 6. *2010 Earthquake-induced normal stress change resolved on the N-striking Planchon-Peteroa magma pathway (PP), using different finite fault models from: (A) Delouis et al. (2010), (B) Koper et al. (2012), (C) Lin et al. (2013), (D) Pollitz et al. (2011), (E) Lorito et al. (2011) and (F) Vigny et al. (2011), (Tab. 3 Chapter 4). Red colours represent a normal static stress reduction on the receiver plane, blue colours represent an increase.*

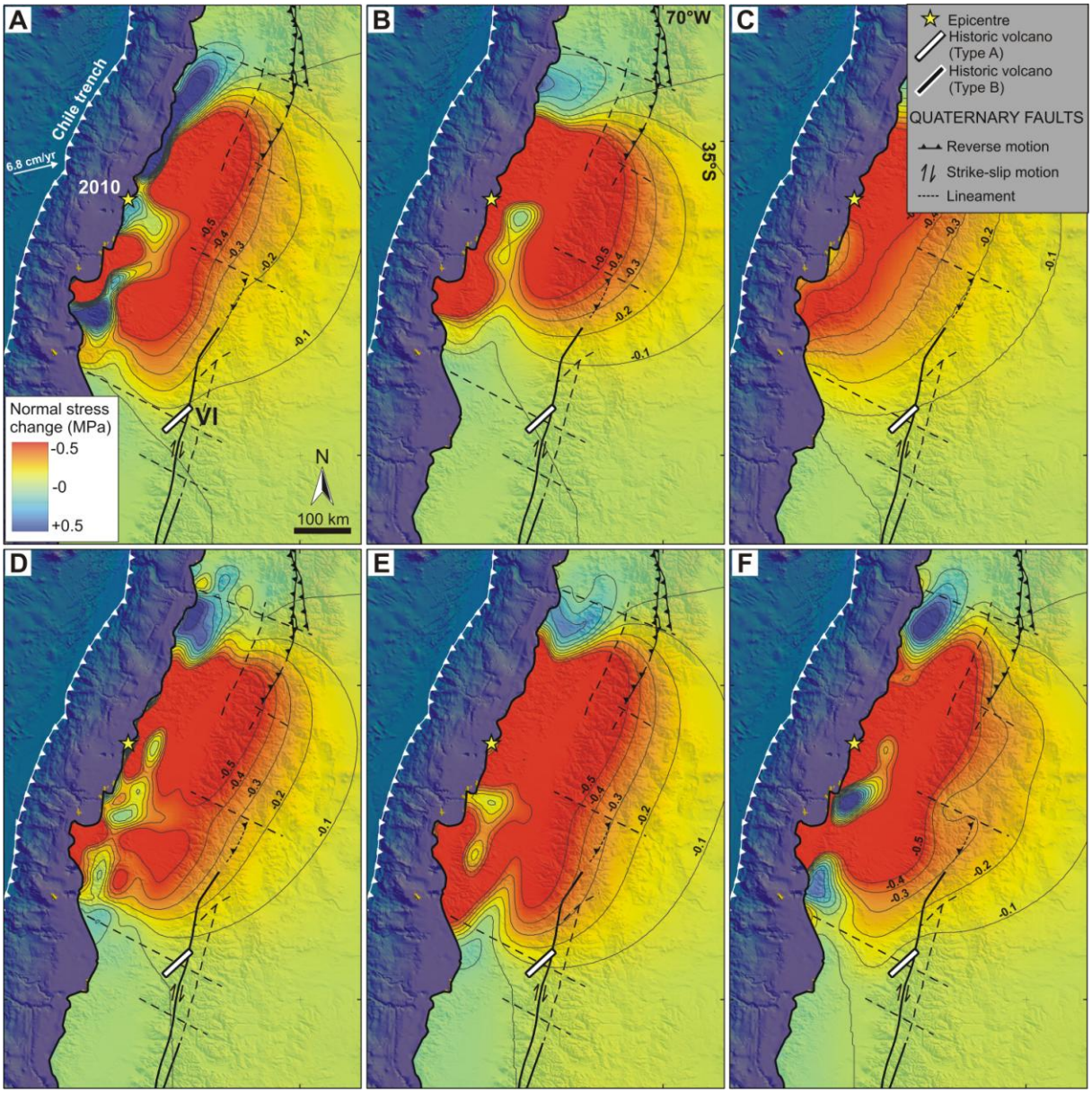

Figure 7. *2010 Earthquake-induced normal stress change resolved on the N47.5°E-striking Villarrica magma pathway (VI), using different finite fault models from: (A) Delouis et al. (2010), (B) Koper et al. (2012), (C) Lin et al. (2013), (D) Pollitz et al. (2011), (E) Lorito et al. (2011) and (F) Vigny et al. (2011), (Tab. 3, Chapter 4). Red colours represent a normal static stress reduction on the receiver plane, blue colours represent an increase.*

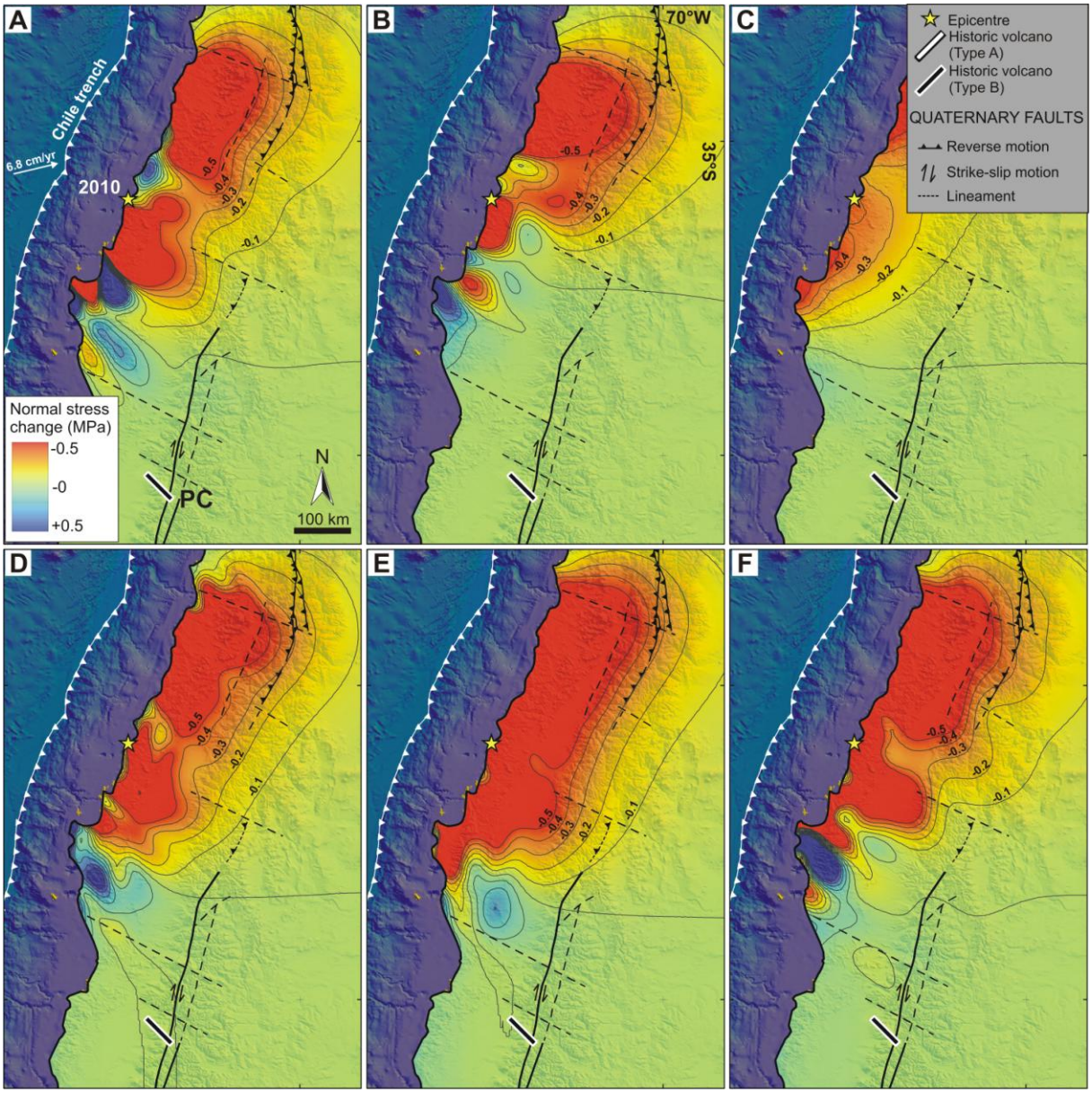

Figure 8. *2010 Earthquake-induced normal stress change resolved on the N135°E-striking Puyehue-Cordón Caulle magma pathway (PC), using different finite fault models from: (A) Delouis et al. (2010), (B) Koper et al. (2012), (C) Lin et al. (2013), (D) Pollitz et al. (2011), (E) Lorito et al. (2011) and (F) Vigny et al. (2011) (Tab. 3, Chapter 4). Red colours represent a normal static stress reduction on the receiver plane, blue colours represent an increase.*

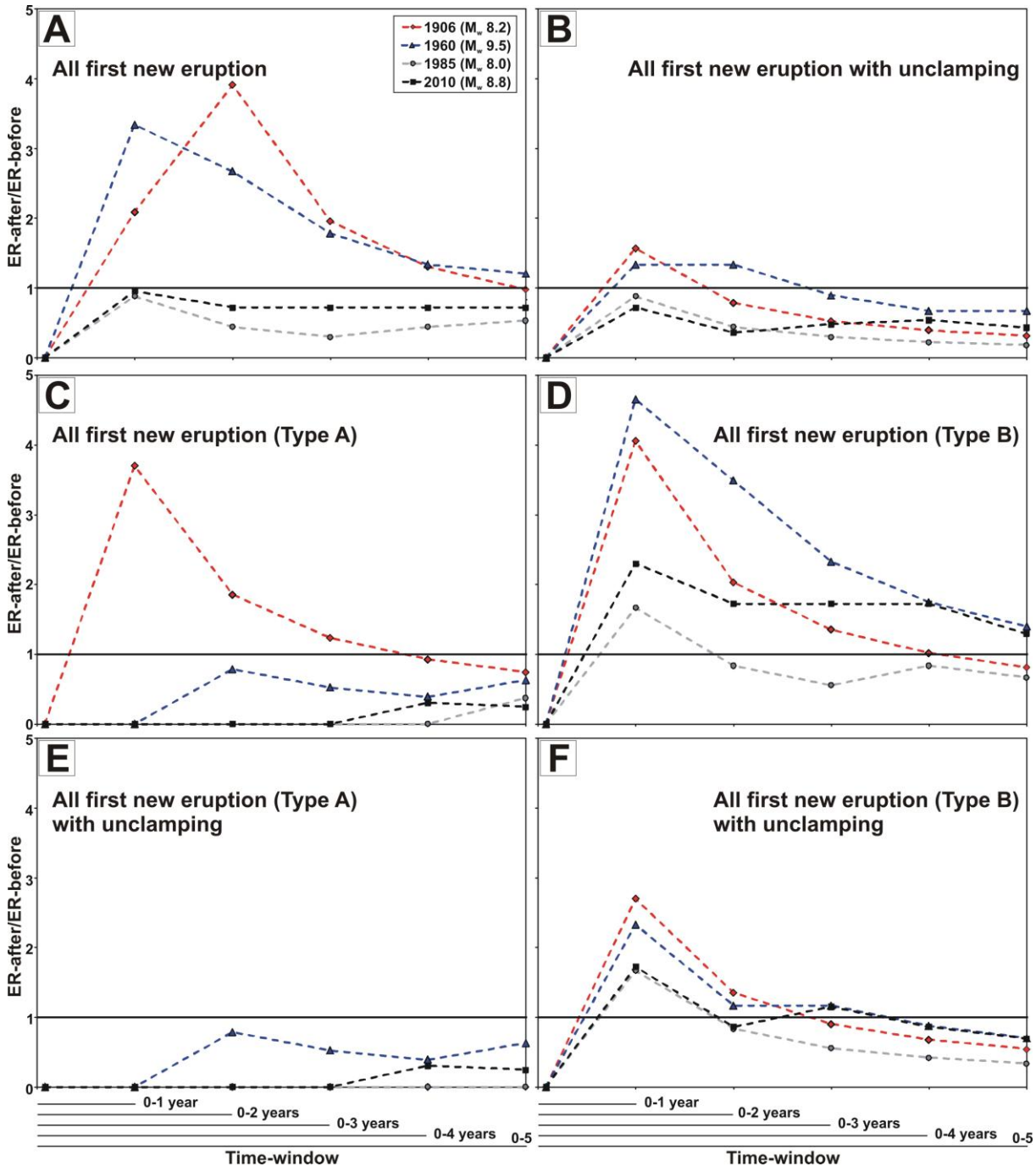

Figure 9. *The graph represents the ratio between the eruption rate (ER) after and before each earthquake (ER-after/ER-before). ER-before is calculated in the 50 years prior to the earthquake, while ER-after is calculated for different increasing time-windows, from 0-1 year to 0-5 years*

6.4.4. Analysis of the primary variables

In this section we compare the available data for the 15 *first new* eruptions (out of 20) occurred only in the time-windows suggested from the eruption rate analysis that has be done for each earthquake. Two out of 15 are the eruptions occurred at volcanoes of Type A, 13 out of 15 occurred at Type B and 9 out of 13 are *awakening events* (Type B+). In particular, to

assess the influence of key volcanic parameters on the feedback between large earthquakes and volcanic events, the following parameters are taken into account: magma chamber depth, silica content of the volcanic products, geometry of the magma pathway, volcano dimension and the tectonic setting of the volcano substratum, distance from the earthquake epicentre and time-gap between earthquake occurrence and *first new* volcanic event.

6.4.4.1. Earthquake-induced static stress change

First new activity took place under very weak clamping (always <0.13 MPa) for both Type A and B, but only in one case it regards an *awakening* (with a large earthquake magnitude and the highest silica content). The other *awakening* events are always under unclamping. Numerical models indicate that the unclamping of magma pathway is higher at closer distances, where the *awakening* events are better represented (Fig. 10A). At large distances, the normal stress change is always null or shows very weak clamping (Tab. 1), as suggested by the class of distance 500-750 km where only one *awakening* event occurred (Fig. 10A). The awakening events are mostly represented within 500 km of distance from the epicentre and in only one case an *awakening* occurred as far as 522 km (Tab. 1). At a general level, *first new* eruptions cluster in the three years after the earthquake, *first new* eruptions didn't occur after 3 years (Fig. 10B). Unclamping promotes *awakening* event that may occur up to three years following the earthquake, and medium and/or high value of unclamping promotes a rapid volcanic response (Fig. 10B and Tab. 1), as where 0-1 month class is present. The energy of the volcanic events may increase with the amount of unclamping, as suggested by the *awakening* events that occurred under unclamping (Fig. 10C). Furthermore it is possible to note that among these events, those with higher VEI values occur at greater distances (Fig. 10A and 10C). Silica content spans 52% to 69% (wt) (Tab. 1): Type A is exclusively characterized by the lowest silica content (about 52% wt) and by shallow chamber depth (Fig. 10D and 10E), Type B is characterised by a higher silica range (63-70%) for shallow depths, and lower silica values (55-60.5%) for deeper chambers with only one case with high silica content (about 67-68%). Magma pathway unclamping increases the occurrence of events at volcanoes with high silica content (Fig. 10D), as particularly shown by *awakening* events; in only one case a high silica content eruption occurred in no unclamping state, at large distance. The amount of unclamping is compared to the depth of magma chamber in Figure 10E. Events at Type A volcanoes correspond only to chambers at shallow depth. *Awakening* events occurred under unclamping, with only one exception for a shallow chamber and high silica content; *awakening* at the deepest chamber occurred under the

highest value of unclamping. It seems that the *awakening* events are associated to a general trend of silica decrease with depth (Fig. 10D and 10E).

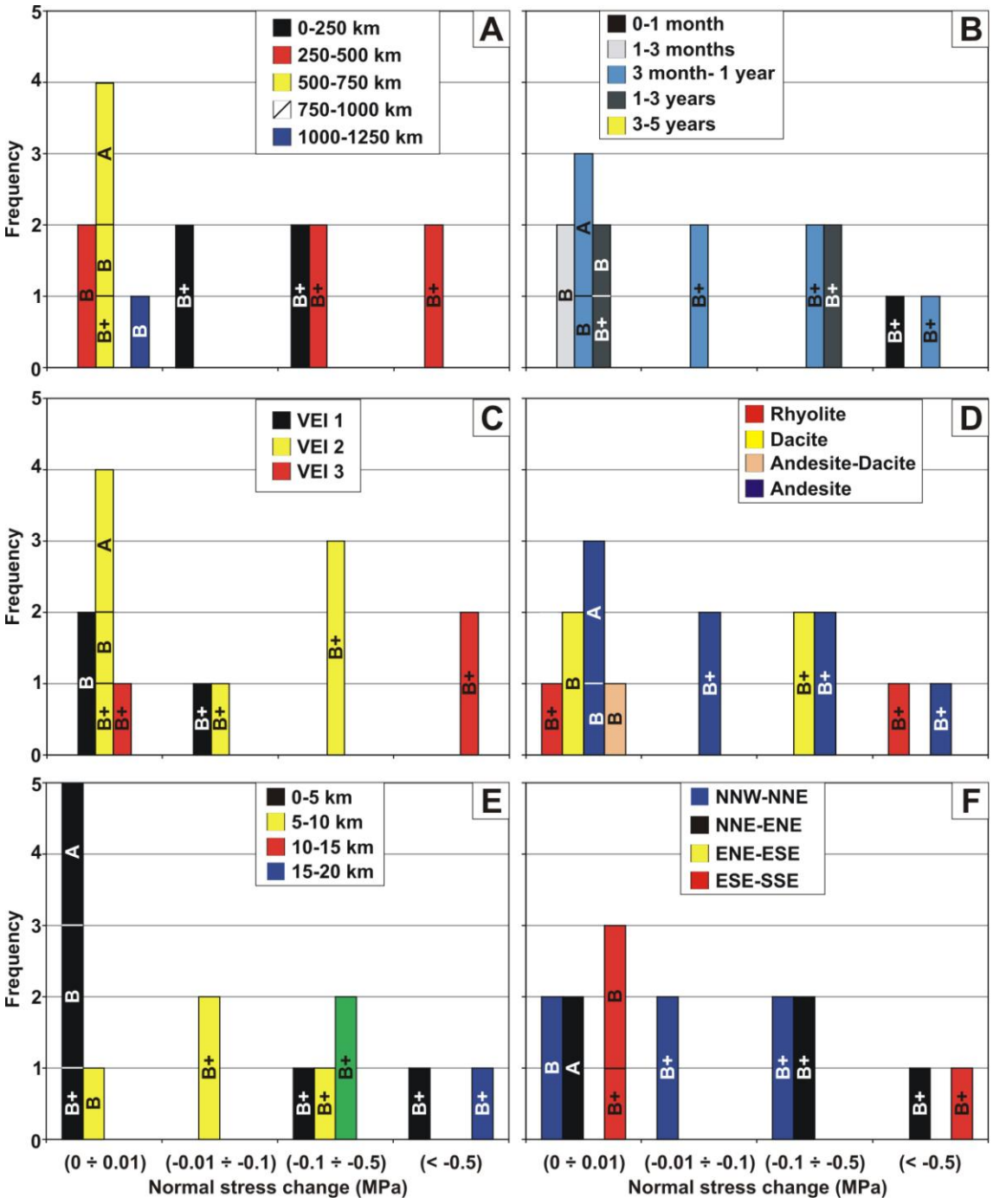

Figure 10. *(A) This graph shows that the first new eruptions occurred under clamping/unclamping and, this correlation is stronger for events of Ttype B at no larger distance. Normal stress change versus: (B) time-gap, (C) VEI, (D) silica content, (E) depth of magma chamber and (F) azimuth of magma pathway. A = Type A volcanoes, B = Type B volcanoes that had eruptions in the five years before the earthquakes, and B+ = volcanoes that had no eruptions in the five years before the earthquakes (awakening events).*

Considering the distance from the epicentre, the depth of magma chamber and the amount of unclamping (Fig. 10A and 10E), it can be seen that: i) shallow magma chambers are present at all distances from the related earthquake epicentre, ii) for such chambers, *awakening* events occur only once at a distances as far as 522 km (Tab. 1), iii) the maximum distance at which an *awakening* can occur decreases with increasing chamber depth, and iv) events at deeper chambers are present within a distance of 500 km and are under unclamping (Fig. 10A and 10E). The time-gap for the *awakening* events shows the widest range for shallow magma chambers, spanning from 2 days to 462 days, whereas this range narrows for deeper chambers to 183-1029 days (Tab. 1). With regard to the azimuth of magma pathways, it can be seen that: i) magma pathways striking in the range NNE-SSW to ENE-WSW are the most represented, and Type A is represented only in this class; ii) magma pathways striking about NW-SE belong all to Type B, along with those striking about N-S; iii) *awakening* events occur associated to a wider azimuth range (Fig. 10F).

6.4.4.2. Tectonics

Five of the 15 *first new* eruptions occurred in the strike-slip fault zone (south of 38°S), while 2 occurred in the transition zone and 7 occurred in the thrust-fault zone (north of 37°S, according to Cembrano and Lara, 2009), while only one occurred in the Austral Volcanic Zone. Differences in silica content are reported between these zones: in the thrust-fault zone, silica content ranges from 60.5 to 68 %, whereas in the strike-slip fault zone it ranges from 52 to 70 % (Fig. 1 and Tab. 1). Another important correlation is the orientation of the magma pathways, with an azimuth ranging N-S to NNE-SSW in the thrust-faults zone, and prevailingly NE-SW to ENE-WSW in the strike-slip fault zone, along with a less represented NW-SE azimuth range (Fig. 4A). Type A is represented only in the NE-SW azimuth range (Tab. 1). Shallow chambers are present in both tectonic settings; those with a top depth of 7 km are present only in the thrust-fault zone, while the two deepest chambers are present in the transition (Copahue) and strike-slip zones (Calbuco) (Fig. 1 and Tab. 1). *Awakening* events at volcanoes that overlie thrust-faults occurred after 183 days (*first new* activity occurred after 49 days), while in the strike-slip zone the *awakening* (and *first new* activity) occurred after 2 days, and in the transitional zone after 405 days (Fig. 1 and Tab. 1). The range in time-gap between the earthquake and the *awakening* spans from 2 to 462 days in the LOFZ zone, while it spans 183-346 days in the fold and thrust-belt; the highest VEI associated to an *awakening* is recorded in the LOFZ. The epicentre-volcano distance is

represented by a 192-316 km range in the fold and thrust-belt and by a 281-522 km range in the LOFZ (Fig. 1).

6.5. Discussion

6.5.1. Earthquake-induced stress changes in promoting awakening event

Linde and Sacks (1998) suggested that an earthquake can induce explosive eruptions up to a distance of 750 km after large earthquakes due to static and dynamic effects. Walter and Amelung (2007) provided numerical models for the four largest earthquakes in the World since 1900 A.D. ($M_w \geq 9$), suggesting that the M_w 9.5 1960 seismic event of Chile induced crustal volumetric dilation below the volcanic arc. In particular Cordón Caulle, Calbuco, Villarrica, and Copahue volcanoes were candidate to erupt. Eggert and Walter (2009) suggested that after a large earthquake ($M_s \geq 7$), the number of eruptions increases at a closer distance from the epicentre (0-250 km), and that such evidence is stronger for not-continuously erupting volcanoes (Type B).

Our data suggest that: i) the number of *awakening* events increases with earthquake magnitude (Fig. 2A), and ii) *awakening* events occur within a distance of 522 km. The number of volcanoes subjected to unclamping increases with earthquake magnitude due to a larger fault slip that is capable to affect magma pathways at larger distances (Fig. 10A): 8 out of 9 *awakening* events occurred under unclamping conditions at distances ranging from 166 to 353 km. Earthquake-induced unclamping by the M_w 8.0 1985 earthquake promoted the *awakening* of Tupungatito, at a distance of 192 km. The M_w 8.2 1906 earthquake promoted the *awakening* of both Tupungatito and Cerro Azul/Quizapu due to unclamping as far as 316 km. Planchón-Peteroa and Copahue volcanoes experienced unclamping due to the M_w 8.8 2010 earthquake, which encouraged new eruptions to a maximum distance of 257 km. The M_w 9.5 1960 earthquake-induced unclamping and consequent *awakening* at Cordon Caulle, Calbuco and Copahue volcanoes as far as 353 km. These results agree with Manga and Brodsky (2006), who suggested that static stress changes may explain processes leading to eruption relatively close to the fault rupture zone and that such stresses decay rapidly with distance. Our results are consistent also with Hill et al (2002) and Walter (2007) who suggested that a decrease in normal stress on the feeding system (unclamping) directly promotes dyke intrusion. In our case, the unclamping-induced *awakening* events always occurred at distances lower than the maximum value of 750 km proposed by Linde and Sacks (1998).

6.5.2. Weak clamping, magma chamber depth and silica content

The only one *awakening* event occurred in very weak clamping conditions: the post-2010 Puyehue-Cordon Caulle eruption (Fig. 3). The analysis of our dataset suggests that *awakening* in very weak clamping state may occur in case of a shallow magma chamber. In fact, shallow chambers at restless volcanoes are present at all distances from the related earthquake epicentre as far as 522 km. On the contrary, *awakening* events associated to deeper chambers occur at shorter distances (≤ 353 km), where an unclamping effect is present.

Woods and Pyle (1997) suggested that pressure evolution of the magma stored in the crust is sensitive to depth, due to cooling and crystallization. For shallow chambers, magma can become vapour-saturated on emplacement, and inter-eruption time-scales are greater for deeper chambers (Woods and Pyle, 1997). Most of the pressure change induced by static stress may be accommodated by the gas phase because its compressibility exceeds that of the melt and of chamber walls. In shallow chambers huge amounts of gas are presents. Since shallow chambers are more prone to be vapour-saturated, this implies that they are more sensitive to earthquake-induced effects because the internal pressure is already high and an external perturbation may promote further gas exsolution/dissolution from the melt, enough to reach the critical overpressure value. In contrast, at deeper magma chambers, magma may be far from vapour saturation conditions, and therefore may not give rise to *awakening* events unless direct unclamping of the magma feeding system occurs. The silica content of the magma appears to be another sensitive parameter, since most of the volcanoes that underwent *awakening* had high silica values (Fig. 10D). Previous volcanic models suggest that basaltic-andesite magmas remain unsaturated unless the pressure is very low or the water content is high (Woods and Pyle, 1997). Also in the case of shallow basaltic-andesite magma chambers, a significant amount of crystallization occurs before the magma becomes gas-saturated. Thus, the probability of inducing sufficient overpressure due to earthquake-induced stress changes is higher for high-silica magma reservoirs. In summary, for the *awakening* events that occurred in a very weak clamping condition, our analysis suggests that magma is always stored at shallow depth, where a vapour-saturated condition is generally expected (Woods and Pyle, 1997). In any case, the static stress change cannot be claimed as a triggering factor and thus another explanation is required and will be given in the next section.

6.5.3. Dynamic stress change

For those volcanoes where static stress change produced weak clamping, an alternative explanation for the eruption-triggering factor must be found. The very weak values of clamping exclude a "toothpaste" or "flask" process due to permanent deformation (e.g. Bautista et al., 1996). Although in this paper we focused only on static stress change, we cannot exclude that also another type of stress change might have produced some triggering effect; in fact, an earthquake generates also dynamic stress changes (transient) (Hill et al., 2002; Manga and Brodsky, 2006). Earthquake-generated seismic waves travel at great distances without losing much of their energy (Hill et al., 2002) and dynamic stress change decreases more slowly than the static stress changes (Hill and Prejean, 2007). Furthermore, dynamic stresses produce greater pressure changes, although these last only seconds (Eggert and Walter, 2009). Such dynamic stress changes may excite and promote ascent of gas bubbles, and consequently magma ascent (Manga and Brodsky, 2006), the details of the feedback mechanisms remaining unclear. Dynamic stresses can also favour bubble growth, including adjective overpressure (Linde et al., 1994), rectified diffusion (Brodsky et al., 1998) and shear strain (Sumita and Manga, 2008). Regarding the rectified diffusion, Ichihara and Brodsky (2006) suggest that such process can cause only a slight pressure increase. In our studied cases, the passage of the seismic wave (dynamic stress) may have encouraged gas exsolution, ascent of gas bubbles and consequently magma rise (Manga and Brodsky, 2006). Shallow magma chambers and high silica contents may be both factors that reflect conditions where seismic wave interactions increase the probability of volcano *awakening* in areas affected by large earthquakes.

6.5.4. Role of tectonic settings

Seven of the 15 *first new* events occurred in the older and thicker crust of the fold and thrust belt at Type-B volcanoes, and four are *awakening* events. Actually, in this area all historical volcanoes are Type-B (Fig. 1), possibly suggesting that this contractional tectonic setting does not favour the maintenance of open magma conduits. The present tectonic state of stress is characterized by horizontal σ_1 and σ_2, a situation that discourages magma upwelling, although more and more active volcanoes in contractional tectonic settings are being reported in the literature (e.g. Tibaldi, 2008; for a review, Tibaldi et al., 2010). N0° to N25°E orientation of magma pathways dominates this zone, being parallel or subparallel to the local strike of the faults. This may imply a direct control of substrate faults on magma pathway

orientation, similarly to the model proposed by Tibaldi (2008). Magma reaches the surface when its pressure is larger than σ_2 if this stress axis lies in the horizontal plane, or when it is larger than σ_3 if there is a very local rotation of the stress tensors with σ_3 assuming a horizontal dip as suggested by Galland et al. (2007). In this contractional zone, the four *awakening* events always occurred under unclamping conditions that may have directly promoted dyke intrusion (Hill et al., 2002; Walter, 2007), irrespective of the tectonic horizontal buttressing.

South of this thrust zone, where strike-slip faulting is predominant (LOFZ, south of 38°S), five *first new* eruptions occurred at both Type A and Type B volcanoes (Fig. 1), along vertical magma pathways with horizontal σ_1 and σ_3. A lower silica content than observed in the thrust-fault zone and the presence also of Type A volcanoes, suggests that a σ_3 lying on the horizontal plane favours magma upwelling and the possibility of preserving more open magma conduits. Another characteristic of this strike-slip fault zone is a predominance of shallow magma chambers with only one deeper chamber. Along the strike-slip LOFZ, most magma pathways strike N40° to N60° (Fig. 4A); this orientation is perpendicular or oblique to σ_3, suggesting that magma uses tension cracks or R' shear planes respectively. Instead, the NW-SE-striking magma paths at two historic volcanoes (Nevados de Chillan and Puyehue-Cordon Caulle) are not easily explained and need further field investigations to elucidate the local Holocene to Present day fault geometry and kinematics.

Different tectonic settings may also influence the time-gap between the earthquake and the volcanic events: i) the *first new* events at volcanoes that overlie thrust-faults occurred after 49 days (*awakening* events after 183 days), and ii) in the LOFZ both *first new* and *awakening* events occurred after 2 days. At a general level, the time-gap between the earthquake and the *awakening* decreases with increasing unclamping (Fig. 10B). This should reflect the larger energy made available by greater earthquakes, which produces larger stress changes capable of overcoming the buttressing exerted by the host-rock or inducing magma overpressure (Manga and Brodsky, 2006). In addition, the highest VEI are reported in the LOFZ associated with the three *awakening* events.

6.5.5. Volcano type and dimensions

Volcanoes of Type B have high values of silica contents that may explain the predominance of the related high values of VEI (2-3). Furthermore, such volcanoes appear capable of erupting at the greatest distance with the highest VEI, and with the two largest earthquake

magnitudes (e.g. Puyehue-Cordon Caulle post-2010 earthquake eruption, Fig. 10A, 10E), suggesting an important role of both seismic wave and static change interactions with crustal fluids in promoting eruptions. Additionally, Type B subvolcanic systems appear to be mostly sealed in the uppermost part due to larger periods of volcanic quiescence and thus dyke cooling, and a larger internal pressure is necessary to open the sealed cracks in order to reach the surface, compared to Type A volcanoes with more open conduits; this internal force reveals with a higher VEI once eruption occurs.

Regarding volcanic edifice dimensions, we found a quite large variability in height among reactivated volcanoes, from 1397 to 2447 m, and very different associated volumes. It has been proposed that the volcanic mass may have effects on magma pathways: increasing load can prevent vertical magma ascent in a volcano axial zone (Kervyn et al., 2009, and references therein). These authors suggested that a key control is the relative magnitude of the dyke driving pressure and edifice load-induced stress; in our study the driving pressure induced by earthquake stress changes is the key factor since our reactivated volcanoes have different dimensions.

6.5.6. Implications for volcanic hazard

The SVZ has had more than 17 earthquakes with M_w greater than 8 since 1750 AD, and thus other large earthquakes are expected in the near future. Our study shows that static stress changes can promote volcano *awakening* after large earthquakes, although other parameters influence whether any individual volcano will erupt. The inherent complexity of magmatic systems, with feedbacks between magma composition, rheology, storage depth, state of volatile saturation and overpressure, and complexity of the magma pathways, together dictate the specific magmatic course followed at a given volcano after large earthquakes. Owing to this complexity, the delay between the earthquake and the volcanic events can be days, months and up to three years. This study helps to constrain the volcanoes that may pose an eruption hazard following a great earthquake. Given a suitable knowledge of the geometry of the magma pathway, the depth of the magma chamber and the tectonic setting, volcanic hazard following great earthquakes could be reasonably assessed.

6.6. Conclusions

I analysed the static stress change induced by four earthquakes with $M_w \geq 8$, which occurred in the Southern Volcanic Zone (SVZ) of Chile since 1906 AD, in order to contribute to understanding the general mechanisms by which earthquakes could trigger new volcanic

activity. I developed a new approach by resolving the earthquake-induced normal static stress change on the magma pathway of each volcano. I also considered other parameters that may lead to eruption, such as magma chamber depth, magma composition and viscosity, local tectonic settings and volcano dimension. The dataset includes a total of 20 *first new* eruptions where the analysis of the eruption rates suggest that 15 out of 20 are related with the earthquakes.

Results indicate that the static stress changes calculated at each single magma pathway depict a more complicate pattern than considering instead the general crustal volume. Unclamping of magma pathway plays a fundamental role in promoting volcano *awakening* at a maximum distance of 353 km from earthquake epicentre, in particular it is a key factor to promote volcano *awakening* at deep magma chambers (>7 km). Its role is also important for shallow chambers (2-3 km), which are expected to be more prone to a critical state due to magma overpressure induced by cooling and crystallising.

Our analysis also suggests that volcanoes characterized by shallow magma chamber and high silica contents (Type B) are good candidates to erupt up to a distance of 522 km, where earthquake-induced dynamic stress may play an important role in triggering volcanic activity under very weak clamping.

In the contractional setting of the fold and thrust belt, volcanic *awakening* occurred due to unclamping, while along the strike-slip Liquiñe–Ofqui fault zone, a rapid volcanic feedback has been more favoured despite smaller stress changes up to a distance of 522 km from earthquake epicentre.

This approach combines a more detailed analysis of static stress changes, linked to the geometry of the magma plumbing system at each volcano, and the analysis of the eruption rates, with other parameters such as silica content, magma chamber depth and tectonic settings. Such approach may contribute to recognize the volcanoes prone to earthquake-induced unrest.

TABLES

Earthquake	Volcano name	Type	Silica (% wt)	Distance (km)	Time-gap (days)	VEI	N.S.C. (MPa)	P-E activity	M.P. (azimuth)	M.C. depth (km)	Height (m)	E.R. analysis
First new volcanic events												
Valparaiso (1906)	Tupungatito	B+	60.5 [2]	210	183	2	-0.044	N	N22.5°E	7-10 [1,2,3]	2000	Y
Valparaiso (1906)	Villarrica	A	52.04-52.71 [5]	712	262±4	2	0.003	Y	N47.5°E	2-3 [1,3]	2447	Y
Valparaiso (1906)	Nevados de Chillan	B	66.6-67.6 [8,9]	432	318±182	1	0.010	Y	N140°E	2-3 [1,2,3]	1912	Y
Valparaiso (1906)	Llaima	A	52.04-52.71 [16]	632	318±182	2	0.005	Y	N62.5°E	2-3 [1,3]	1925	Y
Valparaiso (1906)	Cerro Azul (Quizapu)	B+	67-68 [4]	316	346	2	-0.191	N	N8°E	7-10 [1,2,14]	2288	Y
Valdivia (1960)	Puyehue-Cordon Caulle	B+	68.9-70.01 [12]	281	2	3	-0.512	N	N135°E	2-3 [1,3]	2447	Y
Valdivia (1960)	Planchon-Peteroa	B	63.05-63.12 [11]	391	49	1	0.013	Y	N0°E	2-3 [7]	2107	Y
Valdivia (1960)	Tupungatito	B	60.5 [2]	603	54±5	2	0.005	Y	N22.5°E	7-10 [1,2,3]	2000	Y
Valdivia (1960)	Calbuco	B+	55.76-56.48 [6]	353	255	3	-2.277	N	N45°E	18-24 [6]	1803	Y
Valdivia (1960)	Copahue	B+	54.9-56.9 [13]	166	405±182	-	-0.138	N	N60°E	9-20 [10]	1397	Y
Valdivia (1960)	Villarrica	A	52.04-52.71 [5]	169	405±182	1	-0.823	Y	N47.5°E	2-3 [1,3]	2447	N
Valdivia (1960)	Llaima	A	52.04-52.71 [16]	127	1501±182	2	-0.167	Y	N62.5°E	2-3 [1,3]	1925	N
Valdivia (1960)	Lautaro	B	60.5-67.5 [17, 18]	1207	511±15	2	0.001	Y	NW-SE	-	1670	Y
Santiago (1985)	Tupungatito	B+	60.5 [2]	192	323	1	-0.035	N	N22.5°E	7-10 [1,2,3]	2000	Y
Santiago (1985)	Llaima	A	52 [16]	605	1820	1	0.000	N	N62.5°E	2-3 [1,3]	1925	N
Santiago (1985)	Lonquimay	B+	63.8 [5]	571	1393	3	0.000	N	N50°E	2-3 [1,3]	?	N
Maule (2010)	Planchon-Peteroa	B+	63.05-63.12 [11]	210	191	2	-0.398 ÷ -0.197	N	N0°E	2-3 [7]	2107	Y
Maule (2010)	Puyehue-Cordon Caulle	B+	68.9-70.01 [12]	522	462	3	0.000 ÷ 0.005	N	N135°E	2-3 [1,3]	2447	Y
Maule (2010)	Copahue	B+	54.9-56.9 [13]	257	1029	2	-0.256 ÷ -0.157	N	N60°E	9-20 [10]	1397	Y
Maule (2010)	Villarrica	A	53.77-54.44 [5]	396	1244	1	-0.120 ÷ -0.013	Y	N47.5°E	2-3 [1,3]	2447	N
Other volcanic events												
Valparaiso (1906)	Villarrica	A	52.04-52.71 [5]	712	807	2	-	-	-	-	-	-
Valparaiso (1906)	Villarrica	A	52.04-52.71 [5]	712	1099	2	-	-	-	-	-	-
Valdivia (1960)	Tupungatito	B	60.5 [2]	603	348±4	2	-	-	-	-	-	-
Valdivia (1960)	Tupungatito	B	60.5 [2]	603	1534	2	-	-	-	-	-	-
Valdivia (1960)	Planchon-Peteroa	B	63.05-63.12 [11]	391	603±15	1	-	-	-	-	-	-
Valdivia (1960)	Villarrica	A	52.04-52.71 [5]	168	1009	3	-	-	-	-	-	-
Valdivia (1960)	Villarrica	A	52.04-52.71 [5]	168	1380	2	-	-	-	-	-	-
Santiago (1985)	Tupungatito	B+	60.5 [2]	192	1000	2	-	-	-	-	-	-
Maule (2010)	Planchon-Peteroa	B+	63.05-63.12 [11]	210	355	3	-	-	-	-	-	-

Table 1. *Characteristics of the volcanic events at each volcano following the large earthquakes, including: volcano name, Type, SiO_2 content of erupted lavas, distance from the epicentre, time-gap between the earthquake and the volcanic event, VEI of the eruption, amount of normal stress change (N.S.C.), activity in the five year before the earthquake (P-E activity), azimuth of the inferred magma pathway (M.P.) and depth of the magma chamber (M.C. depth), volcano height and analysis of the eruption rates (E.R. analysis, Y = positive correlation). In light gray are represented the post-2010 minor volcanic events. Data based on satellite images, SRTM90 DEM (srtm.csi.cgiar.org), Global Volcanism Program Digital Information Series (http://www.volcano.si.edu/gvp/world) and data reported in the literature (Hickey-Vargas et al., 1984[1]; Hildreth and Moorbath, 1988[2]; Tormey et al., 1991[3]; Hildreth and Drake 1992[4]; Gonzalez-Ferran, 1995[5]; López-Escobar et al., 1995[6]; Tormey et al., 1995[7]; Dixon et al., 1999[8]; Déruelle and López-Escobar, 1999[9]; Mamaní et al., 2000[10]; Naranjo and Haller, 2002[11]; Lara et al., 2006b[12]; Varekamp et al., 2006[13]; Maskimow et al., 2007[14]; Rea et al., 2009[15]; Reubi et al., 2011[16]; Orinashi et al., 2004[17]; Motoki et al., 2006[18]).*

Name	Valparaiso	Valdivia	Santiago	Maule
Date (dd/mm/year)	17/08/1906	22/05/1960	03/03/1985	27/02/2010
M_w	8.2	9.5	8.0	8.8
Search radius (km)	836	1521	762	1102
Rupture length (km)	330	940	170	460-720
Fault geometry (strike/dip, °)	8°/17°	7°/20°	11°/26°	13.5°-18°/13°-18°
N. of patches	1	864	153	126-375
Average slip (m)	2.6	3.8	1.6	-
Average rake angle (°)	117°	105°	105°	-
Fault top (km)	20.5	0.0	21.8	-
Fault bottom (km)	47.5	153.9	61.3	-
σ_1 (azimuth/plunge, °)	71°/31°	100°/35°	86°/20°	92°/28°
σ_2 (azimuth/plunge, °)	157°/7°	10°/0°	174°/9°	178°/5°
σ_3 (azimuth/plunge, °)	56°/58°	80°/55°	61°/68°	80°/61°

Table 2. *Characteristics for the four $M_w \geq 8$ earthquakes and related finite fault models: date of the event, magnitude, used search radius, fault rupture length (Lomnitz, C., 1970; Kelleher, 1972; Lomnitz, C., 1985; Comte et al., 1986; Okal, 2005; Watt et al. 2009; Servicio Sismológico de la* Universidad de Chile*, http://ssn.dgf.uchile.cl; USGS earthquake hazards program), strike and dip angle of the fault plane, number of patches, averaged fault slip and rake angle, depth of top and bottom of the fault plane, trend and plunge of σ_1, σ_2 and σ_3 (based on Barrientos and Ward, 1990; Yoshida, 1991; Lin and Stein, 2004; USGS earthquake hazards program, http://earthquake.usgs.gov; Okal, 2011, written communication; Kanamori, 2011, written communication). Further details regarding the 2010 earthquake are reported in Table 3, Chapter 4 .*

7. Earthquake-induced magma pathway unclamping in promoting eruptions: the Alaska-Aleutian case

The content of this chapter has been submitted to Tectonophysics as "Bonali, F.L.[1], Tibaldi, A.[1], 2013. Earthquake-induced magma pathway unclamping in promoting eruptions: the Alaska-Aleutian case".

[1]*Department of Earth and Environmental Sciences, University of Milan-Bicocca, Milan, Italy*

Abstract

Five earthquakes with $M_w \geq 8$ occurred in proximity of the Alaska-Aleutian volcanic arc since 1938. We analysed these events by numerical modelling and field data to understand the key attributes of each volcano that may lead to a seismically-triggered eruption and the general mechanisms by which earthquakes could trigger new volcanic activity. We followed a novel approach that resolves the earthquake-induced static stress change normal to the magma pathway of each volcano instead of considering the general crustal volume. We also considered other parameters that may contribute to control eruptions, such as magma composition and viscosity, magma chamber depth and local tectonic settings. The dataset includes 13 first new eruptions following large earthquakes, occurred at 8 different volcanoes. Seven out of these 13 first new eruptions occurred at volcanoes that had no activity in the five years before the earthquake, and four regard volcanoes with non-continuously erupting activity (awakening event). Comparison of the eruption rate before and after each earthquake, suggests that 11 out of the 13 first new eruptions have a positive relation with the studied earthquakes. A total of 7 first new eruptions occurred along NE-striking magma pathways, normal to the subduction direction, and 6 along planes parallel to this direction. The calculation of the earthquake-induced static stress changes indicates a decrease normal to the plumbing system, larger at the NE-striking magma paths. At volcanoes with non-continuously erupting activity, the static stress change was capable of favouring the observed volcanic phenomena up to a distance of 543 km from the epicentre and awakening events at a maximum distance of 290 km.

7.1. Introduction

Several authors suggested that a large earthquake could trigger volcanic eruptions due to stress change in the crust (Linde and Sacks, 1998; Hill et al., 2002; Marzocchi, 2002; Marzocchi et al., 2002; Manga and Brodsky, 2006; Walter and Amelung, 2007; Watt et. al. 2009; Delle Donne et al., 2010; Bebbington and Marzocchi, 2011). This is more evident in the near-field (< 250 km from the epicenter) (Eggert and Walter, 2009) and within a few days after the earthquake (Linde and Sacks, 1998; Manga and Brodsky, 2006; Eggert and Walter, 2009), but it is suggested that the delay between the earthquake occurrence and the following volcanic events can be from seconds to years, owing to the complexity of volcanic systems (Linde and Sacks, 1998; Nostro et al., 1998; McLeod and Tait, 1999; Walter and Amelung, 2007; Eggert and Walter, 2009). For example, Watt et al. (2009) suggested that the overall eruption rate in the Southern Volcanic Zone of the Andes increased after the two Chilean subduction earthquakes of August 1906 (M_w 8.2) and May 1960 (M_w 9.5), considering time windows of one and three years after the earthquakes. Bonali (2013) suggested that the 2010 M_w 8.8 Chile earthquake was capable of promoting eruptions up to three years after the event due to crustal extension (unclamping) perpendicular to magma pathway. Three principal modes for earthquake-induced stress transfer capable of promoting eruptions have been suggested: static, quasi-static and dynamic stress changes (Hill et al., 2002; Marzocchi et al., 2002; Manga and Brodsky, 2006). The static stress change is the difference in the stress field from just before an earthquake to shortly after the seismic waves have decayed (Hill et al., 2002). It may explain processes leading to eruption in regions close to the fault rupture (e.g., Walter and Amelung, 2007; Bonali, 2013; Bonali et al., 2013) up to five years after an earthquake (Marzocchi, 2002). Quasi-static stress change is associated with slow viscous relaxation of the lower crust and upper mantle beneath the epicentre of a large earthquake, and occurs over a period of years to decades (Marzocchi, 2000; Freed and Lin, 2002; Marzocchi et al., 2002). At large distances, dynamic stress associated with the passage of seismic waves is often proposed as a possible eruption trigger (Linde and Sacks, 1998; Manga and Brodsky, 2006; Delle Donne et al., 2010). In the present work we analyze the five $M_w \geq 8$ earthquakes occurred in the Aleutian-Alaska arc after 1938 AD (Tab. 1) and the documented volcanic eruptions (Tab. 2) in the five years following each earthquake. We focus on the contribute given by the earthquake-induced static stress change on the magma feeding system reconstructed at each single studied volcano, and we propose new relations between magma pathway unclamping and time-gap. We take also into consideration: magma chamber depth, magma rheology and tectonic settings. Understanding the relative importance

of the parameters that might control earthquake-favoured volcanism is of paramount importance to achieve the goal of identifying which volcanoes that are more prone to erupt.

7.2. Geological and seismo-tectonic overview

The Aleutian-Alaska arc can be divided into two parts: the western insular arc that resulted from the subduction of the Pacific plate beneath the oceanic part of the American plate, and the eastern arc at the continental margin that resulted from the subduction of the Pacific plate beneath the Mesozoic continental basement of the Alaska Peninsula (Reed and Lanphere, 1973). The arc is 2500 km long from the Hayes volcano west of Anchorage in the Alaska-Aleutian Range, to the Buldir Island in the western Aleutian Islands (Fig. 1), hosting over 80 major volcanic centres of Holocene age. At least 29 of these volcanoes have had historical eruptions (since 1760 AD) while other further 12 volcanic centres are suspected to have had historical eruptions (Miller et al., 2008). A total of 265 eruptions were reported since 1760, which should have been originated from these 41 volcanoes. Further 7 volcanic centres in the Aleutian arc have active fumaroles fields but no reported historical eruptions (Miller et al., 2008). The Aleutian-Alaska arc is also the most seismically active area in the USA. Since 1900, in the area one major earthquake ($M_w \geq 8$) occurred on average every 13 years (Koehler et al., 2012), whereas one M_w 7-8 earthquake occurred every two years and six M_w 6-7 earthquakes occurred per year (Alaska Seismic Hazard Safety Commission, 2012). Tectonic deformation involves also the back-arc region, being distributed over 700 km into the Alaska interior. It is assumed that this widespread deformation zone and the high seismicity are related to the fast plate convergence, in the order of ~5.5 cm/yr, and the gentle subduction angle especially below the eastern part of the arc (Koehler et al., 2012). The consequence has been the generation of multiple large historic earthquakes such those that will be studied here: the 1938 M_w 8.2 Shumagin Islands earthquake near the Alaska Peninsula, the 1946 M_w 8.1 Unimak earthquake, the 1957 M_w 8.6 Fox-Andreanof Islands earthquake and the 1965 M_w 8.7 Rat Islands earthquake along the Aleutian Islands, and the 1964 M_w 9.2 Good Friday earthquake in Alaska mainland (Plafker, 1969; Beck and Christensen, 1991; Christensen and Beck, 1994; Johnson and Satake, 1994; http://earthquake.usgs.gov/). All these major earthquakes are related to ruptures that occurred along the shallow part of the gently dipping thrust interface between the subducting and overriding plates. In particular, west of Kayak Island the main subduction zone is strongly coupled, as reflected by the occurrence of the 1964 earthquake that is the second largest seismic event recorded instrumentally. The 1964 earthquake (Fig. 1) was accompanied by

left-lateral reverse slip of the order of 20 m, which produced also 10 m of uplift of Prince William Sound (Plafker, 1969; Hastie and Savage, 1970). The dimension of the rupture zone was 750 x 200 km (Page et al., 1991). The depth of the hypocenter was restrained to 20 km, although it is sometime regarded as lying between 20 and 50 km (Stauder ad Bollinger, 1966). The 1938 event ruptured a 300-km-long segment of the Alaskan arc, which corresponds to the aftershock area (Johnson and Satake, 1994). The 1946 earthquake has a very small aftershock zone, about 100 km in length (Sykes, 1971), but was accompanied by a very strong tsunami (Johnson and Satake, 1997). The 1957 earthquake has the longest aftershock zone of any earthquake ever recorded, in the order of 1200 km, and has been estimated as the third largest earthquake of the XX Century (Johnson et al., 1994). The 1965 earthquake has dimensions of the aftershock area of 600 km in length (Beck and Christensen, 1991). All these earthquakes are compressional with focal mechanisms of low-angle thrust planes for the 1964 and 1965 earthquakes (Stauder and Bollinger, 1966; Stauder, 1968). The Quaternary crustal faults are known in mainland Alaska and are characterized by the presence of several structures mostly depicting a curved belt with a northward convex side north of the volcanic chain (Fig. 1) (Koehler et al., 2012).

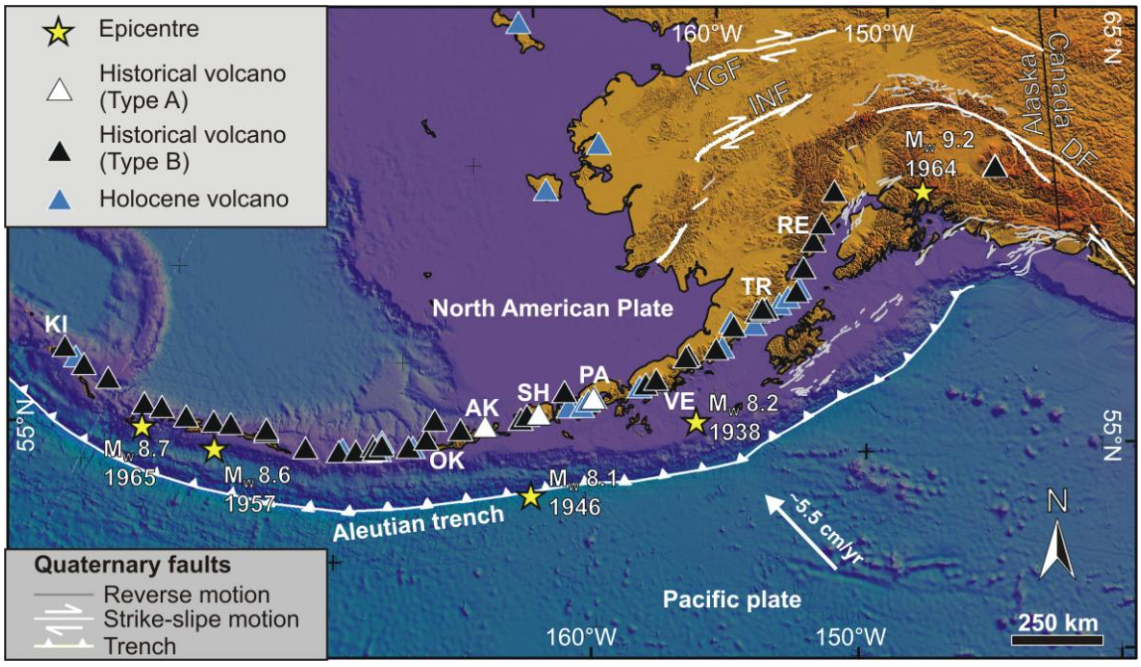

Figure 1. *Active and Holocene volcanoes belonging to the Aleutian-Alaska Arc. The white arrow indicates the approximate convergence direction of the plates and estimated velocity. Main Quaternary intra–arc faults with reverse motions and right-lateral strike–slip motions are reported (redrawn after Koehler et al., 2012). Faults: DF = Denali; KGF = Kaltag; INF = Iditarod-Nixon Fork;. Volcanoes: VE = Veniaminof, OK = Okmok, AK = Akutan, SH = Shishaldin, PA = Pavlof, KI = Kiska, RE = Redoubt, TR = Trident.*

The longest structures here are the Kaltag and Iditarod-Nixon Fork right-lateral strike-slip faults, striking ENE and NE respectively. More to the east, crossing the Alaska-Canada border, the Denali Fault lies along the southern margin of the Alaska Range and was the source of the 2002 M_w 7.9 earthquake (Haeussler et al, 2004, and references therein). This fault has right-lateral strike-slip motions along a plane striking ENE to the west and SE to the east. Closer to the Alaska volcanic chain, there is a series of Quaternary faults with length in the order of tens of km (Fig. 1) (Koehler et al., 2012). These faults strike mostly NNE to NE, parallel to the volcanic alignment, and a few strike N-S. Between the Alaska volcanic belt and the subduction trench, there is a swarm of Quaternary faults striking NE in the western part and E-W in the eastern part at the Alaska-Canada border. All these faults are proposed to have a reverse kinematics (Koehler et al., 2012). Probably more Quaternary/active faults do exist, also in the intra-arc region, but the remote and rugged terrains of this area prevented extensive field studies. Previous data on the structures affecting the Quaternary volcanoes come from studies of the distribution of vents grew on the main volcano slopes (Nakamura, 1977; Nakamura et al, 1977, 1980). These studies indicate that in most of the main Quaternary volcanoes of the Aleutian and Alaska belt, the magma-feeding structures are oriented parallel to the trajectories of the greatest horizontal principal stress (σ_{Hmax}) that is about NW-SE and correlates with the relative motions between the North America and Pacific plates. Local studies suggest the presence also of NE-striking magma paths and normal faults in the intra-arc zone (e.g. Coats et al., 1961).

7.3. Method

We analyzed the earthquake-volcano interactions induced by the studied seismic events (Tab. 2), within a search radius based on Delle Donne's et al. (2010) formula:

$$Mw = -6.4 + 2.17 \log R_{max}$$

relating the earthquake magnitude (M_w) and an empirical maximum distance for volcanic response (R_{max}). In order to have a reliable and homogeneous dataset we consider only the eruptions occurred with certainty in the five years after each earthquake, which are classified as "*confirmed*" in the world catalogue (Global Volcanism Program, http://www.volcano.si.edu/index.cfm). We focused the analysis in the time-frame up to five years to better constrain the contribution of coseismic stress changes in promoting new eruptions (e.g. Marzocchi, 2002), considering also that static stress change is capable of inducing aftershocks (rock failure) up to 3-5 years after an earthquake (Anderson and

Johnson, 1999; Stein, 1999; Hardebeck et al., 1998; Seeber and Armbruster, 2000; R. Stein, written comm., 2012). Similarly to Eggert and Walter (2009) and Walter and Amelung (2007), the analyzed volcanoes are classified in two classes: "Type A" are volcanoes erupting more or less continuously (i.e. more than 20 eruptions since 1900 AD), which are considered as open-conduit systems, and "Type B" are non-continuously erupting volcanoes (less than 20 eruptions). We named as "*first new*" activity the first new eruption after the earthquake within the successive 5 years if a volcano had eruptions also in the preceding 5 years, and "*awakening"* events the *first new* events that occurred at Type B volcanoes that did not have any activity in the 5 years prior to the earthquake (e.g. Bonali et al., 2013). Based on these definitions, Type-A volcanoes cannot have *awakening* events since they are already in a condition of continuous eruptive activity. Type-B volcanoes that didn't have any eruption in the 5 years prior to the earthquake and then experienced *awakening* after the earthquake are defined as Type B+. In order to assess the influence of key volcanic parameters on the feedback between large earthquakes and volcanic events, we compiled all the data available for each volcano: magma chamber depth, silica content of the volcanic products, geometry of the magma pathway and the tectonic setting of the volcano substratum, earthquake magnitude, distance from the earthquake epicentre and time-gap between earthquake occurrence and eruptions. Finally we compare the eruption rate before and after each earthquake, always considering eruptions within the search radius proposed by Delle Donne et al. (2010). The eruption rate before the earthquake (ER-before) has been calculated considering only eruptions occurred in the 50 years before (e.g. Walter and Amelung, 2007), while the eruption rate after the earthquake (ER-after) has been calculated for different increasing time-windows: 0-1 year, 0-2 years, 0-3 years, 0-4 and 0-5 years. This was also done analyzing only the "*first new*" eruptions, distinguishing the volcano Type (A or B) and finally considering only the eruptions occurred under magma pathway unclamping, in order to identify a consistent time-gap between the earthquake and the following volcanic eruptions.

7.3.1 Reconstruction of magma pathway geometry

Here we detail methodology and results because the reconstruction of magma path geometry is a fundamental step in our approach and will be compared with other results in the discussion section. Basic magma is supplied to the surface mostly along planar, steeply-inclined intrusive sheets that may group to form dike swarms (Dieterich, 1988; Carracedo, 1994; Moore et al., 1994; Walter and Schmincke, 2002) and eventually volcanic rift zones

formed by hundreds of parallel dikes (Fiske and Jackson, 1972; Walker, 1999). Volcanic rift zones are usually expressed at the surface by aligned pyroclastic centres and swarms of fissures, dikes and faults (Johnson and Harrison, 1990; Strecker and Bosworth, 1991; Annen et al., 2001; Walter and Schmincke, 2002). Dikes in particular form aligned volcanic centres when magma intercepts the surface; several parallel dikes produce corridors containing tens of pyroclastic cones (e.g. Nakamura, 1977). A more detailed reconstruction of magma paths can be done by combining dike geometry with a series of morphometric parameters of main craters and parasitic vents (Tibaldi, 1995; Corazzato and Tibaldi, 2006; Bonali et al., 2011). When a dike intercepts the volcano slope, it produces scoria ramparts (e.g. Fig. 2A) that are parallel to the dike, or pyroclastic cones with an elongated base and crater (e.g. Fig. 2A) whose azimuth is controlled by the magma path strike (Tibaldi, 1995). Fissure eruptions can also produce closely-spaced vents leading to elongated composite cones (e.g. Figs. 2B and 2D) (Corazzato and Tibaldi, 2006). All these features are thus the surface expression of dikes and tend to be perpendicular to the horizontal least principal stress (σ_{Hmin}). Fissures and faults can also be directly recognized in the substratum surrounding the volcanoes, giving clues to the style and geometry of the fracture field (e.g. Fig. 2C). Geophysical data recorded during magma injection events can also be useful, such as the precise location of volcano-tectonic earthquakes and related focal mechanisms that can be used to resolve the dominant geometry of magma paths. The reconstruction of the azimuth of the Quaternary magma pathways (Tab. 1) was thus based on: i) alignment of secondary closely-spaced vents, ii) alignment of composite craters, iii) preferred distribution of swarms of parasitic and flank cones, iv) trend of elongated vents, v) trend of elongated pyroclastic cone base, and vi) fracture systems. These features were recognized and measured using satellite images, DEM-SRTM90 and geological maps, integrated with the available literature information on field and geophysical data. Akutan volcano in 1996 affected by a swarm of volcano-tectonic earthquakes, opening of N110°E-striking ground cracks on the NW flank and parallel Holocene normal faults that were reactivated in the eastern part (Richter et al., 1998). Interferometric data helped to interpret these features as produced by the propagation of a NW-striking steeply dipping dike propagated to within < 1 km to the surface of the northwest flank and to the volcano summit (Lu et al., 2000). These data together with our observations suggest to assume here a vertical dike plane with a N110°E orientation. Shishaldin Volcano is characterized by the presence of a swarm of pyroclastic cones grew on its NW flank. Most of them show morphometric features compatible with the emplacement of NW-striking dikes (e.g. Fig. 2D). Moran et al. (2002) studied a sequence of tectonic earthquakes preceding the April-May 1999 eruption

and simulated a dike with this strike. This preferred orientation of magma feeding paths was also considered here by Nakamura et al. (1980). At Pavlof and Kiska volcanoes we assigned a N40° and a N50° trend, respectively, for magma paths based on the distribution and morphometric characteristics of pyroclastic cones (Fig. 2B) and elongation of the main cone. In particular at Kiska, Nakamura et al (1980) assigned a magma path trend of N50°, and a geologic survey by Coats et al. (1961) showed the presence, in the surrounding substratum, of N30° and N120°E-striking fractures striking, with a few of them where it has been possible to recognize normal fault movements. We also recognized high-angle faults striking from N-S to NE-SW (e.g. Fig. 2D). Based on these data we assigned to Kiska a magma pathway trending N40°±10°.

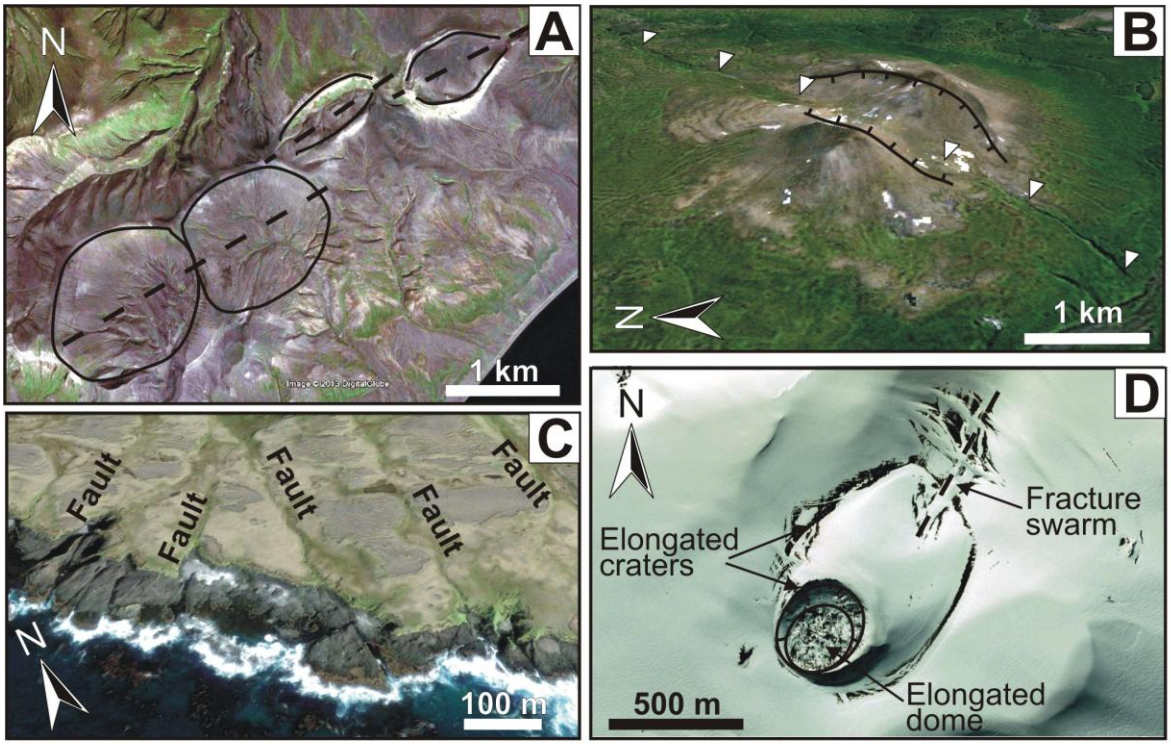

Figure 2. *(A) Example of two scoria ramparts (NE part of the figure) that can be used as indicator of the strike of the fracture feeding magma to the surface (dashed line), and alignment of two coeval pyroclastic cones lying at the foothills of Shishaldin volcano. (B) Example of a composite pyroclastic cone with an elongated base and crater, across which a fracture with the same strike can be recognized (white triangles) at the foothills of Pavlof volcano. (C) Example of fissures and faults recognized in the substratum surrounding the Kiska volcano; note that here fractures strike from N-S to NE-SW and are at high angle, suggesting they can be strike-slip or extensional features. (D) Example of an elongated composite cone and a fracture striking NW-SE at Shishaldin volcano.*

At Redoubt volcano the interpretation of the geometry of the plumbing system is more complicate. Based on the inversion of fault plane solutions of 420 earthquakes occurred below the volcano, Sanchez et al. (2004) showed that during the 1989-90 eruptions, σ_1 and σ_2 were typically sub-horizontal and trending ESE-WNW and NNE-SSW respectively, with a near-vertical σ_3. During July 1991-January 1998 the same authors found a near-vertical σ_1 and sub-horizontal σ_2 and σ_3 striking SSE-NNW and ENE-WSW respectively. This was explained by the initial expansion of a plexus-like magma body, with no-preferred orientation, followed by the 1991-98 period of non-magmatic activity with very little horizontal stress beneath the volcano. In this period the vertical load is the largest principal stress and the σ_{Hmax} of tectonic origin is σ_2 with a SSE-NNW trend. Lahr et al. (1994) showed that a swarm of earthquakes of the 1989-90 eruption has locations consistent with activity occurring along a narrow conduit with a 75 °-dip to the NE in the depth range of 1 to 7 km. Roman and Gardine (2013), studying the shear-wave splitting during the 2005-2006 period of quiescence of Redoubt, found a stress field characterized by a NW-SE σ_{Hmax} that should represent the tectonic stress. The analysis of fault-plane solutions of 210 volcano-tectonic events indicates periods of complex intrusions in 2009, followed by a period with a stable dominant NE-SW-trending P-axis orientation. This trend is perpendicular to the regional σ_{Hmax} and is also characterized by shallow earthquakes located directly below the Redoubt's summit, and has been interpreted as the effect of horizontal displacement of the conduit walls in response to intruding magma (Roman and Gardine, 2013). After that, plane solutions indicate again a period of stable NW-SE-trending P-axis that represents the re-establishment of post-eruptive effect of tectonic stress. A magma path should be perpendicular to the sin-intrusive P-axis and thus we infer that the most probable dike should strike NW-SE, consistent with one of the two solutions proposed by Buurman et al. (2013). A plexus of dikes and sills has been recognized beneath the north volcano flank between 1 and 6 km below sea level, and a conduit zone extends from this area to below the volcano summit (Benz et al., 1996). The same authors showed the distribution of 930 volcano-tectonic earthquakes occurred in July 1991 that in plain view suggest a N15°E trend for the conduit zone. Based on all these data it is possible to resume that the tectonic σ_{Hmax} trends between NNW-SSE and NW-SE, and magma pathways can strike NW-SE and also NNE-SSW. The active Trident volcano is the last centre of a line of Quaternary volcanoes striking NE-SW, whose activity shifted gradually from NE to SW (Hildreth et al., 2001). Dikes, sills or modest pods of magma have been all considered possible for magma pathways. Lu et al. (1997), by using synthetic-aperture-radar interferometry of 1993-95 images, detected 7 cm of uplift

beneath Southwest Trident. They interpreted the apparent ground deformation to reflect inflation of a pressure source at 0.8- to 2-km depth, which they attributed to either magma intrusion or pressurization of the hydrothermal system. Wallmann et al. (1990) described a set of fissures crossing the margins of the 1912 Novarupta crater and striking N140°E, subparallel to the dominant bedrock joint set. These authors suggest that fissures and joints, local plate-motion vector and the inferred regional stress orientation, are consistent with a feeder dike propagating from a reservoir beneath Trident volcano to the eruptive vent. Another set of joints has a N70°E strike subparallel to the line from Mt Katmai to Novarupta. The contemporaneous creation of the Mt Katmai caldera represents a possible magmatic connection between the reservoir beneath this volcano and Trident; this connection has been interpreted as a propagating sill or the failure of septa between NE-aligned batches of magma (Wallmann et al., 1990; Lowenstern et al., 1991; Hildreth and Fierstein, 2000).

7.3.2 Numerical modelling

A series of representative numerical models were developed to investigate how tectonic motions along the fault planes of the five earthquakes transferred static stress on the magma pathways of the eight studied volcanoes (Tab. 1). The numerical models were performed using the Coulomb 3.3 software (Lin and Stein, 2004; Toda et al., 2005), where calculations were made in an elastic halfspace with uniform isotropic elastic properties following Okada's (1992) formulae. These formulae allow to calculate the crustal dilatation as well as the static normal stress change resolved on a receiver surface, independently from the rake angle of the receiver structure and from the friction coefficient used in the model. The normal stress change can produce a clamping (increase in normal stress) or unclamping (decrease in normal stress) effect on any receiver surface (e.g. a magma pathway/feeder dike). The upper crust was modelled with a Young's modulus $E = 80$ GPa and a Poisson's ratio $\nu = 0.25$ based on King et al. (1994), Mithen (1982), Lin and Stein (2004) and Toda et al. (2005); a lower value of Young's modulus would only have the effect of reducing the magnitude of static stress changes. The finite fault models used to simulate the earthquake-induced effects are based on tsunami wave form inversion (Tab. 2). The input stress fields are based on data reported in the World Stress Map database (Heidbach et al., 2008; Tab.2). The subvolcanic magma feeding systems that link the volcanoes with their magma reservoirs are assumed as vertical surfaces for all volcanoes. The stress change over the area of interest has been calculated at a representative depth of 2 km below the volcano base, based on the fact that previous sensitive

analyses show minimum variation of stress change with depths in the range of possible magma chambers (e.g. Bonali, 2013).

7.4. Results

7.4.1 Volcanic events following the earthquakes

A total of 22 eruptions occurred in the five years following the studied earthquakes, at 8 different volcanoes, listed in Table 2. Some volcanoes erupted more than once following the same earthquake or following more than one earthquake, thus 13 of these 22 events are classified as *first new* eruptions. Six *first new* eruptions occurred at volcanoes of Type A, while 7 at Type B volcanoes. Six of the 13 *first new* eruptions represent *awakening* events (occurring at Type B volcanoes that had no activity in the five years before the earthquakes), and 4 of these 6 experienced unclamping of magma pathway (Tab. 2). *First new* eruptions occurred always after each earthquake, while *awakening* events occurred for magnitudes > 8.2 (Fig. 2A) as far as 750 km from the epicentre (Fig. 3B). In particular, no eruption occurred at volcanoes of Type B beyond 750 km, and there is a class of distance (750-1000 km) without eruptions (Fig. 3B). *Awakening* events started after 3 months and are present up to 3-5 years; at a general level the number of all eruptions occurred between 1-3 years as well as the number of first new that comprises both types A and B (Fig. 3C). Regarding the chamber-centred depth, the class with depth of about 0-5 km is the most represented, followed by 5-10 km, and both regard Type A and Type B volcanoes. The deepest class of 15-20 km includes only Type A volcanoes (Fig. 3D). The historical records report two *first new* eruptions that occurred after the M_w 8.2 1938 earthquake (Tab. 2): Veniaminof (Type B+) that erupted on 23/05/1939, and Okmok (Type B+) that erupted in June 1943. Veniaminof erupted also on November 1939. After the M_w 8.1 1946 earthquake, three *first new* eruptions are reported (Tab. 1): Akutan (Type A) on December 1946, Shishaldin (Type A) on August 1946, and Pavlof (Type A) on 31/07/1950. Akutan and Shishaldin erupted also on 29/04/1948 and 1948, respectively. After the M_w 8.6 1957 earthquake, two *first new* eruptions are reported (Tab. 1): Okmok (Type B+) on 14/08/1958, and Kiska (Type B+) on 24/01/1962. Okmok erupted also on 15/10/1960. After the M_w 9.2 1964 earthquake, four *first new* eruptions are reported (Tab. 1): Redoubt (Type B+) on 24/01/1966, Trident (Type B) on 31/05/1964, Pavlof (Type A) on 15/03/1966, and Shishaldin (Type A) on 28/01/1967. Redoubt erupted also on 7/10/1966 while Trident erupted others three times in 1966, on 05/09/1967 and on 13/11/1968. After the M_w 8.7 1965 earthquake, two *first new* eruptions are reported (Tab. 1): Kiska (Type B) on 11/09/1969, and Shishaldin (Type A) on 28/01/1967.

The eruptions occurred at Shishaldin could hav suffered feedback by both the 1964 and 1965 earthquakes.

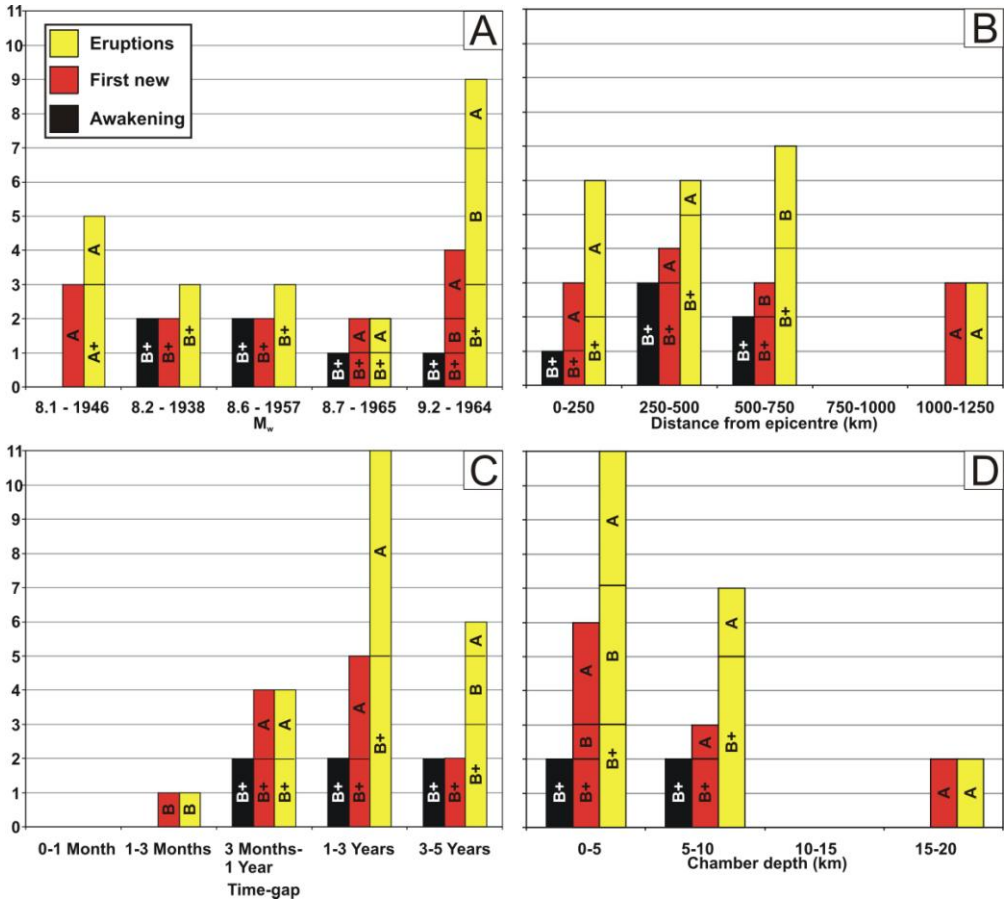

Figure 3. *Volcanic events occurred in the five years following the studied earthquakes, distinguished in Type A and Type B. (A) Number of: volcanic eruptions, first new events and awakening events (volcanoes that had no volcanic events in the five years before the earthquake) versus earthquake magnitude. (B) Number of volcanic events versus the distance from earthquake epicentre (km). (C) Number of volcanic events versus time-gap. (D) Number of volcanic events versus centred-depth of magma (km).*

7.4.2 Numerical modelling of static stress changes

The computation of static stress changes induced by the earthquakes, resolved on the reconstructed magma pathway, indicates that 7 *first new* eruptions occurred at volcanoes that suffered moderate to minor unclamping (-0.541 ÷ -0.001), 2 occurred in cases of no stress change and four of the 13 events occurred at volcanoes where modelling shows a very weak clamping (normal stress increase <0.01 MPa). Specifically, the 1938 earthquake did not induce changes at Okmok volcano (Fig. 4B) and induced unclamping at Veniaminof volcano (Fig. 4C). The 1946 earthquake induced very weak clamping at Akutan and no changes on

Pavlof (Figs. 4D-E), while medium-high unclamping was experienced by Shishaldin (Fig. 4F). The 1957 earthquake induced weak unclamping at Okmok and unclamping at Kiska (Figs. 5A-B). The 1964 earthquake induced medium-high unclamping at Redoubt and Trident (Figs. 5C-D and Figs. 5E-F), while it induced very weak clamping at Pavlof and Shishaldin (Figs. 6A-B). The 1965 earthquake induced medium-high unclamping at Kiska (Fig. 6C) and no changes at Shishaldin (Fig. 6D).

7.4.3. Analysis of the eruption rates

The analysis of the volcanic activity in the 50 years preceding each earthquake and in the following years was done considering the first new eruptions for both types A and B and also the unclamping effect induced by the earthquake. When the ratio ER-after/ER-before > 1, a relation between the earthquake and the following eruptions is supposed. A first analysis of the eruption rates has been done considering all the *first new* eruptions, suggesting that a relation between the earthquake and following eruptions exists for the 1938, 1946, 1957, 1964 and 1965 seismic events for time windows of 0-1, 0-2, 0-2, 0-4 and 0-2 years respectively (Fig. 7A). Considering all the *first new* eruptions occurred at volcanoes that suffered earthquake-induced unclamping effect, a relation exists for the 1938, 1946, 1964 and 1965 seismic events for time windows of 0-1, 0-1, 0-3 and 0-1 years respectively (Fig. 7B). It was also analyzed the eruption rate for different types of volcanoes that erupted after the studied earthquakes. In particular the ER-before and ER-after have been calculated for types A and B respectively. Considering all the *first new* eruptions involving volcanoes of Type A, a relation between the earthquakes and following eruptions exists for the 1946, 1964 and 1965 earthquakes for time windows of 0-5, 0-3 and 0-1 respectively (Fig. 7C). Considering all the *first new* eruptions involving volcanoes of Type B, a relation exists for three of the four studied earthquakes. In particular, for the 1938 earthquake a time window of 0-5 years can be considered, for the 1957 earthquake 0-3 years, for the 1964 earthquake 0-4 years, and for the 1965 earthquake 0-1 year (Fig. 7D). These considerations change for the eruptions occurred at volcanoes that experienced unclamping; in particular, only for the 1946 earthquake a relation exists between earthquakes and eruptions occurred at volcanoes of Type A up to 0-2 years (Fig. 7E). Regarding volcanoes of Type B, for the 1938 earthquake it could be considered a time window of 0-2 years, for the 1964 earthquake 0-4 years, and for the 1965 earthquake 0-1 year (Fig. 7F). Analysis of eruption rates suggests that 11 out of the 13 *first new* eruptions have a positive relation with earthquake (Tab. 2).

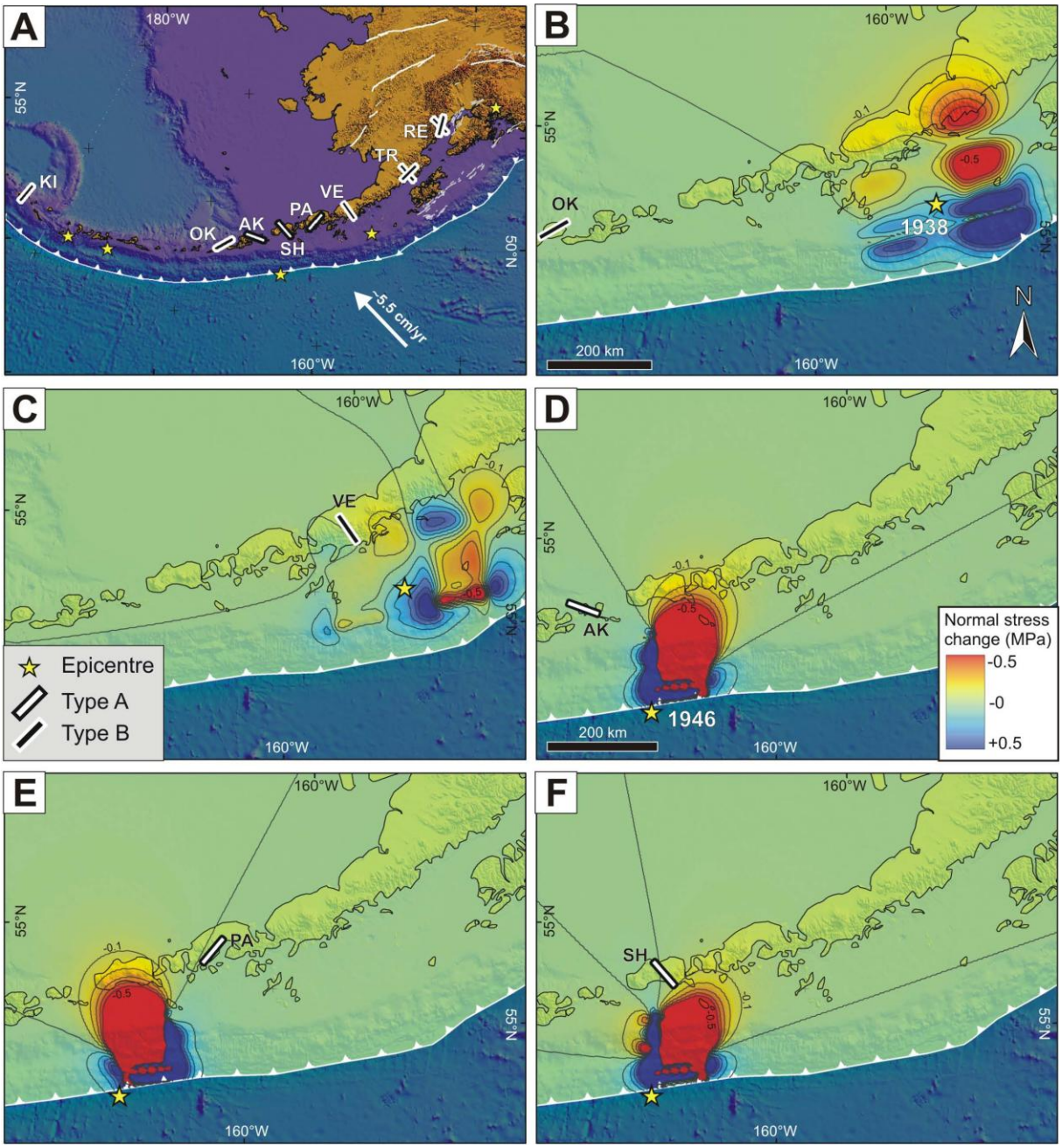

Figure 4. *(A) Reconstructed magma pathway orientation for the studied volcanoes. 1938 Earthquake-induced normal stress change resolved on the (B) N60°E-striking Okmok magma pathway and (C) N145°E-striking Veniaminof magma pathway. 1946 Earthquake-induced normal stress change resolved on the: (D) N110°E-striking Akutan magma pathway, (E) N40°E-striking Pavlof magma pathway and (F) N139°E-striking Shishaldin magma pathway. Depth = 2 km below the volcano bases. Red colours represent a normal static stress reduction on the receiver plane, blue colours represent an increase.*

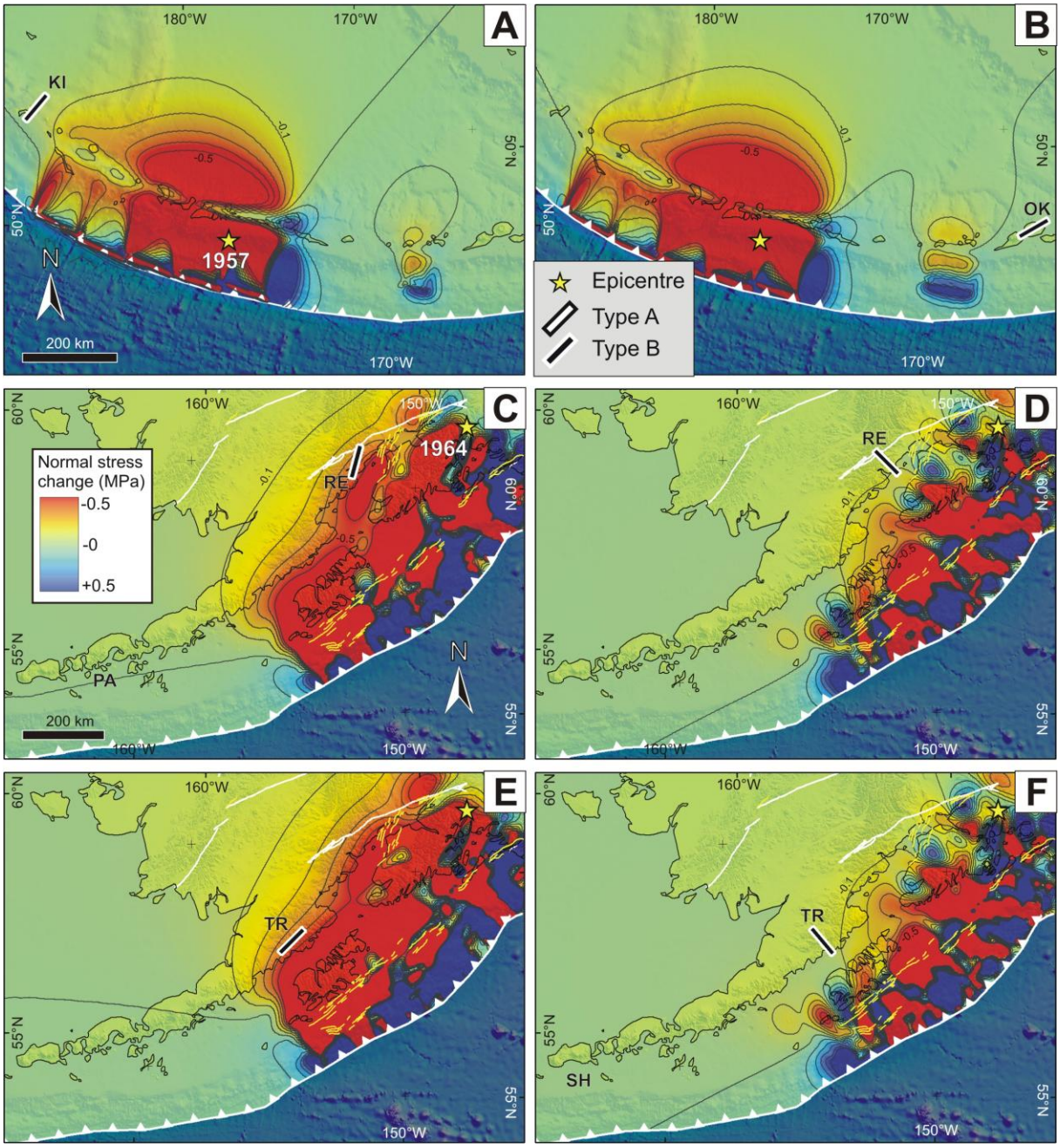

Figure 5. *1957 Earthquake-induced normal stress change resolved on the (A) N40°E-striking Kiska magma pathway and (B) N60°E-striking Okmok magma pathway. 1964 Earthquake-induced normal stress change resolved on the: (C) N15°E-striking and (D) N135°E Redoubt magma pathway, (E) NE-striking and (F) N140°E-striking Trident magma pathway. Depth = 2 km below the volcano bases. Red colours represent a normal static stress reduction on the receiver plane, blue colours represent an increase.*

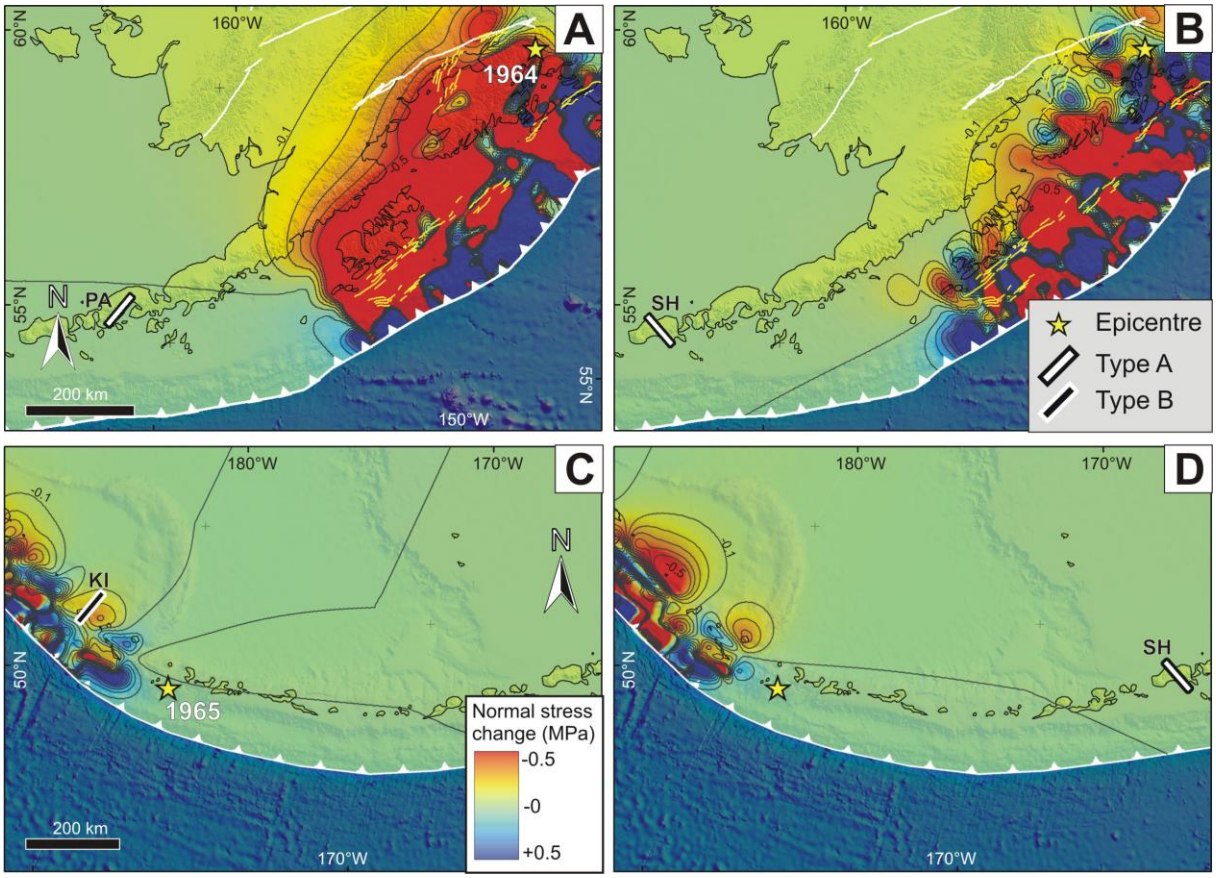

Figure 6. *1964 Earthquake-induced normal stress change resolved on the: (A) N15°E-striking and (B) N135°E Redoubt magma pathway,. 1965 Earthquake-induced normal stress change resolved on the (C) N50°E-striking Kiska magma pathway and (D) E-striking Shishaldin magma pathway. Depth = 2 km below the volcano bases. Red colours represent a normal static stress reduction on the receiver plane, blue colours represent an increase.*

7.4.4 Analysis of the primary variables

In this section we compare the available data for the 11 *first new* eruptions occurred only in the time-windows suggested from the eruption rate analysis that has been done for each earthquake. Five out of these 11 *first new* eruptions occurred at volcanoes of Type A. Six out of 11 occurred at Type B and 4 out of 6 are *awakening* event (Type B+). In particular, to assess the influence of key volcanic parameters on the feedback between large earthquakes and volcanic events, the following parameters are taken into account: distance from the earthquake epicentre, time-gap between earthquake occurrence and *first new* volcanic event, magma chamber depth, silica content of the volcanic products, geometry of the magma pathway and tectonic settings of the volcano substratum.

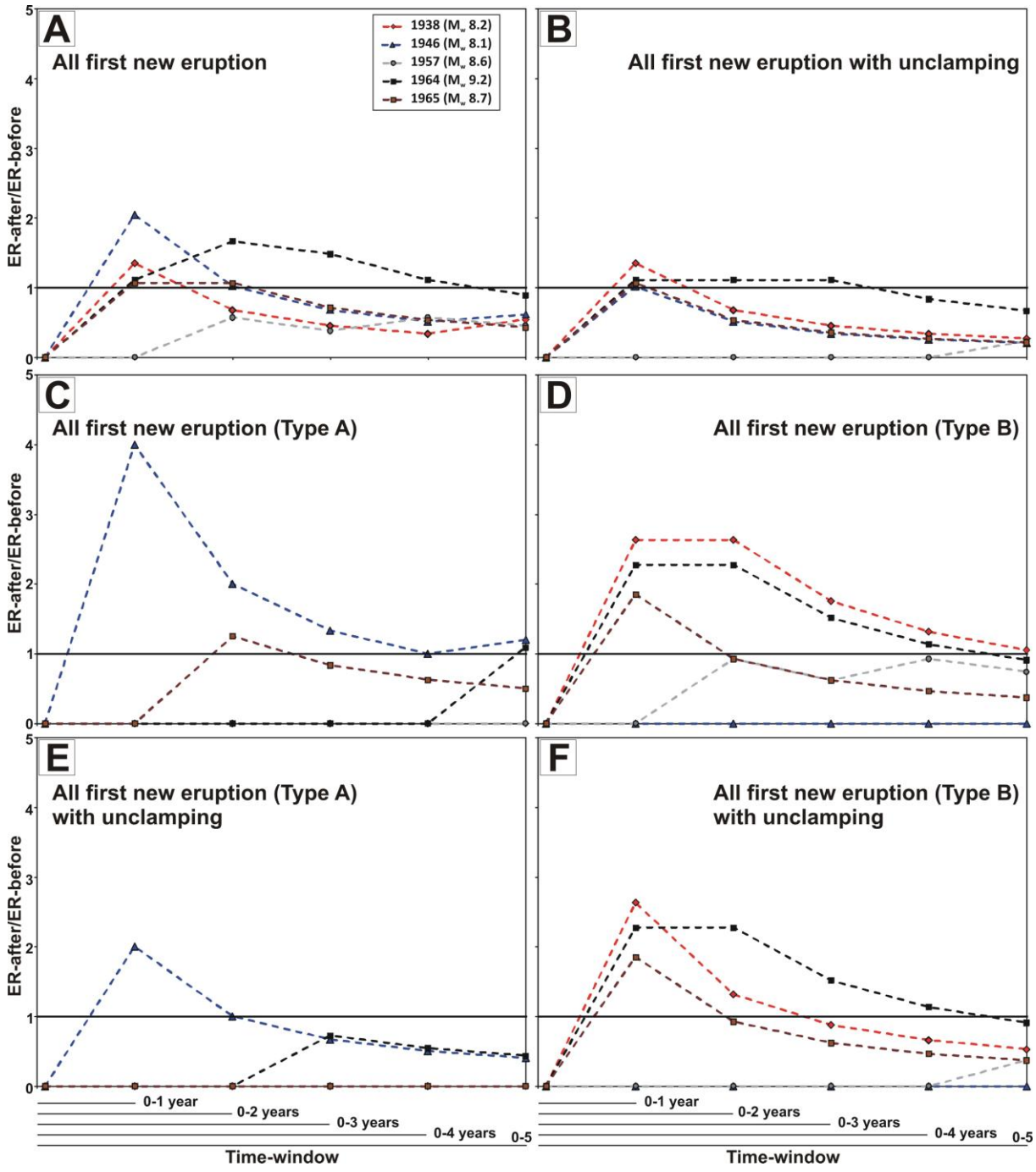

Figure 7. *The graph represents the ratio between the eruption rate (ER) after and before each earthquake (ER-after/ER-before). ER-before is calculated in the 50 years prior to the earthquake, while ER-after is calculated for different increasing time-windows, from 0-1 year to 0-5 years*

Regarding the distances from epicentres, our numerical models indicate that the unclamping of magma pathway occurred as far as 543 km, while *awakening* events occurred up to 730 km (Tab. 2). For distances ≥ 557 km, the normal stress change is always null or shows very low clamping (Tab. 2), while the class of distance 1000-1250 km is represented by Type A volcanoes only (Fig. 8A). Eruptions that occurred in non-unclamping state regard a large number of Type A volcanoes.

Regarding the time gap between earthquake and the occurrence of volcanic event, *first new* eruptions cluster from two months to three years after the earthquake. The class 1-3 months occurred only under unclamping, and the class 3 month-1 year counts three events occurred under unclamping, two of them are *awakening* events. The classes 1-3 years count one event occurred under unclamping while the class 0-5 years does not count any event under unclamping (Fig. 8B). The energy of the volcanic events increases with the amount of unclamping, a large number of eruption with VEI 2-3 occurred under unclamping as represented by *awakening* (Fig. 8C). It is also possible to note that among these events, those with higher VEI values occurred as far as 543 km (Figs. 8A and 8C; Tab. 2). For the rheology of erupted volcanic products, our data suggest that magma pathway unclamping increases the occurrence of events at volcanoes of Type B with high silica content, as well as the number of *awakening* events (Fig. 8D). The magma chamber depth has been compared with the amount of unclamping in Figure 8E. *Awakening* events with deep chamber occurred always under unclamping, while *awakening* with a shallow chamber occurred under no clamping. Type A volcanoes correspond to both shallow and deep chambers. The morphometric indicators of the eruptive centres and the available geophysical data suggest that the magma paths striking NW-SE dominate at Veniaminof, Akutan and Shishaldin volcanoes, whereas the NE-SW planes dominate at Okmok, Pavlof and Kiska volcanoes. Both magma path strikes coexist at Redoubt and Trident volcanoes. These results are consistent with the analysis of the fracture field in the substratum and at the volcano slopes that show the same orientations. Some of the NE-striking faults have uphill-facing scarps that offset glaciated bedrock surfaces suggesting deformations of post-Late Glacial Maximum age. Gullies crossed by these faults do not show any strike-slip offset component; this evidence together with the high-angle dip of fault planes might suggest that most of these faults have dominant normal offsets. Normal fault offsets, in fact, have been observed in the field also by Coats et al. (1961) at Kiska Island along N30°E and N60°E planes, and by Richter et al. (1998) and Lu et al. (2000) at Akutan volcano and surroundings along about N120° planes.

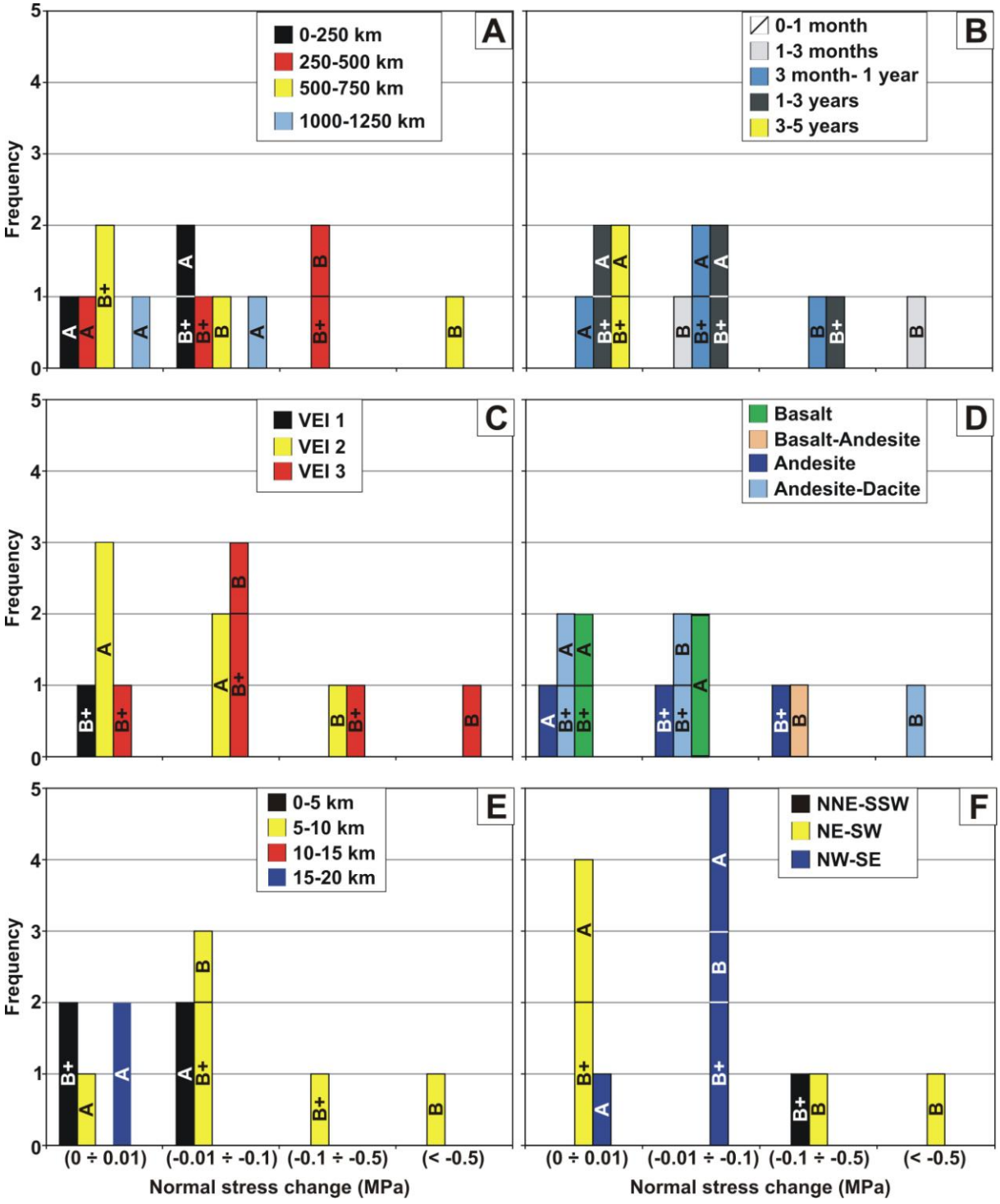

Figure 8. *(A) This graph shows that the new volcanic events and unrests occurred under unclamping and this correlation is stronger for events of Type B at no larger distance. Normal stress change versus: (B) time-gap, (C) VEI, (D) silica content, (E) depth of magma chamber and (F) azimuth of magma pathway. A = Type A volcanoes, B = Type B volcanoes that had eruptions in the five years before the earthquakes, and B+ = volcanoes that had no eruptions in the five years before the earthquakes (awakening events).*

Figure 8F shows that 7 volcanic events occurred by magma paths striking NNE-SSW to NE-SW (from N15°E to N60°E), and 6 along planes striking NW-SE (from N30°W to N60°W). The largest values of unclamping affected the magma-feeding planes striking NNE-SSW to NE-SW. Low unclamping occurred at other NW- and NE-striking planes. No stress variation or very low clamping affected other NE- and NW-striking magma paths.

7.5. Discussion

7.5.1 First new eruptions and eruption rates

We compared the eruption rates before and after each earthquake for volcanoes within the search radius based on Delle Donne's et al. (2010) formula. Our analysis shows that an increase of the eruption rates occurred after all the studied earthquakes. Furthermore, considering the two different types of volcanoes A and B (continuously and non-continuously erupting), it results that 11 out of the 13 *first new* eruptions occurred in a time window where the eruption rate after the earthquake is larger than the eruption rate of the previous 50 years (Tab. 2). In some cases, this time window is larger than the 0-3 years previously proposed by Walter and Amelung (2007). For example, at volcanoes of Type B for the 1938 earthquake it resulted a time window of 0-5 years and for the 1964 earthquake a time window of 0-4 years, (Fig. 7D). At Type A volcanoes, only for the 1946 earthquake it resulted a time window of 0-5 years (Fig. 7C).

These results are consistent with the previous findings of an increase in the number of eruptions after a large earthquake ($M_w \geq 8$), although this has been mainly demonstrated for the near-field (0-250 km from the epicenter) and within a few days (Linde and Sacks, 1998; Manga and Brodsky, 2006; Eggert and Walter, 2009; Watt et. al. 2009). After a very large earthquake, such as a $M_w \geq 9$ event, Walter and Amelung (2007) noted an increase of the eruption rate up to the following three years.

7.5.2 Mechanisms of stress changes

Two main theories have been proposed to explain the seismic-induced changes in a magma body: i) magma is squeezed upward by increased compressional stress in the crust surrounding a magma chamber close to its critical state (e.g. Bautista et al., 1996), but we are inclined to exclude this process in the studied area because the magnitude of the calculated earthquake-induced stress changes are quite low and in particular the very weak values of clamping exclude a "toothpaste" or "flask" process due to permanent deformation. ii) A decrease in compressional stress can promote additional melting, formation of bubbles and

volatiles exsolution, encouraging eruptions in a time frame of years (Hill et al., 2002; Walter and Amelung, 2007). In fact, earthquake-induced static (permanent) normal stress reduction on magma pathway could directly promotes dike intrusion (Hill et al., 2002; Walter, 2007). Some authors suggested that for basaltic magmas an overpressure < 1 MPa is sufficient to generate tensile deviatoric stresses capable of promoting dike formation and propagation without cooling, whereas for more silicic magmas this overpressure has been estimated at 10-100 MPa (Tait et al., 1989; McLeod and Tait, 1999; Jellinek and De Paolo, 2003). In our case, the magnitude of the calculated unclamping is always < 1 MPa, consistent with Manga and Brodsky (2006) who suggested values in the order of $10^{-2} \div 10^{-1}$ MPa for seismic-induced dynamic and static stress changes. The same authors suggested that the overpressure of volcanic system must be within 99%-99.9% of the maximum overpressure for the earthquake to initiate a new eruption. On the contrary, volcanoes showing a longer response may be farther from this tipping point, but stress changes must still be significant to induce permanent pressure changes that could initiate a new eruption in a time frame of years, after an incubation period, where the eruption is the "*failure event*" (e.g. Jupp et al., 2004). Based on the previous considerations, we suggest that the studied *awakening* events occurred under unclamping are good candidate to be classified as eruptions triggered by earthquake-induced static stress changes.

We cannot exclude that in some cases both static and dynamic triggering might have played a role in favouring new eruptions. Dynamic shaking, is another important factor for triggering eruptions that can act up to larger distances than the static effect (Manga and Brodsky, 2006). Dynamic shaking may excite and promote ascent of gas bubbles, and consequently magma ascent (Manga and Brodsky, 2006), the details of the feedback mechanisms remaining unclear. Dynamic effects can also favour bubble growth, including adjective overpressure (Linde et al., 1994), rectified diffusion (Brodsky et al., 1998; Ichihara and Brodsky, 2006) and shear strain (Sumita and Manga, 2008).

7.5.3 Range of distances, time-windows, and magma rheology

Coseismic and postseismic-induced static stress/strain might remotely promote eruptions, particularly for volcanoes close to a critical state (Marzocchi, 2002; Marzocchi et al., 2002; Walter and Amelung, 2007) and may explain processes leading to eruption in regions close to the fault rupture. It is commonly suggested that owing to the complexity of volcanic systems, the delay between the earthquake occurrence and the following volcanic events can be from

seconds to years (Linde and Sacks, 1998; Nostro et al., 1998; McLeod and Tait, 1999; Walter and Amelung, 2007; Eggert and Walter, 2009).

In our study, the *first new* eruptions occurred in a range of distances of 157-1205 km from the epicentres in a time-windows of 2 months up to 4.5 years after the studied earthquakes and unclamping effect was present in the range of 157-1205 km and in a time-window of 2 months-3 years. In particular, eruptions at volcanoes with continuously erupting activity (Type A) occurred in the larger range of distances of 220-1205 km and in a time-window of 4 months-4.5 years. Eruptions at volcanoes with non-continuously erupting activity (Type B), which are considered closer to a critical state (e.g. Walter and Amelung, 2007; Eggert and Walter, 2009), occurred in a shorter range of distances of 157-730 km and in a similar time-window (2 months-4.5 years). Unclamping effects are present at four eruptions that occurred at Type B volcanoes in a range of 157-543 km in a time-window of 2 months-2 years, while *awakening* events with unclamping occurred in a range of 157-300 km in a time-window of 5 months-2 years. Two awakening events occurred in non-unclamping condition in the range 557-730 km in a time-window of 1.4-4.6 years, but they are characterized by a shallow magma chamber (Tab. 2).

Summarizing, *first new* eruptions occurred at volcanoes with non-continuously erupting activity (Type B) and *awakening* events always occurred at a distance < 730 km from the epicentre. We are suggesting that ~730 km could be considered as an upper limit for earthquake-induced new eruptions at volcanoes that are more prone to unrest in the Alaska-Aleutian subduction zone. This is consistent with the authors that usually restricted this kind of analysis up to 750 km from the epicentre (e.g., Linde and Sacks, 1998; Eggert and Walter, 2009), whereas other authors suggest that the volcanic activity may increase also at greater distances (e.g. Delle Donne et al., 2010). Based on our data, unclamping seems capable of promoting *first new* eruptions and *awakening* as far as 543 and 290 km, respectively. Marzocchi (2002) suggested that coseismic stress changes are candidate to promote eruptions at a maximum distance of about 300 km within a time-window of 0-5 years. This time delay can be attributed to the inertia of the volcanic system in reacting to the static stress changes, to a delay due to a non-perfect elasticity of the crust, and/or to stress corrosion effect (e.g., Main and Meredith, 1991). In seismology, the static stress change is candidate to inducing rock failure up to 3-5 years after an earthquake (Anderson and Johnson, 1999; Stein, 1999; Hardebeck et al., 1998; Seeber and Armbruster, 2000; R. Stein, written comm., 2012). In fact, from a seismological perspective, the earthquake-induced static stress changes are evaluated to better constrain the distribution of aftershocks and to understand which faults may be

closer to future failure due to the earthquake-induced stress transfer (Stein, 1999). Post-seismic stress changes were interpreted to be capable of promoting eruptions in 30-35 years after an earthquake, compatibly to the relaxation time of a viscous asthenosphere (Piersanti et al., 1995, 1997; Pollitz et al., 1998; Kenner and Segall, 2000). Marzocchi et al. (2002) showed a more complicate situation, with eruptions occurring in areas where large earthquakes induced strong compression and/or shear perturbations.

Finally, regarding the influence of magma rheology, several authors (e.g., Woods and Pyle, 1997; McLeod and Tait, 1999; Jellinek and De Paolo, 2003) suggested that composition of magmas, storage depth and state of volatile saturation may all play a role. In the studied areas, we noted that unclamping enhanced eruptions preferentially at volcanoes with deep chamber as already proposed (Bonali, 2013; Bonali et al., 2013). For the *awakening* events that occurred in a very weak clamping setting, our analysis suggests that magma is always stored at shallow depth, where a vapour-saturated condition is generally expected due to cooling and crystallizing (Woods and Pyle, 1997).

7.5.4 Magma pathways

The analysis of magma path orientations reveals that three of the studied volcanoes have magma pathways striking NE-SW, other three volcanoes have NW-SE-striking magma paths, and two volcanoes have both magma paths. These data suggest that in the studied volcanic arc segment, magma can intrude along two preferential directions perpendicular and parallel to the Quaternary regional NW-trending σ_{Hmax}. Since also recent normal faulting occurred along planes parallel to these two directions, it must be concluded that two trends of possible dilation might coexist in the studied areas. In the following section we will discuss these trends.

NW-striking dikes and normal faults are consistent with the regional NE-SW trend of the σ_{Hmin}. These NW-SE-striking structures can develop along the volcano slopes at distance from the central plumbing system, as exemplified by the March 1996 intense swarm of volcano-tectonic earthquakes beneath Akutan Island. A dike intrusion produced extensive ground cracks at the north-western part of the island at the lower volcano slope (Lu et al., 2000). At the eastern part, the reactivation of Holocene NW-striking normal faults has been interpreted as the effect of the magma intrusion beneath the volcano and increased extensional strain and/or decreased pore pressure beneath the eastern part of the island (Lu et

al., 2000). This kind of intrusion matches with the Nakamura's (1977), model where at some distance from the central conduit, dikes tend to intrude parallel to the regional σ_{Hmax}.

The NE-striking dikes and normal faults instead developed perpendicularly to the regional σ_{Hmax}. This means two possibilities: 1) the upper crustal magma upwelling follows a trend guided by the deep zone of magma production, the latter being NE-elongated due to the geometry of the subduction zone and associated thermal anomalies. The uppermost crust is mostly dissected by NE-striking fractures and thus magma batches are more facilitated to follow this trend passively instead of creating new NW-striking fractures. This implies in any case that the magmatic stress is larger than the stress acting normal to the NE-striking planes; at Redoubt volcano for example, Sanchez et al. (2004) based on the inversion of fault plane solutions of 420 earthquakes, showed that during the 1991-98 period of non-magmatic activity, the σ_1 was vertical and the $\sigma_{Hmax} = \sigma_2$ = NW-SE. Thus the magmatic stress was sufficient to intrude and dilate the NE-striking planes should have been > σ_2. As possibility 2), we consider that after a long period of compression, the stored energy linked to the NW-trending σ_{Hmax}, is released by a large subduction earthquake. This event can be accompanied by regional vertical differential positive and negative deformations, such as occurred during the 1964 earthquake (Stauder and Bollinger, 1966). The vertical motions can be accompanied by normal faulting along planes parallel to the NE elongation of the uplifting or subsiding blocks. This is validated by the presence of Holocene normal faults very close to some of the studied volcanoes, like at Akutan, Pavlof, Kiska and Redoubt, which represent the weakness zones. The static stress change associated to these large earthquakes produces in the uppermost part of the crust unclamping on NE-striking planes, up to a value of 0.5 MPa, facilitating magma upwelling along this trend.

Finally, those volcanoes that have both the NW- and NE-striking magma paths might be the expression of transient magma stresses dominating over tectonic stresses. In this case magma intrudes in different directions facilitated by the pre-existing mechanical discontinuities in the surrounding rocks. This might preferentially occur in the central conduit zone where the magma force is larger. This interpretation is consistent, for example, with the results coming from the inversion of fault plane solutions of 420 earthquakes at Redoubt volcano by Sanchez et al. (2004). They showed that during the 1989-90 eruptions the stress distribution was coherent with the expansion of a plexus-like magma body with different orientations. A further possibility is here suggested based on the comparison of dike injection geometries at Redoubt volcano during the 1989-90, 1991 and 2009 eruptions. Lahr et al. (1994) showed

that the location of an earthquake swarm of the 1989-90 eruption is consistent with a NE-dipping narrow conduit (i.e. a NW-SE-striking dike), whereas Benz et al. (1996) showed that the successive July 1991 eruption was accompanied by earthquakes compatible with a N15°E-striking conduit zone. The successive eruption of 2009 was immediately followed by a period with volcano-tectonic events indicating a stable NE–SW-trending P-axis orientation corresponding to the horizontal displacement of the conduit walls (Roman and Gardine, 2013) along a possible NW-SE dike. This alternation of intrusions along the two main NW-SE and NE-SW trends suggests that each intrusion might locally modify the stress state within the surrounding rocks favouring the successive emplacement of a dike in a perpendicular direction.

7.6. Conclusions

We analyzed the static stress changes induced by five earthquakes with $M_w \geq 8$, which occurred in the Alaska-Aleutian subduction zone since 1938 AD, in order to contribute to understanding the general mechanisms by which earthquakes could trigger new volcanic activity. We used a novel approach by resolving the earthquake-induced normal static stress change on the magma pathway of each volcano. We also considered other parameters that may contribute to dictate eruption occurrence, such as magma chamber depth, magma composition/viscosity and local tectonic settings. The dataset includes a total of 13 *first new* eruptions (out of 22 total eruptions) occurred at 8 volcanoes.

Eleven eruptions out of 13 have a positive statistical correlation with earthquakes. Results indicate that the static stress changes calculated at each single subvolcanic plumbing system depict a more complex and precise pattern than considering the general crustal volume. Field new data and published geological-geophysical data indicate that the studied volcanoes have magma-feeding planes that strike NE or NW. At two volcanoes, both trends are present. The calculated stress changes suggest unclamping on both planes, with larger values of stress decrease at the planes striking NNE to NE. The activation of one preferential trend depends upon the balance between magmatic stress, tectonic stress and static stress change, in association with the presence of preferential vertical discontinuities in the rocks; the substrates surrounding the studied volcanoes in fact, show preferential NW- or NE-striking fracture fields.

Our data suggest that *first new* eruptions at non-continuously erupting volcano (that are more prone to unrest) occurred as far as 730 km from the epicentres, unclamping promoted *first new* eruptions as far as 543 km and *awakening* as far as 290 km from the epicentre. In

particular, volcano *awakening* has been promoted especially at deep magma chambers. Role of unclamping is also important for shallow chambers, which are expected to be more prone to a critical state due to magma overpressure induced by cooling and crystallizing. We finally suggest that future investigations should be devoted to quantify also the possible contribution of earthquake-induced dynamic stresses, especially in contributing to trigger volcanic activity under very weak clamping conditions.

Name	Shumagin Islands	Unimak Island	Fox-Andreanof Islands	Good Friday	Rat Islands
Date (dd/mm/year)	10/11/1938	01/04/1946	09/03/1957	28/03/1964	04/02/1965
M_w	8.2	8.1	8.6	9.2	8.7
Search radius (km)	836	798	1005	1325	1052
Rupture length (km)	~300 ÷ 400 [1,3]	~100	~1100 ÷ 1200 [3]	~800 [4]; 540 ÷ 740 [5]	~420 ÷ 600 [7,8]
Fault geometry (strike, °/dip, °)	~75 ÷ 80/10 [1,3]	250/6	~70 ÷ 95/15 [3]	216 ÷ 237/6 ÷ 12	290/18 [7]
N. of patches	4 [1,3]	3	12 [3]	95 [4]	14 [8]
Average slip (m)	1.1	7.5	1.6	3.8	1.6
Average rake angle (°)	90.0	90.0	90.0	83.0	90
Fault top (km)	20 [1]	0.0	1.0	5.2	1
Fault bottom (km)	46.0	9.7	39.8	46.8	37.7684
σ_1 (azimuth, °/plunge, °)	154/11 [2]	150/25 [2]	155/24 [2]	165/35 [6]	160/35.5 [9]
σ_2 (azimuth, °/plunge, °)	67/15 [2]	60/4 [2]	63/4 [2]	333/0 [6]	58.5/13.5 [9]
σ_3 (azimuth, °/plunge, °)	29/71 [2]	328/65 [2]	324/66 [2]	243/63 [6]	310.5/50 [9]

Table 1. *Characteristics for the five $M_w \geq 8$ earthquakes and related finite fault models: date of the event, magnitude, used search radius, fault rupture length, strike and dip angle of the fault plane, number of patches, averaged fault slip and rake angle, depth of top and bottom of the fault plane, trend and plunge of σ_1, σ_2 and σ_3 (Johnson and Satake. 1994[1]; Heidbach et al., 2008[2]; Johnson and Satake, 1995[3]; Johnson et al., 1996[4]; Ichinose et al., 2007[5]; Harding and Algermissen, 1969[6]; Johnson and Satake. 1996[7]; Beck and Christensen, 1991[8]; Stauder, 1968[9]; http://earthquake.usgs.gov/).*

Earthquake	Volcano name	Type	Distance (km)	Time-gap (days)	VEI	N.S.C. (MPa)	N.S.C. (MPa)	P-E activity	M.P. (azimuth)	Silica (% wt)	M.C. depth (km)	E.R. analysis
First new volcanic eruptions												
1938	Veniaminof	B+	157	194	3	-0.018	-0.018	N	N35°W [15]	50-63.5 [1,2,14]	Shallow [2], 7.4 [8]	Y
1398	Okmok	B+	730	1678 ± 15	1	0.000	0.000	N	N60°E [15]	51.35 [7]	4 [12]	Y
1946	Akutan	A	222	258 ± 15	2	0.010	0.010	Y	N110°E [11, 21]	52.73 [17]	8 [11], Shallow to moderate < 25 [17]	Y
1946	Shishaldin	A	220	136 ± 15	2	-0.014	-0.014	N	N139°E [15, 22]	49.95-51.94 [19]	3.9 [20]	Y
1946	Pavlof	A	310	1582	2	0.000	0.000	N	N40°E [15]	55.8-65.5 [5]	20 [13]	Y
1957	Okmok	B+	557	523	3	0.008	0.008	N	N60°E [15]	51.35 [7]	4 [12]	Y
1957	Kiska	B+	467	1782	3	-0.045	-0.045	N	N40°E [15, 4]	49.5-59.5 [4,14]	undefined	N
1964	Redoubt	B+	290	667	3	-0.355 / -0.070	-0.355	N	N15°E [24] / NW-SE [23]	59.3-61.9 [16]	6-10 [9]	Y
1964	Trident	B	543	64	3	-0.541 / -0.056	-0.541	Y	NE-SW [25] / N140°E [26]	55.8-65.5 [5]	3 [5], 6 with top at 2	Y
1964	Pavlof	A	1059	717	2	0.006	0.006	Y	N40°E [15]	55.8-65.5 [5]	20 [13]	Y
1964	Shishaldin	A	1205	1036	2	-0.001	-0.001	Y	N139°E [15, 22]	49.95-51.94 [19]	3.9 [20]	Y
1965	Kiska	B	300	285	2	-0.201	-0.201	Y	N40°E [15, 4]	49.5-59.5 [4,14]	undefined	Y
1965	Shishaldin	A	1046	723	2	0.001	0.001	Y	N139°E [15, 22]	49.95-51.94 [19]	3.9 [20]	N
Other volcanic eruptions												
1938	Veniaminof	B+	157	370 ± 15	2	-	-	-	-	-	-	-
1946	Akutan	A	222	759	2	-	-	-	-	-	-	-
1946	Shishaldin	A+	220	822 ± 6 mesi	2	-	-	-	-	-	-	-
1957	Okmok	B+	557	1316 ± 45	3	-	-	-	-	-	-	-
1964	Redoubt	B+	290	923	3	-	-	-	-	-	-	-
1964	Redoubt	B+	290	1045	3	-	-	-	-	-	-	-
1964	Trident	B	543	825 ± 6 mesi	-	-	-	-	-	-	-	-
1964	Trident	B	543	1256	3	-	-	-	-	-	-	-
1964	Trident	B	543	1691	3	-	-	-	-	-	-	-

Table 2. *Characteristics of the volcanic eruptions at each volcano following the large earthquakes, including: volcano name, Type, SiO_2 content of erupted products, distance from the epicentre, time-gap between the earthquake and the volcanic event, VEI of the eruption, amount of normal stress change (N.S.C.), activity in the five year before the earthquake (P-E activity), azimuth of the inferred magma pathway (M.P.) and depth of the magma chamber (M.C. depth), and volcano height. Data based on satellite images, SRTM90 DEM (srtm.csi.cgiar.org), Global Volcanism Program Digital Information Series (http://www.volcano.si.edu/gvp/world) and data reported in the literature. Bacon et al. (2003)[1], Bacon et al. (2007)[2], Byers (1959)[3], Coats et al. (1961)[4], Coombs et al. (2000)[5], Finch (1934)[6], Finney et al. (2008)[7], Fournier and Freymuller (2008)[8], Gerlach et al. (1994)[9], Hildreth (1987)[10], Lu et al. (2000)[11], Masterlark et al. (2012)[12], McNutt and Jacob (1986)[13], Miller et al. (1998)[14], Nakamura (1980)[15], Nye et al. (1994)[16], Romick et al. (1990)[17], Saltuest al. (1991)[18], Stelling et al. (2002)[19], Vergniolle (2006)[20], Richter et al. (1998)[21], Moran et al. (2002)[22], Buurman et al. (2013)[23], Benz et al. (1996)[24], Hildreth et al. (2001)[25], Wallmann et al. (1990)[26].*

8. Discussion and new outcomes

Chapter 8 is based on unpublished data from this doctoral work.

8.1 General

Regarding mud volcanoes, I studied the effect of two earthquakes of M_w 6.18 and 6.08 occurred in the Caspian Sea on November 25, 2000 close to the Baku city, Azerbaijan (Chapter 3). A total of 33 eruptions occurred at 24 mud volcanoes within a maximum distance of 108 km from the epicentres in the five years following the earthquakes. The largest number of eruptions occurred within two years from the earthquakes, with the highest frequency within six months. Our calculated earthquake-induced static effects show that crustal dilatation might have triggered only 7 eruptions at a maximum distance of about 60 km from the epicentres and within 3 years. Based on these new data, dynamic rather than static strain is likely to have been the dominating "promoting" factor because it affected all the studied unrested volcanoes, and its magnitude was much larger.

Regarding magmatic volcanoes I noted a different situation, as it is detailed in the following sections. In Chile four earthquakes with $M_w \geq 8$ occurred in proximity of 60 Holocene volcanoes in the Southern Volcanic Zone of the Andes (SVZ) since 1906. Five earthquakes with $M_w \geq 8$ have occurred in proximity of the Alaska-Aleutian volcanic arc since 1938. I analysed these events by numerical modelling and field data to understand the key attributes of each volcano that may lead to a seismically-triggered eruption, and the general mechanisms by which earthquakes could trigger new volcanic activity. I followed a novel approach that resolves the earthquake-induced static stress change normal to the magma pathway of each volcano instead of considering the general crustal volume. I also considered other parameters that may contribute to control eruptions, such as magma composition and viscosity, magma chamber depth and local tectonic settings. The entire dataset includes a total of 51 eruptions following large earthquakes, 33 representing *first new* eruption occurred at each single volcano. Comparison of the eruption rate before and after each earthquake suggests that 26 out of the 33 first new eruptions have a positive relation with the studied earthquakes (Chapter 6 and 7). 13 out of 26 represent *awakening* events (Type B+): first new eruptions occurred at volcanoes with no continuous eruptive activity that had no eruptions in the five years before the earthquake. Seven eruptions occurred at volcanoes with continuous eruptive activity (Type A) and six occurred at volcanoes with no continuous eruptive activity (Type B). These studies contribute to a possible individuation of those volcanoes that are

more prone to seismically-triggered eruptive events. Two main theories have been proposed to explain the seismically-induced static stress changes in a magma body in promoting eruptions: i) magma is squeezed upward by increased compressional stress in the crust surrounding a magma chamber close to its critical state (e.g. Bautista et al., 1996), but I am inclined to exclude this process in the studied areas because the magnitude of the calculated earthquake-induced stress changes are quite low and in particular the very weak values of clamping exclude a "toothpaste" or "flask" process due to permanent deformation. ii) A decrease in compressional stress can promote additional melting, formation of bubbles and volatiles exsolution, encouraging eruptions in a time frame of years (Hill et al., 2002; Walter and Amelung, 2007). In fact, earthquake-induced static (permanent) normal stress reduction on magma pathway could directly promote dike intrusion (Hill et al., 2002; Walter, 2007). Also postseismically-induced static stress/strain might remotely promote eruptions, particularly for volcanoes close to a critical state (Marzocchi, 2002; Marzocchi et al., 2002; Walter and Amelung, 2007), and may explain processes leading to eruption in regions close to the fault rupture. Dynamic shaking is another important factor for triggering eruptions that can act up to larger distances than the static effect (Manga and Brodsky, 2006).

8.2 Outcomes for the distance from epicentre

In this study, the *first new* eruptions occurred in a range of distances of 157-1207 km from the epicentres; more in detail, eruptions at volcanoes with continuous eruptive activity (Type A) occurred in the range of distances of 220-1205 km, eruptions at volcanoes with non-continuous eruptive activity (Type B), which are considered close to a critical state (e.g. Walter and Amelung, 2007; Eggert and Walter, 2009), occurred in a shorter range of distance of 157-1207 km, and *awakening* events occurred in a range of 157-730 km (Fig. 1). Unclamping effect is present where eruptions occurred at Type B volcanoes in a range of 157-543 km, while *awakening* under unclamping occurred within a range of 157-353 km. Three awakening events occurred in no-unclamping conditions in the range 522-730 km. To summarize, *first new* eruptions occurred at volcanoes with no-continuous eruptive activity (Type B) and *awakening* events always occurred at a distance < 730 km from the epicentre (Fig. 1). Here it is suggested that ~730 km could be considered as the upper limit for earthquake-induced new eruptions at volcanoes that are more prone to unrest in both the Alaska-Aleutian and the Chilean subduction zones. This is consistent with those authors who usually restricted this kind of analysis up to 750 km from the epicentre (e.g., Linde and Sacks, 1998; Eggert and Walter, 2009), whereas other authors suggest that volcanic activity

may have an increase also at greater distances (e.g. Delle Donne et al., 2010). Based on these new data, unclamping seems capable of promoting *first new* eruptions and *awakening* as far as ~550 and ~350 km, respectively. These considerations are in agreement with Marzocchi (2002), who suggested that coseismic stress changes are candidate to promote eruptions at a maximum distance of about 300 km within a time-window of 0-5 years. Finally, I do not exclude that in some cases both static and dynamic triggering might have played a role in favouring new eruptions. Dynamic shaking, is actually another important factor for triggering eruptions that can act up to larger distances than static effect (Manga and Brodsky, 2006). Dynamic shaking may excite and promote ascent of gas bubbles, and consequently magma ascent (Manga and Brodsky, 2006), the details of the feedback mechanisms remaining unclear. I cannot therefore exclude that in some cases both static and dynamic triggering might have played a role in favouring new eruptions. Dynamic effects can also favour bubble growth, including adjective overpressure (Linde et al., 1994), rectified diffusion (Brodsky et al., 1998; Ichihara and Brodsky, 2006) and shear strain (Sumita and Manga, 2008).

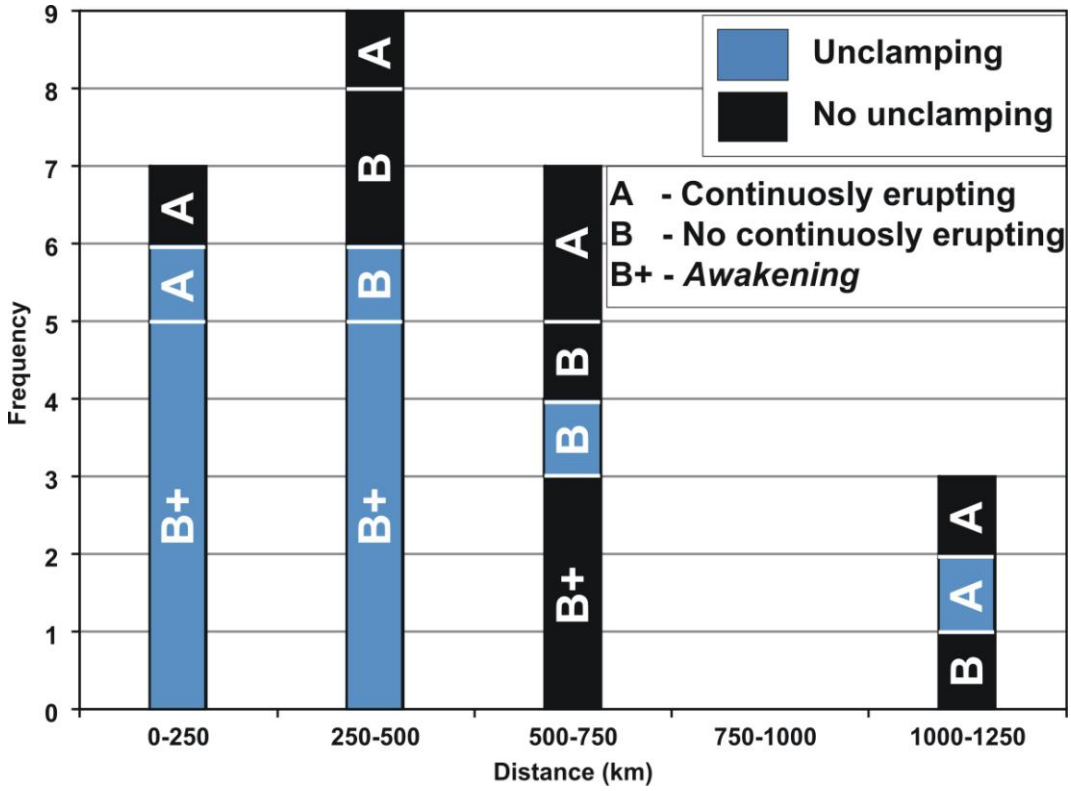

Figure 1. *Volcanic eruptions versus the distance from earthquake epicentre. A = Volcanoes with continuous volcanic activity; B = Volcanoes with no continuous volcanic activity; B+ = B volcanoes that had no volcanic events in the five years before the earthquake.*

8.3 Time-gap

It is commonly suggested that owing to the complexity of volcanic systems, the delay between the earthquake occurrence and the following volcanic events can be from seconds to years (Linde and Sacks, 1998; Nostro et al., 1998; McLeod and Tait, 1999; Walter and Amelung, 2007; Eggert and Walter, 2009).

In this work, *first new* eruptions occurred in a time-window of 2 days up to 4.5 years after the studied earthquakes, and *first new* eruptions under unclamping occurred in a time-window of 2 days up to 3 years.

In particular, *first new* eruptions at volcanoes with continuously erupting activity (Type A) occurred in a time-window of 4 months-4.5 years, eruptions at volcanoes with no-continuous eruptive activity (Type B) occurred in a time-window of 2 days-4.5 years. Unclamping effect promoted eruptions at Type B volcanoes and *awakening* in a time-window of 2 days-3 years (Fig. 2).

In seismology, the static stress change is candidate to inducing rock failure up to 3-5 years after an earthquake (Anderson and Johnson, 1999; Stein, 1999; Hardebeck et al., 1998; Seeber and Armbruster, 2000; R. Stein, written comm., 2012).

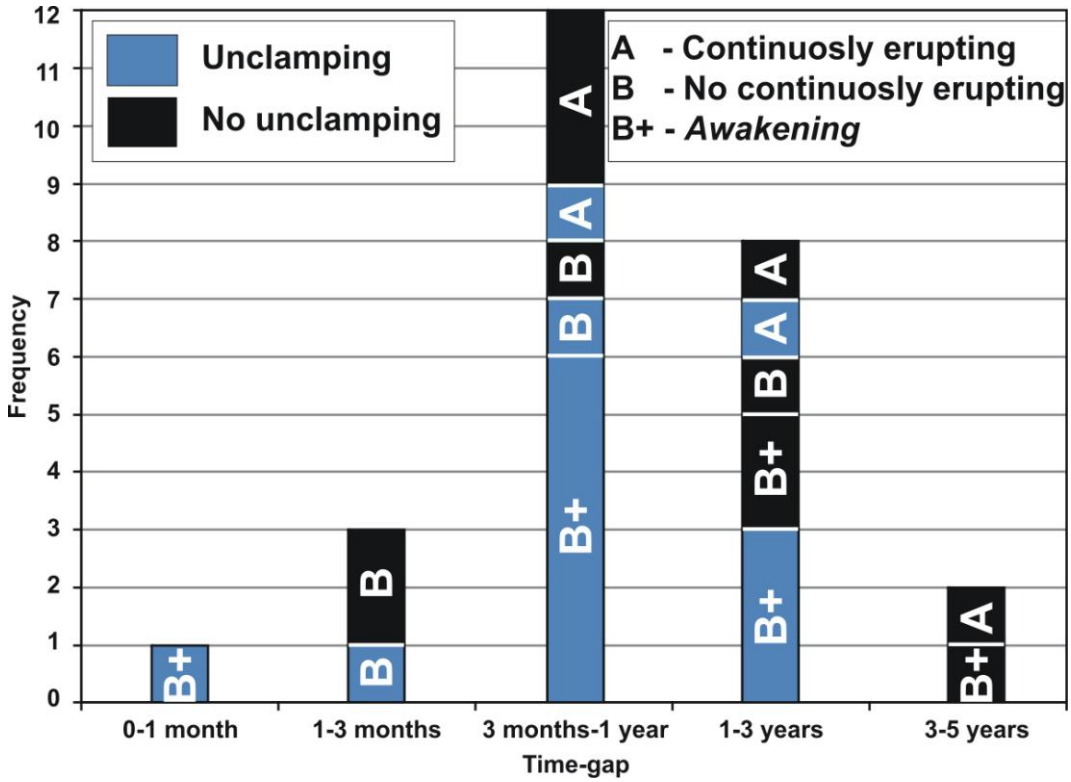

Figure 2. *Volcanic eruptions versus the time-gap. A = Volcanoes with continuous volcanic activity; B = Volcanoes with no-continuous volcanic activity; B+ = B volcanoes that had no volcanic events in the five years before the earthquake.*

In fact, from a seismological perspective, the earthquake-induced static stress changes are evaluated to better constrain the distribution of aftershocks and to understand which faults may be closer to future failure due to the earthquake-induced stress transfer (Stein, 1999).

For volcano-earthquake relations, Marzocchi (2002) noted that the largest explosive eruptions of the last Century in the World occurred within 0-5 and 30-35 years after $M_s \geq 7$ earthquakes, at distances up to 1000 km.

Postseismic stress changes were interpreted to be capable of promoting eruption in 30-35 years after earthquakes, compatibly to the relaxation time of a viscous asthenosphere (Piersanti et al., 1995, 1997; Pollitz et al., 1998; Kenner and Segall, 2000).

Coseismic stress changes are candidate to promote eruptions in the 0-5 years after earthquakes, where the eruptions occurred at a distance within 100-300 km (Marzocchi, 2002).

The time delay of 0-5 years can be attributed to the inertia of the volcanic system in reacting to the static stress changes, to a delay due to a non perfect elasticity of the crust, and/or to the stress corrosion effect (e.g., Main and Meredith, 1991). Finally, I suggest that unclamping is capable of promoting eruption up to 3 years after a large earthquake.

8.4 Magma chamber depth, magma rheology and VEI

Several authors suggested that composition of magmas, storage depth and state of volatile saturation may all play a role (e.g., Woods and Pyle, 1997; McLeod and Tait, 1999; Jellinek and De Paolo, 2003).

In the studied cases, I noted that unclamping enhanced eruptions preferentially at volcanoes with deep chamber (> 5 km) (Fig. 3). For the *awakening* events that occurred in conditions of no unclamping, this analysis suggests that magma is always stored at shallow depth (Fig. 3), where a vapour-saturated condition is generally expected due to cooling and crystallizing (Woods and Pyle, 1997).

Some authors suggested that for basaltic magmas an overpressure < 1 MPa is sufficient to generate tensile deviatoric stresses capable of promoting dike formation and propagation without cooling, whereas for more silicic magmas this overpressure has been estimated at 10-100 MPa (Tait et al., 1989; McLeod and Tait, 1999; Jellinek and De Paolo, 2003).

In the cases I studied, the magnitude of the calculated unclamping is always < 1 MPa, consistently with Manga and Brodsky (2006) who suggested values in the order of $10^{2} \div 10^{-1}$ MPa for seismically-induced dynamic and static stress changes. The same authors suggested that the overpressure of a volcanic system must be within 99%-99.9% of the maximum

overpressure for the earthquake to initiate a new eruption. On the contrary, volcanoes showing a longer response may be farther from this tipping point, but unclamping must still be significant enough to induce permanent pressure changes that could initiate a new eruption in a time frame of 3 years (as suggested above), after an incubation period, where the eruption is the "*failure event*" (e.g. Jupp et al., 2004).

Among the studied cases, only the Calbuco eruption, occurred after the 1960 M_w 9.5 earthquake and emitting andesitic products, took place under an unclamping > 1 MPa (Fig. 4A).

However, *awakening* events with products that span from basalt-andesite to rhyolite are almost always associated to earthquake-induced unclamping. Only one eruption occurred in no unclamping and emitted rhyolitic products, but the volcano is characterized by a shallow magma chamber as discussed above.

The VEI of the eruptions spans in a range 1-3; in particular, it seems that the energy of the volcanic eruptions increases with unclamping, a large number of eruption with VEI 2-3 having occurred under unclamping and being represented by *awakening* (Fig. 4B).

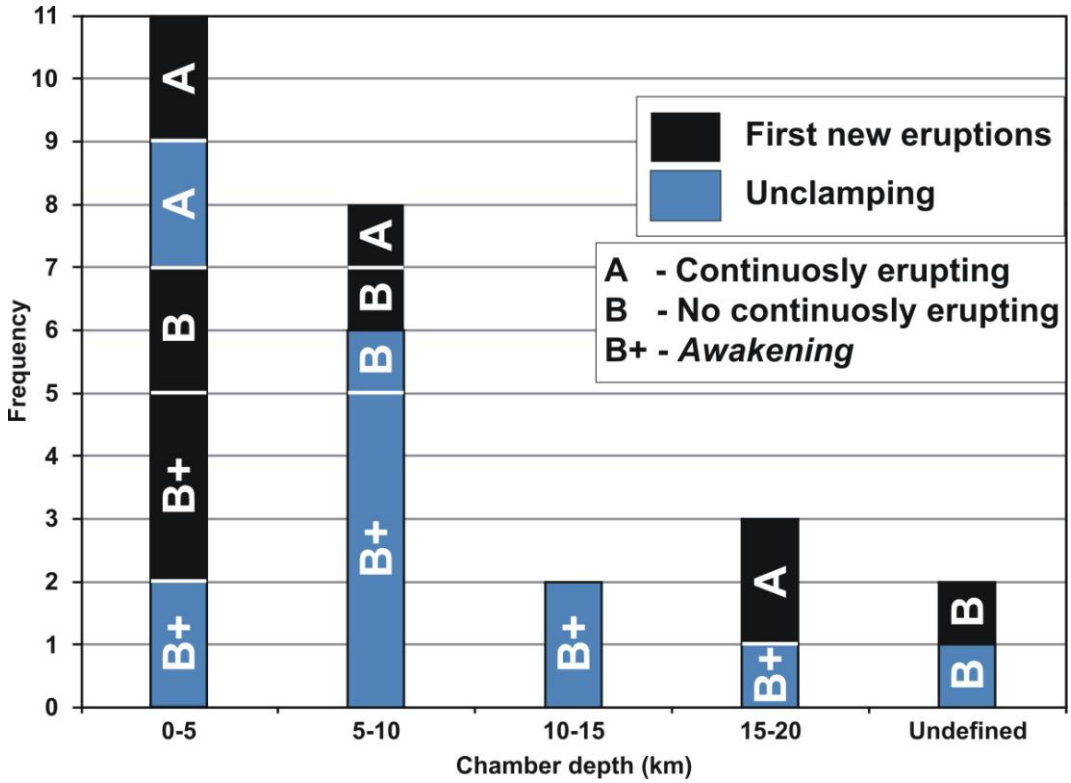

Figure 3. *Volcanic events versus centred depth of the magma chamber. A = Volcanoes with continuous volcanic activity; B = Volcanoes with no-continuous volcanic activity; B+ = B volcanoes that had no volcanic events in the five years before the earthquake.*

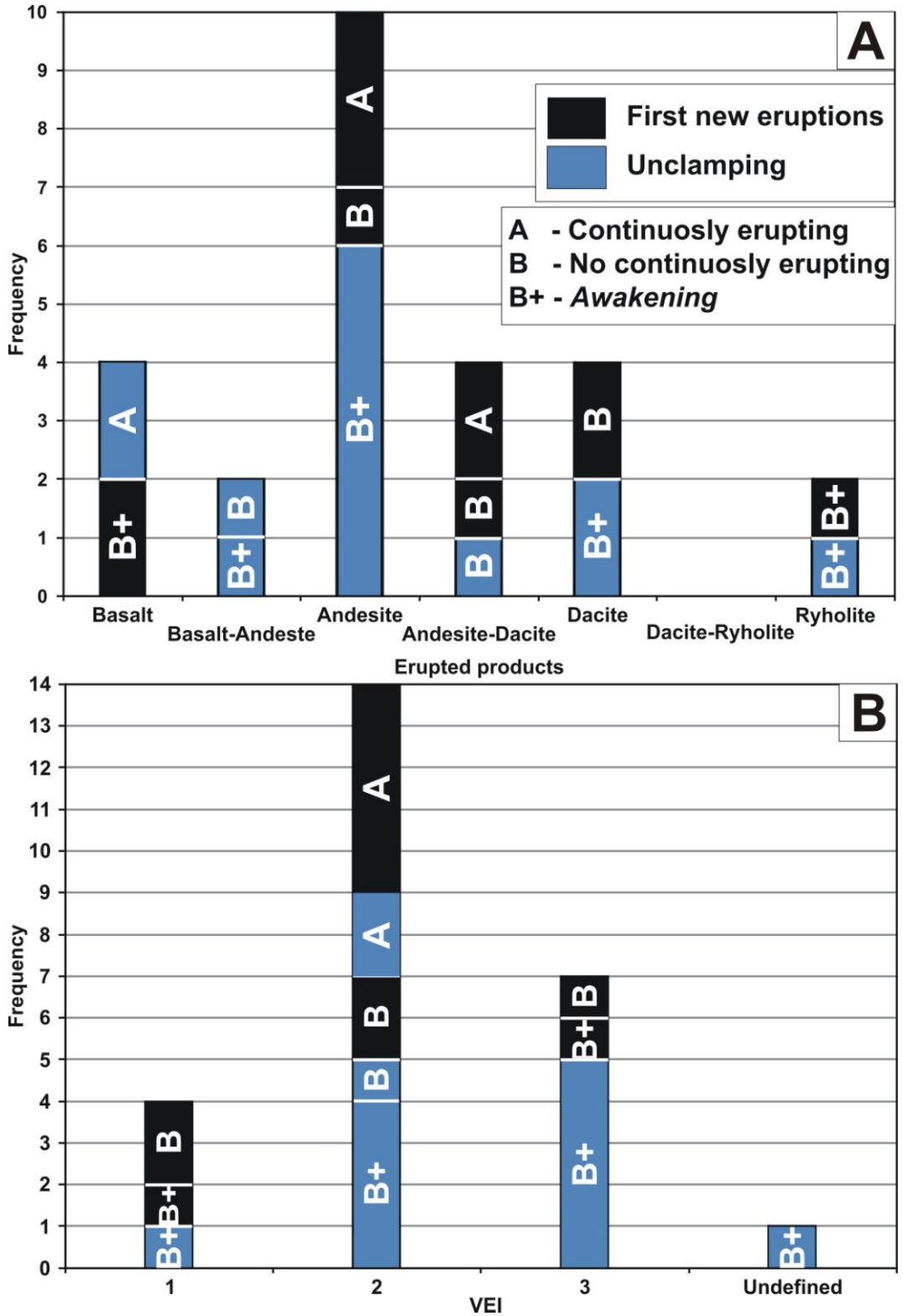

Figure 4. (A) *Number of volcanic eruptions versus erupted products classified by silica content. (B) Volcanic events versus the Volcanic Explosivity index (VEI). A = Volcanoes with continuous volcanic activity; B = Volcanoes with no-continuous volcanic activity; B+ = B volcanoes that had no volcanic events in the five years before the earthquake.*

8.5 Outcomes for magma pathway azimuth

Results indicate that the static stress changes calculated at each single subvolcanic plumbing system depict a more complex and precise pattern than considering the general crustal volume. Delle Donne et al (2010) suggested that volcanoes that responded to earthquakes are characterized by an azimuth within 30° of the fault strike for the associated earthquake. They explain such relation with a scenario where the radiation pattern of Love waves is larger along the fault strike (Kanamori, 1970) and did not exclude that the propagation of fault rupture may have a fundamental role in focusing the stress in a well-defined direction. The sensitivity analysis done for the 2010 Chile earthquake (Chapter 4) shows that the N-S- and NE-SW-striking magma pathways suffered a larger unclamping in comparison with those striking NW-SE and E-W. Magma pathways parallel or subparallel to the strike of modelled faults suffered the highest unclamping, and this evidence was also noted in the Alaska-Aleutian volcanic arc (Chapter 7). The results of the sensitivity analysis show that the magma pathway geometry controls the magnitude of the static stress change induced by large earthquakes, with differences of up to 8 times among magma-feeding planes of different orientation at the same volcano. This range of diverse values is larger for volcanoes closer to the epicentre. The possible error in the estimate of magma chamber depth has a minimum effect on the results, since the sensitivity analysis shows that the range of stress changes with depth is about 1.5 orders of magnitude smaller than the range linked to variations of the magma pathway strike.

In the Alaska-Aleutian volcanic arc, new field data and published geological-geophysical data indicate that the studied volcanoes have magma-feeding planes that strike NE or NW (Fig. 5). At two volcanoes both trends are present. The calculated stress changes suggest unclamping on both planes, with larger values of stress decrease at the planes striking NNE to NE (Chapter 7). The activation of one preferential trend depends upon the balance between magmatic stress, tectonic stress and static stress change, in connection with the presence of preferential vertical discontinuities in the rocks; the substrate surrounding the studied volcanoes, in fact, shows preferential NW- or NE-striking fracture fields. Based on the World Stress Map data (Heidbach et al., 2008), the σ_{Hmax} affecting the upper plate in the Western insular arc strikes N151°E, while in the eastern arc it strikes N130°E (Fig. 5).

In the SVZ, *first new* eruptions occurred in the older and thicker crust of the fold and thrust belt dominated by Type B volcanoes (Fig. 6), possibly suggesting that this contractional tectonic setting does not favour the preservation of open magma conduits.

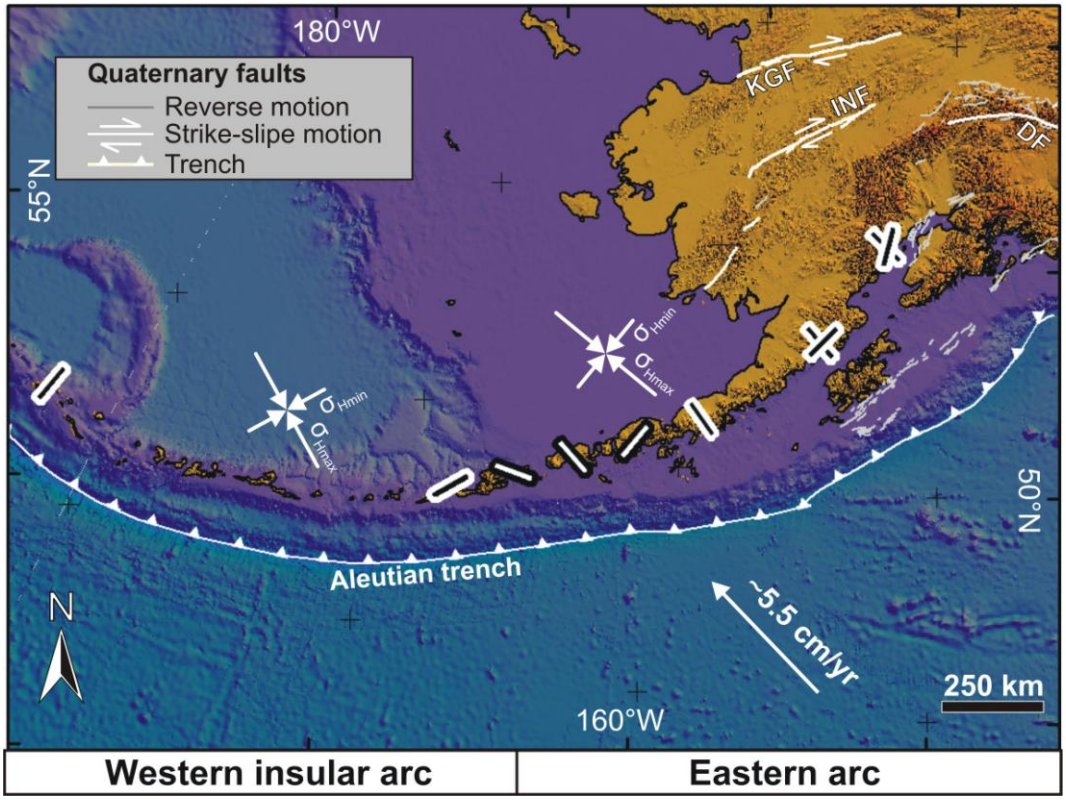

Figure 5. *Reconstructed magma pathway orientation for the studied volcanoes. The white arrow indicates the approximate convergence direction of the plates and estimated velocity. Main Quaternary intra–arc faults with reverse motions and right-lateral strike–slip motions are reported (redrawn after Koehler et al., 2012).*

The present tectonic state of stress is characterized by horizontal σ_1 and σ_2, a situation that discourages magma upwelling, although more and more active volcanoes in contractional tectonic settings are being reported in the literature (e.g. Tibaldi, 2008; for a review, Tibaldi et al., 2010). N0° to N25°E orientation of magma pathways dominates this zone, being parallel or subparallel to the local strike of the faults. This may imply a direct control of substrate faults on magma pathway orientation, similarly to the model proposed by Tibaldi (2008).

Magma reaches the surface when its pressure is larger than σ_2 if this stress axis lies in the horizontal plane, or when it is larger than σ_3 if there is a very local rotation of the stress tensors with σ_3 assuming a horizontal dip as suggested by Galland et al. (2007). In this contractional zone, the four *awakening* events always occurred under unclamping conditions that may have directly promoted dyke intrusion (Hill et al., 2002; Walter, 2007), irrespective of the tectonic horizontal buttressing. South of this thrust zone, where strike-slip faulting is

predominant (LOFZ, south of 38°S), *first new* eruptions occurred at both Type A and Type B volcanoes (Fig. 6), along vertical magma pathways with horizontal σ_1 and σ_3.

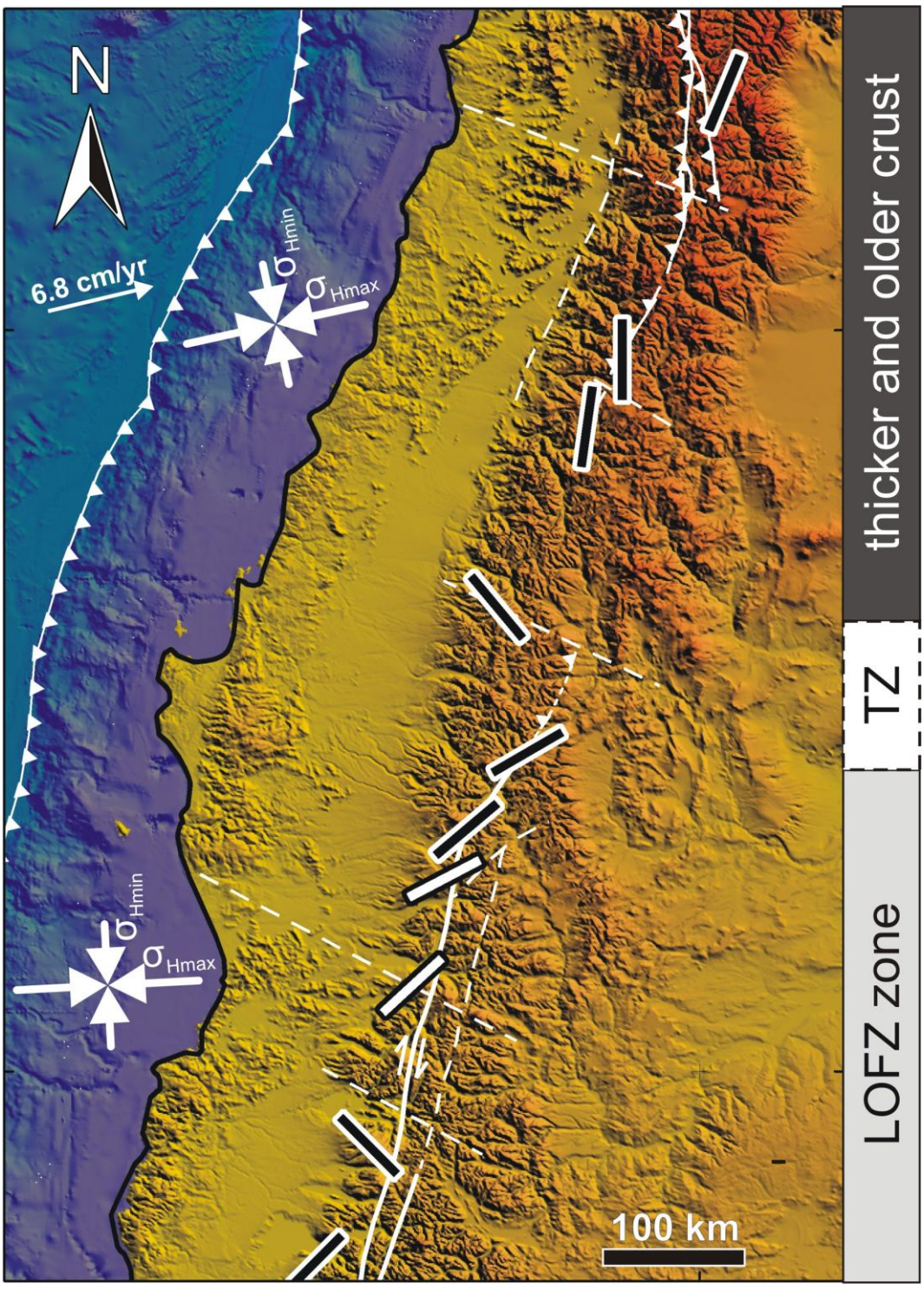

Figure 6. *Reconstructed magma pathway orientation for the studied volcanoes. The white arrow indicates the approximate convergence direction of the plates and estimated velocity. Main intra–arc faults with reverse motion in the north, and right-lateral strike-slip motion in the south (redrawn after Cembrano and Lara, 2009), are reported; TZ = Transition Zone. LOFZ = Liquiñe–Ofqui Fault Zone.*

A lower silica content than observed in the thrust-fault zone (Chapter 5) and the presence also of Type A volcanoes, suggest that a σ_3 lying in the horizontal plane favours magma upwelling and the possibility of preserving more open magma conduits. Another characteristic of this strike-slip fault zone is the predominance of shallow magma chambers over only one deeper chamber (Chapter 5).

Along the strike-slip LOFZ, most magma pathways strike N40° to N60° (Fig. 6); this orientation is perpendicular or oblique to σ_3, suggesting that magma uses tension cracks or R' shear planes respectively. Instead, the NW-SE-striking magma paths at two historic volcanoes (Nevados de Chillàn and Puyehue-Cordon Caulle) are not easily explained and need further field investigations to elucidate the local Holocene to Present-day fault geometry and kinematics. Based on World Stress Map data (Heidbach et al., 2008), the σ_{Hmax} affecting the older and thicker crust strikes N83°E, while in the LOFZ strikes N88°E (Fig. 6). The azimuth of each magma pathway has been compared with the azimuth of the σ_{Hmax} affecting the upper plate (Fig. 7), based on World Stress Map data (Heidbach et al., 2008).

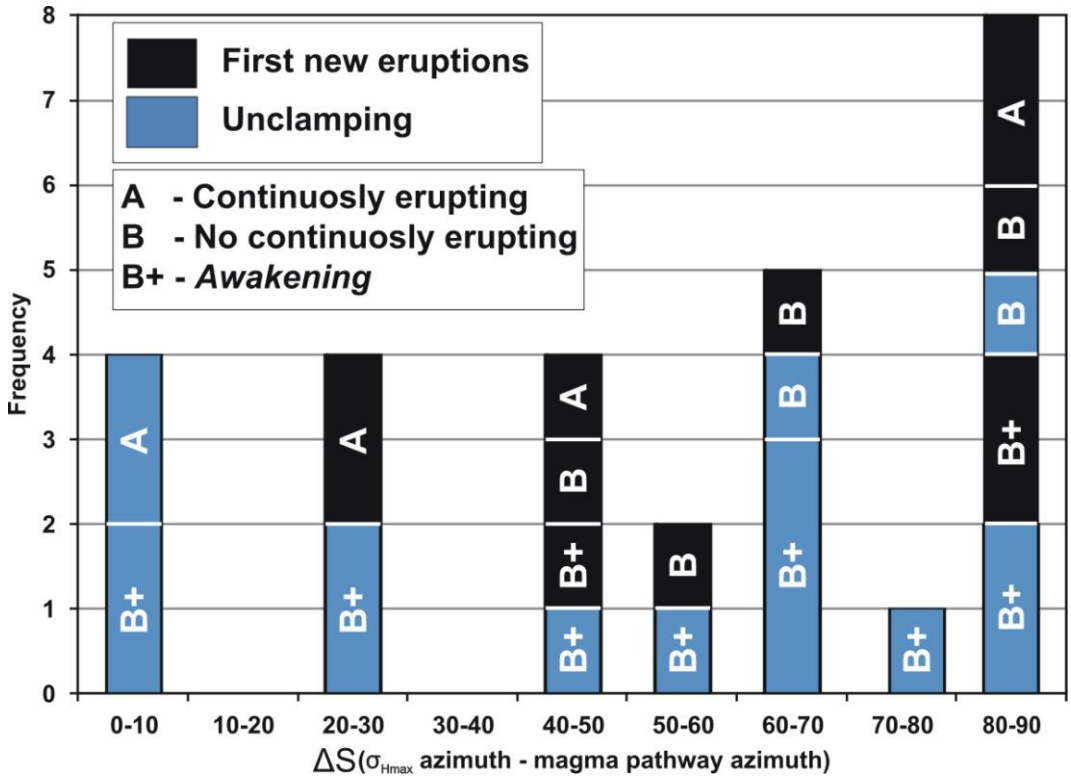

Figure 7. *Number of volcanic eruptions versus the angle between maximum horizontal stress and magma pathway strikes. A = Volcanoes with continuous volcanic activity; B = Volcanoes with no-continuous volcanic activity; B+ = B volcanoes that had no volcanic events in the five years before the earthquake.*

Result suggest that 4 *awakening* events occurred along magma pathways parallel or subparallel to the σ_{Hmax}, and they are always under unclamping. Eleven *awakening* events occurred along magma pathways that have an angle ranging 40-90° respect to the $\sigma_{Hmax,}$ thus unclamping favoured 8 of these events (Fig. 7).

Nakamura and Uyeda (1980) suggest that along subduction zones a stress gradient exists and it is manifested by a zonal pattern of different tectonics. In particular, moving away from the trench axis, zones are first predominantly characterized by thrust faults, then by strike-slip faults as a result of stress field rotation, and volcanic arcs take place in this strike-slip regime. This work suggests that large earthquakes along the Alaska-Aleutian subduction zone could impart a maximum decrease of stress along a defined surface up to about 0.5 MPa, while a large earthquake along the Chile subduction zone could impart a maximum decrease of stress along a defined surface up to about 1-2 MPa. Mount and Suppe (1987) suggest that the deviatoric stress in the crust could be a value of 100 MPa in the San Andreas fault zone, while other authors suggest, also providing numerical models, to assume a deviatoric stress of about 10 MPa (King et al., 1994; Hardebeck and Hauksson, 2001). In particular, in the crust above the subduction zone in the Andes, it is assumed less than 10 MPa (Husson and Ricard, 2004). Based on the results from this work, earthquake-induced stress change can favor magma rise by imparting stress field modifications of the deviatoric stress acting on magma pathway in a percentage up to 5-10 %, increasing the efficiency of magma rise and consequent dyke intrusion (e.g. Hill et al., 2002; Walter, 2007), also where the tectonic regime does not favour magma rise (e.g. in the older and thicker crust in Chile).

9. Final remarks

- Regarding mud volcanoes, I studied the effects of two earthquakes of M_w 6.18 and 6.08 occurred in the Caspian Sea on November 25, 2000 close to Baku city, Azerbaijan. A total of 33 eruptions occurred at 24 mud volcanoes within a maximum distance of 108 km from the epicentres in the five years following the earthquakes. Results show that crustal dilatation might have triggered only 7 eruptions at a maximum distance of about 60 km from the epicentres and within 3 years. Dynamic rather than static strain is thus likely to have been the dominating "promoting" factor because it affected all the studied unrested volcanoes and its magnitude was much larger.

- Regarding magmatic volcanoes, the entire dataset includes a total of 51 eruptions following 9 large earthquakes ($M_w \geq 8$); 33 represent *first new* eruptions occurred at each single volcano. Comparison of the eruption rate before and after each earthquake suggests that 26 out of the 33 first new eruptions have a positive relation with the studied earthquakes; 13 out of 26 represent *awakening* events, which are first new eruptions occurred at volcanoes with not-continuous eruptive activity that had no eruptions in the five years before the earthquake.

- I followed a novel approach that resolves the earthquake-induced static stress change normal to the magma pathway of each volcano instead of considering the general crustal volume. I also considered other parameters that may contribute to control eruptions, such as magma composition and viscosity, magma chamber depth and local tectonic settings.

- The sensitivity analysis performed for the 2010 Chile earthquake shows that the N-S- and NE-SW-striking magma pathways suffered a larger unclamping in comparison with those striking NW-SE and E-W. Magma pathway parallel or subparallel to the strike of modelled faults suffered the highest unclamping, and this was also evident in the Alaska-Aleutian arc. Magma pathway geometry controls the magnitude of the static stress change induced by large earthquakes, with differences of up to 8 times among magma-feeding planes of different orientation at the same volcano. This range of diverse values is larger for the volcanoes closer to the epicentre. The possible error in the estimate of magma chamber depth has a minimum effect on the results since the sensitivity analysis shows that the range of stress changes with depth is about 1.5 orders of magnitude smaller than the range linked to variations in the magma pathway strike.

- Unclamping effect promoted eruptions that occurred at non-continuously erupting volcanoes (Type B) in a range of 157-543 km, while *awakening* under unclamping occurred in a range of 157-353 km. Unclamping promoted eruptions at Type B volcanoes and *awakening* in a time window of 2 days-3 years.

- In the studied cases, it was noted that unclamping enhanced eruptions preferentially at volcanoes with a deep magma chamber (> 5 km).

- Results suggest that 4 *awakening* events occurred along magma pathways parallel or subparallel to the σ_{Hmax}, and they are always under unclamping. Eleven *awakening* events occurred along magma pathways that have an angle from 40° to 90° respect to the σ_{Hmax}, thus unclamping favoured 8 of these events.

- Based on the results from this work, earthquake-induced stress changes can favor magma rise by imparting stress field modifications of the deviatoric stress acting on magma pathway in a percentage up to 5-10 %, increasing the efficiency of magma rise and consequent dyke intrusion also where the tectonic regime doesn't favour magma rise (e.g. in the older and thicker crust in Chile under contractional tectonics).

10. Acknowledgements

This work was carried out in the framework of the International Lithosphere Program-Task Force II “Volcanoes and society: environment, health and hazards”.

Coulomb 3.3 software is provided freeware for research and teaching purposes from ww.coulombstress.org.

I greatly acknowledge Ross E. Stein, Jian Lin and Min Ding for providing the Coulomb input file for the 1960 Chile earthquake.

Emile A. Okal and Hiroo Kanamori kindly provided the focal mechanism data for the 1906 and 1960 earthquakes.

Fred F. Pollitz, Thorne Lay, Anthony Sladen, Christophe Vigny and Stefano Lorito are acknowledged for kindly providing the 2010 Chile earthquake finite fault models.

Federico A. Pasquarè, Annalisa Tunesi and Maria Luce Frezzotti are acknowledged for useful comments to the work.

Mara Limonta and Marco A. Paolini are acknowledged for their support.

11. References

Adriasola, A.C., Thomson, S.N., Brix, M.R., Hervé, F., Stockhert, B., 2006. Postmagmatic cooling and Late Cenozoic denudation of the North Patagonian Batholith in the Los Lagos Region of Chile, 41°S-42°S. International Journal of Earth Sciences 95, 504-528.

Agabekov, M.G., Allakhverdiev, R.A., 1972. Geology and oil-and-gas bearing of upper part of Jeyrankehmez river (South-eastern subsidence of Greater Caucasus). Baku, Elm 178.

Akker, S., Bommer, J., 2010. Empirical Equations for the Prediction of PGA, PGV, and Spectral Accelerations in Europe, the Mediterranean Region, and the Middle East Seismological Research Letters 81, 2, 195-206.

Alaska Seismic Hazards Safety Commission, 2012, Annual Report to the Governor and State Legislature, http://seismic.alaska.gov/.

Aliyev, A.A., Guliyev, I.S., Rakhmanov, R.R., 2009. Catalogue of mud volcano eruptions of Azerbaijan (1810-2007 yrs). Nafta-Press 110.

Anderson, G., Johnson, H., 1999. A new statistical test for static stress triggering: Application to the 1987, Superstition Hills earthquake sequence. Journal of geophysical research 104, 20153-20168.

Angermann, D., Klotz, J., Reigber, Ch., 1999. Space-geodetic estimation of the Nazca-South America Euler vector. Earth and Planetary Science Letters 171, 3, 329-334.

Annen, C., Lénat, J-F., Provost, A., 2001. The long-term growth of volcanic edifices: numerical modelling of the role of dyke intrusion and lava flow emplacement. Journal of volcanology and geothermal research Res 105, 263-289.

Arancibia, G., Cembrano, J., Lavenu, A., 1999. Transpresión dextral y partición de la deformación en la Zona de Falla Liquiñe-Ofqui, Aisén, Chile (44-45°S). Revista Geológica de Chile 26, 1, 3-22.

Asano, Y., Saito, T., Ito, Y., Shiomi, K., Hirose H., Matsumoto, T., Aoi, S., Hori, S., Shoji, S., 2011. Spatial distribution and focal mechanisms of aftershocks of the 2011 off the Pacific coast of Tohoku Earthquake. Earth Planets Space 63, 669-673.

Babayev, G.R., 2010. About some aspects of probabilistic seismic hazard assessment of Absheron peninsula. Republican Seismic Survey Center of Azerbaijan National Academy of Sciences. Catalogue of Seismoforecasting Research Carried Out in Azerbaijan Territory in 2009. Tекnur Baku, 59-64 (in Russian).

Babayev, G., Ismail-Zadeh, A., Le Moüel, J-L., 2010. Scenario-based earthquake hazard and risk assessment for Baku (Azerbaijan). Natural Hazards and Earth System Sciences 10, 2697-2712.

Baciu, C., Etiope, G., 2005. Mud volcanoes and seismicity in Romania. In Mud Volcanoes, Geodynamics and Seismicity, NATO Sci Ser Earth Environ, Edited by G. Martinelli and B. Panahi, Springer, New York 51, 77-88.

Bacon, C.R., Calvert, A.T., Nye, C., Sisson, T.W., 2003. History and Eruptive Style of Mount Veniaminof, a Huge Alaskan Basalt-to-Dacite Volcano With Pleistocene and Holocene Caldera-Forming Eruptions. American Geophysical Union, Fall Meeting 2003, abstract #V32D-1048.

Barber, A.J., Tjokrosapoetro, S., Charlton, T.R., 1986. Mud volcanoes, shale diapirs, wrench faults, and melanges in accretionary complexes, Eastern Indonesia. Am Assoc Petrol Geol Bull 20, 11, 1729-1741.

Barrientos, S.E., Ward, S.N., 1990. The 1960 Chile earthquake: inversion for slip distribution from surface deformation. Geophysical Journal International 103, 589-598.

Barrientos, S.E., Acevedo-Ardnguiz, P.S., 1992. Seismological aspects of the 1988-1989 Lonquimay (Chile) volcanic eruption. Journal of Volcanology and Geothermal Research 53, 73-87.

Barrientos, S.E., 1994. Large thrust earthquakes and volcanic eruptions. Pure and Applied Geophysics 142, 225-237.

Bautista, B.C., Bautista, L.P., Barcelona, E.S., Punongbayan, R.S., Laguerta, E.P., Rasdas, A.R., Ambubuyog, G., Amin, E.Q., Stein, R.S., 1996. Relationship of regional and local structures to Mount Pinatubo activity. In: Newhall, C.G., Punongbayan, R.S. (Eds.), The 1991-1992 Eruptions of Mount Pinatubo, Philippines. Univ. of Wash. Press, Seattle, 351-370.

Bebbington, M.S.,Marzocchi,W., 2011. Stochastic models for earthquake triggering of volcanic eruptions. Journal of Geophysical Research 116, B05204.

Beck, S.L., Christensen, D.H., 1991. Rupture process of the February 4, 1965, Rat Islands earthquake: Journal of Geophysical Research 96, B2, 2205-2221.

Benz H.M., B.A. Chouet, P.B. Dawson, J.C. Lahr, R.A. Page, J.A.H, 1996. Three-dimensional P and S wave velocity structure of Redoubt Volcano, Alaska. Journal of Geophysical Research 101, B4, 8111-8128.

Beresnev, .IA., Johnson, P.A., 1994. Elastic-wave stimulation of oil production: a review of methods and results. Geophysics 59, 6, 1000-1017.

Blake, S., 1984. Volatile oversaturation during the evolution of silicic magma chambers as an eruption trigger. Journal of Geophysical Research 89, 8237-8244.

Boghdanovitch, G., 1904. Remarques sur ke tremblement de terre a chemakha le 31 janvier 1902. Comptes Rendue des Seances, Tome I Academie Imperiale des Sciences St.-Petersbourg, 282-291.

Bonali F.L., Corazzato C., Tibaldi A., 2011. Identifying rift zones on volcanoes: an example from La Réunion island, Indian Ocean. Bulletin of Volcanology 73, 3, 347-366.

Bonali, F.L., Corazzato, C., Tibaldi, A., 2012, Elastic stress interaction between faulting and volcanism in the Olacapato-San Antonio de Los Cobres area (Puna plateau, Argentina).

Bonali, F.L., 2013. Earthquake-induced static stress change on magma pathway in promoting the 2012 Copahue eruption. Tectonophysics 608, 127-137.

Bonali, F.L., Tibaldi, A., Corazzato, C., Tormey, D., Lara, L.E., 2013. Quantifying the effect of large earthquakes in promoting eruptions due to stress changes on magma pathway: The Chile case. Tectonophysics 583, 54-67.

Bonini, M., 2012. Mud volcanoes: Indicators of stress orientation and tectonic controls. Earth-Science Reviews 115, 121-152.

Bonini, M., Mazzarini, F., 2010. Mud volcanoes as potential indicators of regional stress and pressurized layer depth. Tectonophysics 494, 32-47.

Boore, D.M., Atkinson, G.M., 2008. Ground-Motion Prediction Equations for the Average Horizontal Component of PGA, PGV, and 5%-Damped PSA at Spectral Periods between 0.01 s and 10.0 s. Earthquake Spectra 24, 1, 99-138.

Brodsky, E.E., Sturtevant, B., Kanamori, H., 1998. Volcanoes, earthquakes and rectified diffusion. Journal of Geophysical Research: Solid Earth 103, 23827-23838.

Brodsky, E.E., Roeloffs, E.A., Woodcock, D., Gall, I., Manga, M., 2003. A mechanism for sustained groundwater pressure changes induced by distant earthquakes. Journal of Geophysical Research: Solid Earth 108, B8, 2390-2399.

Brown, K.M., 1990. The nature and hydrogeologic signifi cance of mud diapirs and diatremes for accretionary systems. Journal of Geophysical Research 95, 8969-8982.

Buurman H., West, M.E., Roman, D.C., 2013. Using repeating volcano-tectonic earthquakes to track post-eruptive activity in the conduit system at Redoubt Volcano, Alaska. Geology 41, 511-514.

Byers, F.M., 1959. Geology of Umnak and Bogoslof Islands, Aleutian Islands, Alaska: U.S. Geological Survey Bulletin 1028-L, 167-369.

Carracedo, J.C., 1994. The Canary Islands - an example of structural control on the growth of large oceanic-island volcanoes. Journal of Volcanology and Geothermal Research 60, 225-241.

Cas, R.A.F., Wright, J.V., 1987. Volcanic Successions. Allen & Unwin, London 528.

Caselli, A.T., Agusto, M.R., Vélez, M.L., 2013. Volcan Copahue (Argentina-Chile): La erupción del 22 de diciembre de 2012, https://vhub.org/resources/2175.

Cayol, V., Dieterich, J.H., Okamura, A., Miklius, A., 2000. High magma storage rates before the 1983 eruption of Kilauea, Hawaii. Science 288, 2343-2346.

Cembrano, J., Hervé, F., Lavenu, A., Shermer, E., Lavenu, A., Sanhueza, A., 1996. The Liquiñe Ofqui fault zone: a long-lived intra-arc fault system in southern Chile. Tectonophysics 259, 1-3 55-66.

Cembrano, J., Shermer, E., Lavenu, A., Sanhueza, A., 2000. Contrasting nature of deformation along an intra-arc shear zone, the Liquiñe-Ofqui fault zone, southern Chilean Andes. Tectonophysics 319, 129-149.

Cembrano, J., Lara, L.E., 2009. The link between volcanism and tectonics in the Southern Volcanic Zone of the Chilean Andes: A review. Tectonophysics 471, 96-113.

Chigira, M., Tanaka, K., 1997. Structural features and the history of mud volcanoes in southern Hokkaido, northern Japan. Journal-Geological society of Japan103, 781-791.

Chinn, D.S., Isacks, B.L., 1983. Accurate source depths and focal mechanisms of shallow earthquakes in western South America and in the News Hebrides islands arc. Tectonics 2, 529-563.

Chinn, D.S., Isacks, B.L., 1983. Accurate source depths and focal mechanisms of shallow earthquakes in western South America and in the News Hebrides islands arc. Tectonics 2, 529-563.

Chiou, B.S-J., Youngs, R.R., 2008. An NGA Model for the Average Horizontal Component of Peak Ground Motion and Response Spectra. Earthquake Spectra 24, 1, 173-215.

Chouet, B.A., 1996. Long-period volcano seismicity: its source and use in eruption forecasting. Nature 380, 309-316.

Christensen, D.H., Beck, S.L., 1994. The rupture process and tectonic implications of the Great 1964 Prince William Sound earthquake. Pure and Applied Geophysics 142, 1, 29-53.

Cisternas, M., Atwater, B.F., Torrejon, T., Sawai, Y., Machuca, G., Lagos, M., Eipert, A., Youlton, C., Ignacio, S., Kamataki, T., Shishikura, M., Rajendran, C. P., Malik., J.K., Rizal., Y., Husni, M., 2005. Predecessors of the giant 1960 Chile earthquake. Nature 437, 404-407.

Coats, R.R., Nelson, W.H., Lewis, R.Q., Powers, H.A., 1961. Geologic reconnaissance of Kiska Island, Aleutian Islands, Alaska: U.S. Geological Survey Bulletin 1028-R, 563-581.

Cockerham, R.C., Corbett, E.J., 1987. The July 1986 Chalfant Valley, California, earthquake sequence: Preliminary results. Bulletin of the Seismological Society of America 77, 280-289.

Collini, E., Osores, M.S., Folch, A., Viramonte, J.G., Villarosa, G., Salmuni, G., 2013. Volcanic ash forecast during the June 2011 Cordón Caulle eruption. Natural Hazards 6, 389-412.

Comte, D., Eisenberg, A., Lorca, E., Pardo, M., Ponce, L., et al., 1986. The central Chile earthquake of 3 March 1985: a repeat of previous great earthquakes in the region? Science 233, 449–453.

Coombs, M.L., Eichelberger, J.C., Rutherford, M.J., 2000. Magma storage and mixing conditions for the 1953–1974 eruptions of Southwest Trident volcano, Katmai National Park, Alaska. Contributions to Mineralogy and Petrology 140, 1, 99-118.

Corazzato C., Tibaldi A., 2006. Basement fracture control on type, distribution, and morphology of parasitic volcanic cones: an example from Mt. Etna, Italy. In: Tibaldi A. and Lagmay M. (eds.), "Interaction between Volcanoes and their Basement". Journal of Volcanology and Geothermal Research Special issue 158, 177-194.

Darwin, C., 1840. On the connexion of certain volcanic phenomena in South America; and on the formation of mountain chains and volcanos, as the effect of the same power by which continents are elevated: Geological Society. Transactions of the Geological Society of London 2, 5, 601-631.

Davis, M., Koenders, M.A., Petford, N., 2007. Vibro-agitation of chambered magma. Journal of Volcanology and Geothermal Research 167, 24-36.

Delisle, G., von Rad, U., Andruleit, H., van Daniels, C., Tabreez, A.A.I., 2002. Active mud volcanoes on- and offshore eastern Makran, Pakistan. International Journal of Earth Sciences 91, 1, 93-110.

Delle Donne, D., Harris, A.J.L., Ripepe, M., Wright, R., 2010 Earthquake-induced thermal anomalies at active volcanoes. Geology 38, 9, 771-774.

Delouis, B., J.-M. Nocquet, Vallée, M., 2010. Slip distribution of the February 27, 2010 Mw = 8.8 Maule earthquake, central Chile, from static and high-rate GPS, InSAR, and broadband teleseismic data. Geophysical Research Letters 37, L17305.

Delpino, D., Bermúdez, A., 1993. La actividad del Volcán Copahue durante 1992. Erupción con emisiones de azufre piroclastico, Provencia del Neuquen, Argentina: Congreso Geológico Argentino XII y Congreso de Exploración de Hidrocarburos II, Actas 4, 292-301.

Delpino, D., Bermúdez, A., 1995, Eruptions of pyroclastic sulphur at crater lake of Copahue volcano, Argentina: International Union of Geodesy and Geophysics, General Assembly XXI, Abstracts, p. B410.

Déruelle, B., López-Escobar, L., 1999. Basaltes, andesites, dacites et rhyolites des stratovolcans des Nevados de Chillán et de l'Antuco (Andesméridionales): la remarquable illustration d'une différenciation par cristallisation fractionnée. Comptes Rendus de l'Academie des Sciences Series IIA Earth and Planetary Science 329, 337–344

Dieterich, J.H., 1988. Growth and persistence of Hawaiian volcanic rift zones. Journal of Geophysical Research, Solid Earth 93, 4258-4270.

Dixon, J.E., Stolper, E.M., Holloway, J.R., 1995. An experimental study of water and carbon dioxide solubilities in mid-ocean ridge basaltic liquids; Part I, Calibration and solubility models. Journal of Petrology 36, 1607-1631.

Dixon, H.J., Murphy, M.D., Sparks, S.J., Chavez, R., Naranjo, J.A., Dunkley, P.N., Young, S.R., Gilbert, J.S., Pringle, M.R., 1999. The geology of Nevados de Chillan Volcano, Chile. Revista Geológica de Chile 26, 227–253.

Eggert, S., Walter, T.R., 2009. Volcanic activity before and after large tectonic earthquakes: Observations and statistical significance. Tectonophysics 471, 14-26.

Eichelberger, J.C., 1980. Vesiculation of mafic magma during replenishment of silicic magma reservoirs. Nature 288, 446-450.

Farías, M., 2007. Tectónica y erosión en la evolución del relieve de los Andes de Chile Central durante el Neógeno. Ph.D. Thesis, Universidad de Chile, Santiago, Chile.

Feuillet, N., Nostro, C., Chiarabba, C., Cocco, M., 2004. Coupling between earthquake swarms and volcanic unrest at the Alban Hills volcano (central Italy) modelled through elastic stress transfer. Journal of Geophysical Research: Solid Earth 109, B02308.

Feyzullayev, A.A., 2012. Mud volcanoes in the South Caspian basin: Nature and estimated depth of its products. Natural Science 4, 445-453.

Finch, R.H., 1934. Shishaldin Volcano: Proceedings of the Fifth Pacific Science Conference Canada 3, 2369-2376.

Finney, B., Turner, S., Hawkesworth, C., Larsen, J., Nye, C., George, R., Bindeman, I., Eichelberger, J., 2008. Magmatic Differentiation at an Island-arc Caldera: Okmok Volcano, Aleutian Islands, Alaska. Journal of Petrology 49, 5, 857-884.

Fiske, R.S., Jackson, E.D., 1972. Orientation and growth of Hawaiian volcanic rifts: the effect of regional structure and gravitational stresses. Proceedings of the Royal Society of London 329, 299-326.

Folguera, A., Ramos, V.A., Melnick, D., 2002. Partición de la deformación en la zona del arco volcánico de los Andes neuquinos (36-39°S) en los últimos 30 millones de años. Revista Geológica de Chile 29, 2, 151-165.

Folguera, A., Ramos, V.A., Gonzalez Dıaz, E., and Hermanns, R., 2006, Late Cenozoic evolution of the Eastern Andean Foothills of Neuqu´en between 37° and 37°30'S. In Late Cretaceous to Recent Magmatism and Tectonism of the Southern Andean Margin at the Latitude of the Neuquen Basin (36-39◦S) (eds. Kay, S.M. & Ramos, V.A.), Geol. S. Am. S. 407, 247-266.

Fournier, T., Freymueller, J., 2008. Inflation detected at Mount Veniaminof, Alaska, with campaign GPS. Geophysical Research Letters 35, 20.

Freed, A.M., Lin, J., 2002. Accelerated stress buildup on the southern San Andreas Fault and surrounding regions caused by Mojave Desert earthquakes. Geology 30, 6, 571-574.

Freed, A.M., 2005. Earthquake triggering by static, dynamic, and postseismic stress transfer. Annual Review of Earth and Planetary Sciences 33, 335-367.

Frey, F. A., Gerlach, D. C., Hickey, R. L., López-Escobar, L., and Munizaga-Villavicencio, F., 1984, Petrogenesis of the Laguna del Maule volcanic complex, Chile (36°S). Contributions to Mineralogy and Petrology 88, 133-149.

Fujita, E., Kozono, T., Ueda, H., Kohno, Y., Yoshioka, S., Toda, N., Kikuchi, A., Ida, Y., 2013. Stress field change around the Mount Fuji volcano magma system caused by the Tohoku megathrust earthquake, Japan. Bulletin of Volcanology 75, 679.

Galland, O., Cobbold, P.R., Bremond d'Ars, J. de, Hallot, E. 2007. Rise and emplacement of magma during horizontal shortening of the brittle crust : Insights from experimental modeling. Journal of Geophysical Research 112, B6.

Galli, P., 2000. New empirical relationships between magnitude and distance for liquefaction. Tectonophysics 324, 169-187.

Gerlach, T.M., Westrich, H.R., Casadevall, T.J., Finnegan, D.L., 1994. Vapor saturation and accumulation in magmas of the 1989-1990 eruption of Redoubt Volcano, Alaska. Journal of Volcanology and Geothermal Research 62, 1-4, 317-337.

Germa, A., Quidelleur, X., Gillot, P.-Y., Tchilinguirian, P., 2007, Volcanic evolution of the back-arc complex of Payun Matru (Argentina) and its geodynamic implications for caldera-forming eruption in a complex slab geometry setting. IUGG 2007, Perugia, abstract 6761.

Gilbert, J.S., Stasiuk, M.V., Lane, S., Adam, C.R., Murphy, M.D., Sparks, R.S.J., Naranjo, J.A., 1996, Non-explosive, constructional evolution of the ice-filled caldera at Volcan Sollipulli, Chile. Bulletin of Volcanology 58, 67-83.

Glazner, A.F., 1991. Plutonism, oblique subduction, and continental growth: An example from the Mesozoic of California. Geology 19, 784-786.

Global Volcanism Program Digital Information Series, http://www.volcano.si.edu/gvp/world.

Gomberg, J., Davis, S., 1996. Stress/strain changes and triggered seismicity at the Geysers, California. Journal of geophysical research 101, 733-749.

Gonzalez-Ferran, O., 1995. Volcanes de Chile. Instituto Geografico Militar, Santiago de Chile.

Guliev, I.S., Feyzullayev, A.A., 1997. All about Mud Volcanoes. Nafta Press Baku 52.

Haeussler, P.J., Schwartz, D.P., Dawson, T.E., Stenner, H.D., Lienkaemper, J.J., Sherrod, Brian, Cinti, F.R., Montone, Paola, Craw, P.A., Crone, A.J., and Personius, S.F., 2004. Surface rupture and slip distribution of the Denali and Totschunda faults in the 3 November 2002 M 7.9 earthquake, Alaska. Bulletin of the Seismological Society of America 94, 6B, 23-52.

Hamilton, W.B., 1995. Subduction systems and magmatism. In: Smellie, J.R. (Ed.), Volcanism associated with extension to consuming plate margins. Geolical Society London Special Publication 81, 3-28.

Hardebeck, J.L., Nazareth, J.J., Hauksson, E., 1998. The static stress change triggering model: Constraints from two southern California aftershocks sequences. Journal of Geophysical Research: Solid Earth 103, 24427-24437.

Hardebeck, J.L., Nazareth, J.J., Hauksson, E., 1998. The static stress change triggering model: Constraints from two southern California aftershocks sequences. Journal of Geophysical Research 103, 24427-24437.

Hardebeck, J.L., Hauksson, E., 2001. Crustal stress field in southern California and its implications for fault mechanics. Journal of Geophysical Research: Solid Earth 106, B10, 21859-21882.

Harding, S. T., and S. T. Algermissen, 1969. Focal mechanism of the Prince William Sound, Alaska earthquake of March 28, 1964. Bulletin of the Seismological Society of America 59, 799-811.

Harris, R.A., 1998. Introduction to special section: Stress triggers, stress shadows, and implications for seismic hazard. Journal of Geophysical Research: Solid Earth103, 24347-24358.

Hastie, L. M., Savage, J.C., 1970. A dislocation model for the 1964. Alaska earthquake. Bulletin of the Seismological Society of America 60, 1389-1392.

Heidbach, O., Tingay, M., Barth, A., Reinecker, J., Kurfeß, D., Müller, B., 2008. The World Stress Map database release 2008.

Hickey-Vargas, R., Gerlach, D., Frey, F., 1984. Geochemical variations in volcanic rocks from central-south Chile (33°–42°S): implications for their petrogenesis. In: Harmon, R., Barreiro, B. (Eds.), Andean Magmatism: Chemical and Isotopic Constraints. Shiva Publishing Limited, England 72-95.

Hieke, W., 2004. The August 27, 1886 earthquake in Messenia (Peloponnesus) and reported flames over the Ionian Sea a Mediterranean Ridge gas escape event? Marine Geology 207, 1-4, 259-265.

Hildreth, W., 1987. New perspectives on the eruption of 1912 in the Valley of Ten Thousand Smokes, Katmai National Park, Alaska. Bulletin of Volcanology 49, 680-693.

Hildreth, W., Moorbath, S., 1988. Crustal contributions to arc magmatism in the Andes of Central Chile. Contributions to Mineralogy and Petrology 98, 455-489.

Hildreth W., Drake R.E., 1992. Volcan Quizapu, Chilean Andes. Bulletin of Volcanology, 54 , 93-125.

Hildreth, W., Fierstein, J., 2000. Katmai volcanic cluster and the great eruption of 1912. Bulletin of The Geological Society of America 112, 10, 1594-1620.

Hildreth W., Fierstein, J., Lanphere, M.A., Siems, D.F., 2001. Trident Volcano: Four Contiguous Stratocones Adjacent to Katmai Pass, Alaska Peninsula. Studies by the U.S. Geological Survey in Alaska, U.S. Geological Survey Professional Paper 1678.

Hill, D.P., et al 1993. Seismicity remotely triggered by the magnitude 7.3 Landers, California, earthquake. Science 260, 1617-1622.

Hill, D.P., 1977. Model for earthquake swarms. Journal of Geophysical Research 82, 1347-1352.

Hill, D.P., Reasenberg. P.A., Michael, A., Arabaz, W., Beroza, G., Brumbaugh, D., Brune, J.N, Castro, R., Davis, S., dePolo, D., Ellsworth, W.L., Gomberg, J., Harmsen, S., House, L., Jackson, S.M., Johnston, M.J.S., Jones, L., Keller, R., Malone, S., Munguia, L., Nava, S., Pechmann, J.C., Sandford, A., Simpson, R.W., Smith, R.B., Stark, M., Stickney, M., Vidal, A., Walter, S., Wong, V., Zollweg., J., 1993. Seismicity in the western United States remotely triggered by the M 7.4 Landers, California, earthquake of June 28, 1992. Science 260, 16171623

Hill, D.P., Pollitz, F., Newhall, C., 2002. Earthquake-volcano interactions. Physics Today 55, 41-47.

Hill, D.P., Prejean, S.G., 2007. Dynamic triggering, in Treatise on Geophysics. In: Kanamori, H. (Ed.), Earthquake Seismology, 4. Elsevier, Amsterdam, 257-292.

Hill, D.P., 2008. Dynamic stresses, coulomb failure, and remote triggering. Bulletin of the Seismological Society of America 98, 66-92

Holzer, T.L., Noce, T.E., Bennett, M.J., Alessandro, C.D., Boatwright, J., John, C., Tinsley, I., Sell, R.W., Rosenberg, L.I., 2004. Liquefaction-induced lateral spreading in Oceano, California, during the 2003 San Simeon earthquake. Open-File Report 2004-1269 US Geological Survey.

Husen, S., Taylor, R., Smith, R.B., Heasler, H., 2004. Changes in geyser eruption behavior and remotely triggered seismicity in Yellowstone National Park produced by the 2002 M7.9 Denali fault earthquake, Alaska. Geology 32, 537-540

Husson, L., Ricard, Y., 2004 .Stress balance above subduction: application to the Andes. Earth and Planetary Science Letters 222, 1037-1050.

Hutchinson, R.A., 1985. Hydrothermal changes in the Upper Geyser Basin, Yellowstone National Park, after the 1983 Borah Peak, Idaho, earthquake. In: Stein RS (Ed.) Proceedings of Workshop XXVIII on the Borah Peak, Idaho, Earthquake, 3–6 October 1984, U.S. Geological Survey Open-File Report 85-290.

Ichihara, M., Brodsky, E.E., 2006. A limit on the effect of rectified diffusion in volcanic systems. Geophysical Research Letters 33, L02316.

Ichinose, G., Somerville, P., Thio,H.K., Graves, R., O'Connell, D., 2007. Rupture process of the 1964 Prince William Sound, Alaska, earthquake from the combined inversion of seismic, tsunami, and geodetic data. Journal of Geophysical Research 112, B07306.

Ishihara, K., 1984. Post-earthquake failure of a tailings dam due to liquefaction of the pond deposit. In: Prakash, S. (Ed.), International Conference on Case Histories in Geotechnical Engineering 3, 1129-1146.

Ismail-Zadeh, A., 1996. Migration of seismic activity in the Caspian Sea. In: Chowdhury DK (Ed) Computational seismology and geodynamics 3 Am Geophys Un Washington DC: 125-129.

Jackson, J., Priestley, K., Allen, M., Berberian, M., 2002. Active tectonics of the south Caspian Basin. Geophysical Journal International 148, 214-245

Jacques, E., King, G.C.P., Tapponnier, P., Ruegg, J.C., Manighetti, I., 1996. Seismic activity triggered by stress changes after the 1978 events in the Asal rift, Djibouti. Geophysical Research Letters 23, 2481-2484.

Jellinek, A.M., DePaolo, D.J., 2003. A model for the origin of large silicic magma chambers: precursors of caldera-forming eruptions. Bulletin of Volcanology 65, 363-381.

Jellinek, A.M., Manga, M., Saar, M.O., 2004. Did melting glaciers cause volcanic eruptions in eastern California? Probing the mechanics of dike formation. Journal of Geophysical Research 109, B09206.

Johnson, C.A., Harrison, C.G.A., 1990. Neotectonics in central Mexico. Physics of the Earth and Planetary Interiors 64, 187-210.

Johnson, J.M., Satake, K., 1994. Rupture extent of the 1938 Alaskan earthquake as inferred from tsunami waveforms. Geophysical Research Letters 21, 8, 733-736.

Johnson, J.M., Tanioka, Y., Ruff, L.J., Satake, K., Kanamori, H., Sykes, L.R., 1994. The 1957 Great Aleutian earthquake. Pure and Applied Geophysics 142, 1, 3-28.

Johnson, J.M., Satake, K., 1995. Source parameters of the 1957 and 1938 alaskan earthquakes from tsunami waveforms. Tsunami: Progress in Prediction, Disaster Prevention and Warning, advances in Natural and Technological Hazards Research 4, 71-84.

Johnson, J.M., Satake, K., 1996. The 1965 Rat Islands earthquake: A critical comparison of seismic and tsunami wave inversions. Seismological Society of America 86, 5, 1229-1237.

Johnson, J.M., Satake, K., Holdahl, S.R., Sauber, J., 1996. The 1964 Prince William Sound earthquake: Joint inversion of tsunami and geodetic data. Journal of Geophysical Research: Solid Earth 101, B1, 523-532.

Johnson, J.M., Satake, K., 1997. Estimation of seismic moment and slip distribution of the April 1, 1946, Aleutian tsunami earthquake. Journal of Geophysical Research 102, B6, 1765-1774.

Johnson, J.M., and Satake, K., 1999. Asperity distribution of the 1952 great Kamchatka earthquake and its relation to future earthquake potential in Kamchatka: Pure and Applied Geophysics 154, 541-553.

Jolly, R., Lonergan, L., 2002. Mechanisms and controls on the formation of sand intrusions. Journal of the Geological Society 159, 605-617.

Jupp, T.E., Pyle, D.M., Mason, B.G., Dade,W.B., 2004. A statistical model for the timing of earthquakes and volcanic eruptions influenced by periodic processes. Journal of Geophysical Research: Solid Earth 109, B2.

Kadirov, F.A, 2000. Application of the Hartley transform for interpretation of gravity anomalies in the Shamakhy-Gobustan and Absheron oil- and gas-bearing regions, Azerbaijan. Journal of applied geophysics 45, 49-61.

Kadirov, F.A., Floyd MAlizadeh, A., Guliev, I., Reilinger, R., Kuleli, S., King, R., Toksoz, M., 2012. Kinematics of the Caucasus near Baku, Azerbaijan. Natural hazards 63, 997-1006.

Kanamori, H., 1970, Synthesis of long-period surface waves and its application to earthquake source studies-Kurile Islands earthquake of October 13, 1963. Journal of Geophysical Research 75, 5011-5027.

Kanno, T., Narita, A., Morikawa, N., Fujuwara, H., Fukushima, Y., 2006. A new attenuation relation for strong ground motion in Japan based on recorded data. Bulletin of the Seismological Society of America 96, 3, 879-897.

Karato, S., Wu, P., 1993. Science 260, 5109, 771-778.

Kelleher, J.A., 1972. Rupture zones of large South American earthquakes and some predictions. Journal of Geophysical Research 77, 2087–2103.

Kenner, S. J., Segall, P., 2000. Postseismic deformation following the 1906 San Francisco earthquake. Journal of Geophysical Research: Solid Earth 105, 13195-13209.

Kervyn, M., Ernst, G. G. J., van Wyk de Vries, B. , Mathieu, L., Jacobs, P., 2009. Volcano load control on dyke propagation and vent distribution: Insights from analogue modeling. Journal of Geophysical Research: Solid Earth 114, B03401.

King, G.C.P., Stein, R.S., Lin, J., 1994. Static stress changes and the triggering of earthquakes. Bulletin of the Seismological Society of America 84, 935-953.

Koehler, R.D., Farrell, R-E., Burns, P.A.C., Combellick, R.A., 2012. Quaternary faults and folds in Alaska: A digital database. Alaska Division of Geological & Geophysical Surveys, Miscellaneous Publication 141, 31 pp.

Kohlstedt, D.L., Evans, B., Mackwell, S.J., 1995. Strength of the lithosphere: Constraints imposed by laboratory experiments. Journal of Geophysical Research 100, B9, 17587-17617.

Kondorskaya, N., Hrometskaya, A., Grishiani, A., 1982. New catalogue of strong earthquakes in the USSR from ancient times through 1975. World Data Centre for Solid Earth Geophysics, Moscow Nauka 535.

Koper, D.D., Hutko, A.R., Lay, T., Sufri, O., 2012. Imaging short-period seismic radiation from the 27 February 2010 Chile (M_W 8.8) earthquake by back-projection of P, PP, and PKIKP waves. Journal of geophysical research 117, 1-16.

Kopf, A.J., 2002. Significance of mud volcanism. Reviews of Geophysics 40, 1005.

Kopf, A.J., 2008. Making calderas from mud. Nature Geoscience 1, 500-501.

Kopf, A.J., Behrmann, J.H., 2000. Extrusion dynamics of mud volcanoes on the Mediterranean Ridge accretionary complex. Geological Society London Special publication 174, 169-204.

Koyama, M., 2002. Mechanical Coupling Between Volcanic Unrests and Large Earthquakes; A Review of Examples and Mechanisms, Correlation and Triggering Between Earthquakes and Volcanic Eruptions. Tokyo Geographical Society, Tokyo, Japan, 222-232.

Lahr J.C., B.A. Chouet, C.D. Stephens, J.A. Power, R.A. Page, 1994. Earthquake classification, location, and error analysis in a volcanic environment: implications for the magmatic system of the 1989-1990 eruptions at Redoubt Volcano, Alaska. Journal of Volcanology and Geothermal Research 62, 137-151.

Lange, D., Cembrano, J., Rietbrock, A., Haberland, C., Dahm, T., Bataille, K., 2008. First seismic record for intra-arc strike-slip tectonics along the Liquiñe-Ofqui fault zone at the obliquely convergent plate margin of the southern Andes. Tectonophysics 455, 14-24.

Lara, L.E., Naranjo, J.A., Moreno, H., 2004a. Rhyodacitic fissure eruption in Southern Andes (Cordón Caulle, 40.5°S) after the 1960 (M_w 9.5) Chilean earthquake: a structural interpretation. Journal of Volcanology and Geothermal Research 138, 127-138.

Lara, L.E., Naranjo, J.A., Moreno, H., 2004b. Lanín volcano (39.5°S), Southern Andes: geology and morphostructural evolution. Revista Geológica de Chile 31 2, 241-257.

Lara, L.E., Lavenu, A., Cembrano, J., Rodríguez, C., 2006a. Structural controls of volcanism in transversal chains: resheared faults and neotectonics in the Cordón Caulle–Puyehue area (40.5°S), southern Andes. Journal of Volcanology and Geothermal Research 158, 70-86.

Lara, L.E., Moreno, H., Naranjo, J.A., Matthews, S., Pérez de Arce, C., 2006b. Magmatic evolution of the Puyehue–Cordón Caulle Volcanic Complex (40° S), Southern Andean Volcanic Zone: from shield to unusual rhyolitic fissure volcanism. Journal of Volcanology and Geothermal Research 157, 343-366.

Lavenu, A., Cembrano, J., 1999. Compressional and transpressional-stress pattern for Pliocene and Quaternary brittle deformation in fore and intra-arc zones (Andes of Central and Southern Chile). Journal of Structural Geology 21, 1669-1691.

Lemarchand, N., Grasso, J.R., 2007. Interactions between earthquakes and volcano activity. Geophysical Research Letters 34, 24, L24303.

Levitski, G., 1902. Bulletin de la Commission Centrale Sismique Permanente (Annee 1902. Janvier-juin). Academie Imperiale des Sciences, St.-Petersbourg.

Lin, J., Stein, R.S., 2004. Stress triggering in thrust and subduction earthquakes, and stress interaction between the southern San Andreas and nearby thrust and strike-slip faults. Journal of Geophysical Research: Solid Earth 109, B02303.

Lin, Y.N, Sladen, A., Ortega-Culaciati, F., Simons, M., Avouac, J-P., Fielding, E.J., Brooks, B.A., Bevis, M., Genrich, J., Rietbrock., A., Vigny, C., Smalley., R., Socquet, A., 2013. Coseismic and Postseismic Slip Associated with the 2010 Maule Earthquake, Chile: Characterizing the Arauco Peninsula Barrier Effect. Journal of Geophysical Research 118, 6, 3142-3159.

Linde, A.T., Sacks, I.S., 1998. Triggering of volcanic eruptions. Nature 395, 888-890.

Linde, A.T., Sacks, I.S., Johnston, M.J.S., Hill, D.P., Bilham, R.G., 1994. Increased pressure from rising bubbles as a mechanism for remotely triggered seismicity. Nature 371, 408-410.

Lomnitz, C., 1970. Major earthquakes and tsunamis in Chile during the period 1535 to 1955. Geologische Rundschau 59, 938-960.

Lomnitz, C., 1985. Tectonic feedback and the earthquake cycle. Pure and applied geophysics. 123, 667-682.

Lopez-Escobar, L., Vergara, M., and Frey, F.A., 1981, Petrology and geochemistry of lavas from Antuco volcano, a basaltic volcano of the southern Andes (37° 25' S). Journal of Volcanology and Geothermal Research, 11, 329-352.

López-Escobar, L., Cembrano, J., Moreno, H., 1995. Geochemistry and tectonics of the Chilean Southern Andes basaltic quaternary volcanism (37-46°S). Revista Geológica de Chile 22, 2, 219-234.

López-Escobar, L., Parada, M. A., Hickey-Vargas, R., Frey F. A., Kempton, R D., Moreno, H., 1995. Calbuco Volcano and minor eruptive centers distributed along the Liquiñe-Ofqui Fault Zone, Chile (41°-42°S): contrasting origin of andesitic and basaltic magma in the Southern Volcanic Zone of the Andes. Contributions to Mineralogy and Petrology, 119, 345-361.

Lorito, S., Romano, F., Atzori, S., Tong, X., Avallone, A., McCloskey, J., Cocco, M., Boschi, E., Piatanesi, A., 2011. Limited overlap between the seismic gap and coseismic slip of the great 2010 Chile earthquake. Nature Geoscience 4,173-177.

Lowenstern, J.B., P.C. Wallmann, D.D., Pollard, 1991. The west Mageik lake sill complex as an analogue for magma transport during the 1912 eruption at the valley of Ten Thousand Smokes, Alaska. Geophysical Research Letters 18, 8, 1569-1572.

Lu, Z., Fatland, R., Wyss, M., Li, S., Eichelberger, J., Dean, K., Freymueller, J., 1997. Deformation of New Trident Volcano measured by ERS-1 SAR interferometry, Katmai National Park, Alaska. Geophysical Research Letters 24, 6, 695-698.

Lu, Z., Wicks Jr., C., Power, J.A., Dzurisin, D., 2000. Ground deformation associated with the March 1996 earthquake swarm at Akutan volcano, Alaska, revealed by satellite radar interferometry. Journal of Geophysical Research: Solid Earth 105, B9, 21483-21495.

Main, I.G., Meredith, P.G., 1991. Stress corrosion constitutive laws as a possible mechanism of intermediate-term and short-term seismic quiescence, Geophysical journal international 107, 363-372.

Maksimov, A.P., 2007. A physicochemical model for deep degassing of water-rich magma. Journal of Volcanology and Seismology 2, 5, 356-363.

Mamani, M.J., Borzotta, E., Venencia, J.E., Maidana, A., Moyano, C.E., Castiglione, B., 2000. Electric structure of the Copahue Volcano (Neuquén Province, Argentina), from magnetotelluric soundings: 1D and 2D modellings. Journal of South American Earth Sciences 13, 147-156.

Manga, M., Brodsky, E.E., 2006. Seismic triggering of eruptions in the far field: volcanoes and geysers. Annual Review of Earth and Planetary Science 34, 263-291.

Manga, M., 2007. Did an earthquake trigger the May 2006 eruption of the Lusi mud volcano? EOS 88, 201.

Manga, M., Brumm, M., Rudolph., M., 2009. Earthquake triggering of mud volcanoes. Marine and Petroleum Geology 26, 1785-1798.

Martinelli, G., Dadomo, A., 2005. Volcano monitoring and seismic events in Mud Volcanoes. Geodynamics and Seismicity, NATO Sci. Ser. Earth Environ. edited by G. Martinelli and B. Panahi, Springer New York 51, 211-220.

Marzocchi, W., 2002. Remote seismic influence on large explosive eruptions. Journal of Geophysical Research 107, B1, 2018.

Marzocchi, W., 2002. Remote seismic influence on the large explosive eruptions, Journal of Geophysical Research 107, EPM 6-1.

Marzocchi, W., Casarotti, E., Piersanti, A., 2002. Modeling the stress variations induced by great earthquakes on the largest volcanic eruptions of the 20th century. Journal of Geophysical Research, 107, B11, 2320.

Marzocchi, M., Zacarelli, L., Boschi, E., 2004. Phenomological evidence in favor of a remote seismic coupling for large volcanic eruptions, Geophysical Research Letters 31, L04601.

Masterlark, T., Feigl, K. L., Haney, M., Stone, J., Thurber, C., Ronchin, E., 2012. Nonlinear estimation of geometric parameters in FEMs of volcano deformation: Integrating tomography models and geodetic data for Okmok volcano, Alaska. Journal of Geophysical Research: Solid Earth, 117, B02407.

Mazzini, A., Svensen, H., Akhmanov, G., Aloisi, G., Planke, S., Malthe-Sørenssen, A., Istadi, B. 2007. Triggering and dynamic evolution of Lusi mud volcano, Indonesia. Earth and Planetary Science Letters 261, 375-388.

Mazzini, A., Nermoen, A., Krotkiewski, M., Podladchikov, Y., Planke, S., Svensen, H., 2009. Strike-slip faulting as a trigger mechanism for overpressure release through piercement structures. Implications for the Lusi mud volcano, Indonesia. Marine and Petroleum Geology 26, 1751-1765.

Mau, S., Rehder, G., Arroyo, I.G., Gossler, J., Suess, E., 2007. Indications of a link between seismotectonics and CH4 release from seeps off Costa Rica. Geochemistry, Geophysics, Geosystems 4, 1-13.

McGuire, W.J., Howard, R.J., Firth, C.R., Solow, A.R., Pullen, A.D., Saunders, S.J., Stewart, I.S., Vita-Finzi, C., 1997. Correlation between rate of sea level change and frequency of explosive volcanism in the Mediterranean. Nature 389, 473-476

McLeod, P., Tait, S., 1999. The growth of dykes from magma chambers. Journal of Volcanology and Geothermal Research 92, 231-246.

McMillan, N.J., Harmon, R.S., Moorbath, S., Lopez-Escobar, L., and Strong, D., 1989. Crustal sources involved in continental arc magmatism: a case study of Volcan Mocho-Choshuenco, southern Chile. Geology 17, 1152-1156.

McNutt, S.R., Jacob, K.H., 1986. Determination of large-scale velocity structure of the crust and upper mantle in the vicinity of Pavlof Volcano, Alaska. Journal of Geophysical Research: Solid Earth 91, B5, 5013-5022.

Mellors, R., Kilb, D., Aliyev, A., Gasanov, G., Yetirmishli, G., 2007. Correlations between earthquakes and large mud volcano eruptions. Journal of Geophysical Research: Solid Earth 112, B04304.

Melnick, D., 2000. Geometrìa y estructuras de la parte norte de la zona de falla de Liquiñe-Ofqui (38°S): interpretación de sensores remotos. IX Congreso Geológico Chileno (Puerto Varas), Abstracts 1, 796-799.

Melnick, D, Folguera, A., Ramos, V.A., 2006. Structural control on arc volcanism: The Caviahue–Copahue complex, Central to Patagonian Andes transition (38°S). Journal of South American Earth Sciences 22, 66-88.

Miller, T.P., McGirnsey, R.G., Richter, D.W., Riehle, J.R., Nye, C.J., Yaunt, M.E., Durnoufin, J.A., 1998. Catalog of the historically active volcanoes of Alaska. U.S. Geological Survey, Open File Report, 98-582, 104 pp.

Miller, S.A., Cristiano, C., Chiaraluce, L., Cocco, M., Barchi, M., Kaus, B.J.P., 2004. Aftershocks driven by a high-pressure CO2 source at depth. Nature 427, 724-727.

Mithen, D.P., 1982. Stress amplification in the upper crust and the development of normal faulting. Tectonophysics 83, 121-130.

Moore, J.G., Normark, W.R., and Holcomb, R.T., 1994, Giant hawaiian landslides. Annual Review of Earth and Planetary Sciences 22, 119-144.

Moran, S.C., Stihler, S.D., Power, J.A., 2002. A tectonic earthquake sequence preceding the April-May 1999 eruption of Shishaldin Volcano. Alaska. Bulletin of Volcanology 64, 520-524.

Moran, S.C., Power, J.A., Stihler, S.D., Sanchez, J.J., Caplan-Auerbach, J., 2004. Earthquake triggering at Alaskan volcanoes following the 3 November 2002 Denali Fault earthquake. Bulletin of the Seismological Society of America 94, 300-309.

Moreno, H., Lahsen, A., 1986. El volcán Callaqui: ejemplo de vulcanismo fisural en los Andes del Sur. Revista de la Asociación Geológica Argentina 42, 1-8.

Moreno, H., and Naranjo, J.A., 1991. The southern Andes volcanoes (33°-41° 30' S), Chile. 6th Geol. Congr. Chile, Excur PC-3, 26.

Morley, C.K., 2003. Outcrop examples of mudstone intrusions from the Jerudong Anticline. In: Subsurface Sediment Remobilization (Ed by P Vanrensenbergen RR Hillis AJ Maltman & CK Morley) Geological Society of London Special Publlication 216, 381-394.

Morley, C.K., Crevello, P., Ahmad, Z.H., 1998. Shale tectonics associated with active diapirism; The Jerudong Anticline, Brunei Darussalam. Journal of the Geological Society 155, 3, 475-490.

Motagha, M., Schurr, B., Anderssohn, J., Cailleauc, B., Walter, T.R., Wang, R., Villotte, J-P., 2010. Subduction earthquake deformation associated with 14 November 2007, Mw 7.8 Tocopilla earthquake in Chile: Results from InSAR and aftershocks. Tectonophysics 490, 60-68.

Nakamukae, M., Haraguchi, T., Nakata, M., Ozono, S., Tajika, J., Ishimaru, S., Fukuzumi, T., Inoue, M., 2004. Reactivation of the Niikappu mud volcano following the Tokachi-oki earthquake in 2003. Japan Earth and Planetary Science 2004 (Joint meeting, Chiba, Japan).

Nakamura, K., 1977. Volcanoes as possible indicators of tectonic stress orientation-principle and proposal. Journal of Volcanology and Geothermal Research 2, 1-16.

Nakamura, K., Jacob, K.H, Davies, J.N., 1977. Volcanoes as possible indicators of tectonic stress orientation – Aleutinian and Alaska. Pure and Applied Geophysics 115, 87-112.

Nakamura, K., Uyeda, S., 1980. Stress gradient in arc-back arc regions and plate subduction. Journal of Geophysical Research: Solid Earth 85, B11, 6419-6428.

Nakamura, K., Plakfer, G., Jacob, K.H., Davies, J.N., 1980. A tectonic stress trajectory map of Alaska using information from volcanoes and faults. Bulletin of the Earthquake Research Institute 55, 89-100.

Naranjo, J.A,. Haller, M.J., 2002, Erupciones holocenas principalmente explosivas del volcán Planchón, Andes del sur (35°15'S). Revista geológica de Chile 29, 1, 93-113.

Naranjo, J.A., Polanco, E., 2004. The 2000 AD eruption of Copahue volcano, southern Andes. Revista geológica de Chile, 31, 279-292.

Nostro, C., Stein, R.S., Cocco, M., Belardinelli, M.E., Marzocchi, W., 1998. Two-way coupling between Vesuvius eruptions and southern Apennine earthquakes, Italy, by elastic stress transfer. Journal of Geophysical Research 103, 24487-24504.

Nye, C.J., Swanson, S.E., Avery, V.F., Miller, T.P., 1994. Geochemistry of the 1989-90 eruption of Redoubt Volcano: Part I. Whole-rock major and trace element chemisv. In: T.P. Miller and B.A. Chouet (Editors), The 1989-90 eruptions of Redoubt volcano, Alaska. Journal of Volcanology and Geothermal Research 62, 429-452.

Okada, Y., 1992. Internal deformation due to shear and tensile faults in a half-space. Bulletin Seismological Society of America 82, 1018-1040.

Okal, E.A., 2005. A re-evaluation of the great Aleutian and Chilean earthquakes of 1906 August 17. Geophysical Journal International, 161, 268-282.

OVDAS-SERNAGEOMIN, www.sernageomin.cl.

Page, R. A., Biswas, N. N., Lahr, J. C., Pulpan, H., 1991. Seismicity of continental Alaska. In Slemmons, D. B., Engdahl, E. R., Zoback, M. D., Blackwell, D. D., Eds. Neotectonics of North America: Boulder, Colorado. Geological Society of America, Decade Map, 1.

Palma, J.L., Calder, E.S., Basualto, D., Blake, S., Rothery, D.A., 2008. Correlations between SO_2 flux, seismicity, and outgassing activity at the open vent of Villarrica volcano, Chile. Journal of Geophysical Research 113, B10.

Pardo-Casas, F., Molnar, P., 1997. Relative motion of the Nazca (Farallón) and South American plates since late Cretaceous times. Tectonics 6, 233-248.

Pardo, M., Vera, E., Monfret, T., Yánez, G., Eisenberg, A., 2006. Sismicidad cortical superficial bajo Santiago: implicaciones en la tectónica andina y evaluación del peligro sísmico. Actas XI Congreso Geológico Chileno 1, 443-446.

Piersanti, A., Spada, G., Sabadini, R., Bonafede, M., 1995. Global postseismic deformation, Geophysical Journal International 120, 544-566.

Piersanti, A., Spada, G., Sabadini R., 1997. Global postseismic rebound of a viscoelastic Earth: Theory for finite faults and application to the 1964 Alaska earthquake, Journal of Geophysical Research: Solid Earth 102, 477-492.

Plafker, G., 1969. Tectonics of the March 17, 1964, Alaska earthquake, U.S. Geological Survey Professional Paper, 543-I, I1–I74, 2 sheets, scale 1:500 000.

Planke, S., Svensen, H., Hovland, M., Banks, D.A., 2003. Mud and fluid migration in active mud volcanoes in Azerbaijan. Geo-Marine Letters 23, 258-268.

Pollitz, F. F., Bürgmann, R., Romanowicz, B., 1998. Viscosity of oceanic asthenosphere inferred from remote triggering of earthquakes. Science 280, 1245-1249.

Pollitz, F.F., Sacks, I.S., 1977. The 1995 Kobe, Japan, earthquake: A long-delayed aftershock of the offshore 1944 Tonankai and 1946 Nankaido earthquakes. Seismological Society of America 87, 1, 1-10.

Pollitz, F.F., Brooks, B., Tong, X., Bevis, M.G., Foster, J.H., Bürgmann, R., Smalley, R.,Jr., Vigny, C., Socquet, A., Ruegg, J-C., Campos, J., Barrientos, S., Parra, H., Soto, J.C.B., Cimbaro, S., Blanco, M., 2011. Coseismic slip distribution of the February 27, 2010 M_w 8.8 Maule, Chile earthquake. Geophysical Research Letters 38, L09309.

Potent, S., Reuther, C.D., 2001. Neogene Deformationsprozesse im aktiven magmatischen Bogen Sudcentralchiles zwichen 37° und 39°S. Mitteilungen aus dem Geologisch-PalaÉontologischen Institut der UniversitaÉt Hamburg 85, 1-2.

Power, J.A., Moran, S.C., McNutt, S.R., Stihler, S.D., Sanchez, J.J., 2001. Seismic response of the Katmai volcanoes to the 6 December 1999 magnitude 7.0 Larluk Lake earthquake, Alaska. Bulletin of the Seismological Society of America 91, 57-63.

Prejean, S.G., Hill, D.P., Brodsky, E.E., Hough, S.E., Johnston, M.H.S., Malone, S.D., Oppenheimer, D.H., Pitt, A.M., Richards-Dinger, K.B., 2004. Remotely triggered seismicity on the United States west coast following the M 7.9 Denali fault earthquake. Bulletin of the Seismological Society of America 94, S348-S359.

Rea, J.C., Varekamp, J.C.,Mandeville, C., Goss, A.R., Colvin, A., 2009. Regional magmatic setting of Callaqui Volcano (S-Andes, Chile). Geological Society of America AnnualMeeting (Portland, 18–21 October 2009), Abstracts with Programs 41, 7, p. 111.

Reed, B.L., Lanphere, M.A., 1973.Alaska-Aleutian Range Batholith: Geochronology, Chemistry, and Relation to Circum-Pacific Plutonism. Geological Society of America Bulletin 84, 8, 2583-2610.

Reilinger, R., et al. 2006 GPS constraints on continental deformation in the Africa-Arabia-Eurasia continental collision zone and implications for the dynamics of plate interactions. Journal of Geophysical Research: Solid Earth 111, B5.

Reubi, O., Bourdon, B., Dungan, M.A., Koornneef, J.M., Sellés, D., Langmuir, C.H., Aciego, S., 2011. Assimilation of the plutonic roots of the Andean arc controls variations in U-series disequilibria at Volcan Llaima, Chile. Earth and Planetary Science Letters 303, 37-47.

Richter, D.H., Waythomas, C.F., McGimsey, R.G., Stelling, P.L., 1998. Geologic map of Akutan Island, Alaska. U.S. Geological Survey. Open File Report, 98-135, 22 pp.

Roberts, K.S., Davies, R., Stewart, S., 2010. Structure of exhumed mud volcano feeder complexes, Azerbaijan. Basin Research 22, 439-451.

Rockstroh, E., 1903. Recent Earthquakes in Guatemala. Nature 67, 1734, 271.

Roeloffs, E., Sneed, M., Galloway, D.L., Sorey, M.L., Farrar, C.D., Howle, J.F., Hughes, J., 2003. Water-level changes induced by local and distant earthquakes at Long Valley caldera, California. Journal of Volcanology and Geothermal Research 127, 269-303.

Rojstaczer, S., Galloway, D.L., Ingebritsen, S.E., Rubin, D.M., 2003. Variability in geyser eruptive timing and its causes: Yellowstone National Park. Geophysical Research Letters 30, 18, 1953.

Roman, D.C., Gardine, M.D., 2013. Seismological evidence for long-term and rapidly accelerating magma pressurization preceding the 2013 eruption of Redoubt Volcano, Alaska. Earth and Planetary Science Letters 371-372, 226-234.

Romick, J. D., Perfit, M.R., Swanson, S.E., Shuster, R.D., 1990, Magmatism in the eastern Aleutian Arc: temporal characteristic of igneous activity on Akutan Island. Contributions to Mineralogy and Petrology 104, 700-721.

Rosenau, M., 2004. Tectonics of the southern Andean intra-arc zone (38°-42°S). Ph.D. thesis, 159 pp. (Free University, Berlin, Germany).

Rosenau, M., Melnick, D., Echtler, H., 2006. Kinematic constraints on intra-arc shear and strain partitioning in the Southern Andes between 38°S and 42°S latitude. Tectonics 25, TC4013.

Sahagian, D.L., Proussevitch, A.A., 1992. Bubbles in volcanic systems. Nature 359, 485.

Sanchez, J.J, Wyss, M., McNutt, S.R., 2004. Temporal-spatial variations of stress at Redoubt volcano, Alaska, inferred from inversion of fault plane solutions. Journal of Volcanology and Geothermal Research 130, 1-30.

Shikhalibeyli, E., 1972. Location of Azerbaijan in general structure of the Caucasus and surrounding folded region. In: Azizbekov, Sh.A. Ed., Geology of the USSR, Azerbaijan vol XLVII Nedra Moscow, 286-290 (in Russian).

Shikhalibeyli, E., 1996. Some Aspects of Geological Structures and Tectonics of Azerbaijan. Elm Baku 82 (in Russian).

Saint Blanquat, M., Tikoff, B., Teyssier, C., Vigneresse, J.L., 1998. Transpressional kinematics and magmatic arcs. In: Holdsworth, R.E., Strachan, R.A., Dewey, J.F. (Eds.), Continental Transpressional and Transtensional Tectonics. Geological Society London Special Publications 135, 327-340.

Savage, J.C., Clark, M.M., 1982. Magmatic resurgence in Long Valley caldera, California: Possible cause of the 1980 Mammoth Lakes earthquakes. Science 217, 531-533, 1982.

Seeber, L., Armbruster, J.G., 2000. Earthquakes as beacons of stress change. Nature 407, 69-72.

Sepulveda, F., Lahsen, A., Bonvalot, S., Cembrano, J., Alvarado, A., Letelier, P., 2005. Morpho-structural evolution of the Cordón Caulle geothermal region, Southern Volcanic Zone, Chile: Insights from gravity and 40Ar/39Ar dating. Journal of Volcanology and Geothermal Research 148, 207-233.

Siebert, L., Simkin, T., 2010. Volcanoes of the world: an illustrated catalog of Holocene volcanoes and their eruptions. Smithsonian Institution, Global Volcanism Program Digital Information Series, GVP-3, http://www.volcano.si.edu/world/.

Silver, P.G., Valette-Silver, N.J., 1992. Detection of hydrothermal precursors to large Northern California earthquakes. Science 257, 1363-1368.

Somoza, R., 1998. Updated Nazca (Farallon)-South America relative motions during the last 40 My: implications for the mountain building in the central Andean region. Journal of South American Earth Sciences 11, 211-215.

Sparks RSJ, Sigurdsson H, Wilson L. 1977. Magma mixing: a mechanism for triggering acid explosive eruptions. Nature 267, 315-18.

Sruoga, P., Llambías, E.J., Fauqué, L., Schonwandt, D., Repol, D.G., 2005. Volcanological and geochemical evolution of the Diamante Caldera-Maipo volcano complex in the Southern Andes of Argentina (34°10'S). Journal of South American Earth Sciences19, 399-414.

Steacy, S., Gomberg, J., Cocco, M., 2005. Introduction to special section: Stress transfer, earthquake triggering, and time-dependent seismic hazard. Journal of Geophysical Research: Solid Earth 110, B05S01.

Stauder, W., 1968. Mechanisms of the Rat Island earthquake sequence of February 4. 1965, with relation to island arcs and seafloor spreading. Journal of Geophysical Resource 73, 3847-3857.

Stein, R.S., 1999. The role of stress transfer in earthquake occurrence. Nature 402, 605-609.

Steinberg, G.S., Steinberg, A.S., Merzhanov, A.G., 1989. Fluid mechanism of pressure growth in volcanic (magmatic) systems. Mod. Geol. 13, 257-266.

Stelling, P., Beget, J., Nye, C., Gardner, J., Devine, J., George, R., 2002. Geology and petrology of ejecta from the 1999 eruption of Shishaldin Volcano, Alaska. Bulletin of Volcanology 64, 8, 548-561.

Strecker, M., Bosworth, W., 1991. Quaternary stress-field change in the Gregory Rift, Kenya. Eos Trans., AGU 72, 17-22.

Sumita, I., Manga, M., 2008. Suspension rheology under oscillatory shear and its geophysical implications. Earth and Planetary Science Letters 269, 468-477.

Sykes, L., 1971. Aftershock zones of great earthquakes, seismicity gaps and earthquake prediction for Alaska and the Aleutians. Journal of Geophysical Resource 76, 8021-8041.

Tait S, Jaupart C, Vergniolle S. 1989. Pressure, gas content and eruption periodicity of a shallow crystallizing magma chamber. Earth and Planetary Science Letters 92, 107-123.

Telesca, L., Babayev, G., Kadirov, F., 2012. Temporal clustering of the seismicity of the Absheron-Prebalkhan region in the Caspian Sea area. Natural Hazards and Earth System Sciences12, 3279-3285.

Thatcher, W., Savage, J.C., 1982. Triggering of large earthquakes by magma-chamber inflation, Izu Peninsula. Japan, Geology 10, 12, 637-640.

Tibaldi, A., 1992. The role of transcurrent intra-arc tectonics in the configuration of a volcanic arc. Terra Nova 4, 567-577.

Tibaldi A., 1995. Morphology of pyroclastic cones and tectonics. Journal of Geophysical Research 100, B12, 24521-24535.

Tibaldi, A., 2008. Contractional tectonics and magma paths in volcanoes. Journal of volcanology and geothermal research 176, 291-301.

Tibaldi, A., Romero, J.L., 2000. Morphometry of Late Pleistocene-Holocene faulting in the southern Andes of Colombia and volcano-tectonic relationships. Tectonics 19, 2, 358-377.

Tibaldi, A., Pasquarè, F.A., Tormey, D., 2010. Volcanism in reverse and strike-slip fault settings. In: New Frontiers in Integrated Solid Earth Sciences, Ed S Cloetingh J Negendank, Springer-Verlag, 315-348.

Tilling, R.I., Koyanagi, R.Y., Lipman, P.W., Lockwood, J.P., Moore, J.G., Swanson, D.A., 1976. Earthquake and related catastrophic events, Island of Hawaii, November 29, 1975: A preliminary report: U.S. Geological Survey Circular 740, 33 pp.

Tingay, M.R.P., Heidbach, O., Davies, R., Swarbrick, R., 2008. Triggering of the Lusi Mud Eruption: Earthquake Versus Drilling Initiation. Geology 36, 8, 639-642.

Toda, S., Stein, R.S., Richards-Dinger, K., Bozkurt, S., 2005. Forecasting the evolution of seismicity in southern California: Animations built on earthquake stress transfer. Journal of Geophysical Research: Solid Earth 110, B05S16-17.

Toda, S., Stein, R.S., Lin, J., Sevilgen, K., 2011. Coulomb 3.3 User Guide pp. 63.

Toda S., Lin J., Stein, R.S., 2011a. Using the 2011 Mw 9.0 off the Pacific coast of Tohoku Earthquake to test the Coulomb stress triggering hypothesis and to calculate faults brought closer to failure. Earth Planets Space 63, 725-730.

Toda S., Stein, R.S., Lin J., 2011b. Widespread seismicity excitation throughout central Japan following the 2011 M=9.0 Tohoku earthquake and its interpretation by Coulomb stress transfer. Geophysical research letters 38, L00G03.

Tormey, D.R., Hickey-Vargas, R., Frey, F.A., and López-Escobar, L., 1991. Recent lavas from the Andean volcanic front (33 to 42°S); interpretations of along-arc compositional features. In Andean Magmatism and its Tectonic Setting (eds. Harmon, R.S., & Rapela, C.W.), Geol. S. Am. S., 265, 57-77.

Tormey, D.R., Frey, F.A., Lopez-Escobar, L., 1995. Geochemistry of the active Azufre-Planchon-Peteroa volcanic complex, Chile (35°15′S): evidence for multiple sources and processes in a Cordilleran arcmagmatic system. Journal of Petrology 36, 265-298.

Wallmann P.C., D.D. Pollard, Hildreth, W., Eichelberger, J.C., 1990. New structural limits on magma chamber locations at the Valley of Ten Thousand Smokes, Katmai National Park, Alaska. Geology 18, 1240-1243.

Varekamp, J.C., Ouimette, A.P., Herman, S.W., Bermudez, A., Delpino, D., 2001. Hydrothermal element fluxes from Copahue, Argentina: a "beehive" volcano in turmoil. Geology 29, 1059-1062.

Varekamp, J.C., Maarten de Moor, J., Merrill, M.D., Colvin, A.S., Goss, A.R., Vroon, P.Z., Hilton, D.R., 2006. Geochemistry and isotopic characteristics of the Caviahue–Copahue volcanic complex, Province of Neuquen, Argentina. Evolution of an Andean Margin: A Tectonic and Magmatic View from the Andes to the Neuquen Basin (35–39 S). Geological Society of America Special Paper 407, 317-342.

Veber, M.V., 1904. Recherches preliminaries sur le tremblement de terre a Chamakha. Comptes Rendue des Seances, Tome I. Academie Imperiale des Sciences, St.-Petersbourg, 238-241.

Vergniolle, S., Caplan-Auerbach, J., 2006. Basaltic thermals and Subplinian plumes: Constraints from acoustic measurements at Shishaldin volcano, Alaska. Bulletin of Volcanology 68, 611-630.

Vigny, C., Socquet, A., Peyrat, S., Ruegg, J.-C., Métois, M., Madariaga, R., Morvan, S., Lancieri, M., Lacassin, R., Campos, J., Carrizo, D., Bejar-Pizarro, M., Barrientos, S., Armijo, R., Aranda, C., Valderas-Bermejo, M.-C., Ortega, I., Bondoux, F., Baize, S., Lyon-Caen, H. , Pavez, A., Vilotte, J.P., Bevis, M., Brooks, B., Smalley, R., Parra, H., Baez, J.-C., Blanco, M., Cimbaro, S., Kendrick, E., 2011. The 2010 Mw 8.8 Maule Megathrust Earthquake of Central Chile, Monitored by GPS. Science 332, 1417-1421.

Walker, G.P.L., 1999. Volcanic rift zones and their intrusion swarms. Journal of Volcanology and Geothermal Research 94, 21-34.

Walter, T.R., Schmincke, H.-U., 2002. Rifting, recurrent landsliding and Miocene structural reorganization on NW-Tenerife (Canary Islands). International Journal of Earth Sciences 91, 615-628.

Walter, T.R., 2007. How a tectonic earthquake may awake silent volcanoes: Stress triggering during the 1996 earthquake-eruption sequence at the Karymsky Volcanic Group, Kamchatka. Earth and Planetary Science Letters 264, 3-4, 347-359.

Walter, T.R., Amelung, F., 2007. Volcanic eruptions following M≥9 megathrust earthquakes: Implications for the Sumatra-Andaman volcanoes. Geology 35, 539-542.

Walter, T.R., Wang, R., Acocella, V., Neri, M., Grosser, H., Zschau, J., 2009. Simultaneous magma and gas eruptions at three volcanoes in southern Italy: An earthquake trigger? Geology 37, 3, 251-254.

Wang, C-Y., 2007. Liquefaction beyond the near field. Seismological Research Letters 78, 5, 512–517.

Watanabe, T., Koyaguchi, T., Seno, T., 1999. Tectonic stress controls on ascent and emplacement of magmas. Journal of Volcanology and Geothermal Research 91, 65-78.

Watt, S.F.L., Pyle, D.M., Mather, T.A., 2009. The influence of great earthquakes on volcanic eruption rate along the Chilean subduction zone. Earth and Planetary Science Letters 277, 399-407.

Wells, D.L., Coppersmith, K.J., 1994. New empirical relationships among magnitude, rupture length, rupture width, rupture area, and surface displacement. Bulletin of Seismological Society of America 84, 974-1002.

Woods AW, Cardoso SSS. 1997. Triggering basaltic volcanic eruptions by bubble melt separation. Nature 385, 518-520.

Woods, A.W., Pyle, D.M., 1997. The control of chamber geometry on triggering volcanic eruptions. Earth and Planetary Science Letters 151, 155-166.

Zeng, Y., 2001. Viscoelastic stress-triggering of the 1999 Hector Mine Earthquake by the 1992 Landers Earthquake. Geophysical Research Letters 28, 15, 3007-3010.